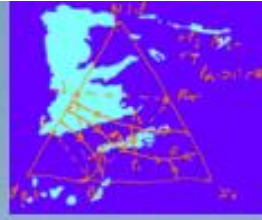**8ª Reunión del Grupo Ibérico de Petrología, Geoquímica y Geocronología.**

Guía de campo. Crecimiento temprano y evolución geológica de la Isla de Fuerteventura.

Comisión de Petrología, Geoquímica y Geocronología de Rocas Ígneas y Metamórficas de la Sociedad Geológica de España.
Fuerteventura, 14 de Junio a 17 de Junio de 2023.

Sociedad Geológica España

SGE

Vicerrectorado de Investigación y Transferencia
Universidad de La Laguna

Cátedra Cultural "Telesforo Bravo" de la Universidad de La Laguna.

CABILDO DE FUERTEVENTURA

Fuerteventura
Reserva de la Biosfera

Crecimiento temprano y evolución geológica de la Isla de Fuerteventura.

Guía de Campo

Autores:

Casillas, Ramón [1]
Fernández, Carlos [2]
Colmenero, Juan Ramón [3]

[1] Departamento de Biología Animal, Edafología y Geología, Universidad de La Laguna, 38206 La Laguna, Santa Cruz de Tenerife, Islas Canarias, España.
[2] Departamento de Geodinámica, Estratigrafía y Paleontología, Universidad Complutense de Madrid, 28040 Madrid, España.
[3] Departamento de Geología, Universidad de Salamanca, 37001 Salamanca, España (Jub.).

SGE – Universidad de La Laguna – Universidad Complutense de Madrid - Universidad de Salamanca.

8ª Reunión del Grupo Ibérico de Petrología, Geoquímica y Geocronología.

Comisión de Petrología, Geoquímica y Geocronología de rocas ígneas y metamórficas de la Sociedad Geológica de España.

Fuerteventura, Junio 2023.

INDICE:

A.- INTRODUCCIÓN

Este documento pretende ante todo dar a conocer a los participantes en la VIII Reunión del Grupo Ibérico de Petrología, Geoquímica y Geocronología las principales características geológicas de la isla de Fuerteventura. En ningún modo pretende ser un compendio exhaustivo. Antes bien, en aras de que resulte una guía ágil y amena, hemos intentado abreviar las descripciones en la medida de lo posible, para que no resulten prolijas en exceso. Con independencia de lo anterior, la presentación de los rasgos geológicos de la isla se ha hecho con el mayor rigor de que hemos sido capaces. Hemos procurado respetar el principio de objetivad científica en la discusión de las interpretaciones, especialmente cuando se dispone de varias hipótesis complementarias o alternativas para explicar el mismo hecho. Pedimos disculpas de antemano para los casos en los que no lo hayamos conseguido.

Debemos reconocer que el grueso de nuestro trabajo en Fuerteventura se centra en las formaciones más antiguas de la isla. Es por eso, y porque el análisis de estas unidades constituye el objetivo esencial de la excursión, que el énfasis principal de esta memoria recae en ellas. Dado que es en estas rocas más antiguas, donde se observan las estructuras tectónicas más abundantes, espectaculares e importantes para conocer el origen de la isla, y, por ende, de todo el archipiélago canario, por lo que esperamos que los participantes en la reunión del Grupo Ibérico de Petrología, Geoquímica y Geocronología sepan comprender este sesgo en nuestro acercamiento geológico a la isla. En cualquier caso, ofrecemos en las referencias bibliográficas un buen número de trabajos en los que el lector interesado podrá acercarse a la descripción geológica de otras unidades menos favorecidas en esta memoria. Como documentación adicional, hemos incluido en el Anexo de esta memoria cinco de nuestras contribuciones sobre la evolución temprana de la isla de Fuerteventura.

Pero este documento es también la guía de una excursión. En la segunda parte de la memoria trataremos con cierto detalle la descripción de las distintas paradas previstas. En ningún modo pueden considerarse descripciones cerradas. Los afloramientos geológicos son como las buenas obras de arte, que siempre tienen cosas nuevas que ofrecernos, algo que sabían bien los maestros de nuestra ciencia como Hans Cloos. Nuestro deseo es conseguir interesar lo suficiente a los participantes en esta excursión como para que puedan contribuir activamente, con todo su bagaje de conocimientos y experiencia, en la descripción e interpretación de cada afloramiento. Estaríamos completamente satisfechos si pudiésemos alcanzar este objetivo.

No querríamos acabar esta introducción sin rendir un pequeño homenaje a la protagonista de la excursión. Se dice que los alemanes sienten tanto apego por Fuerteventura, que intentaron comprársela al gobierno español durante la dictadura franquista. Es también conocido el hecho de que dispusieron de una mansión en el extremo sur de la isla, desde la que proporcionaban ayuda logística y refugio a las tripulaciones de submarinos que operaban en el Atlántico durante la Segunda Guerra Mundial. Modernamente, es lugar habitual de llegada de los cayucos procedentes del África sub-sahariana, destino turístico privilegiado de media Europa y conocido enclave de *windsurfistas*. Pero ni eso, ni las historias de piratas berberiscos o de incursiones militares inglesas, ni la sombra de un Unamuno desterrado, constituyen datos suficientes para apreciar el sabor y la infinidad de matices de esta tierra sorprendente. Estamos seguros de que estos días en el campo podrán entender y quizá compartir con nosotros esta pasión indefinible por Fuerteventura. Es la ventaja y el privilegio de dedicarnos a la Geología.

B.- DESCRIPCIÓN GEOLÓGICA DE LA ISLA DE FUERTEVENTURA

B.1.- SITUACIÓN Y CARACTERÍSTICAS GEOGRÁFICAS

La isla de Fuerteventura se localiza en la parte oriental del archipiélago canario, a unos 100 km de la costa del continente africano y se levanta más de 3000 m por encima del fondo oceánico del Atlántico (Fig. 1).
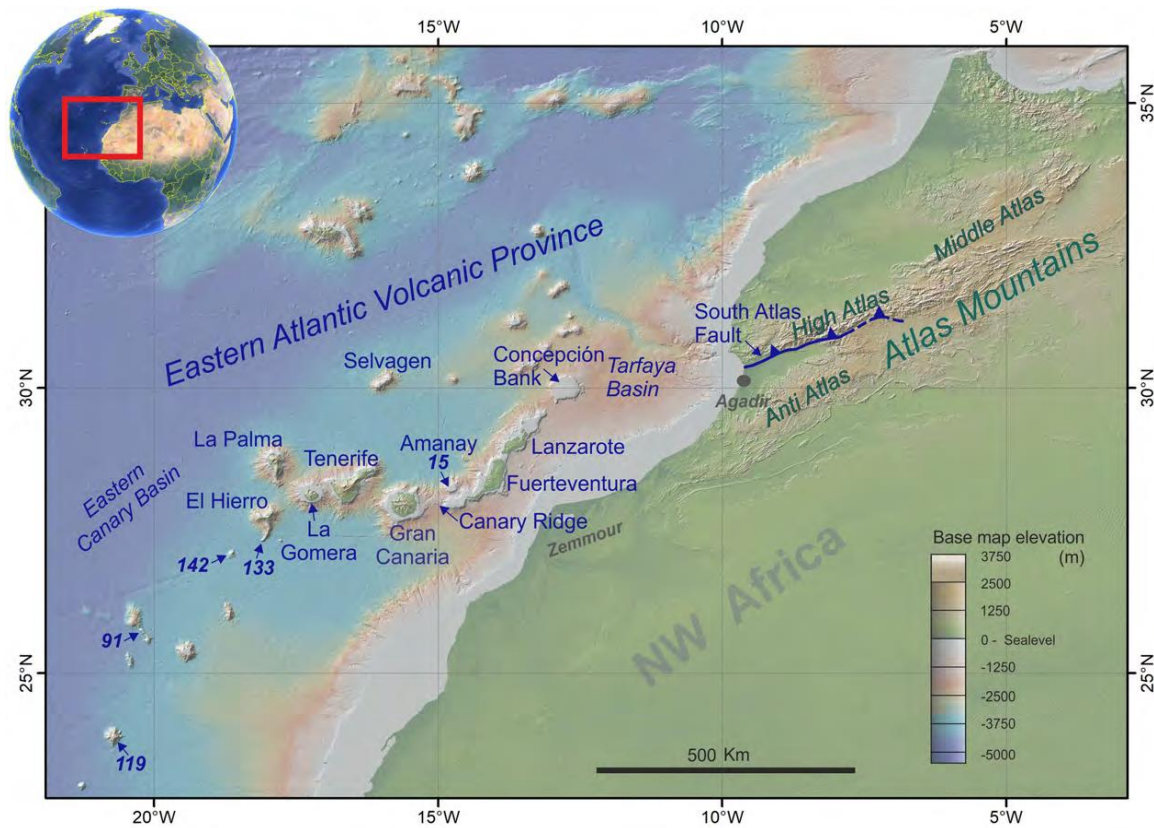
Fig. 1.- Situación general de Fuerteventura dentro del archipiélago canario, con indicación de la batimetría en ese sector del Atlántico Norte. (tomado de Anguita et al., enviado a ESR).

La isla se alarga más de 100 km en la dirección NNE-SSO y, con una superficie de 1.662 km^2, incluida la isla de Lobos, es la segunda isla en extensión del archipiélago canario. Frente a este notable tamaño, su cota máxima no alcanza los 1000 m (pico de la Zarza, 807 m), siendo exigua la superficie situada por encima de los 600 m. Es posible distinguir en Fuerteventura cinco comarcas fisiográficas claramente diferenciadas (Fig. 2) (Criado, 1991):

Fig. 2.- Modelo de elevación digital del terreno con indicación de las principales comarcas fisiográficas de Fuerteventura (iluminación desde el NO). La mayor parte de estas comarcas están condicionadas por unidades geológicas bien diferenciadas, como se indica en el texto (véase la Fig. 3).

1. El Norte. Abarca los espacios situados al norte de la línea constituida por el barranco de Tebeto, La Oliva y la montaña de Escanfraga. Se trata de un área con escasos desniveles y con una altitud que, salvo algunos puntos concretos (montaña de Tindaya y montaña de la Arena), no supera los 200 m. Esta parte de la isla está constituida fundamentalmente por pequeños conos de escorias y malpaíses, producidos en erupciones relativamente recientes de los últimos episodios del segundo ciclo de vulcanismo subaéreo plio-cuaternario y del vulcanismo subreciente.

2. La Llanura Central. Al sur de Montaña Quemada se abre la llanura interior, que es una de las regiones fisiográficas más características de la isla. Esta llanura aparece alterada por la presencia de pequeños tableros alargados de una veintena de metros de altura y algunas montañas que se levantan un centenar de metros sobre el relieve circundante, como montaña de Gairía. Hacia el sur, el Valle Central se estrecha progresivamente hasta desaparecer en el Valle del Tarajal de Sancho. Esta llanura central constituye un bloque hundido con respecto al sector más occidental, y su origen ha estado condicionado por la actividad tectónica.

3. Los Valles y Cuchillos orientales. Esta unidad se localiza desde montaña de Escanfraga, al norte, hasta el istmo de Jandía, al sur. La característica esencial es la presencia de un relieve que se estructura en valles, la mayoría sin cabeceras bien desarrolladas, con vertientes cóncavas y fondo plano. Los interfluvios están constituidos por cordales que normalmente superan los 400 m (cuchillos). Estos cuchillos representan los restos de la gran Dorsal Inicial de la Isla y los Edificios en Escudo Miocenos Norte y Central.

4. El Macizo de Betancuria. Este macizo se localiza desde el curso medio del barranco de Los Molinos, al norte, hasta el margen occidental del barranco de Chilegua. El contacto con la llanura central es bastante brusco, sobre todo entre Antigua y Tuineje. Este macizo presenta, como rasgos diferenciales, acusados desniveles y una notable compartimentación del relieve. En este sector afloran gran parte de los materiales más antiguos de la isla: la corteza oceánica mesozoica, el Complejo Plutónico Ultra-alcalino, la Dorsal Inicial y los complejos plutónico-filonianos relacionados con los Edificios en Escudo Miocenos Norte y Central.

5. La Península de Jandía. Separada del resto de la isla por el istmo de la Pared, presenta dos vertientes claramente diferentes. La vertiente de barlovento presenta un talud cóncavo y un escarpe donde se alcanzan las mayores cotas de la isla (pico de la Zarza, 807 m). La vertiente de sotavento se caracteriza por la presencia de una red de barrancos estrechos y cortos, en disposición casi radial que parten del escarpe. Desde Morro Jable hacia el oeste, los barrancos terminan en una planicie costera, levantada unos 10 metros sobre el nivel del mar. Algunos sectores como el istmo de Jandía o el Jable de Salinas, se caracterizan por la presencia de formaciones dunares de arenas bioclásticas movilizadas por el viento, y sobre las que se han

producido importantes encostramientos. En general, la península de Jandía representa los restos de la parte más meridional de la gran Dorsal Inicial de la isla y del Edificio en Escudo Mioceno Sur.

B.2.- PRINCIPALES UNIDADES GEOLÓGICAS

Desde el punto de vista geodinámico, el archipiélago canario y, por tanto, Fuerteventura, está situado dentro de la placa de Nubia, en una posición tectónica de intraplaca, en ambiente oceánico y cercano al borde continental de tipo pasivo del noroeste africano. El espesor de la corteza oceánica bajo Canarias varía desde los 12 km en La Palma hasta los 15 a 20 km entre Fuerteventura y Lanzarote (Bosshard & Macfarlane, 1970; Banda *et al.*, 1980; Banda *et al.*, 1981). Por tanto, la isla de Fuerteventura se asienta sobre una corteza de espesor anormalmente grueso para ambientes oceánicos, que puede ser interpretada como oceánica engrosada o incluso como corteza de transición. Su estructura consiste (Banda *et al.*, 1980; Banda *et al.*, 1981) en una primera capa de rocas volcánicas que se extiende hasta los 3 km de profundidad, y una capa de rocas ígneas plutónicas de posible composición gabroica y ultramáfica que alcanza los 15 km de profundidad. Entre los 15 y 20 km aparece una zona de tránsito entre la corteza oceánica y el manto, caracterizada por una baja velocidad de propagación de las ondas sísmicas P (7.4 km/s) si la comparamos con velocidades típicas de propagación de dichas ondas en el manto litosférico (8.0 km/s). Esta capa puede corresponder a un conjunto de rocas máficas y ultramáficas producidas por el magmatismo asociado a la pasada actividad ígnea de la isla (Holik *et al.*, 1991). Esta capa de baja velocidad sísmica ha sido encontrada en otros contextos de magmatismo intraplaca (Caress *et al.*, 1995).

En el conjunto del archipiélago es posible reconocer la existencia de direcciones estructurales de primer orden que han sido interpretadas clásicamente como debidas a importantes fracturas o fallas en la corteza oceánica. Las orientaciones de estas fracturas parecen concentrarse en cuatro grandes poblaciones fundamentales o directrices (Carracedo, 1984) que han condicionado la génesis y formación del archipiélago y están íntimamente ligadas a la evolución tectónica del océano Atlántico, al desplazamiento de la placa de Nubia y al campo de esfuerzos local provocado por la supuesta existencia de un penacho mantélico o de una amplia zona de anomalía térmica en el manto superior sub-litosférico (Anderson *et al.*, 1992):

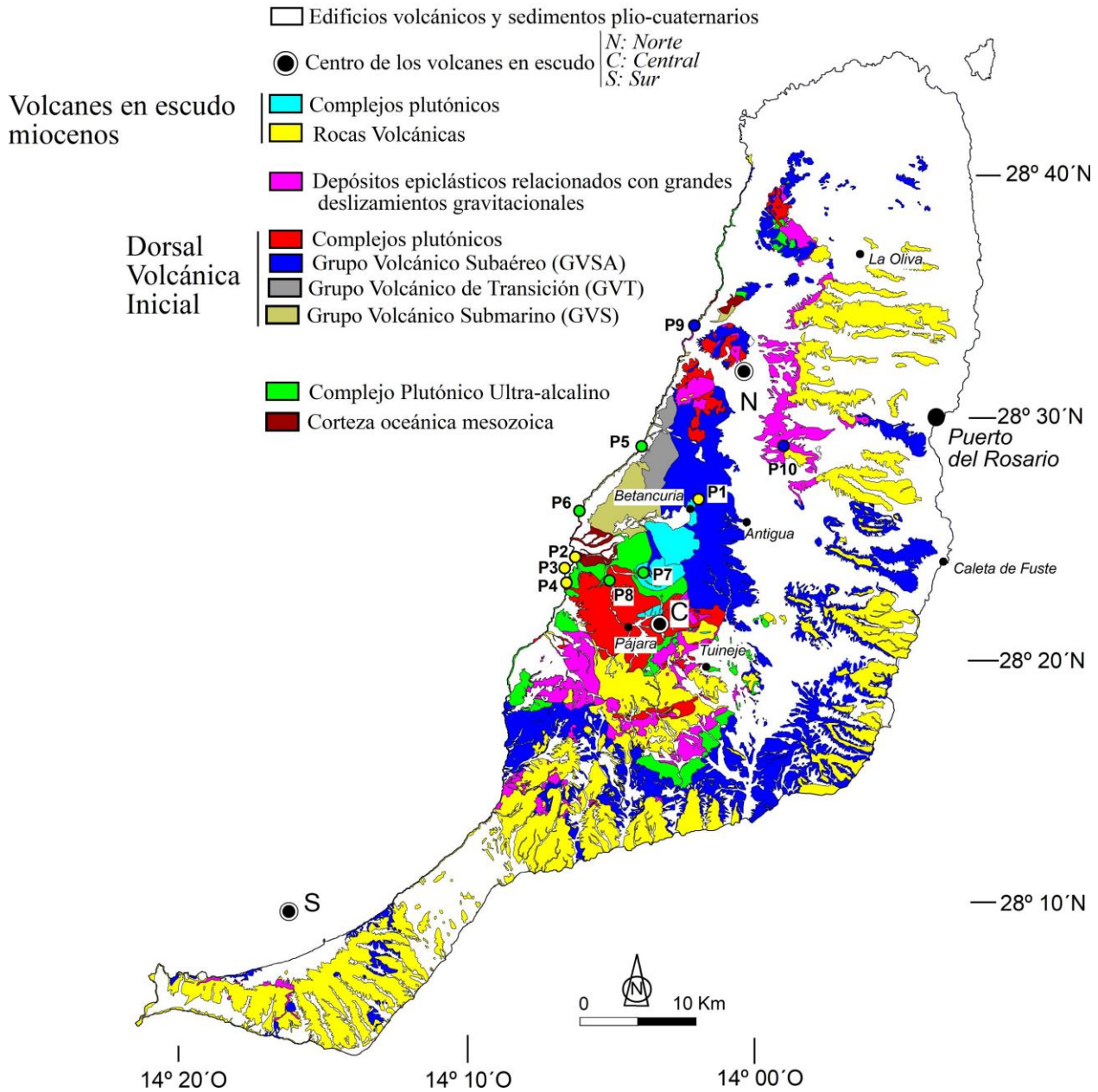Fig. 3.- Mapa geológico de la isla de Fuerteventura (modificado de Balcells *et al.,* 2006) mostrando las principales unidades, la localización de los centros de los edificios volcánicos miocenos (N: Norte, C: Central, S: Sur), y la posición de las paradas de esta excursión (P1 a P10). El principal afloramiento de las rocas más antiguas, en la zona centro-occidental de la isla, es el llamado macizo de Betancuria.

1. N35ºE (NE-SO). Es la llamada dirección *africana* (alineación de Fuerteventura y Lanzarote, así como un gran número de estructuras observables en estas y otras islas).

2. N110ºE (NO-SE). Dirección *atlántica* (alineación definida por las islas de La Palma, Tenerife y Gran Canaria, y numerosas estructuras observables en el archipiélago).

3. N60-65ºE. Dirección también *atlásica* (aunque definida por las islas de Tenerife, La Gomera y El Hierro y por diversas estructuras en las distintas islas).

4. N-S. Orientación de la red de diques en La Palma.

El nacimiento y emersión de Fuerteventura y su posterior evolución se ha llevado a cabo, de forma similar a como ocurre en las otras islas, según dos ciclos fundamentales (crecimiento submarino y subaéreo), que han dado lugar a la formación de diversas rocas representadas en la isla por seis grandes formaciones litológicas (Ancochea *et al.,* 1993) (Fig. 3 y Fig. 4):

1). La Corteza oceánica mesozoica.

2). El Complejo Plutónico Ultra-alcalino.

3). La Dorsal Volcánica Inicial.

4). Los grandes edificios en escudo miocenos.

5). Los edificios volcánicos plio-cuaternarios.

6). Los sedimentos plio-cuaternarios.

La corteza oceánica mesozoica, el Complejo Plutónico Ultra-alcalino, parte de la Dorsal Inicial y los complejos plutónicos-filonianos asociados a los grandes edificios en escudo miocenos constituyen el Complejo Basal, de acuerdo con la terminología clásica empleada por los investigadores de la escuela del Prof. Fúster. Siguiendo esta misma terminología, parte de la Dorsal Volcánica Inicial y los grandes edificios en escudo miocenos constituyen la Serie I, mientras que los edificios volcánicos plio-cuaternarios forman las Serie II, III y IV.

A continuación, se describirán con más detenimiento cada una de estas grandes unidades geológicas.
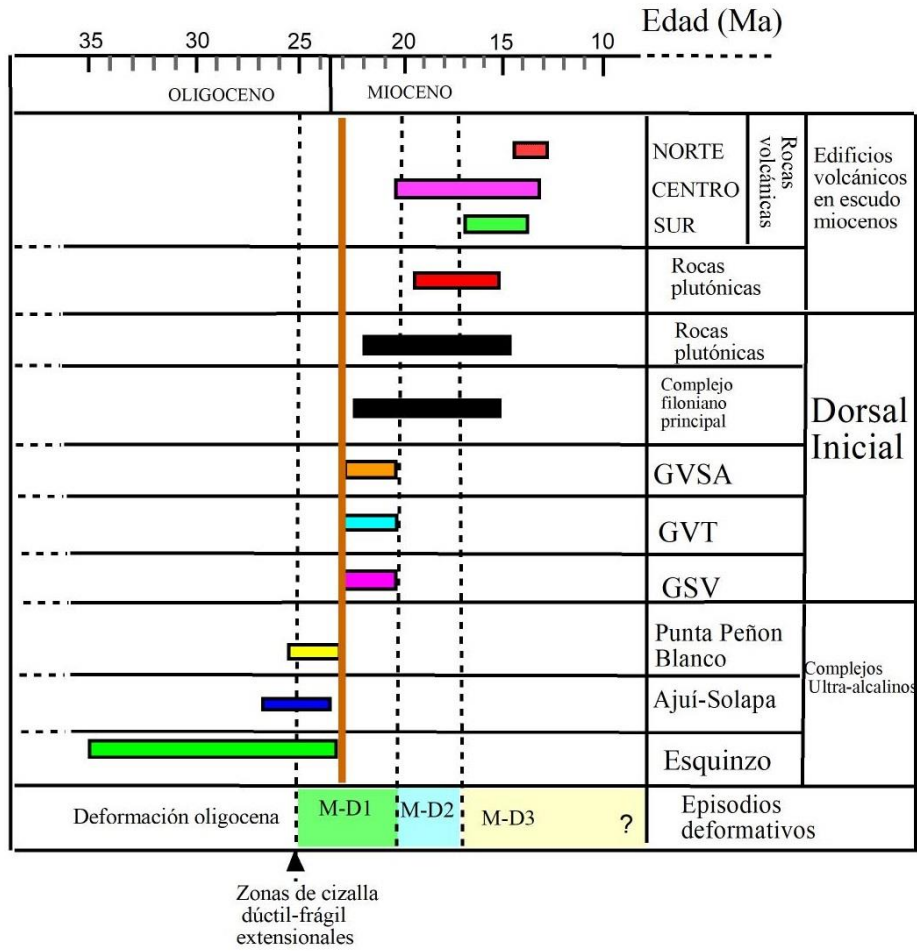
Fig. 4.- Esquema de evolución temporal de las diferentes unidades geológicas tempranas relacionadas con la formación de Fuerteventura y etapas de deformación. En color naranja se muestra la posición geocronológica de la discordancia existente bajo las rocas volcánicas de la Dorsal Inicial.

B.2.1. La corteza oceánica mesozoica.

La corteza oceánica mesozoica pre-volcánica aparece en dos sectores de la costa occidental de la isla (Fig. 3): entre la Piedra de La Playa y el Pardero en la costa norte (Fúster *et al.*, 1968a; Robertson & Stillman, 1979a; Roberston & Bernouilli, 1982), donde se encuentra muy fracturada e hidrotermalizada, y entre la playa de Los Muertos y la caleta de la Peña Vieja en Ajuy (Fúster *et al.*, 1968a; Rothe, 1968; Robertson & Stillman, 1979a; Fúster *et al.*, 1980; Roberston & Bernouilli, 1982; Fúster *et al.*, 1984a y b; Renz *et al.*, 1992). En este último sector, esta secuencia presenta un espesor aproximado de 1600 m. Se han diferenciado cinco unidades en estos sedimentos (Steiner *et al.*, 1998, Fig. 5).
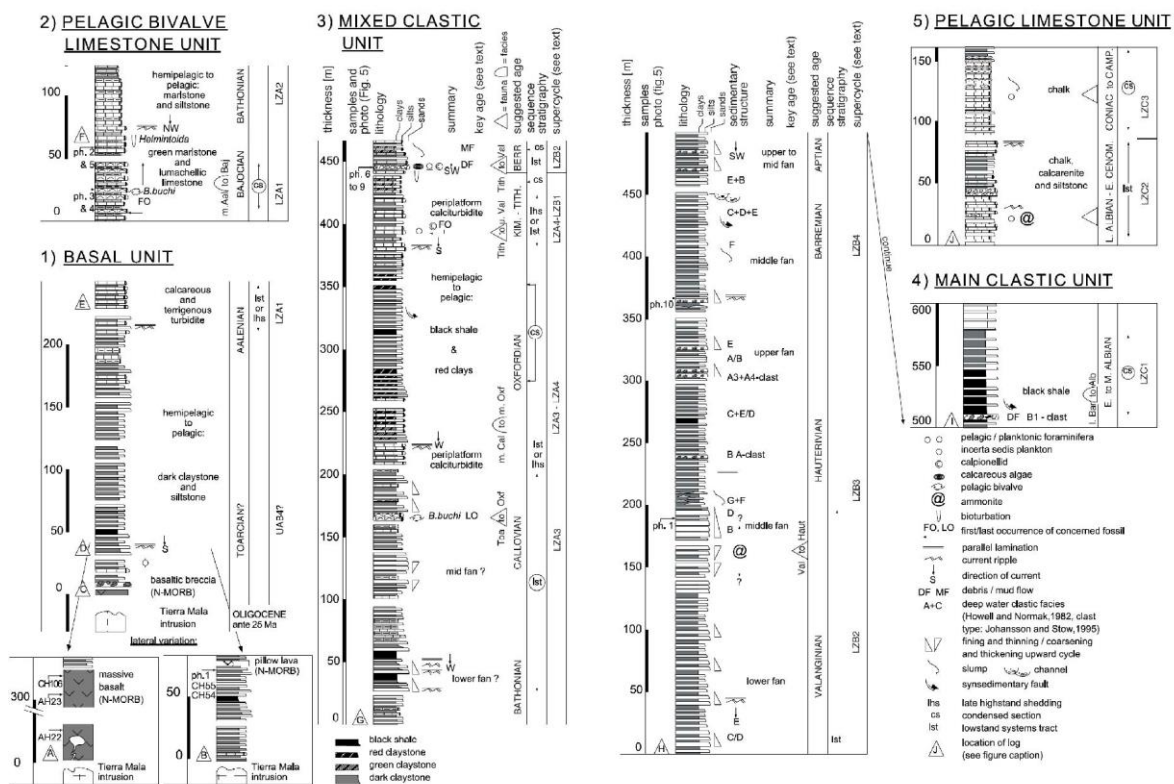
Fig. 5.- Columnas estratigráficas de la corteza oceánica mesozoica aflorante en la región de Ajuy, al SO de Betancuria (Fig. 3). Incluyen tanto las rocas volcánicas N-MORB de la Unidad Basal, como los sedimentos jurásicos y cretácicos que las recubren. Tomado de Steiner *et al.* (1998).

- Unidad Basal. En la base de la secuencia, los sedimentos mesozoicos están intercalados con basaltos toleíticos de tipo N-MORB, de edad Jurásico inferior, que representan los materiales

más antiguos de la corteza oceánica en el Atlántico Central. Estos basaltos aparecen en la playa de Los Muertos, en el barranco de La Majada de La Perra y en el barranco de La Potranca. Los basaltos están cubiertos por unos 150 metros de argilitas y limolitas depositadas en aguas profundas, por debajo del nivel de compensación de carbonatos.

- Unidad de Calizas con bivalvos pelágicos. Aflora en el Barranco de Ajuy y a lo largo de la costa, al norte del puerto de La Peña. Consiste en unos 150 metros de calizas, argilitas y margas. En las margas aparecen numerosas impresiones del bivalvo *Bositra buchi,* identificadas por Rothe (1968) como *Posidonia bronni*. La asociación de facies de esta unidad indica que la sedimentación se produjo entre la parte media del talud continental y la llanura abisal, por encima del nivel de compensación de carbonatos. La edad de esta unidad es Jurásico inferior - Jurásico superior.

- Unidad Clástica Mixta. Aflora a lo largo de la costa, entre la caleta Negra y la desembocadura del barranco de la Peña, con una potencia de 470 metros. Marca el retorno a la sedimentación clástica y está compuesta principalmente por arenas y limos turbidíticos, con margas y pizarras negras subordinadas, depositadas en un ambiente marino profundo. Los foraminíferos y el alga verde encontrada en el techo de esta unidad aportan una edad Jurásico-Cretácico inferior (*Nautiloculina* sp., *Mesoendothyra* sp. y *Ophatalmidium* sp.) y Oxfordiense a Valanginiense (*Salpingoporella pygmaea*).

- Unidad Clástica Principal. Aflora a lo largo de la costa entre la desembocadura del barranco de La Peña y el sur de la caleta de la Peña Vieja, y está compuesta por 500 metros de arenas turbidíticas. La base, de edad Valanginiense-Hauteriviense, se ha datado a partir de la aparición del ammonites *Neocomites* sp. (Renz *et al.*, 1992). Los últimos 100 metros de esta unidad están compuestos principalmente por pizarras negras que marcan el final del sistema de abanico submarino. Considerando la edad de la siguiente unidad, las pizarras negras podrían corresponderse con el más antiguo de los eventos oceánicos anóxicos del Cretácico (Berriasiense- Albiense; Jenkyns, 1980).

- Unidad de Calizas Pelágicas. Aflora principalmente en la caleta de la Peña Vieja y en la parte media del barranco de la Peña. Está compuesta por 150 metros de depósitos de talud, principalmente margas. Se corresponde con la unidad F y G de Robertson & Stillman (1979a). Robertson & Bernoulli (1982) asignan una edad Albiense-Cenomaniense inferior a la unidad F basándose en la aparición del ammonites *Partschiceras* cf. *whiteavesi* y a la siguiente asociación de foraminíferos planctónicos: *Schakoina galdolfii* Reichel, *Rotalipora* sp., *Hedbergella* sp. y *Gabonella* sp. A la unidad G se le atribuye una edad Senoniense por la presencia de Globotruncánidos y Heterohelícidos, asociados con foraminíferos bentónicos del género *Stensiöina*, *Gavelinella*, *Polimorphina* y *Reussella*.

B.2.2.- El Complejo Plutónico Ultra-alcalino.

Las rocas que forman este Complejo son, junto con las de la Dorsal Inicial, las que tienen una mayor extensión geográfica de todas las que forman la isla, estando sólo ausentes en la península de Jandía. Por el norte (Fig. 3) se extienden hasta la montaña de Los Frailes y la playa del Águila, cerca de El Cotillo (Fúster *et al.,* 1980; Barrera *et al.,* 1986). Por el sur llegan, por la costa, hasta cerca de la desembocadura del barranco de Amanay (Le Bas *et al.,* 1986; Ahijado y Hernández-Pacheco, 1990; Ahijado y Hernández-Pacheco, 1992; Ahijado *et al.,* 1992; Mangas *et al.,* 1994: Ahijado, 1999). Por el suroeste hasta la montañita de Agando, junto al caserío de Violante. Por el este, hasta el Roque del Buey, al este de la montaña de Gairía.

Se trata fundamentalmente de piroxenitas, kaersutiitas, gabros anfibólicos, ijolitas-melteigitas-urtitas, malignitas, sienitas, sienitas nefelínicas, traquitas porfídicas y carbonatitas (Fúster *et al.,* 1968; Muñoz, 1969; Barrera *et al.*, 1981; Le Bas *et al.*, 1986; Ahijado y Hernández-Pacheco, 1990; Ahijado y Palacios, 1991; Hoernle y Tilton, 1991; Ahijado *et al.*, 1992; Ahijado y Hernández-Pacheco, 1992; Cantagrel *et al.*, 1993; Sagredo *et al.*, 1996; Demeny *et al.*, 1998; Ahijado 1999; Hoernle *et al.*, 2002; Demeny *et al.*, 2004; Muñoz *et al.*, 2005; De Ignacio *et al.*, 2006). Estas últimas aparecen, principalmente, concentradas en tres macizos: Esquinzo, Ajuy-Solapa (Punta de la Nao-Caleta de la Cruz) y Punta del Peñón Blanco (Barrera *et al.,* 1981; Ahijado y Hernández-Pacheco, 1990; Ahijado y Hernández-

Pacheco, 1992; Ahijado *et al.,* 1992; Mangas *et al.,* 1992, 1993, 1994; Ahijado, 1999; Muñoz *et al.*, 2005). Algunos afloramientos más dispersos aparecen en la montaña de Los Frailes, al norte; en el barranco del Cortijo (Violante) al sur y en el barranco de Los Arrabales (Tiscamanita), en el centro de la isla.

Se trata del Grupo A1 y A2 definidos por Balogh *et al.*, (1999); o el Grupo EM-1 definido por Muñoz *et al.*, (2005).

Las rocas plutónicas de la serie ultra-alcalina inicial están afectadas por zonas de cizalla dúctil o dúctil-frágil (Casillas *et al.,* 1994; Fernández *et al.,* 1997) de movimiento transcurrente y normal (Casillas *et al.,* 1994; Fernández *et al.,* 1997). Esta deformación parece estar causada por la existencia de un régimen extensional para el tránsito Oligoceno-Mioceno y en el Mioceno (Fernández *et al.,* 2006); responsable, como veremos más adelante, de la formación de la Dorsal Inicial y de su complejo filoniano de dirección NNE-SSO que llega a representar un 50% de dilatación cortical (Stillman, 1987; Ahijado *et al.,* 2001; Fernández *et al.,* 2006). Alguna de estas zonas de cizalla se describirá con más detalle y será objeto de una de las paradas (P4) durante esta excursión.

En la costa norte, en La Piedra de la Playa, contactan con los sedimentos de la corteza oceánica a través de una zona de falla de dirección NE-SO. En el entorno de Ajuí, el contacto con los materiales de la secuencia invertida de la corteza oceánica es intrusivo, aunque se encuentra retocado por las zonas de cizalla dúctil o dúctil-frágil mencionadas anteriormente.

La edad de las rocas de este complejo se sitúa entre los 23 y los 35 Ma (Fig. 4, Cantagrel *et al.,* 1993; Balogh *et al.,* 1999; Muñoz *et al.*, 2005; Sagan *et al.,* 2020), siendo más antiguas en el norte que en el sur (Sagan *et al.,* 2020).

B.2.3.- La Dorsal Volcánica Inicial.

Sobre las rocas de la corteza oceánica y del Complejo Plutónico Ultra-alcalino, a través de una discordancia erosiva que recorre la isla de norte a sur (Fig. 6), aparecen las rocas volcánicas que constituyen la Dorsal Volcánica Inicial (23 Ma.-20,5 Ma) que se extendería desde la península de Jandía hasta el extremo norte de la isla, sin descartarse que pudiera tener continuidad más hacia el norte en Lanzarote, llegando hasta el Banco de Concepción (descrita ya por Fúster 1975, como "dorsal canaria"). El término "dorsal volcánica" alude a edificios volcánicos alargados, en forma de "tejado a dos aguas", generalmente asociados a erupciones de tipo fisural, y no tiene relación con el concepto de dorsal oceánica utilizado en tectónica.

Esta discordancia basal de la Dorsal Volcánica Inicial aparece representada, en la zona central y occidental de la isla por brechas y conglomerados submarinos, mientras que en la parte septentrional, meridional y centro-oriental de la misma aparecen paleosuelos ferruginosos, conglomerados y arenas aluviales. En las brechas y conglomerados son muy frecuentes los fragmentos de sedimentos de la corteza oceánica, piroxenitas, ijolitas, sienitas y traquitas. En Esquinzo, estos materiales detríticos fueron descritos por primera vez por Fúster *et al.* (1968) e interpretados, posteriormente por Barrera *et al.* (1981) como una brecha de fluidificación formada por la acción de fluidos hidrotermales tardíos relacionados con las intrusiones ultra-alcalinas.

Sobre los depósitos detríticos anteriores aparecen los materiales volcánicos que representan el crecimiento de la gran Dorsal Inicial de la Isla. Dicha Dorsal está integrada por tres grandes unidades litoestratigráficas transicionales y/o superpuestas (Figuras 3, 4, 6, 7 y 8) (Gutiérrez, 2000; Gutiérrez *et al.,* 2006): el Grupo Volcánico Submarino (GVS), constituido por rocas volcánicas submarinas emplazadas sobre la discordancia basal que se apoya en el Complejo Ultra-alcalino o en la corteza oceánica; el Grupo Volcánico de Transición (GVT), constituido por rocas formadas en ambientes de transición submarino-subaéreo, y, finalmente, el Grupo Volcánico Subaéreo (GVSA), integrado por las rocas volcánicas emplazadas sobre la discordancia en condiciones subaéreas, entre los que se incluyen los niveles más bajos de los Edificios Subaéreos Meridional, Central y/o

Septentrional Inferiores, definidos, previamente por Ancochea *et al*. (1993) y Ancochea *et al*. (1996).
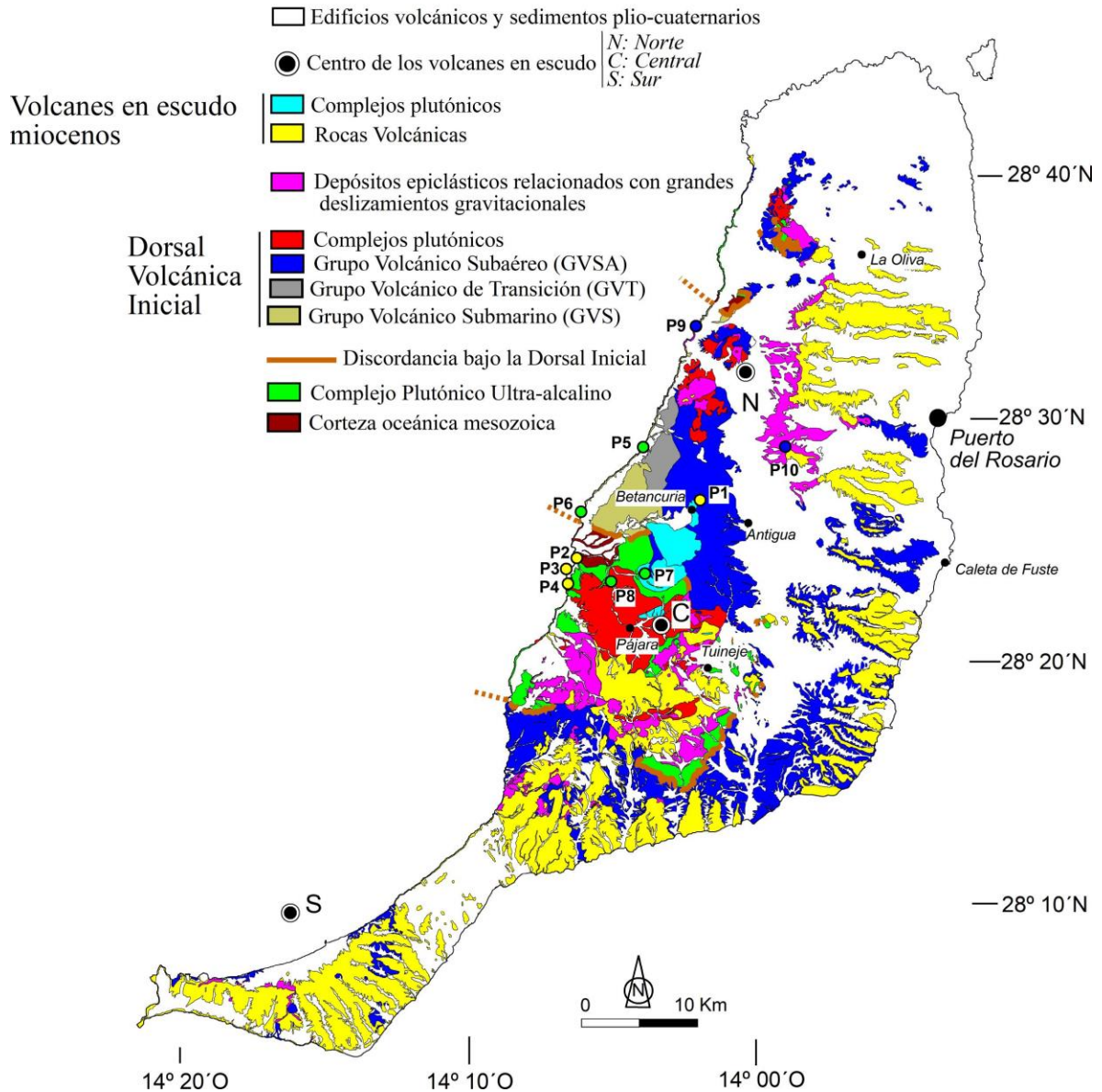

Fig. 6.- Localización de la discordancia (en línea de color naranja) bajo la Dorsal Inicial. Mapa geológico de Fuerteventura modificado de Balcells *et al.,* 2006.

Las relaciones entre estas unidades y sus principales características litoestratigráficas pueden observarse en la Fig. 8, y serán descritas a continuación.

FORMACIONES POST-COMPLEJO BASAL
- Formaciones sedimentarias plio-cuaternarias (FS)
- Coladas basálticas Pliocenas (Serie II)
- Brecha de Salinas (S)
- Brechas tipo "Ampuyenta" (Am)

OTRAS UNIDADES DEL COMPLEJO BASAL
- Intrusión masiva tardía de diques traquíticos
- Melanogabros y leucogabros. Edificio Morro del Sol (MS)
- Sienitas. Edificio Betancuria (Be2)
- Tobas y brechas traquíticas. Edificio Betancuria (Be1)
- Grupo Volcánico Subaéreo (GVSA)

GRUPO VOLCÁNICO DE TRANSICIÓN
- Fm. calcarenitas y calciruditas bioclásticas del Bco. de la Fuente Blanca (G5)
- Formación conglomerados y areniscas de Garcey (G4)
- Formación basaltos flogopítico-anfibólicos de Piedra de Fuera (G3)
- Formación traquitas de la Caleta del Barco (G2)
- Formación traquitas de la Caleta del Barco (G1)

GRUPO VOLCÁNICO SUBMARINO
- Formación basaltos del Valle (F)
- Formación limolitas y areniscas de Toscano (E)
- Formación basaltos de La Gatera (D)
- Formación brechas, areniscas y limolitas de Los Negros (C)
- Formación basaltos y fonolitas de La Herradura (B)
- Formación basaltos y nefelinitas del Barranco del Tarajalito (A)

- SERIE MESOZOICA (M)

So
Anticlinal (fase D2)
Fallas normales
Sinclinal (fase D2)

N

2 Km.

La equidistancia entre curvas de nivel es de 100 m.
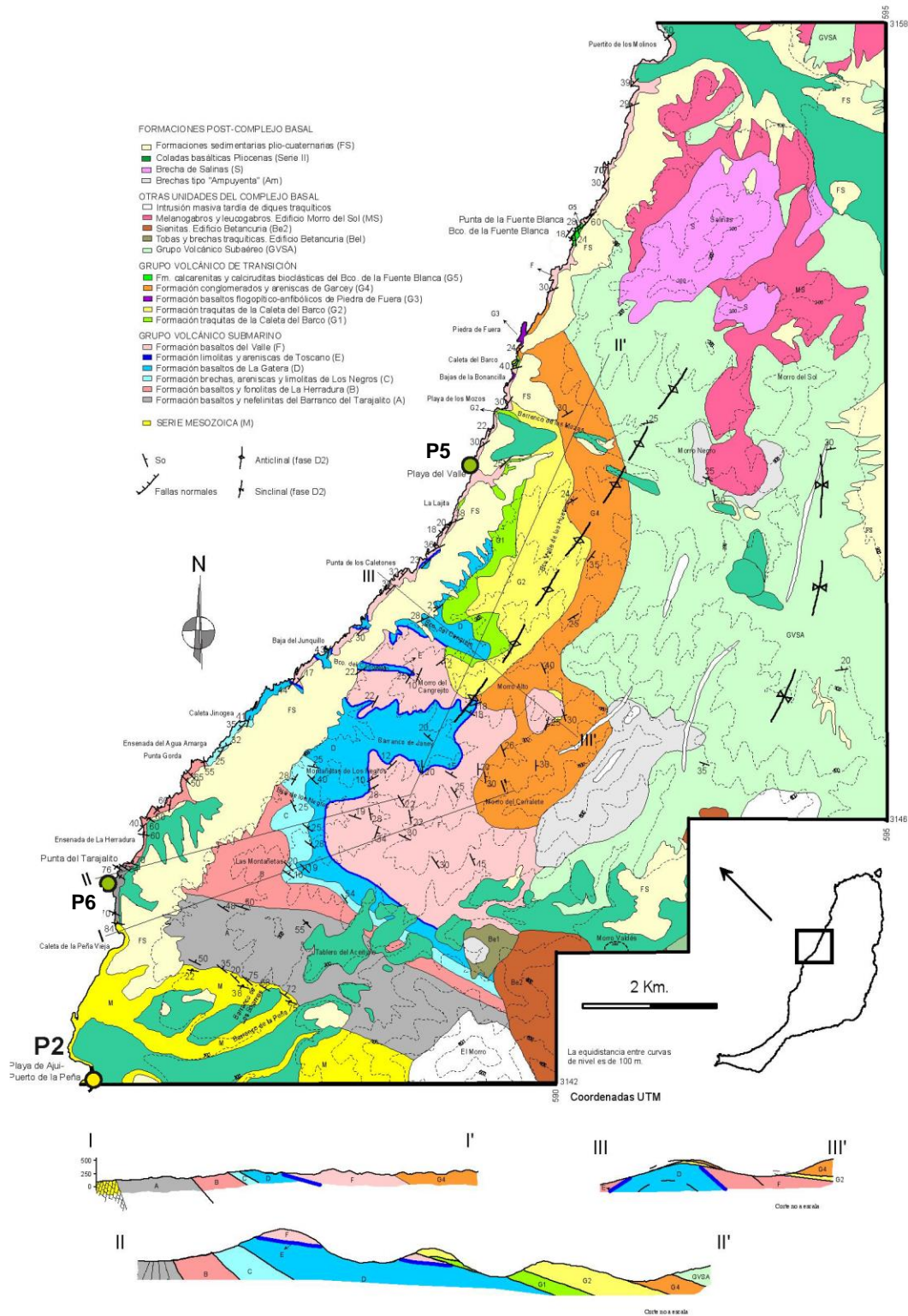
Coordenadas UTM

P5
P6
P2

Fig. 7.- Mapa y cortes geológicos de las unidades aflorantes en el macizo de Betancuria, según Gutiérrez (2000). P2, P5 y P6 indican la localización de varias de las paradas de la excursión.
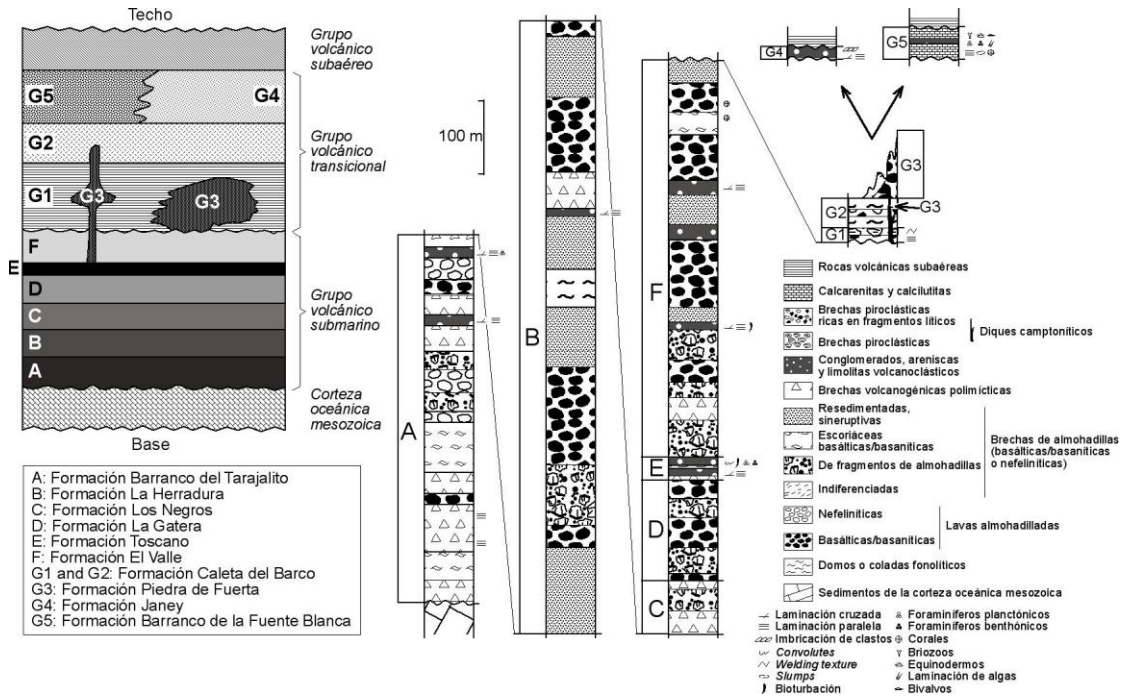
Fig. 8.- Columnas esquemáticas de las unidades volcánicas correspondientes al crecimiento submarino (GVS) y al tránsito a las condiciones de crecimiento subaéreo (GVT) aflorantes en el macizo de Betancuria, según Gutiérrez *et al.* (2006).

Grupo Volcánico Submarino (GVS)

Aparece en el sector centro-occidental de la isla, fundamentalmente, a lo largo de su costa occidental desde El Pardero, al norte de Los Molinos, hasta la caleta de la Peña Vieja (Fig. 7).

Unidades litoestratigráficas

En el GVS se han diferenciado varias formaciones en función de sus características estratigráficas, sedimentológicas y petrográficas (Gutiérrez, 2000; Gutiérrez *et al.,* 2006) (Fig. 8):

1) *Formación basaltos y nefelinitas del Barranco del Tarajalito* (A). Se apoya de manera

discordante sobre los sedimentos de fondo oceánico de la serie mesozoica. Esta unidad se caracteriza por la aparición de rocas de afinidad ultra-alcalina (nefelinitas, fonolitas nefelínicas) junto a otras fuertemente alcalinas (basanitas). En ella se diferencian dos asociaciones de facies. Una está integrada por rocas volcánicas primarias de composición basanítica, constituidas por lavas almohadilladas, brechas de fragmentos de almohadillas más o menos resedimentadas y brechas de almohadillas escoriáceas; esta asociación de facies se generó a través de erupciones subaéreas cuyas coladas llegaron al mar formando deltas lávicos (Fig. 9a). La otra asociación de facies es de naturaleza volcanogénica, formada, principalmente por conglomerados, brechas, areniscas y limolitas volcánicas, depositadas a través de flujos subacuáticos en relación con la destrucción parcial de complejos ultra-alcalinos situados en la zona oriental.

2) *Formación basaltos y fonolitas de La Herradura* (B). Está constituida principalmente por depósitos proximales (lavas almohadilladas, brechas de almohadillas escoriáceas y brechas de fragmentos de almohadillas) de composición basanítica. Eventualmente tuvieron lugar erupciones efusivas de coladas fonolíticas que dieron lugar a depósitos hialoclastíticos de la misma composición (Fig. 9b).

3) *Formación brechas, areniscas y limolitas de Los Negros* (C). Compuesta fundamentalmente por depósitos volcanogénicos en los que predominan los fragmentos de composición basanítica, con ocasionales fragmentos de fonolitas**.** Estos niveles se depositaron por flujos gravitatorios, principalmente *debris-flows* y flujos granulares de densidad modificada subacuáticos (Fig. 9c). Algunos de los depósitos presentan una alta concentración de fragmentos bioclásticos (foraminíferos bentónicos, bivalvos, gasterópodos, etc.)

4) *Formación basaltos de La Gatera* (D). Formada por lavas almohadilladas de considerable tamaño, asociadas a depósitos autoclásticos (brechas de almohadillas y brechas de fragmentos de almohadillas) (Fig. 9d).
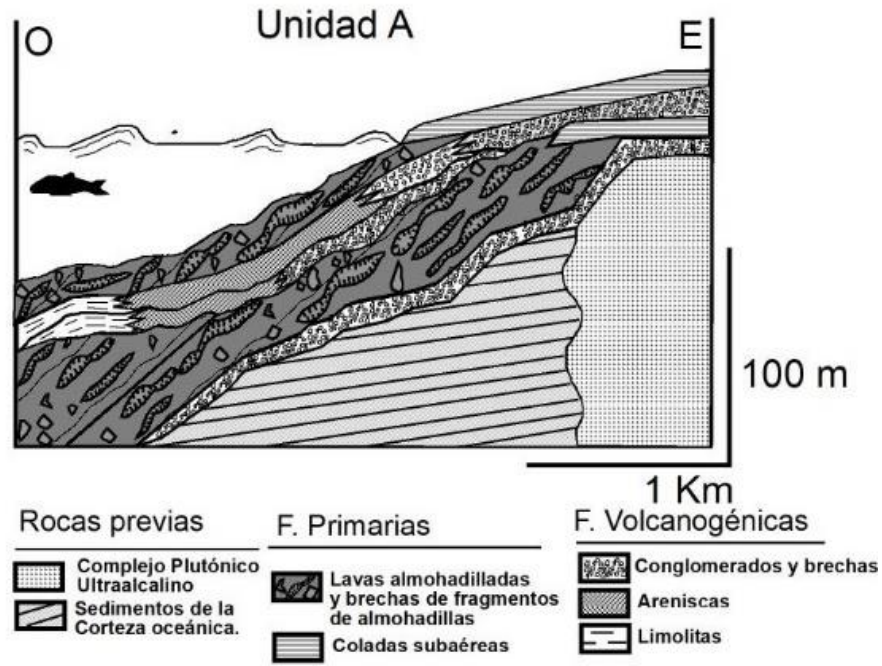
Unidad A

Rocas previas
- Complejo Plutónico Ultraalcalino
- Sedimentos de la Corteza oceánica.

F. Primarias
- Lavas almohadilladas y brechas de fragmentos de almohadillas
- Coladas subaéreas

F. Volcanogénicas
- Conglomerados y brechas
- Areniscas
- Limolitas

Fig. 9a.- Esquema de interpretación paleogeográfica de la unidad A del Grupo Volcánico Submarino (Gutiérrez *et al.*, 2006).

Unidad B

Rocas previas
- Sustrato

R. Basálticas
- Lavas almohadilladas y brechas de fragmentos de almohadillas
- Coladas subaéreas

R. Fonolíticas
- Lóbulos e hialoclastitas
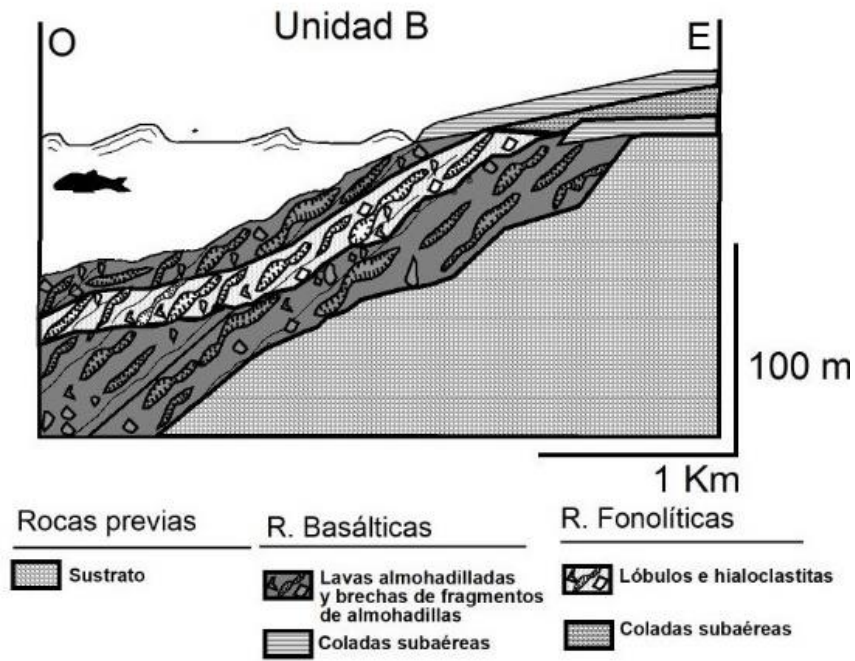- Coladas subaéreas

Fig. 9b.- Esquema de interpretación paleogeográfica de la unidad B del Grupo Volcánico Submarino (Gutiérrez *et al.*, 2006).
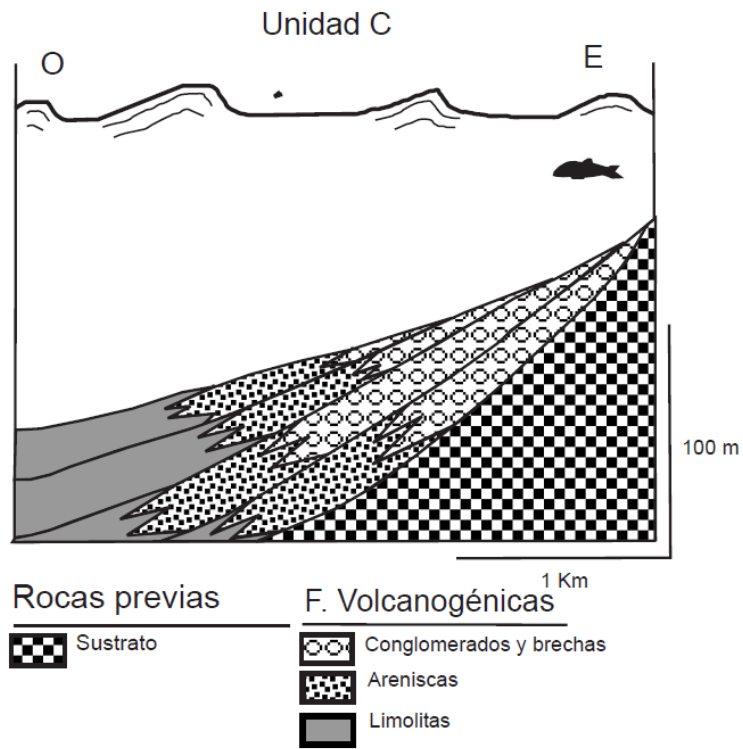
24

Fig. 9c.- Esquema de interpretación paleogeográfica de la unidad C del Grupo Volcánico Submarino (Gutiérrez *et al.*, 2006).

Fig. 9d.- Esquema de interpretación paleogeográfica de la unidad D del Grupo Volcánico Submarino (Gutiérrez *et al.*, 2006).

Fig. 9e.- Esquema de interpretación paleogeográfica de la unidad E del Grupo Volcánico Submarino (Gutiérrez *et al.*, 2006).

Fig. 9f.- Esquema de interpretación paleogeográfica de la unidad F del Grupo Volcánico Submarino (Gutiérrez *et al.*, 2006).
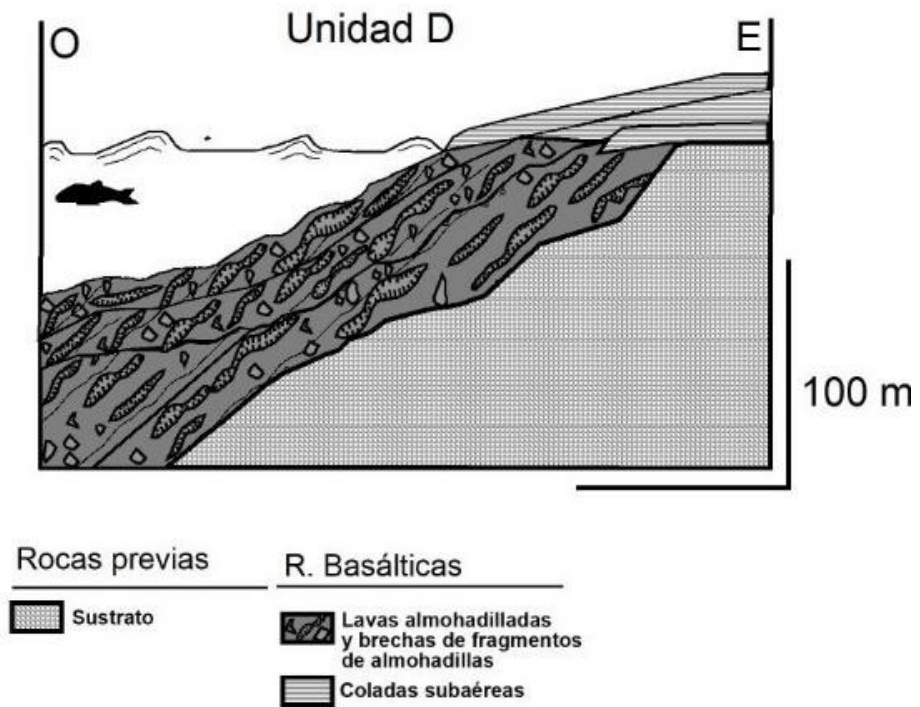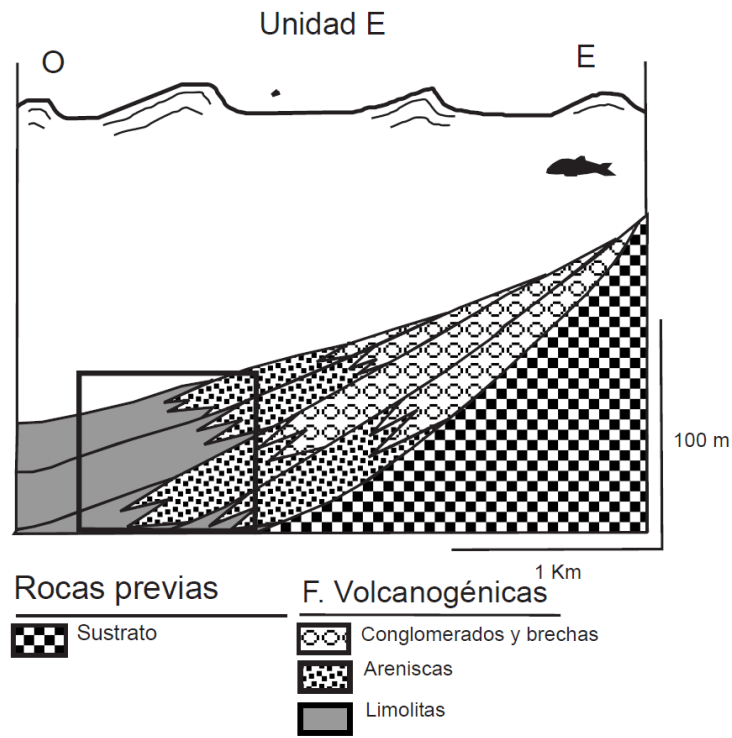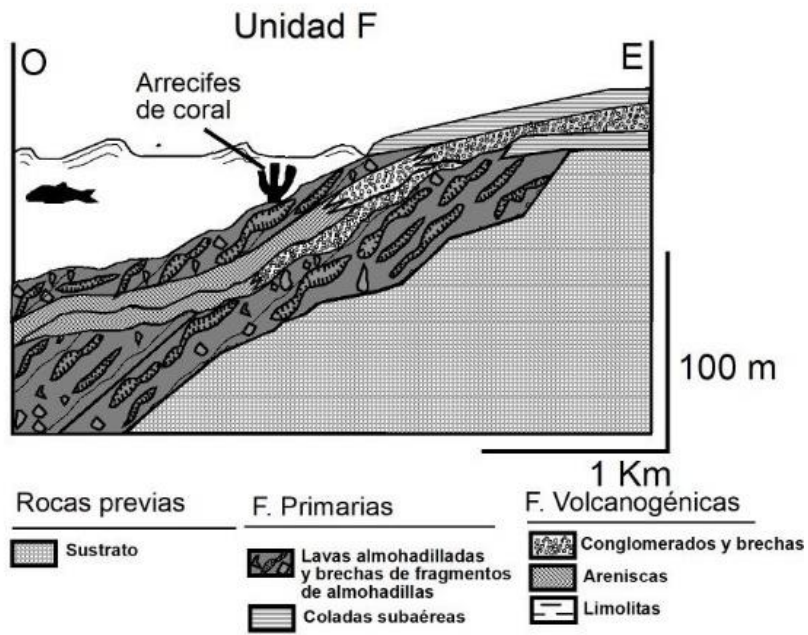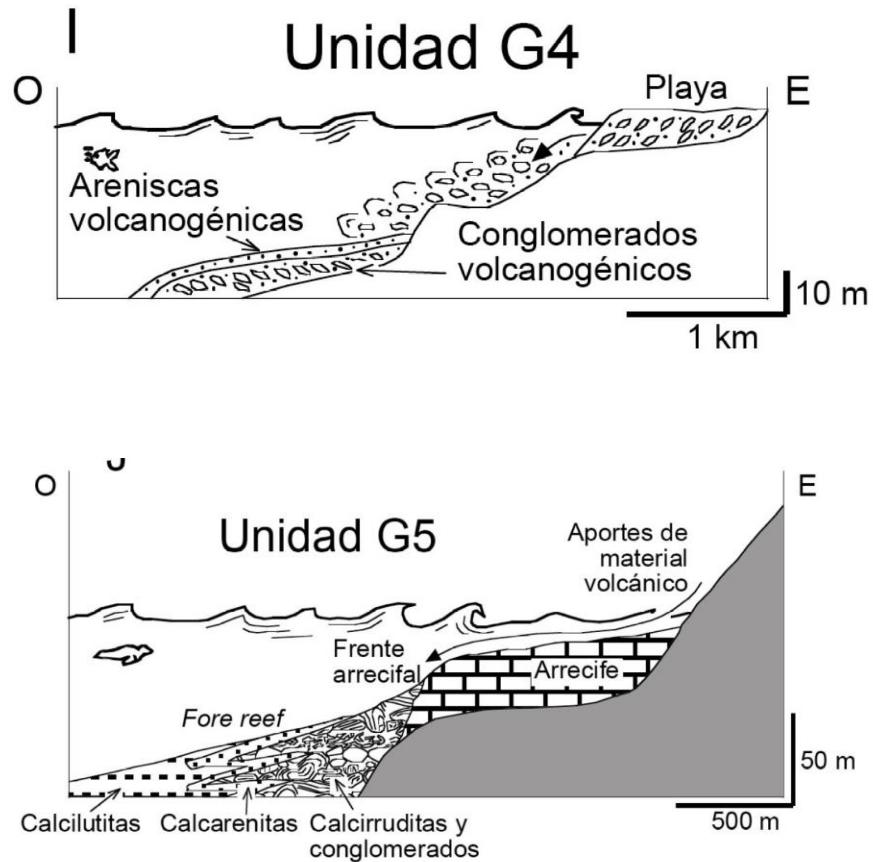
Fig. 9g.- Esquema de interpretación paleogeográfica de las unidades G4 y
G5 del Grupo Volcánico de Transición (Gutiérrez *et al.*, 2006).

5) *Formación areniscas y limolitas de Toscano* (E). Integrada principalmente por alternancias de areniscas y limolitas, depositadas a través de flujos gravitatorios, que se han sedimentado en las partes distales de abanicos submarinos (Fig. 9e).

6) *Formación basaltos del Valle* (F). Consiste fundamentalmente en lavas almohadilladas y depósitos autoclásticos asociados (brechas de almohadillas y brechas de fragmentos de almohadillas), depósitos sineruptivos resedimentados (brechas de fragmentos de almohadillas resedimentadas) y niveles volcanogénicos (areniscas y brechas volcánicas). La presencia de corales coloniales incrustados en la corteza externa de algunas lavas

almohadillas, junto a evidencias de abrasión significativa en los cantos en algunos niveles volcanogénicos y la existencia de estructuras tractivas en niveles altos de la unidad, sugieren un depósito a escasa profundidad y cercano a la línea de costa. (Fig. 9f). La composición de los materiales es fundamentalmente basanítica, restringiéndose los materiales sálicos a algunos niveles volcanogénicos de grano fino.

Características petrológicas

Desde el punto de vista geoquímico y petrográfico, en el Grupo Volcánico Submarino puede distinguirse la existencia de dos componentes fundamentales superpuestos: rocas de series ultra-alcalinas, presentes en los niveles detríticos volcanogénicos de la base del grupo (Formación basaltos y nefelinitas del Barranco del Tarajalito, A), y rocas de una serie fuertemente alcalina, dominando el resto de esta sucesión. Los fragmentos de los niveles detríticos volcanogénicos de composición ultraalcalina están constituidos fundamentalmente por melanefelinitas y nefelinitas *s.s.* y fonolitas nefelínicas, apareciendo además sus equivalentes plutónicos (ijolitas, melteigitas, sienitas nefelínicas). Diversas evidencias petrográficas, geoquímicas y geocronológicas, sugieren que estos niveles detríticos volcanogénicos proceden de la erosión subaérea de las rocas del Complejo Plutónico Ultra-alcalino.

Las rocas de la serie fuertemente alcalina son, fundamentalmente, diversos tipos de basaltos/basanitas y fonolitas. En cuanto a los términos básicos se han diferenciado basaltos/basanitas olivínico-piroxénicos, basaltos/basanitas piroxénicas, basaltos/basanitas anfibólicos y basaltos/basanitas piroxénico-anfibólicos. Estas rocas incorporan enclaves de piroxenitas, ijolitas y kaersutiitas, relacionados con la con el Complejo Plutónico Ultra-alcalino (fragmentos de roca de caja arrancados por el magma durante su ascenso). Los términos más diferenciados de esta serie se corresponden con fonolitas, que contienen en ocasiones enclaves, seguramente comagmáticos, de sienitas.

Grupo Volcánico de Transición (GVT)

Las rocas volcánicas que constituyen el GVT marcan el tránsito hacia el vulcanismo subaéreo representado por el Grupo Volcánico Subaéreo. Aunque alguna de las unidades que lo integran se depositaron bajo el mar, todas ellas presentan evidencias de haberse formado una vez que la isla estaba parcialmente emergida. Aparece en el sector centro-occidental de la isla, fundamentalmente, a lo largo de su costa occidental, desde la desembocadura del barranco de la Fuente Blanca, al norte, hasta La Lajita, al sur (Fig. 7).

Unidades litoestratigráficas (Fig. 8)

1) *Formación traquitas de la Caleta del Barco.* Constituida principalmente por niveles de brechas polimícticas resedimentadas generadas en flujos gravitatorios subacuáticos procedentes de la destrucción de complejos lóbulo-hialoclastíticos submarinos (G1) y de coladas sálicas acumuladas durante periodos de emisión efusiva, en gran parte, subacuáticas, pudiendo formar complejos lóbulo-hialoclastíticos (G2).

2) *Formación basaltos flogopítico-anfibólicos de Piedra de Fuera* (G3). Formada por coladas subaéreas que eventualmente llegaron al mar originando deltas de lava, lavas almohadillas y brechas de almohadillas escoriáceas extruídas en aguas someras.
Aparecen también diques de considerable espesor. Este episodio de vulcanismo está ligado temporal y espacialmente a la emisión de traquitas de la unidad G2.

3) *Formación conglomerados y areniscas de Janey (*G4). Constituida por conglomerados y areniscas depositados en ambientes marinos muy someros por flujos gravitatorios de sedimentos, procedentes de la erosión y retrabajamiento de los materiales emergidos de las formaciones anteriormente descritas en este GVT y de otras más antiguas (Corteza oceánica mesozoica, Complejo Plutónico Ultra-alcalino).

4) *Formación calcirruditas y calcarenitas del Barranco de la Fuente Blanca* (G5). Está constituida por conglomerados, calcirruditas y calcarenitas procedentes de la destrucción de un arrecife coralino que bordeaba a la isla. Se corresponde a los niveles bioclásticos

estudiados por Robertson y Stillman (1979b) y en ella se reconocen tres litofacies (Figs. 8 y 9g):

-A: alternancias rítmicas de calcarenitas bioclásticas y calcilutitas limosas pelágicas, formando una secuencia grano y estratocreciente. Presentan cuerpos esféricos de más de 5 cm con laminación concéntrica que incorporan conchas finamente fragmentadas.

-B: calcirruditas conglomeráticas, calcarenitas bioclásticas y calcilutitas con intraclastos de pizarras negras dispersos, ordenadas en capas amalgamadas granodecrecientes. Hacia el techo aparecen intercalaciones de areniscas y limolitas volcanoclásticas.

 -C: calcarenitas y areniscas volcanoclásticas.

Características petrológicas

Los materiales volcánicos básicos emitidos durante este periodo tienen afinidad fuertemente alcalina. Por otro lado, su estrecha relación espacial y temporal con las rocas traquíticas plantea la posibilidad de que ambos tipos de rocas estén genéticamente relacionadas y que la fraccionación de la kaersutita, durante un proceso de cristalización fraccionada condujera a la saturación en sílice del magma residual y originara los términos traquíticos. Otra posibilidad es que, aunque ambos tipos de roca aparezcan asociados, no tengan ninguna relación genética entre ellas.

Grupo Volcánico Subaéreo (GVSA)

Las rocas volcánicas que constituyen el GVSA constituyen el volumen más importante de la Dorsal Inicial y aparecen, fundamentalmente en la parte central y occidental de la isla, en el macizo de Betancuria, y en la base de los cuchillos de la parte oriental de la isla. También forman las partes más bajas de la península de Jandía. Salvo en esta península, se apoyan discordantemente sobre las rocas del Complejo plutónico Ultra-alcalino a través de paleosuelos ferruginosos, conglomerados y arenas aluviales. Hacia el

Oeste, en el macizo de Betancuria, las rocas del GVSA pasan transicionalmente al GVT y a las rocas del GVS.

El GVSA está compuesto por coladas vesiculadas de composición basáltica-traquibasáltica y niveles fragmentarios monomícticos que parecen corresponder con zonas escoriáceas entre estas coladas de emisión subaérea. En la zona central del macizo de Betancuria se encuentran intensamente intruidas por los diques del complejo filoniano relacionados con el interior de la Dorsal Inicial.

B.2.3.1.- Intrusiones plutónicas y enjambres filonianos asociados a la gran Dorsal Inicial.

Atravesando las rocas volcánicas de la Dorsal Inicial (Fig. 4) aparece un importante complejo filoniano constituido por una red de diques de extraordinaria densidad (Fig. 10), que en muchos casos constituyen el 95% al 99% del afloramiento rocoso (Fúster *et al.,* 1968a; López-Ruiz, 1970; Stillman, 1987; Ahijado *et al.,* 2001). Suelen disponerse en posición subvertical, pero también aparecen rotados e inclinados hacia el este o el oeste (Fig. 10). La dirección más corriente es NNE-SSO, aunque también aparecen algunos con dirección NE-SO y NO-SE. Su composición es variable predominando los tipos basálticos y traquibasálticos. Este complejo filoniano representa la parte más profunda de esta gran Dorsal Inicial.

Por otro lado, asociados a esta Dorsal Inicial aparecen numerosos cuerpos plutónicos e hipoabisales (Fig. 3, Fig. 4). Las intrusiones plutónicas forman una serie de cuerpos independientes en la parte central y septentrional de la isla (serie gabroide-piroxenítica de Fúster *et al.,* 1968a; Gastesi, 1969a; Gastesi, 1969b; Gastesi, 1973; Muñoz y Sagredo, 1975; Stillman *et al.,* 1975; Fúster *et al.,* 1980; Fúster *et al.,* 1984a y b; Le Bas *et al.,* 1986; Stillman, 1987; Sagredo *et al.,* 1989; Muñoz y Sagredo, 1989, 1994; Cantagrel *et al.,* 1993; Grupo A3 de Balogh *et al.*, 1999; Grupo EM-2 de Muñoz *et al.*, 2005), de forma alargada según la dirección NNE-SSO y NO-SE (Gastesi, 1969a; Gastesi, 1969b, Gastesi, 1973) cuya intrusión produce intensos fenómenos de metamorfismo de contacto en las rocas encajantes (Muñoz y Sagredo, 1975; Stillman *et al.,* 1975; Muñoz y Sagredo, 1989) y, algunos de los cuales han sido datados en 22 M.a. (PX1, Allibon *et al.*, 2011b). Como consecuencia del intenso

metamorfismo de contacto llega a producirse la anatexis de las rocas preexistentes (Hobson *et al.*, 1998; Holloway & Bussy, 2008; Holloway *et al.*, 2008) y la formación esporádica de metacarbonatitas (Casillas *et al.*, 2008; Casillas *et al.*, 2011).

Estas rocas plutónicas posiblemente representan los restos de las cámaras magmáticas que alimentaron a la Dorsal Inicial (Ancochea *et al.*, 1996; Allibon *et al.*, 2011a; Allibon *et al.*, 2011b; Tornare *et al.*, 2016).
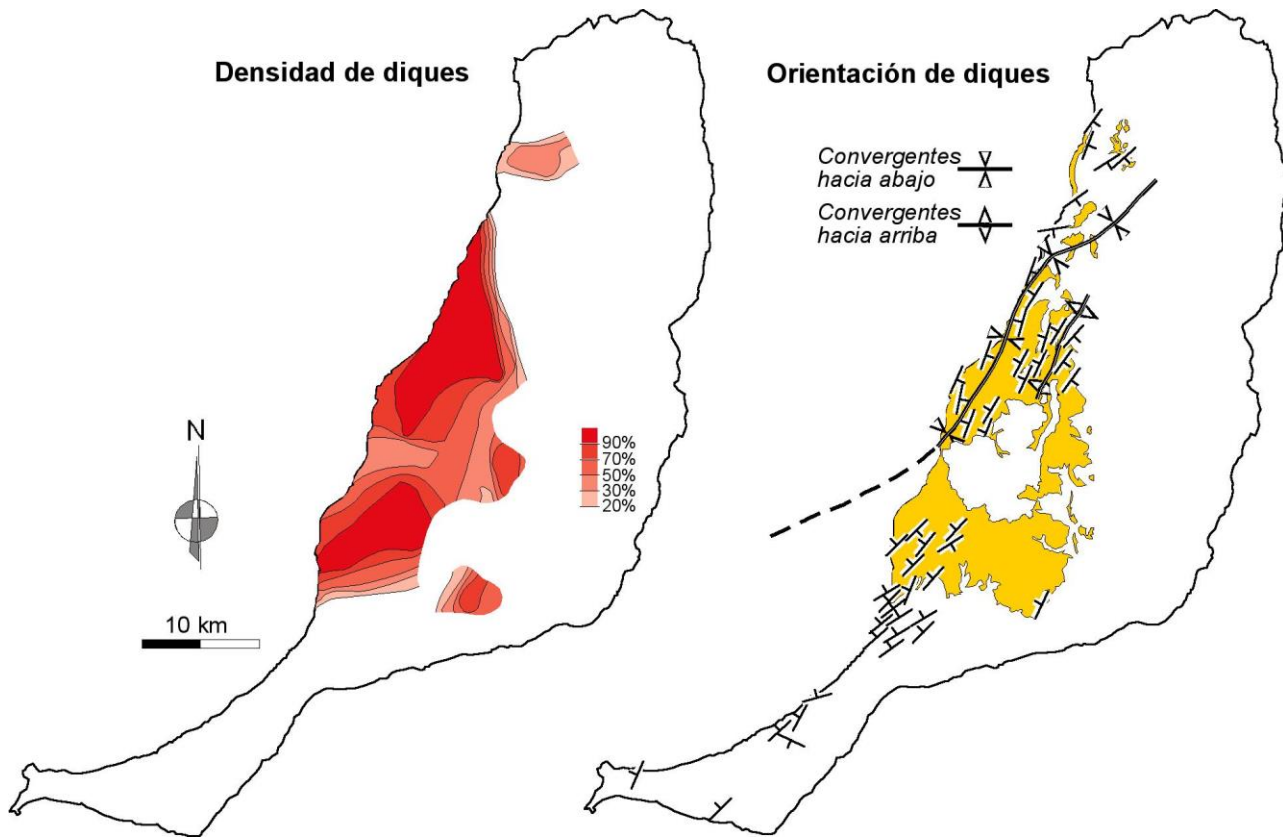
Fig. 10.- Esquemas mostrando la distribución espacial de la densidad de la red de diques básicos del complejo filoniano (izquierda), así como la orientación promedio de dichos diques medida en distintas estaciones (derecha). Obsérvese cómo los diques se disponen formando enormes abanicos asociados a la estructura a gran escala de la Dorsal Inicial. Según Fernández *et al.* (2006).

La Dorsal Inicial pudo alcanzar más de 3000 metros de altura (Javoy *et al.*, 1986), volviéndose un edificio volcánico muy inestable, de tal manera que sufrió varios

deslizamientos gravitacionales, todos orientados hacia el oeste o noroeste, entre los que podemos destacar los siguientes (Fig. 11):

-A). Al norte, el deslizamiento de Puerto del Rosario Norte (Acosta *et al.*, 2003; Casillas *et al.*, 2012; Casillas *et al.,* 2019), que afectó a la parte de la Dorsal que hoy se corresponde con la parte norte de la isla de Fuerteventura, acaecido hace unos 14.5 Ma.

-B). En el centro, el deslizamiento de Puerto del Rosario Sur (Acosta *et al.*, 2003) que afectó a la parte de la Dorsal que hoy se corresponde con la parte central de la isla de Fuerteventura, acaecido hace unos 20.5 Ma.

-C). En el sur, el deslizamiento de Jandía (Casillas y Martín, 2021), que afectó a la parte de la Dorsal que hoy se corresponde con la península de Jandía, acaecido entre hace 21,5 y 17 Ma.
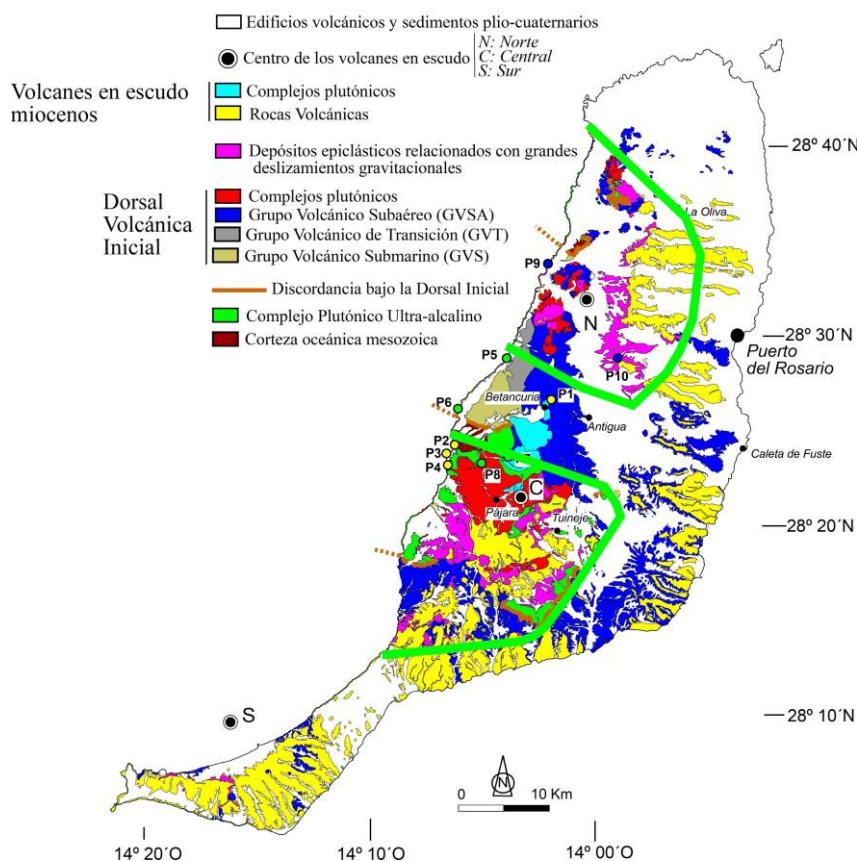

Fig. 11.- Posición deducida (líneas verdes) de los anfiteatros producidos por los deslizamientos gravitacionales de Puerto del Rosario Norte y Puerto del Rosario sur. Mapa geológico de Fuerteventura modificado de Balcells *et al.,* 2006.

Como consecuencia de estos megadeslizamientos gravitacionales se produjeron deslizamientos menores secundarios, así, como, en el caso del deslizamiento de Puerto del Rosario Norte, un fenómeno de *blast* (Casillas *et al.*, 2012).

Como producto de todos estos deslizamientos se generaron depósitos de avalancha rocosa *(debris avalanches)* que pueden ser observados en tierra (motivo de la parada nº 10), aunque el mayor volumen de ellos se extienden en el fondo del océano, ocupando varios kilómetros del margen submarino occidental de la isla (al deslizamiento de Puerto del Rosario Norte se vincula un megabloque kilométrico situado a unos 50 kilómetros al noroeste de la isla, que por sus dimensiones se le considera el segundo de mayor tamaño encontrado hasta la fecha en deslizamientos de flancos de islas volcánicas oceánicas, Casillas *et al*., 2019).

Posteriormente, la erosión de las paredes de los anfiteatros generados dio lugar a depósitos de coladas de derrubios *(debris flows)* y aluviales que fueron rellenando y colmatando los anfiteatros a medida que se fue reanudando la actividad volcánica que dio lugar a la formación de los tres grandes edificios volcánicos en escudo anidados.

B.2.4.- Los grandes edificios en escudo miocenos.

Tras el desarrollo de los grandes deslizamientos gravitacionales que afectaron a la Dorsal Inicial de la isla, la actividad volcánica se reanudó y dando lugar a tres grandes edificios volcánicos en escudo (Fig. 4), anidados dentro de los anfiteatros resultantes de los deslizamientos. Este vulcanismo subaéreo, cuya edad estaría comprendida entre los 20,5 y 12,8 Ma. (Abdel Monem *et al*., 1971; Fearud, 1981; Coello *et al*., 1992; Ancochea *et al.*, 1993; Balcells *et al.*, 1994; Ancochea *et al.*, 1996; Pérez-Torrado *et al*., 2023), dio lugar en la isla a la construcción de tres edificios volcánicos en escudo (parecidos a los que aparecen en Hawai), cuyos centros principales de emisión se situarían al oeste de la pared de Jandía, entre Pájara y Toto, y al este del puertito de Los Molinos (Fig. 3):

-Edificio Norte. Construido entre los 14,5 Ma y 12,8 Ma (Fig. 4) (Abdel Monem *et al.*, 1971; Fearud, 1981; Coello *et al.*, 1992; Ancochea *et al.*, 1993; Balcells *et al.*, 1994; Ancochea *et al.*, 1996; Pérez-Torrado *et al.*, 2023).

-Edificio Central. Construido entre los 20,5 Ma y 13,2 Ma (Fig. 4) (Abdel Monem *et al.*, 1971; Fearud, 1981; Coello *et al.*, 1992; Ancochea *et al.*, 1993; Balcells *et al.*, 1994; Ancochea *et al.*, 1996; Pérez-Torrado *et al.*, 2023).

-Edificio Sur. Construido entre los 17 Ma y 13,7 Ma (Fig. 4) (Abdel Monem *et al.*, 1971; Fearud, 1981; Coello *et al.*, 1992; Ancochea *et al.*, 1993; Balcells *et al.*, 1994; Ancochea *et al.*, 1996; Pérez-Torrado *et al.*, 2023).

Los restos de estos edificios se pueden observar en las laderas de los "cuchillos" que limitan los grandes valles en "U" de la parte oriental de la isla (Fig. 2). Estos volcanes se formaron por acumulación de grandes volúmenes de coladas de lavas muy fluidas y material piroclástico, en erupciones fisurales de altas tasas eruptivas (Ancochea *et al.,* 1993; Ancochea *et al.,* 1996). Con posterioridad, alguno de estos edificios volcánicos también sufrieron importantes deslizamientos gravitacionales que dieron lugar depósitos de avalancha de derrubios y al posterior relleno de las depresiones formadas por depósitos de coladas de derrubios y aluviales.

Los materiales basálticos de estas formaciones están también profusamente atravesados por numerosos diques de diversa naturaleza y composición y por algunos pitones sálicos (p. ej., la Montaña de Tindaya, Cubas *et al.*, 1989).

B.2.4.1.- Intrusiones plutónicas y enjambres filonianos asociados a los grandes edificios volcánicos en escudo.

Asociados al edificio volcánico en escudo central aparecen numerosos cuerpos plutónicos e hipoabisales, en forma de complejos circulares (Fig. 3), entre los que podemos destacar el de Vega de Río Palmas, con una serie de intrusiones anulares de gabros y sienitas (18.7-16,05 Ma), que dan lugar en el terreno a la aparición de crestas circulares como la que se

encuentra en el embalse de Las Peñitas (Muñoz, 1969). Otros cuerpos lo constituyen las sienitas de Toto (19,5 Ma) y las sienitas de Betancuria (15.1. Ma). Todos estos macizos fueron definidos como Grupo A4 por Balogh *et al.*, (1999); y Grupos EM-3 y EM-4 definidos por Muñoz *et al.*, (2005).

B.2.5.- Los edificios volcánicos plio-cuaternarios.

Una vez formados los edificios volcánicos miocenos y tras un intenso período erosivo, a finales del Plioceno (5 Ma), se renueva la actividad volcánica y se forman una serie de pequeños volcanes en escudo (Ventosilla, Cercado Viejo, Betancuria, Antigua, etc), cuyas coladas de lava basáltica fueron rellenando algunos paleorelieves. Con posterioridad se producen algunas pequeñas erupciones que forman conos de *cinder* alineados a lo largo de fracturas y coladas derivadas de extensión variable (Cendrero, 1966). Intercalados entre las sucesiones volcánicas de este último ciclo aparecen numerosos niveles de playas levantadas cuyo origen debe relacionarse con movimientos de elevación de bloques insulares y/o movimientos eustáticos.

B.2.4.- Los sedimentos plio-cuaternarios.

En tres ocasiones, tránsito Mio-Plioceno, Pleistoceno superior y Holoceno, se producen depósitos marinos relacionados con pequeños episodios transgresivos. Las playas levantadas correspondientes a los dos primeros episodios contienen faunas de invertebrados de aguas cálidas, mientras que en el último se ha encontrado fauna similar a la que actualmente habita en el medio marino canario. A estos depósitos se les superpusieron formaciones dunares (Plioceno-Pleistoceno superior-Holoceno) con aluviones y paleosuelos intercalados que han quedado parcialmente cubiertas por lavas basálticas.

B.2.4.1.- El Plioceno de Fuerteventura

Los depósitos marinos del tránsito Mioceno-Plioceno (datados entre 5,8 y 6,6 Ma) aparecen hoy emplazados a 10-14 m de altura sobre el nivel del mar, aunque, por la acción de movimientos tectónicos locales, llegan a situarse a unos 55 m de altura en Morro Jable. Están constituidos por niveles delgados (hasta 1 m de potencia) de conglomerados y areniscas bioclásticas con gran riqueza en fauna y flora calcárea (algas incrustantes). Esta extraordinaria riqueza calcárea les ha hecho constituir la materia prima de los costrones calcáreos (Meco, 1977, 1993; Meco & Pomel, 1985).

En Fuerteventura han sido estudiadas numerosas localidades con depósitos marinos del Plioceno que se extienden a lo largo de su costa occidental, desde el Aljibe de la Cueva al norte, hasta la Punta Cotillo en el sur. En la costa oriental sólo aparecen en la península de Jandía, concretamente en Morro Jable (Meco, 1977). Las asociaciones de invertebrados de los depósitos marinos pliocenos varían de unas localidades a otras, pero todas ellas se caracterizan por la presencia de especies de carácter cálido como *Strombus coronatus* (playa del Aljibe de La Cueva; Puerto de la Peña), o las acumulaciones de *Saccostrea cucullata* en la playa del Valle.

Existen pocos estudios paleontológicos sobre depósitos terrestres del Plioceno de Fuerteventura, y, en general, de todas las Canarias. No obstante, en estos materiales arenosos calcificados (calcarenitas) aparecen restos de tortugas gigantes y gasterópodos terrestres pertenecientes al Plioceno inferior, aunque algunos depósitos pudieran ser del límite Mioceno–Plioceno.

En Agua Tres Piedras, en el istmo de la Pared, es donde mejor se pueden observar las formaciones dunares del Plioceno de Fuerteventura. Según Meco (1977) estas dunas se formaron por la removilización de arenas puestas al descubierto durante la fase de regresión del nivel del mar. Intercalados entre ellas aparecen paleosuelos que indican varias pausas lluviosas durante este período.

B.2.4.2.- El Cuaternario de Fuerteventura

Durante el Pleistoceno superior se produjeron varios ascensos relativos del nivel del mar debido a un aumento global de la temperatura durante los periodos interglaciales. Estos cambios han quedado registrados en las costas de Fuerteventura, en los depósitos que Meco & Petit-Maire (1986) denominan Jandiense, que pertenecen, al menos, a los estadios isotópicos 5 y 7 y se sitúan a unos 5 m sobre el actual nivel del mar (Meco *et al*., 1992; Zazo *et al*., 1997). La localidad tipo de esta playa levantada jandiense es Las Playitas (Gran Tarajal) (Meco & Petit-Maire, 1986). Está constituida por areniscas muy cementadas de color claro con *Strombus bubonius*, sobre las que suele aparecer un conglomerado de unos 2 a 3 m de espesor con numerosos cantos redondeados de basalto.

En el Holoceno se produjo una nueva elevación del nivel del mar dando lugar a varios depósitos marinos de edades entre 5.640 años y 3.400 años, que se localizan a 3-4 m sobre el nivel de la marea baja. Este episodio transgresivo fue denominado por Meco & Petit-Maire (1986) como Erbanense, siendo su localidad tipo La Jaqueta (sur de Fuerteventura). Otros afloramientos son los de Corralejo y El Cotillo. Los restos de esta playa son eminentemente conglomeráticos con cantos rodados de la arenisca jandiense sobre la cual directamente se sitúan cuando corresponden al relleno de cubetas; en otras ocasiones lo hacen sobre un delgado depósito continental de color asalmonado con clastos angulosos y conchas de gasterópodos terrestres. El punto más alto, correspondiente a la berma se encuentra a casi dos metros de altura sobre la berma actual.

Las dunas eólicas están bien representadas por toda la isla. Los cambios del nivel del mar favorecieron el ataque de la base de los acantilados de la costa norte de la península de Jandía, dejando expuestas las calcarenitas y las areniscas grises cementadas, que, por acción del viento, formarán las dunas del Pleistoceno superior y del Tardiglacial en la zona del istmo de Jandía y el norte de Fuerteventura (Meco *et al.*, 1992). Dentro de estas dunas se pueden encontrar frecuentemente niveles con celdillas de insectos y restos de gasterópodos como los de *Theba costillae* n. sp.

La alternancia de dunas y paleosuelos, así como el estudio de depósitos de materiales finos procedentes del Sahara, han permitido establecer las sucesiones de eventos paleoclimáticos de Fuerteventura (Meco, 1975; Meco & Petit-Maire, 1986; Rognon & Coudé-Gaussen, 1987; Rognon *et al.,* 1989).

B.3.- EVOLUCIÓN ESTRUCTURAL

La historia estructural de la isla es tan dilatada como su evolución magmática. La región se ha visto afectada por varias etapas de deformación tectónica. Es importante remarcar que, en Fuerteventura, tanto la corteza mesozoica como los materiales volcánicos submarinos se encuentran basculados. En la costa, las unidades del GVS muestran una geometría en abanico y se apoyan sobre los sedimentos oceánicos que se encuentran invertidos y definiendo un gran pliegue cuyo eje se orienta en dirección ONO-ESE (Fig. 12). Por su parte, hacia el interior de la isla, las rocas del GVS buzan hacia el norte y descansan discordantes sobre los sedimentos mesozoicos y las rocas del Complejo Ultra-alcalino. Esta compleja estructura es todavía mal conocida. La serie mesozoica constituye el basamento de dicha discordancia y se encuentra invertida (Robertson & Stillman, 1979a), habiendo sido afectada por una tectónica contractiva con dirección de acortamiento NNE-SSO. Se ha estimado que la corteza oceánica ha podido ascender más de 3 km, debido en parte a esta deformación, favoreciendo que en la actualidad llegue a aflorar por encima del nivel del mar. Este levantamiento explica que las unidades del GVS se hayan generado bajo láminas de agua de profundidad moderada o somera. Aunque esta etapa pudo haber involucrado también a las unidades más bajas del GVS (por ejemplo, la unidad A que parece mostrar una estructura similar a la de los sedimentos oceánicos: Fig. 12b), su edad es incierta, pudiendo considerarse genéricamente como paleógena y, probablemente, pre-oligocena. Las rocas del Complejo Plutónico Ultra-alcalino (de edad entre 35 y 23 Ma) intruyen a los sedimentos mesozoicos ya deformados.
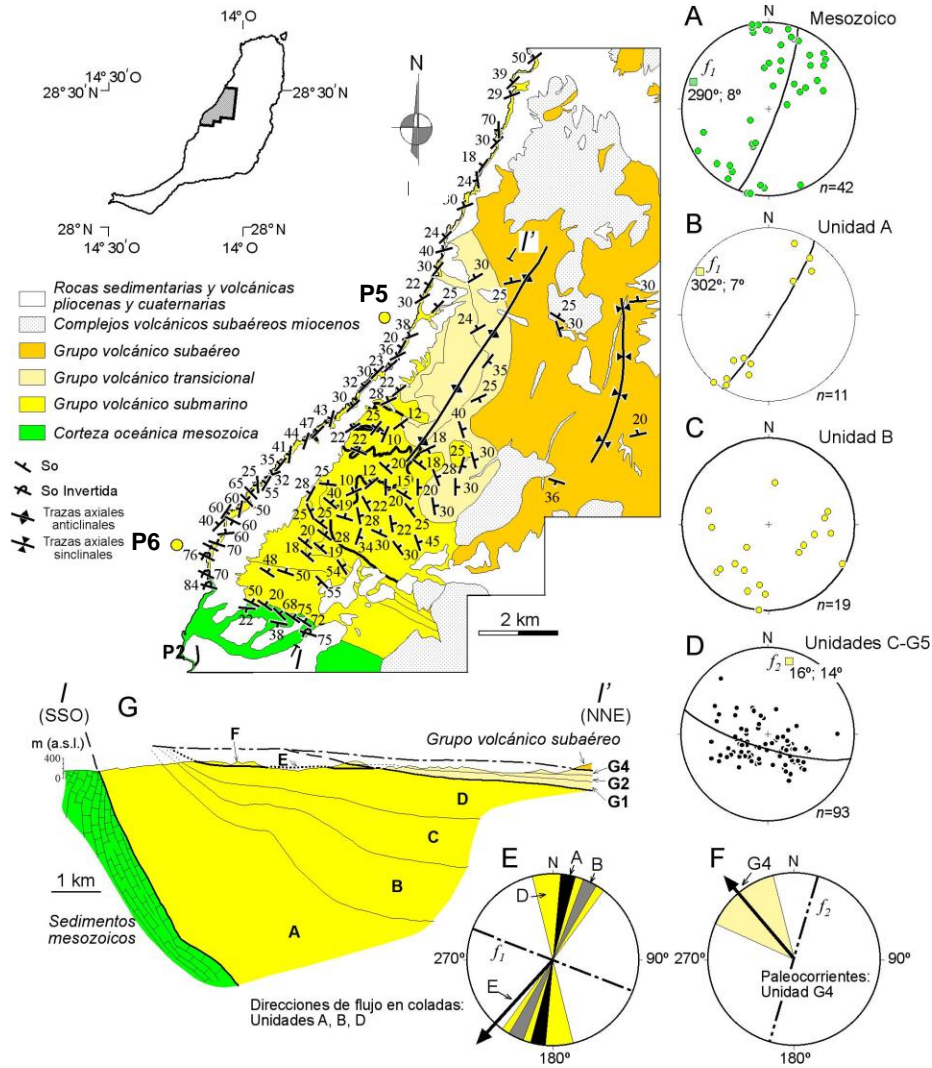
Fig. 12.- Mapa estructural y corte geológico del Complejo Basal al oeste de Betancuria (Gutiérrez *et al.*, 2006). A-D: Proyección equiareal en el hemisferio inferior de datos de estratificación y ajuste estadístico al eje del pliegue. E y F: rosas de direcciones de paleocorrientes.

El segundo periodo de deformación es de edad miocena. Fernández *et al.* (2006) han reconocido tres fases tectónicas sucesivas, las tres extensionales. La importancia y características de esta etapa de extensión han llevado a Fernández *et al.* (2006) a hablar del *rifting* mioceno de Fuerteventura, retomando antiguas propuestas de Fúster (1975). La primera fase (M-D$_1$), que es la más importante, ha sido datada entre 25 y 20 Ma, y se habría caracterizado por una extensión de dirección ONO-ESE a NO-SE, es decir, prácticamente ortogonal a la dirección de acortamiento de la fase contractiva anterior responsable de la inversión que sufren los sedimentos de la corteza oceánica. Las estructuras debidas a esta fase son muy abundantes en Fuerteventura, llegando a constituir la impronta estructural

más marcada y característica de la isla (Fig. 12). Durante el inicio de esta etapa, en la transición entre la fase contractiva anterior y M-D_1, tuvo lugar la formación de zonas de cizalla dúctil y dúctil-frágil (que se describirán con más detalle en la explicación de la Parada 4). Estas zonas de cizalla son posteriores al Complejo Ultra-alcalino (35-23 Ma) y anteriores a las primeras rocas de la Dorsal Inicial (23 Ma). La fase M-D_1, en sentido estricto, se caracteriza por la formación de grandes pliegues de *rollover* con trazas axiales de dirección NE-SO (Fig. 12), un espectacular haz de diques (Fig. 10), abundantes sistemas de fallas normales y normal-direccionales, y una intensa actividad eruptiva fisural subaérea. La posición cartográfica actual del Complejo Basal se debe a su localización en el núcleo de grandes estructuras antiformales (Fig. 13). La orientación y posición de la zona de máxima densidad de diques coincide también con la región afectada por los grandes arqueamientos antiformales de las rocas del Complejo Basal (compárense las Figs. 10 y 13). La base de la Dorsal Inicial constituiría la serie sintectónica relacionada con esta fase M-D_1 extensional.

De acuerdo con la interpretación dada por Fernández *et al.* (2006), la estructura a gran escala estaría dominada por uno o más despegues principales con desplazamiento del bloque de techo predominantemente hacia el ONO (corte de la Fig. 13). Esto explica la tendencia de la Dorsal Inicial a colapsar precisamente en esa dirección (Ancochea *et al.,* 1996; Stillman, 1999). En planta, las estructuras de fase M-D_1 dibujan grandes formas arqueadas (Fig. 13) que recuerdan las observadas en zonas de *rift* continental (Rosendahl, 1987) y cuya geometría condicionó probablemente la posición y alineación de los principales centros de emisión volcánica (Fig. 3).
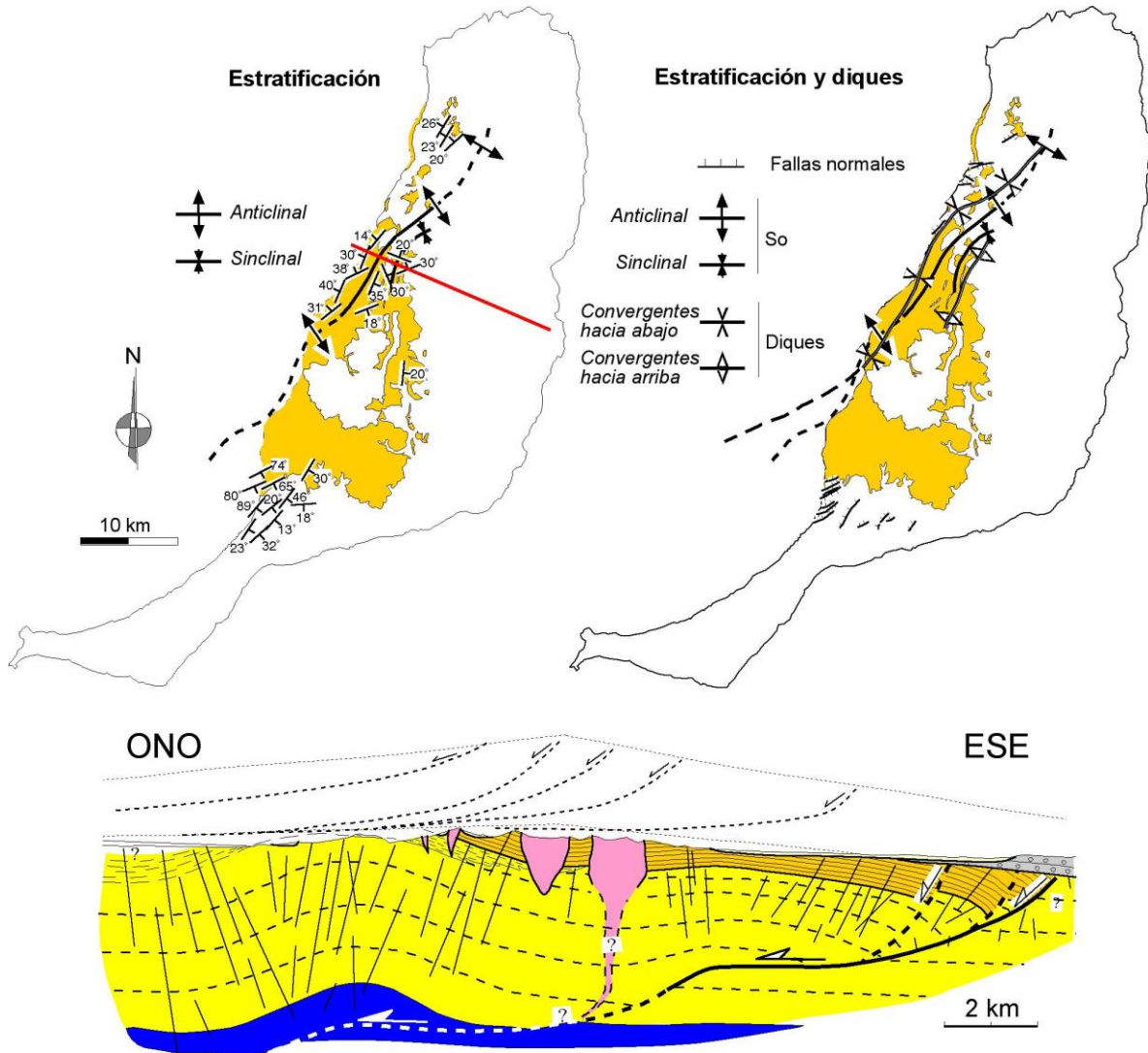
Fig. 13.- Esquemas estructurales del Complejo Basal, mostrando la orientación media de la estratificación en distintos afloramientos (izquierda) y su comparación con la orientación promedio de los diques del complejo filoniano (derecha). La estructura general dibuja grandes antiformes y sinformes que han sido tentativamente interpretados como debidos a un despegue extensional de geometría escalonada. En el corte (localización en la figura superior izquierda) se representa la corteza oceánica en azul, el GVS y el GVT en amarillo, el Grupo Volcánico Subaéreo en naranja, las rocas plutónicas tardías relacionadas con los grandes edificios en escudo miocenos, en rosa, y las rocas de estos edificios miocenos en gris (Fernández *et al.*, 2006).
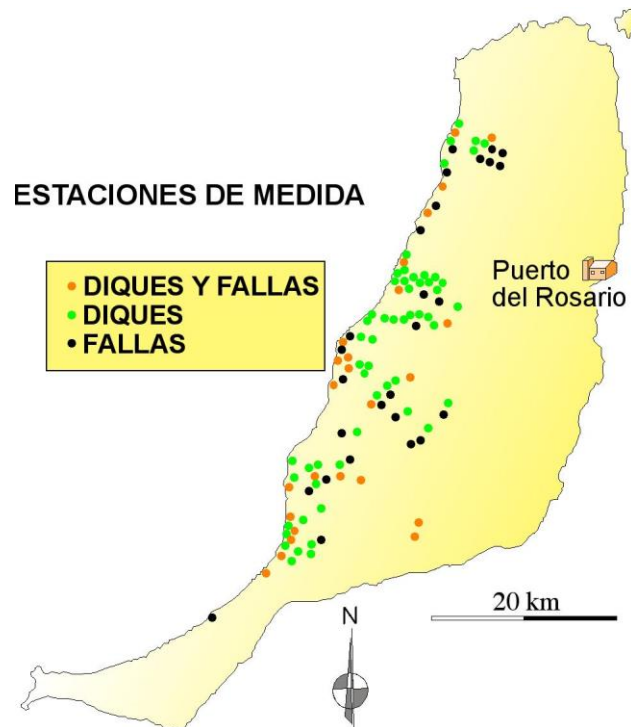
Fig. 14.- Distribución de las estaciones de medida de fallas (1780 fallas medidas en 55 estaciones) y de diques básicos del complejo filoniano (2996 datos tomados en 96 estaciones). Modificado de Fernández *et al.* (2006).

La dirección de extensión ha sido también ratificada mediante el uso de las técnicas de análisis de poblaciones de fallas y de orientación de haces de diques (Fernández *et al.*, 2006). Las estaciones utilizadas para esta determinación se distribuyen por todas las rocas de la corteza oceánica, del Complejo Ultra-alcalino, de la Dorsal Inicial y de los edificios volcánicos en escudo miocenos (Fig. 14). El máximo estiramiento en la horizontal se orienta en la dirección ONO-ESE para gran parte de la isla durante la fase M-D1 (Figs. 15 y 16), con excepción de la región de la península de Jandía (extremo sur de Fuerteventura), en donde la dirección de extensión gira hacia NNO-SSE. Este cambio puede estar relacionado con la geometría arqueada en planta que presentan las grandes estructuras extensionales, como se ha indicado antes. Al mismo tiempo, puede asociarse también a la conexión hacia el oeste de las estructuras extensionales de Fuerteventura con las que hipotéticamente deberían encontrarse en la cercana isla de Gran Canaria (cubiertas por materiales más recientes).
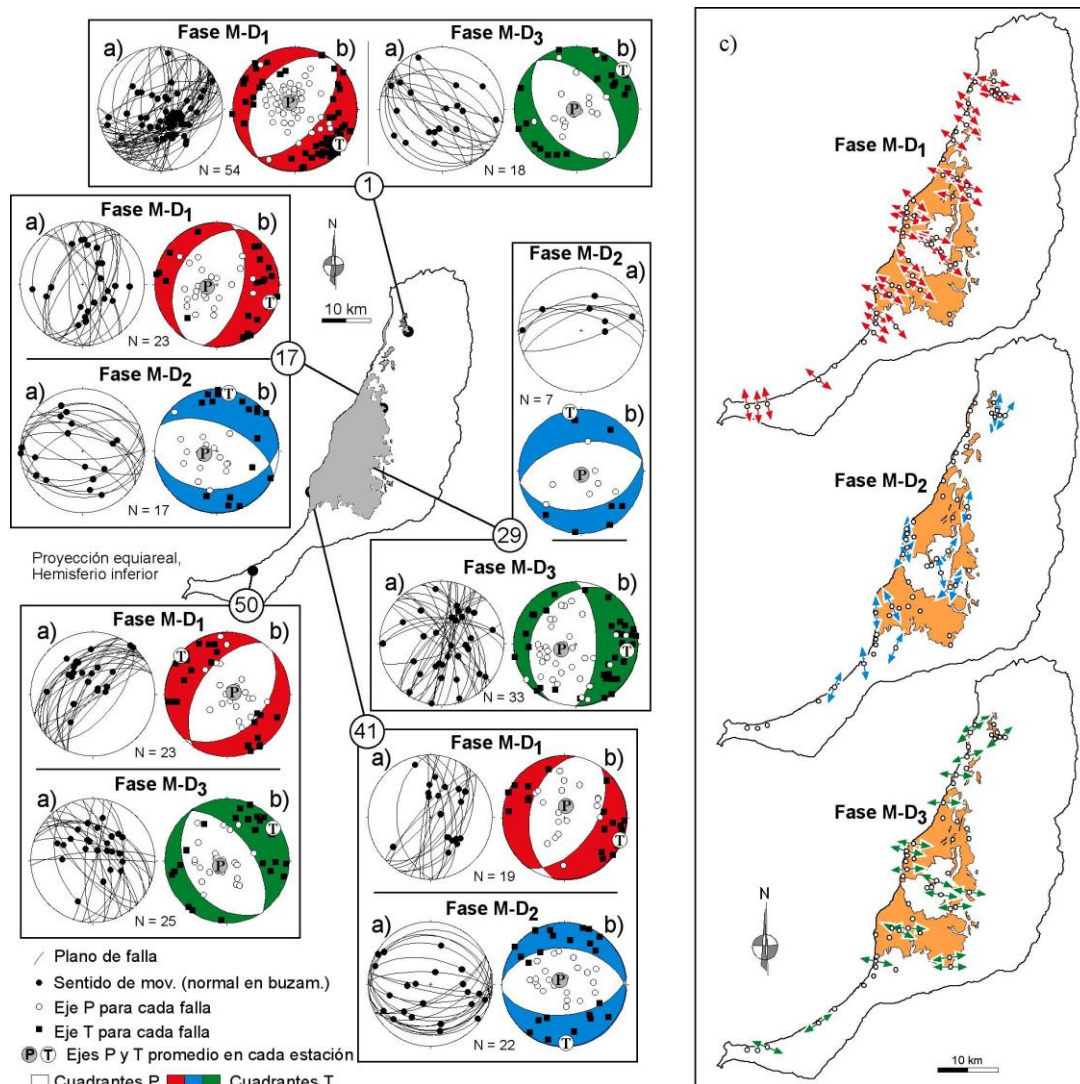
Fig. 15.- Resultados del análisis de poblaciones de fallas mediante el uso del método PT de Marrett y Allmendinger (1990). Izquierda: Ejemplos tomados de estaciones seleccionadas (a: planos de fallas, estrías y sentidos de movimiento; b: resultados del método PT). Derecha (c): Distribución espacial de los ejes T (máximo estiramiento) para las tres fases extensionales miocenas (M-D$_1$ a M-D$_3$). Modificado de Fernández *et al.* (2006).

El cambio en la dirección de extensión que tuvo lugar hace unos 20 Ma marca el paso a la segunda fase de deformación miocena (M-D$_2$), que se extendería entre los 20 y los 17 Ma, coincidiendo con el deslizamiento de la parte central de la Dorsal Inicial y la formación del deslizamiento de Puerto del Rosario Sur. M-D$_2$ se caracteriza por la formación de sistemas de diques y de fallas que reflejan extensión en dirección NNE-SSO

(Figs. 15 y 16). La actividad volcánica pasaría de fisural a central, dándose las condiciones mecánicas adecuadas para el inicio de la formación de los grandes edificios en escudo miocenos, comenzando por el edifico Central (Fig. 3).
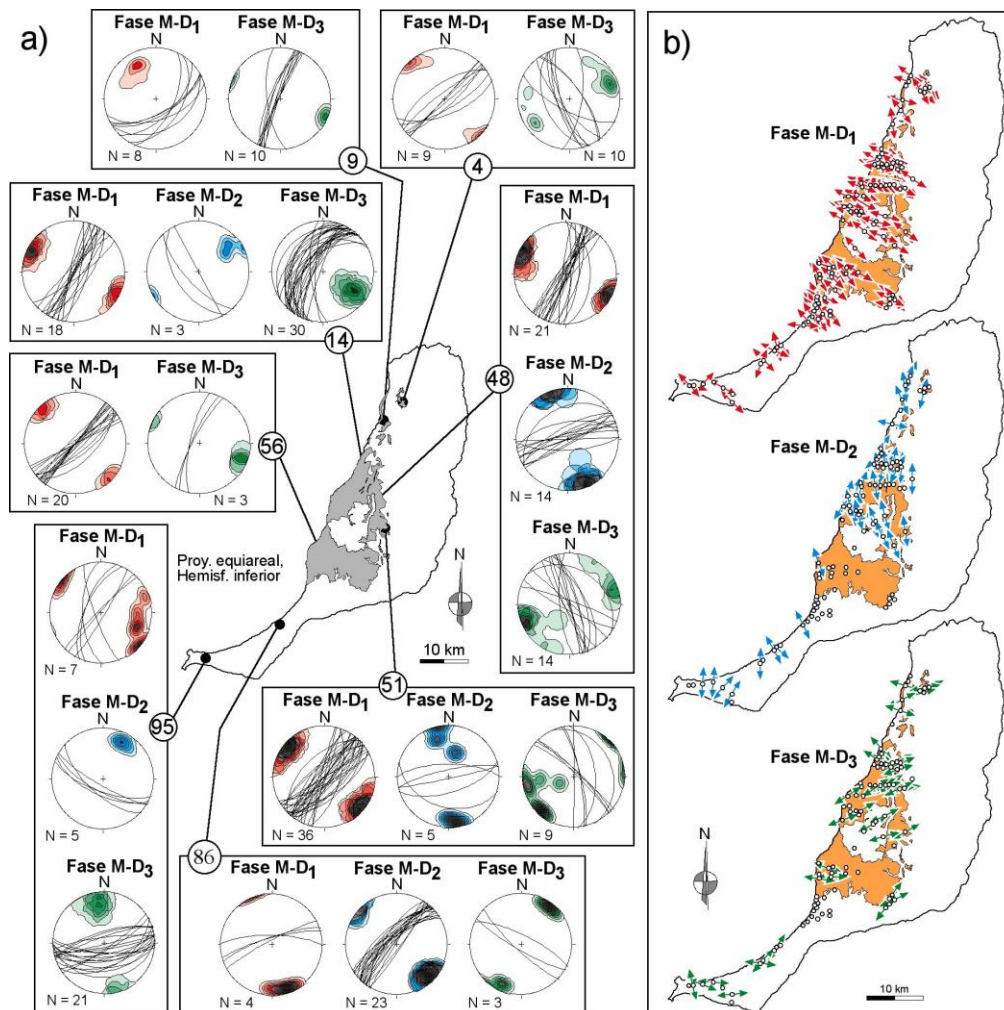
Fig. 16.- Resultados de la medición de diques básicos del complejo filoniano. a) Ejemplos seleccionados de estaciones con diques atribuidos (en función de sus relaciones de corte) a las diferentes fases extensionales. Diagramas de densidad con intervalo de contornos de 5 veces la desviación típica. b) Distribución espacial de los ejes T (máximo estiramiento) para las tres fases de deformación extensional miocena. Según Fernández *et al.* (2006).

Finalmente, entre 17 y 12 Ma se habría desarrollado la tercera fase de deformación miocena (M-D$_3$), coincidiendo con el deslizamiento de la parte norte y sur de la Dorsal Inicial y la consiguiente formación de los edificios en escudo miocenos Norte y Sur,

caracterizada por una dirección de extensión E-O a ENE-OSO (Figs. 15 y 16). Las fases M-D_2 y M-D_3 son responsables de diversas discordancias observadas por Ancochea *et al.* (1996) en los edificios volcánicos en escudo miocenos. La dirección de acortamiento horizontal deducida para la fase M-D_3 por Fernández *et al.* (2006) coincide con la dirección local de movimiento relativo actual entre las placas de Nubia y euroasiática (Fig. 17). Aunque en Fuerteventura no se han encontrado pruebas de la actuación de fases más recientes que M-D_3, la información obtenida por Marinoni & Pasquarè (1994) en la cercana Lanzarote sugiere que el campo de deformaciones relacionado con M-D_3 podría continuar activo hasta la actualidad.
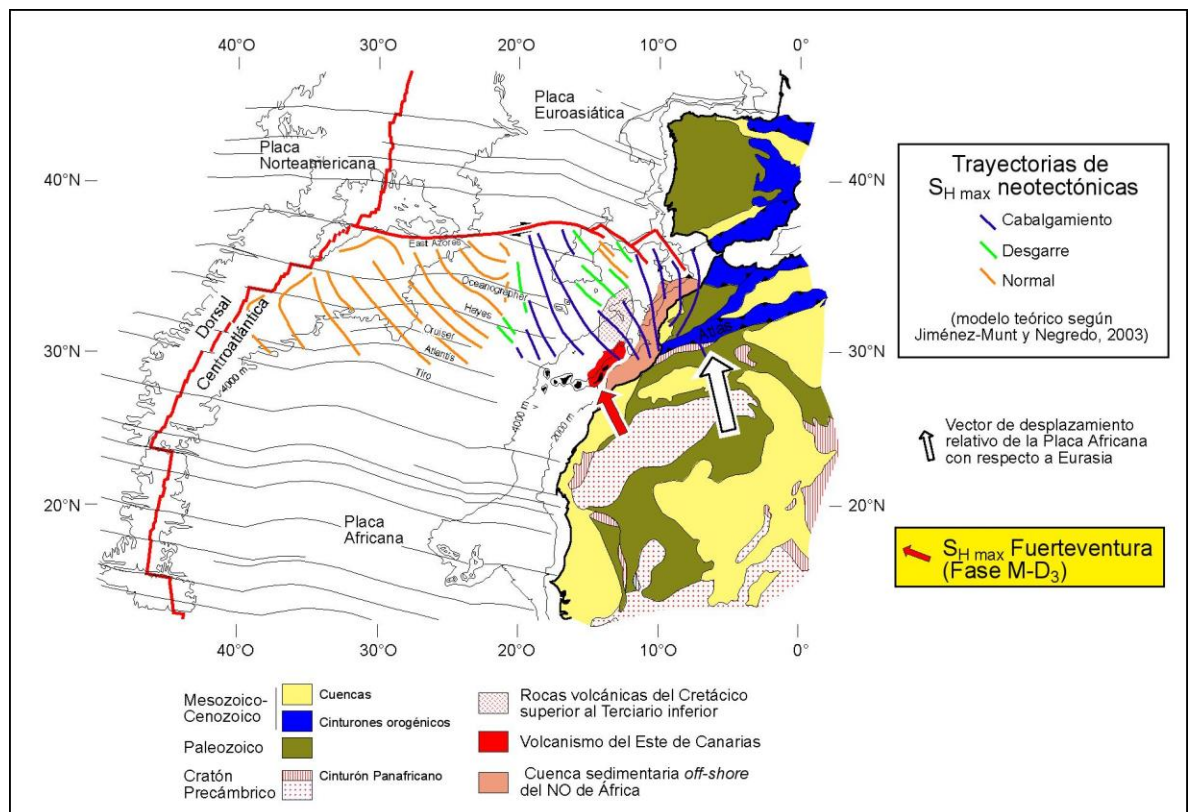
Fig. 17.- Situación tectónica de la Isla de Fuerteventura en el contexto de las placas de Nubia, Euroasiática y Norteamericana, con la comparación entre la dirección de acortamiento horizontal deducida para M-D_3 por Fernández *et al.* (2006), el vector de acercamiento relativo entre las placas de Nubia y Euroasiática y con la orientación de la máxima compresión horizontal deducida a partir de un modelo numérico por Jiménez-Munt y Negredo (2003).

La evolución tectónica pre-miocena y miocena de Fuerteventura parece condicionada tanto por causas locales y regionales, probablemente sub-litosféricas, como por el contexto global de movimientos relativos entre las placas de Nubia y Euroasiática. Esta evolución tectónica habría determinado la actividad magmática en la isla.

Fig. 18.- Modelo de evolución tectónica de Fuerteventura desde el Oligoceno superior-Mioceno inferior hasta el Mioceno medio (parcialmente tomado de Fernández *et al.*, 2006).

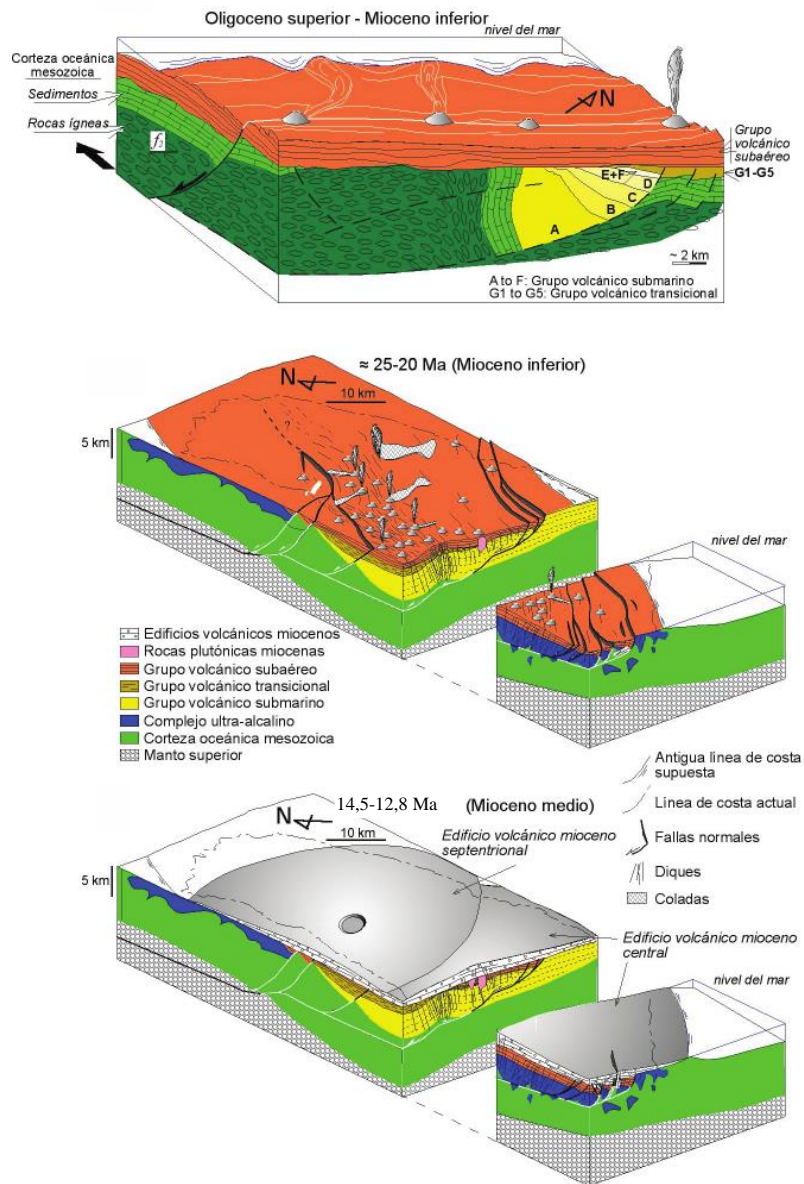La evolución tectónica pre-miocena es todavía bastante desconocida, aunque una fase contractiva con dirección de acortamiento NNE-SSO fue responsable de la inversión de la corteza mesozoica y, en parte, de su levantamiento. Durante la formación de la Dorsal Inicial, se desarrolló la fase M-D$_1$, que originó el *rifting* de la corteza oceánica y la emisión de grandes volúmenes de rocas volcánicas, incluyendo buena parte de la Dorsal Volcánica Inicial (Fig. 18 c1 y c2). La dirección de extensión se orientó en dirección ONO-ESE. Finalmente, siempre en un contexto extensional, pero con deformaciones mucho más moderadas, y con direcciones de extensión cambiantes, se suceden las fases M-D$_2$ y M-D$_3$ (Fig. 18d), asociadas a los grandes deslizamientos que sufrió la Dorsal Inicial y al crecimiento anidado de los tres volcanes en escudo miocenos de Fuerteventura.

Es posible también detectar los efectos de deformaciones muy recientes, posiblemente neotectónicas, en la alineación de conos volcánicos plio-cuaternarios, en la distinta elevación a lo largo de la isla, y especialmente en la costa occidental, de los niveles de playa de esa misma edad, en el encajamiento de barrancos en sus propios sedimentos, y en la presencia de piedemontes basculados, entre otras evidencias. No obstante, no se dispone de datos para caracterizar con precisión estos eventos tectónicos modernos.

C.- DESCRIPCIÓN DE LAS PARADAS

C.1.- PROGRAMA DE LA EXCURSIÓN

Día 14 de junio: 19:00 a 20:30 h. Reunión de la Comisión de Petrología, Geoquímica y Geocronología de Rocas Ígneas y Metamórficas en los apartamentos Broncemar Beach. Presentación de la excursión y sesión ordinaria de la Comisión de Petrología, Geoquímica y Geocronología de Rocas Ígneas y Metamórficas de la SGE. Antes de la reunión, llegada al Caleta de Fuste (Antigua) Broncemar Beach Suites y recogida de vehículos todoterreno.

Día 15 de junio: Itinerario 1 (Figs. 3 y 19). Paradas 1 a 4. La corteza oceánica aflorante. El Complejo Ultra-alcalino y sus deformaciones: Punta de la Nao-Caleta de la Cruz. Salida de Caleta de Fuste a las 9:00 h. Comida (bolsa facilitada por la organización) hacia las 14:00 h en Ajuí. Vuelta a Caleta de Fuste a última hora de la tarde.

Día 16 de junio: Itinerario 2 (Figs. 3 y 19). Paradas 5 a 8. Evolución submarina y emersión de la isla. Intrusiones plutónicas asociadas a la Dorsal inicial de la isla y a los edificios en escudo miocenos: El Complejo Circular de Vega de Río Palmas. Salida de Caleta de Fuste a las 9:00 h. Comida (bolsa facilitada por la organización) hacia las 14:00 h en Pájara. Vuelta a Caleta de Fuste a última hora de la tarde.

Día 17 de junio: Itinerario 3 (Figa. 3 y 19). Paradas 9 y 10. Los grandes deslizamientos gravitacionales en Fuerteventura: el deslizamiento del Puerto de Rosario Norte. Salida de Caleta de Fuste a las 9:00 h. Comida (bolsa facilitada por la organización) hacia las 14:00 h. Final de la excursión y de la Reunión a primera hora de la tarde.
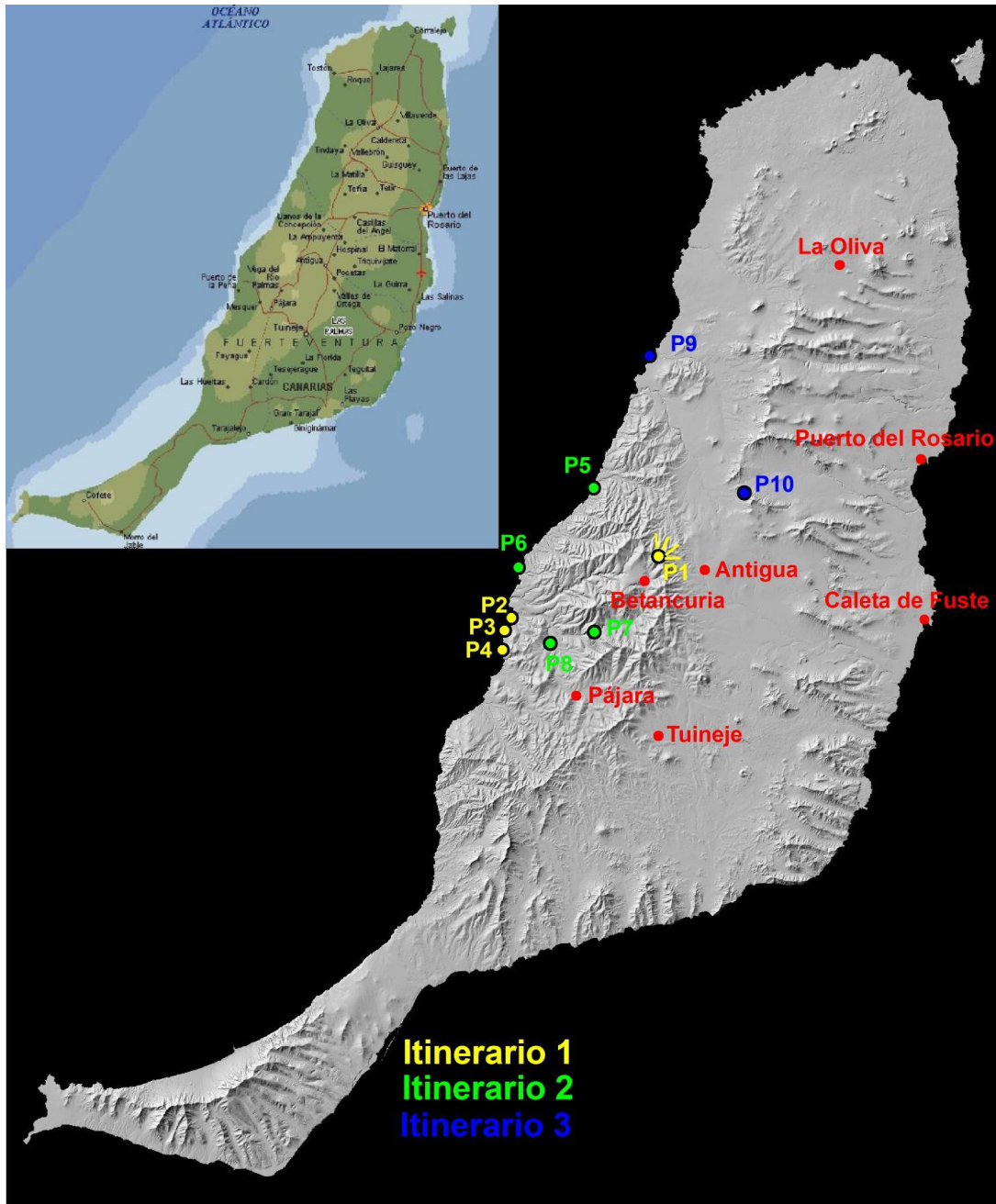
Fig. 19.- Situación de las paradas de la excursión y de las capitales de los municipios de Fuerteventura. Los apartamentos se localizan en Caleta de Fuste.

C.2.-ITINERARIO 1.

Definición de las principales unidades geográficas y geológicas de la isla. Las formaciones más antiguas: la corteza oceánica mesozoica y el Complejo Plutónico Ultra-alcalino (piroxenitas, ijolitas, melteigitas, sienitas y carbonatitas) y las deformaciones tectónicas que los afectan (Figs. 2, 3, 4, 5 y 19).

Parada 1.

Definición de las principales unidades geológicas de la isla: el mirador del Morro de la Velosa.

Desde este impresionante mirador, a nuestro alrededor podemos observar las cinco comarcas fisiográficas más importantes del centro y norte de Fuerteventura, que responden a diferentes unidades geológicas claramente diferenciadas (Fig. 2, Criado, 1991): El Norte, el Valle Central, Los Valles y Cuchillos Orientales, el Macizo de Betancuria y la Península de Jandía. En este punto, y aprovechando la panorámica, se discutirá la conformación geológica general de la isla, y su influencia en la formación y evolución de sus principales rasgos geográficos. El mirador servirá también como lugar privilegiado para explicar y justificar la localización de las diferentes paradas de esta excursión.

Parada 2

La corteza oceánica aflorante: las lavas almohadilladas y los sedimentos de fondo oceánico mesozoicos (la Unidad Basal: la Playa de los Muertos y el Puerto de la Peña) (Figs. 3, 4 y 5)*.*

En el afloramiento de la playa de los Muertos podemos observar los niveles más bajos de la *Unidad Basal* de la secuencia mesozoica, que muestran el tránsito de la capa 1 a la capa 2 de la corteza oceánica jurásica en este sector del Atlántico (Steiner *et al*., 1998). Se trata de una serie de flujos de basaltos toleíticos (con características geoquímicas de N-MORB) que se encuentran muy deformados y alterados. En estos niveles es posible adivinar alguna estructura almohadillada (Fig. 20).

Fig. 20.- Estructuras almohadilladas en las rocas de composición N-MORB
de la playa de los Muertos (vista hacia el este).

Más hacia el norte (parte más septentrional de la playa de los Muertos y en el puerto de la Peña) aparece una secuencia alternante de areniscas, argilitas y limolitas que representan un conjunto de turbiditas de abanico submarino profundo. Estos niveles se orientan según la dirección N70-75ºE y buzan 45-60º hacia el SSE. La serie se encuentra invertida, como demuestran los criterios de polaridad proporcionados por las estructuras sedimentarias que presentan estas secuencias turbidíticas (Fig. 21b). Estos materiales están afectados por una densa red de diaclasas que llegan a constituir una verdadera foliación de fractura según la dirección N-S a NE-SO, y por abundantes fallas de desplazamiento centimétrico a decimétrico (Fig. 21a, d). Toda esta unidad se halla atravesada por diques basálticos y traquíticos, estos últimos más tardíos.
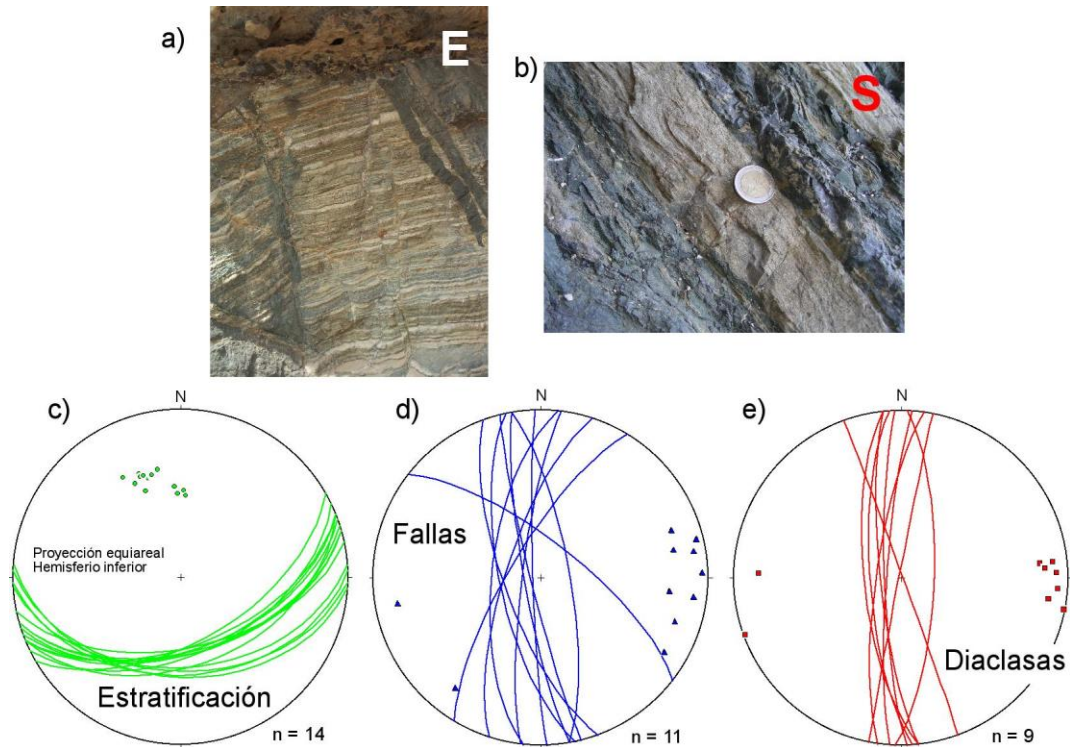
Fig. 21.- (a) Aspecto de la serie sedimentaria mesozoica turbidítica en el puerto de la Peña (vista hacia el norte). Obsérvense las fallas de pequeño desplazamiento que la afectan. (b) Criterios de polaridad en las secuencias de tipo Bouma indicando techo hacia el norte. (c, d, e) Datos estructurales en el afloramiento del puerto de la Peña.

En el puerto de la Peña, por encima de los sedimentos mesozoicos y en posición discordante, se sitúa una playa levantada pliocena, constituida por arenas y conglomerados (Fig. 22). Encima de ellas aparecen coladas basálticas subaéreas que continúan hacia el mar formando lavas almohadilladas e hialoclastitas. En la parte más alta del acantilado la playa levantada contiene numerosos cantos rodados de coladas basálticas y tobas palagoníticas. El acantilado termina en un depósito de arenas litorales y eólicas que se encuentran interestratificadas con conglomerados aluviales.
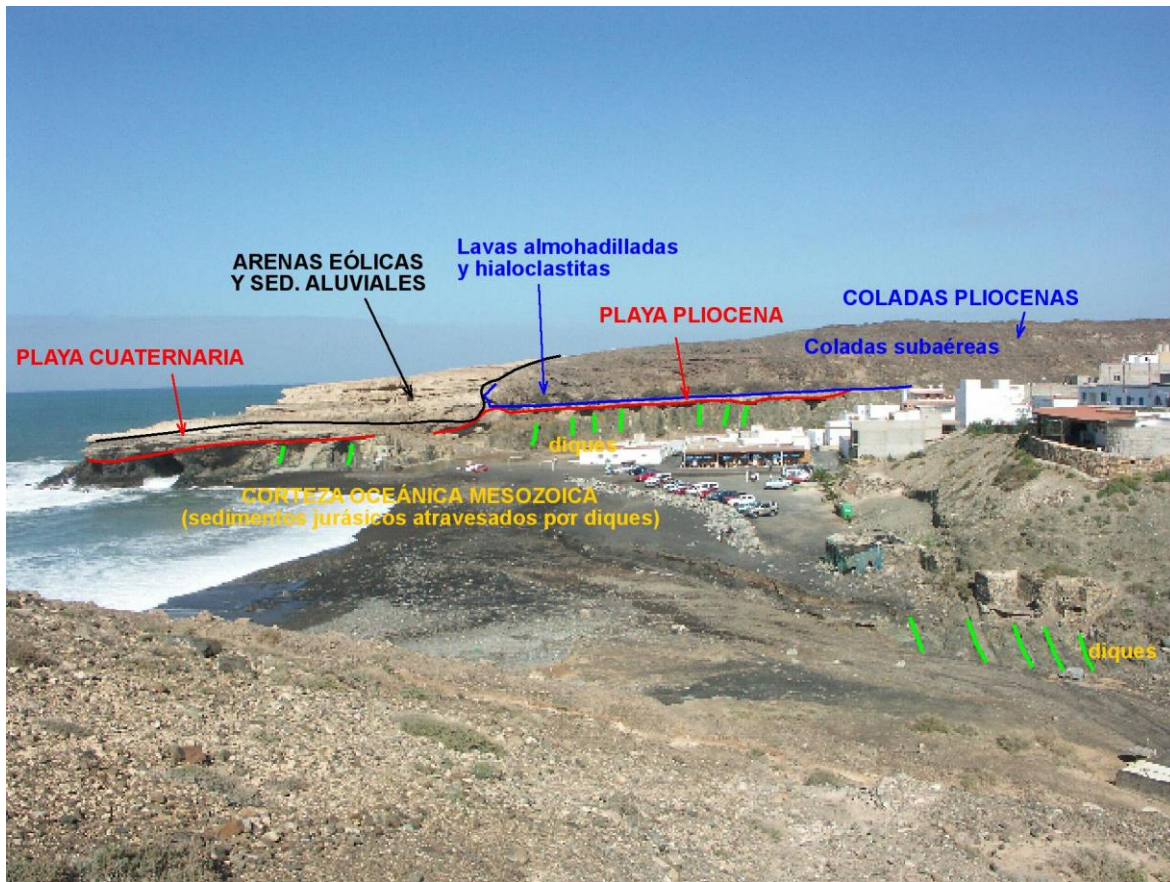
Fig. 22.- Discordancia entre la corteza oceánica mesozoica, profusamente atravesada por diques del complejo filoniano, y las series volcánicas y sedimentarias plio-cuaternarias. Puerto de la Peña.

Parada 3.

El Complejo Ultra-alcalino (piroxenitas, melteigitas, ijolitas, sienitas y carbonatitas). Aspecto de las carbonatitas sin deformación (la Punta de la Nao). (Fig. 3 y 4).

En esta zona de la costa podemos observar uno de los afloramientos de carbonatitas de la isla de Fuerteventura. Se trata de rocas poco frecuentes que en nuestro caso tienen la peculiaridad de representar, junto a las encontradas en el archipiélago de Cabo Verde, uno de los escasos afloramientos de carbonatitas emplazadas en ambiente oceánico (Fúster *et al.,* 1968a).

Las carbonatitas son rocas ígneas compuestas por más de un 50% de carbonatos. Las carbonatitas de Fuerteventura son siempre variedades calcíticas, formadas fundamentalmente

por calcita, flogopita, feldespato potásico, nefelina, augita egirínica, apatito, magnetita, esfena, circón y pirocloro. Las carbonatitas se encuentran asociadas a diversos tipos de rocas silicatadas alcalinas, fundamentalmente sienitas nefelínicas, ijolitas, melteigitas, urtitas y piroxenitas (Fig. 23). Este Complejo plutónico Ulta-alcalino, por el norte (Fig. 3) se extienden hasta la montaña de Los Frailes y la playa del Águila, cerca de El Cotillo (Fúster *et al.,* 1980; Barrera *et al.,* 1981). Por el sur llegan, por la costa, hasta cerca de la desembocadura del barranco de Amanay (Le Bas *et al.,* 1986; Ahijado y Hernández-Pacheco, 1992; Ahijado *et al.,* 1992; Mangas *et al.,* 1994). Por el suroeste hasta la montañita de Agando, junto al caserío de Violante. Por el este, hasta el roque del Buey, al este de la montaña de Gairía. Este Complejo Ultra-alcalino se emplazó desde los 35 a los 23 Ma, entre el Oligoceno y el Mioceno inferior (Cantagrel *et al.,* 1993, Balogh *et al.,* 1999, Muñoz *et al.,* 2005; Sagan *et al.*, 2020).
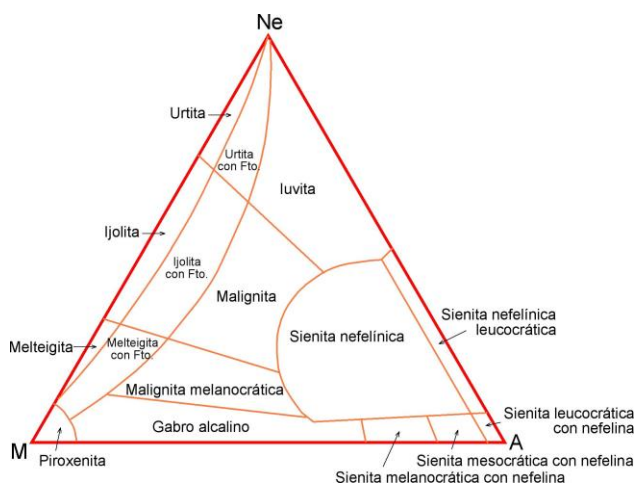
Fig. 23- Triángulo de clasificación de las rocas silicatadas alcalinas.

En la zona costera comprendida entre la Punta de la Nao y la Punta del Viento (Fig. 24), carbonatitas, sienitas, ijolitas y rocas asociadas, se observan formando diques que intruyen a las piroxenitas y rocas asociadas del Complejo Ultra-alcalino.
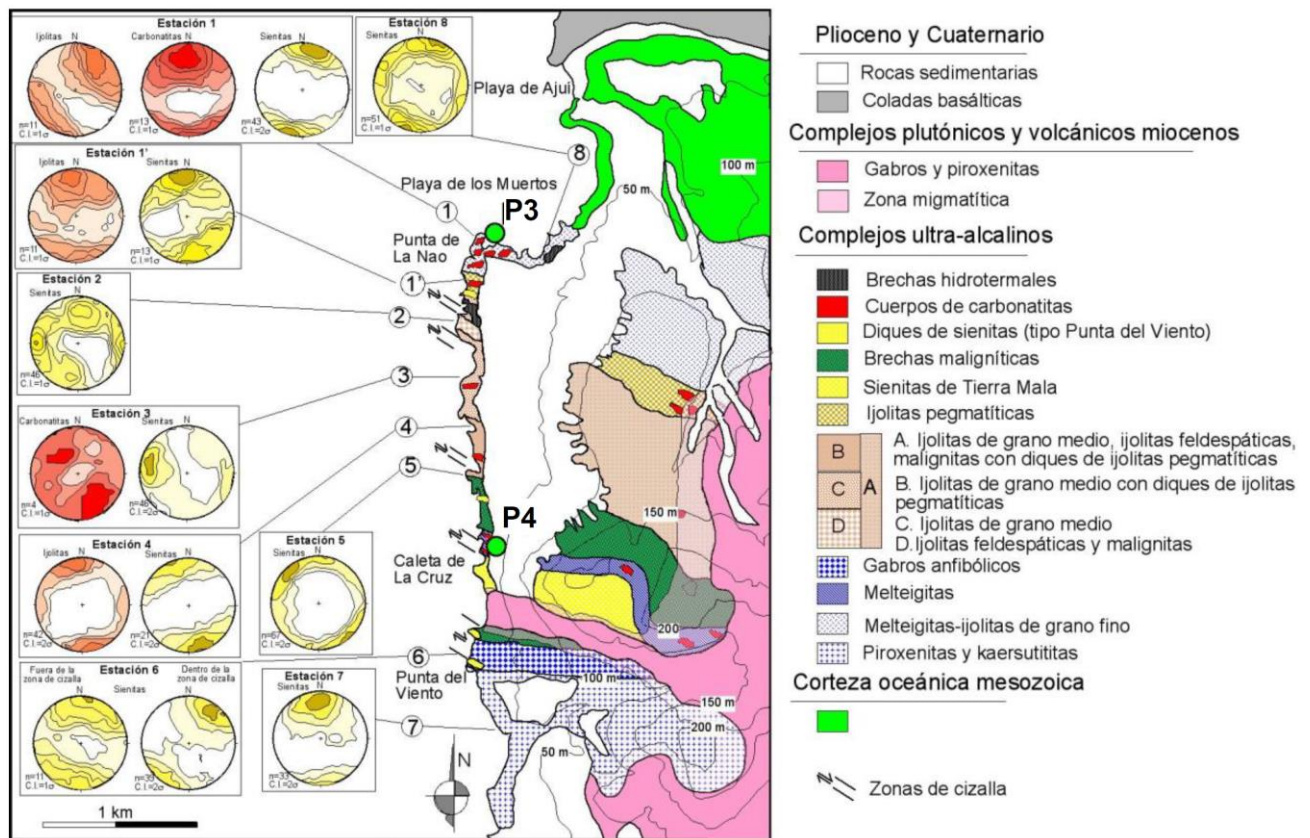
Fig. 24.- Mapa del Complejo Ultra-alcalino de la Punta de la Nao mostrando
la orientación de los diques de ijolita, sienita y carbonatita.

En algunos afloramientos (Esquinzo y Punta de la Nao) las carbonatitas forman diques de potencia métrica. En concreto, en el afloramiento de la Punta de la Nao podemos observar un dique compuesto formado por sienita nefelínica-carbonatita, así como diversas relaciones de corte entre los diques de ijolita, carbonatita y sienita (Fig. 25, foto superior). Estas relaciones, que son sistemáticas en todo el afloramiento, sugieren que los diques de sienita son posteriores a todos los demás en este sector (salvando los diques básicos del complejo filoniano).
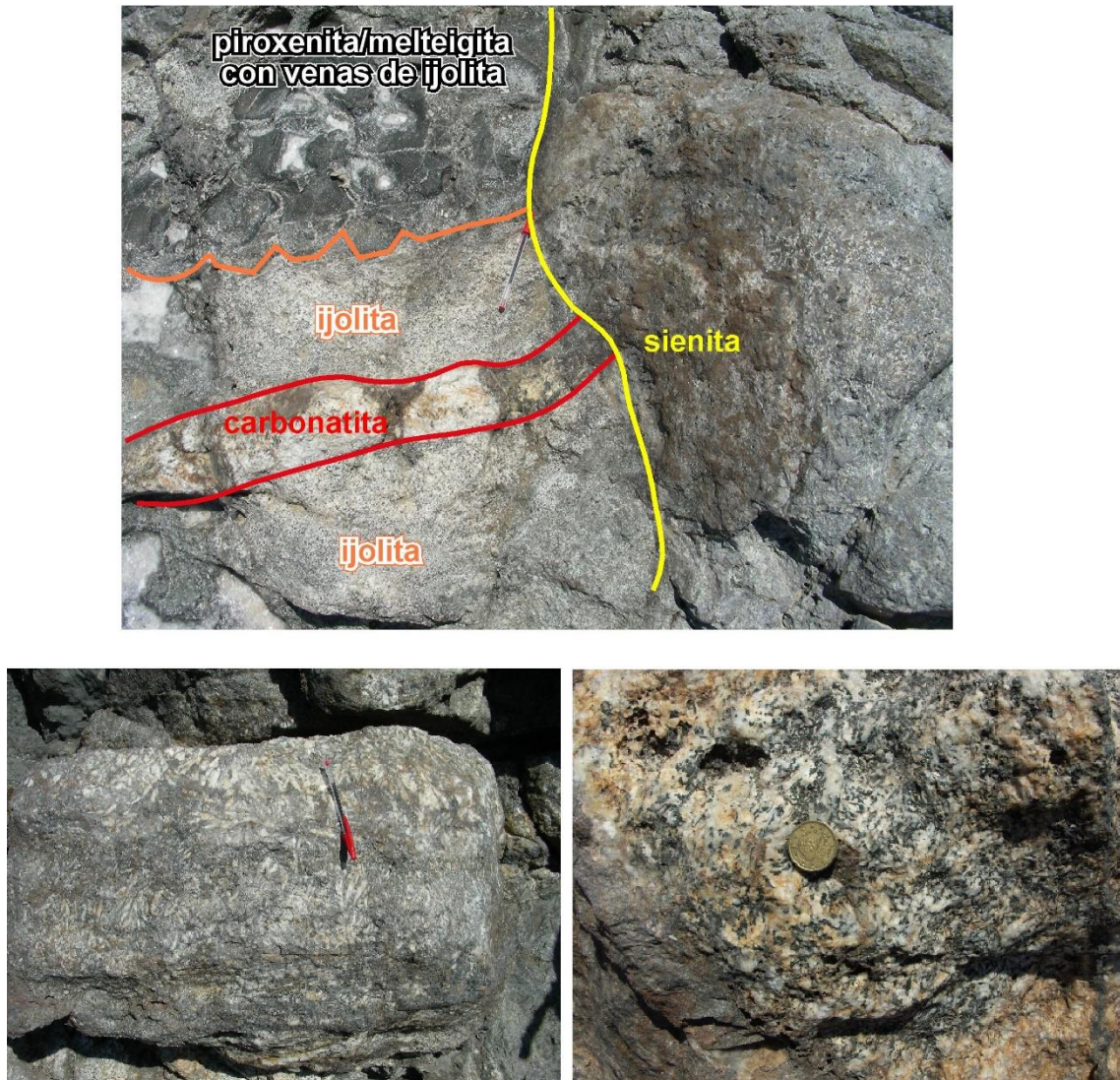
Fig. 25.- Aspecto de campo de los diques de carbonatita, sienita e ijolita de la
Punta de la Nao. Superior: Relaciones de corte entre los distintos tipos de
diques. Inferior: diques de carbonatita.

Es común observar la textura *spinifer* (en peine) de los feldespatos alcalinos dentro de
los diques de carbonatita (Fig. 25, inferior izquierda).

Parada 4.

La zona de cizalla de la Caleta de la Cruz (Fig. 3).

La zona de cizalla de la Caleta de la Cruz, con un grosor de unos 20 m, y producida
durante D-M_1, afecta a piroxenitas, melteigitas, sienitas y carbonatitas del Complejo Ultra-

alcalino de Ajuy-Solapa. El principal afloramiento de esta zona de cizalla se localiza en una estrecha franja de erosión costera, algo más de 2 km al sur del puerto de la Peña (Figs. 3 y 24). Su prolongación tierra adentro se encuentra cubierta por sedimentos plio-cuaternarios.

La calidad del afloramiento en la Caleta de la Cruz ha permitido levantar una cartografía de detalle (Fig. 26). Se trata de una zona de cizalla subvertical y de dirección NO-SE. La deformación en su interior es frágil-dúctil y marcadamente heterogénea, con abundantes bandas de cizalla menores anastomosadas que limitan bloques de piroxenita, melteigita y sienita. En el borde de la zona de cizalla, estas estructuras son frágiles, y aparecen rellenas por la carbonatita que se acumuló en zonas dilatantes como *releasing bends* de bandas de cizalla menores y sombras de presión alrededor de los bloques de piroxenita. Las intrusiones carbonatíticas generaron la fenitización de los bordes de los bloques piroxeníticos y melteigíticos lo que condujo a la formación de agregados de flogopita y albita. Tanto la carbonatita, como los agregados de flogopita y albita son más dúctiles bajo las condiciones de la deformación (unos 500 ºC y 1 kbar) que la roca original, lo que produjo una transición hacia condiciones de ductilidad a medida que progresaba el cizallamiento.
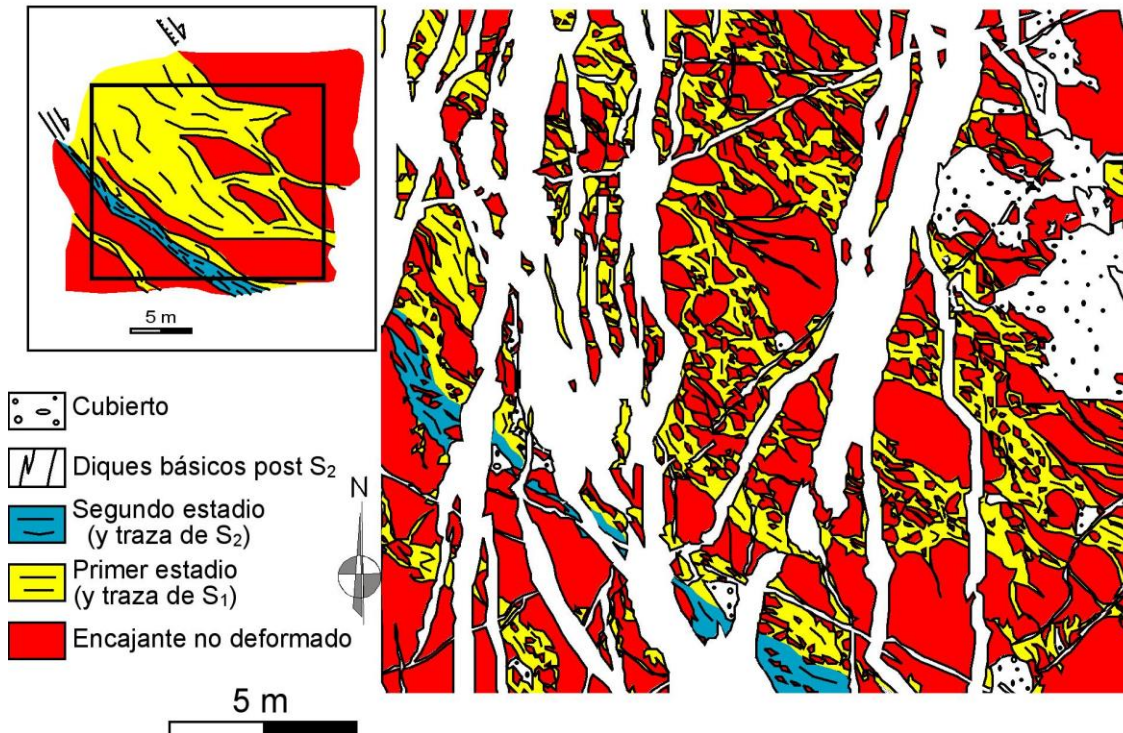
Fig. 26.- Cartografía de detalle de la zona de cizalla de la Caleta de la Cruz.

Las principales estructuras originadas en esta cizalla (algunas de las cuales pueden observarse en la Fig. 27) son una foliación milonítica y una lineación de estiramiento (Fig. 28), además de pliegues asimétricos y de charnela curva (Fig. 28a), fábricas planares compuestas de tipo S-C y bandas de cizalla menores, tanto sintéticas como antitéticas (Fig. 28c). Todos los criterios cinemáticos coinciden en indicar una componente predominante de desplazamiento lateral derecho (Figs. 27 y 28). El cizallamiento se produjo durante, al menos, dos estadios distintos, entre los cuales se produjo la intrusión de diques básicos que aparecen desplazados por la segunda etapa de cizallamiento (Fig. 27e). La cinemática de la segunda etapa de deformación apenas difiere de la deducible para la primera etapa e indicada antes.
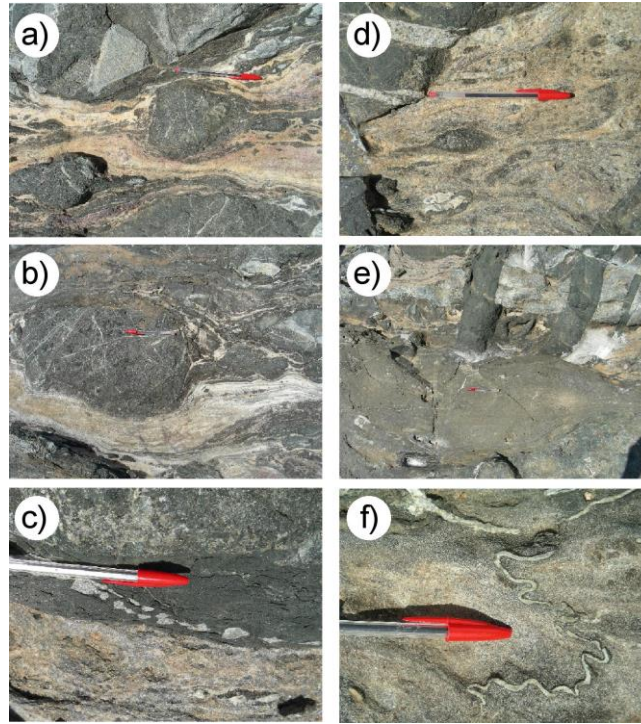
Fig. 27.- Aspecto de campo de las estructuras de deformación en la zona de cizalla de la Caleta de la Cruz. (a y b) Foliación rodeando asimétricamente fragmentos de piroxenita. (c) *Boudinage* en vena de sienita incluida dentro de una zona fenitizada y deformada por la cizalla. (d) Detalle de la fenitización afectando a un pequeño fragmento de piroxenita (debajo del bolígrafo). (e) Diques básicos desplazados por el segundo evento de cizallamiento. (f) Pliegues en venillas de sienita. En todas las fotos el este se sitúa a la derecha. El componente de cizallamiento en dirección es derecho.
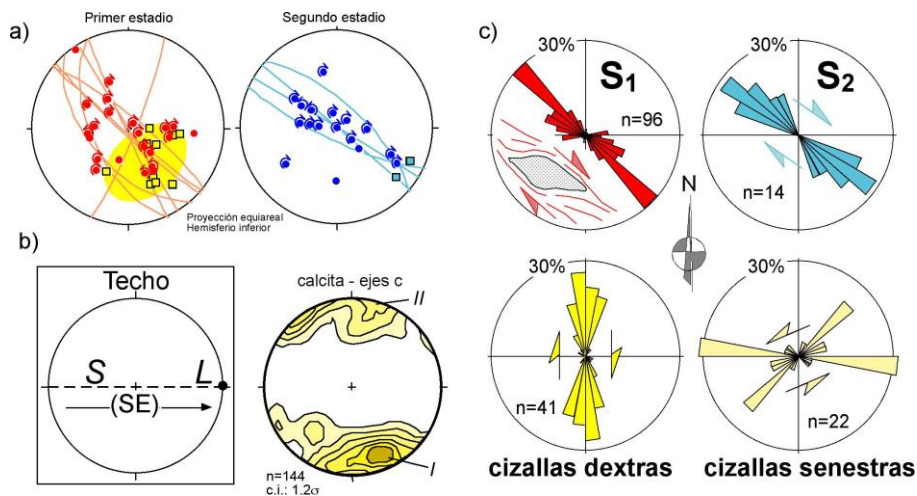
Fig. 28.- Datos estructurales de la zona de cizalla de la Caleta de la Cruz. (a) Foliación (ciclográficas), lineación (cuadrados) y ejes de pliegues (círculos) con indicación de la asimetría. (b) Fábrica cristalográfica de ejes *c* de calcita en las carbonatitas cizalladas. (c) Rosas de direcciones de la foliación y de las zonas de cizalla menores asociadas a la principal.

C.3.- ITINERARIO 2.

La Dorsal Inicial de la isla: el Grupo Volcánico Submarino. (Figs. 3, 4, 6, 7, 8 y 9).

Parada 5.
El Grupo Volcánico Submarino en posición levemente inclinado al Oeste, Formación basaltos del Valle (F) (Barranco del Valle) (Figs. 6, 7, 8 y 9).

En los alrededores de la playa del Valle, la *Formación basaltos del Valle (F)* está representada por niveles de lavas almohadilladas y brechas de fragmentos de almohadillas. Entre estos niveles aparecen algunas areniscas y limolitas volcánicas.

Las lavas almohadilladas aparecen apiladas y tienen tamaños decimétricos y se caracterizan por la presencia de anillos concéntricos de vesículas (Fig. 29, foto inferior). Presentan un borde vítreo de pequeño grosor, formado por el enfriamiento brusco de la lava al entrar en contacto con el agua. Composicionalmente, son basaltos/basanitas piroxénicas con texturas microporfídicas. El material intersticial es de naturaleza hialoclastítica y está formado por fragmentos angulosos vítreos despegados de los bordes de las almohadillas, con formas de astillas, empastados en carbonatos. Estas lavas aparecen atravesadas por diques de lamprófidos camptoníticos con grandes cristales y agregados de flogopita y anfíbol, de composición similar a las rocas de la *Formación basaltos flogopítico-anfibólicos de Piedra de Fuera* (G3, Grupo Volcánico de Transición).
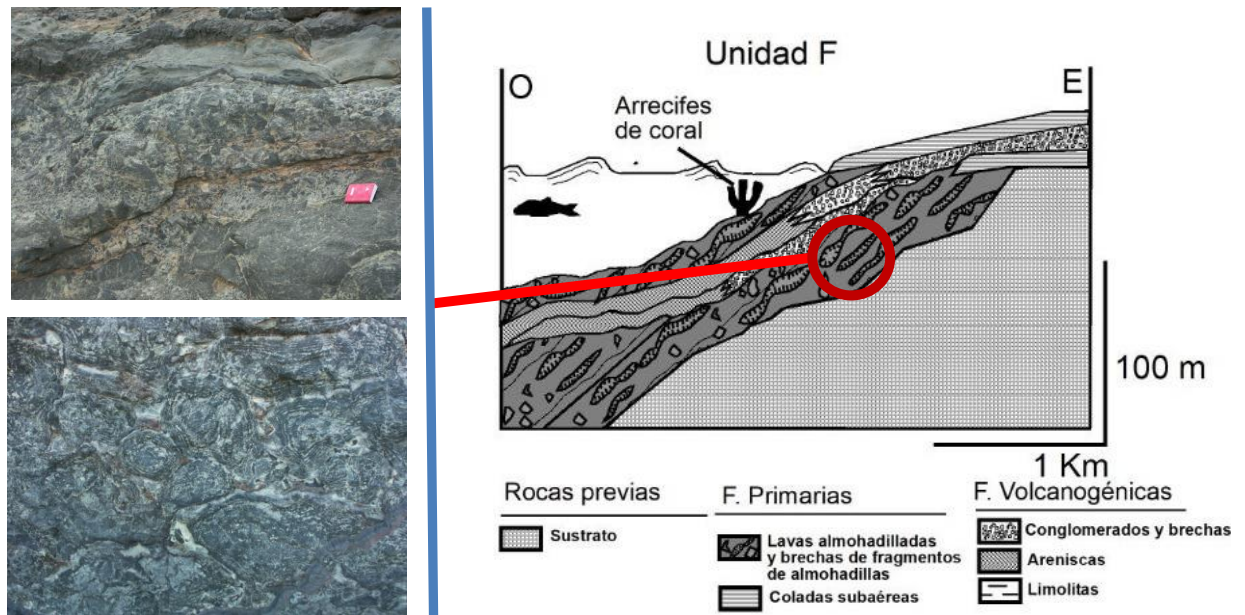
Fig. 29.- Aspecto de campo de las características volcanológicas de la Formación basaltos del Valle en la zona de la parada 5. Las fotos se sitúan en el contexto de la interpretación volcanogénica de la unidad (ver también la Fig. 9). En las fotos la vista es hacia el este.

Es frecuente que los tubos de lava se fragmenten al avanzar en el *foreset* del delta de lava formándose brechas de fragmentos de almohadillas (*pillow fragment breccia* o *broken pillow breccia*). En esta zona existen excelentes afloramientos de este tipo de brechas asociados a los niveles de *pillow lavas* (Fig. 29, foto superior), donde se pueden observar las típicas formas de trozo de tarta en los fragmentos, generadas cuando las almohadillas se rompen a favor de las fracturas radiales. Estos fragmentos tienen el lado curvo vítreo y anillos de vesículas concéntricos. Estas brechas no suelen presentar ningún tipo de organización: el transporte sufrido suele ser muy reducido y su depósito está asociado a flujos gravitatorios en masa. Se diferencia además otro tipo de brechas de fragmentos de almohadillas, en este caso resedimentadas. En ellas es posible observar una organización del depósito en secuencias granocrecientes (Fig. 29, foto superior). En el *foreset* de estos deltas de lavas se depositan brechas de fragmentos de almohadillas resedimentadas (asociación de facies volcanoclástica resedimentadas) a través de flujos granulares de densidad modificada. Tanto las lavas almohadilladas como los fragmentos de las brechas se caracterizan por presentar un elevado índice de vesicularidad que sugiere que la lava que penetró en el mar se encontraba en proceso de desgasificación intensa a poca profundidad.

Toda la serie volcánica submarina se halla atravesada por un denso enjambre filoniano que en ocasiones tiene densidades superiores al 90%. En este punto se observan, como hemos indicado anteriormente, antiguos diques de lamprófidos camptoníticos, biotítico-anfibólicos, con bordes irregulares.

Parada 6.

El Grupo Volcánico Submarino en posición vertical o invertida: Formación basaltos y nefelinitas del Barranco del Tarajalito (A) (Barranco del Tarajalito) (Figs. 6, 7, 8 y 9).

El Grupo Volcánico Submarino aflora de forma continua en la costa occidental de Fuerteventura desde el contacto con los sedimentos mesozoicos, en la Caleta de la Peña Vieja, hasta más al norte del Puertito de los Molinos.

En la desembocadura del barranco del Tarajalito y en la costa adyacente podemos observar las características sedimentológicas y petrológicas de la *Formación basaltos y nefelinitas del Barranco del Tarajalito* (A). Esta formación se caracteriza por la aparición de rocas de afinidad ultra-alcalina (nefelinitas, fonolitas nefelínicas) junto a otras fuertemente alcalinas (basanitas). La secuencia aparece invertida con fuerte buzamiento al sur. En este lugar está bien representada una asociación de facies volcanogénicas formada fundamentalmente por conglomerados, brechas, areniscas y limolitas volcánicas, depositadas a través de flujos subacuáticos relacionados con la destrucción parcial de complejos ultra-alcalinos situados en la zona oriental (Fig. 30, fotos situadas en la parte izquierda).
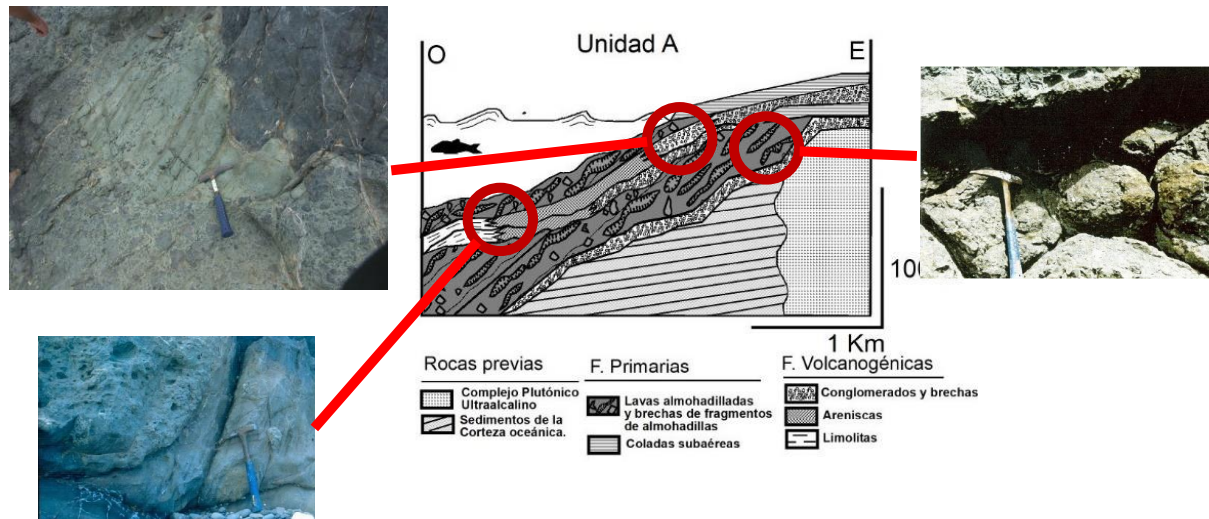
Fig. 30.- Aspecto de campo de las características volcanológicas de la Formación basaltos y nefelinitas del barranco del Tarajalito en la zona de la parada 6. Las fotos se sitúan en el contexto de la interpretación volcanogénica de la unidad (ver también la Fig. 9). En las fotos la vista es hacia el este.

La asociación de facies volcánicas primarias está representada por lavas almohadilladas de composición basanítica con numerosos micro-enclaves de ijolitas y sienitas nefelínicas, apiladas con poco material intersticial (Fig. 30, foto situada a la derecha). Los niveles de lavas almohadilladas se forman en erupciones subacuáticas en deltas de lava formados por la llegada de coladas subaéreas a la línea de costa y aparecen espacialmente relacionados con niveles de brechas de fragmentos de almohadillas más o menos resedimentadas, generadas a través de mecanismos de fragmentación no explosivos de las lavas almohadilladas en los *foreset* de los deltas de lava.

La asociación de facies volcanogénica (brechas volcánicas, conglomerados, areniscas y limolitas) se caracteriza por un predominio de las facies de grano grueso, principalmente niveles de brechas volcánicas depositadas a través de flujos gravitatorios de alta concentración. Gran parte de los niveles de brechas con gradaciones inversas pueden haberse depositado a partir de flujos granulares de densidad modificada, mientras que los

niveles masivos, con selección muy pobre y sin organización interna, se depositarían a partir de corrientes de tipo *cohesionless debris flows*. Por otro lado, el elevado tamaño medio de los fragmentos indica que esas granulometrías estaban disponibles en la fuente y/o que los depósitos son relativamente proximales. Estos depósitos de grano grueso son característicos de zonas distales de los deltas de lava, donde las pendientes acusadas favorecen la movilización gravitatoria de los materiales no consolidados. En estos deltas lávicos, puntualmente tienen lugar colapsos gravitatorios de mayor escala que originan las brechas con grandes bloques de rocas consolidadas como los que se observan en algún nivel de brechas (Fig. 30). Los niveles de areniscas y limolitas finamente estratificados, asociados a brechas volcánicas parecen haberse formado por corrientes de turbidez de alta y baja densidad. Los términos de grano más fino representan las facies distales de los abanicos que rodean a los deltas de lava. Ambos tipos de turbiditas pudieron estar inicialmente asociadas a corrientes de tipo *debris flow*, que se transformarían durante el flujo en corrientes de turbidez diluidas.

La abundancia de depósitos vo1canogénicos en esta formación puede estar relacionada con una actividad tectónica acusada en la cuenca, que provocaría la inestabilidad gravitatoria de los materiales depositados en los deltas lávicos y su resedimentación a través de flujos gravitatorios.

Parada 7.
El complejo circular de Vega de Río Palmas.

Este complejo circular (Fig. 31) está constituido por varios cuerpos de rocas ígneas de geometría anular: sienitas, traquitas y gabros (Muñoz, 1969). Estas masas rocosas se encuentran asociadas a un posible estratovolcán vinculado a la evolución del edificio volcánico en escudo central (Fig. 32), actualmente muy erosionado, que existió en la parte central de Fuerteventura hace entre 18,7 y 16,05 Ma. Los gabros y las sienitas se formaron por la cristalización, a una profundidad de varios kilómetros, bajo el gran volcán, del magma que alimentaba las erupciones que se producían en él. Los anillos de sienitas y traquitas, más resistentes a la erosión, destacan en el paisaje formando relieves destacados en el centro de la

isla y estando atravesados por el río Palmas. Precisamente, el lecho seco del río Palmas va a permitirnos realizar un recorrido a lo largo de todo el complejo, acercándonos a las "entrañas del volcán" (Figs. 31 y 32).

En el primer punto del itinerario (P-7.1) visitamos el anillo más interno de sienitas, llamadas del Sargento. Se trata de sienitas nefelínicas de grano grueso o muy grueso, en la que destacan los cristales prismáticos bien formados de feldespato alcalino (ortosa), de núcleo gris y bordes blancos, entre los que aparece intersticialmente la nefelina. Los cristales más oscuros son de piroxeno, anfíbol y biotita. En algunas zonas de la sienita se observa cómo los cristales de feldespato alcalino se orientan (Fig. 32a) dando lugar a una estructura planar vertical de dirección norte-sur. Se trata de una evidencia del flujo del magma en el momento en el que se estaba solidificando bajo el edificio volcánico dentro del dique anular. Este flujo se orientó paralelamente a las márgenes del dique anular y quedó "congelado" en el momento de la final solidificación del magma.
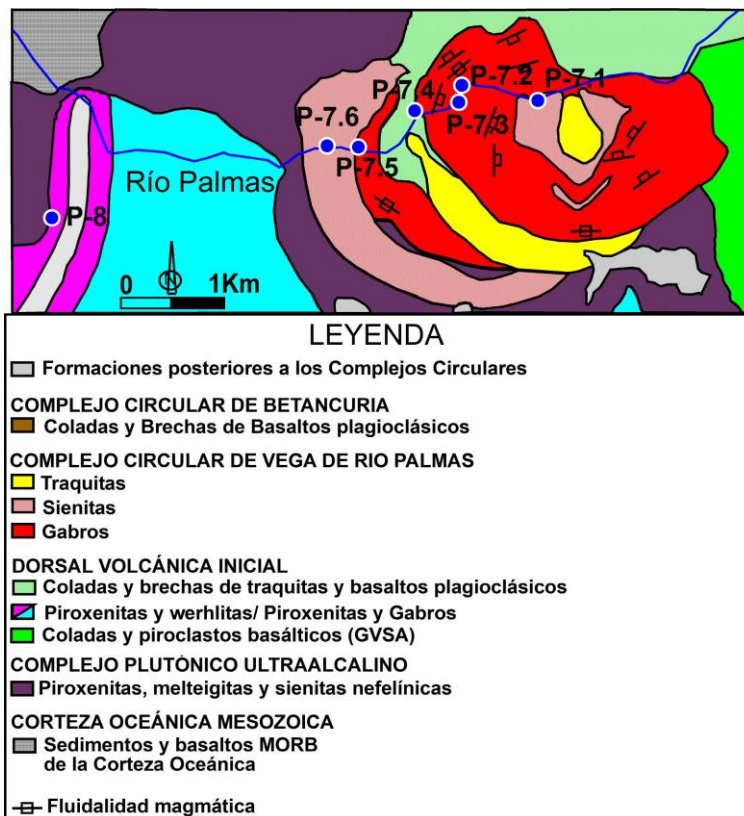
Fig. 31.- Mapa Geológico de la zona del complejo circular de Vega de Río Palmas. Se muestran las paradas 7 y 8 del itinerario. Tomado de Fúster *et al.* (1984a).

Las sienitas se ven atravesadas por diques de sienitas de grano fino (de bordes lobulados e irregulares) y por diques basálticos de color negro, de bordes más netos y rectos más tardíos, que cortan o atraviesan a los diques de sienitas de grano fino.

Tras caminar algunos cientos de metros por el fondo del barranco (P-7.2) nos encontramos con un leucogabro de grano medio-grueso, que constituye el siguiente dique anular del Complejo. En estos leucogabros los cristales blancos son de plagioclasa, los más oscuros de piroxeno, anfíbol y biotita. En ocasiones los minerales oscuros se concentran dando lugar a "bandas" también llamados *schlierens,* que diseñan una estructura planar que, como en el caso de las sienitas del Sargento, reflejan el flujo del magma en el interior del anillo poco antes de su total cristalización. En este punto este bandeado es vertical y se encuentra orientado al noreste. Los gabros se encuentran atravesados por diques de melanogabros de grano fino y leucogabros de grano fino.
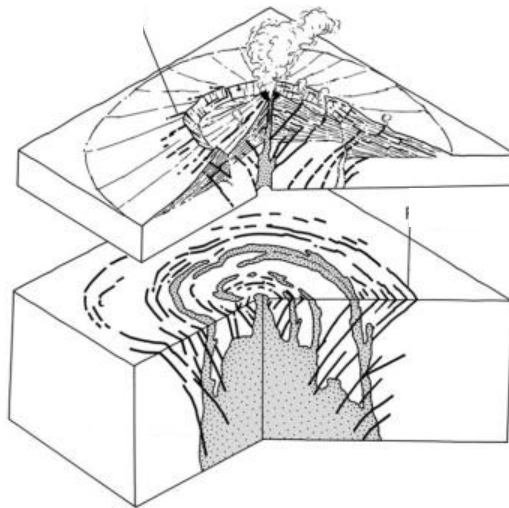
Fig. 32.- Reconstrucción del edificio volcánico asociado al Complejo Circular de Vega de Rio Palmas. Tomado de B. Natalin (Lecture 1: Introduction, geological structures, primary structures. En: Kinematic analysis of deformation. https://slideplayer.com/slide/8628093/).

Algunos metros más abajo del cauce (P-7.3) continuamos observando los leucogabros de grano medio-grueso con marcado flujo magmático. En este punto del itinerario aparece un contacto vertical entre los leucogabros de grano medio-grueso con melanogabros de grano

medio-fino que forman la parte más externa de este dique anular de gabros. En esta parte más externas del dique anular, el magma gabroideo cristalizó a mayor velocidad que en la parte más interna, debido al fuerte contraste de temperatura entre la roca encajante (más fría) y el propio magma (a unos 1000º C de temperatura), generando un mayor número de cristales pero que no pudieron crecer demasiado, dando lugar a un melanogabro de grano medio-fino, con cristales más pequeños que el leucogabro de grano medio-grueso de la parte más interna del dique anular.
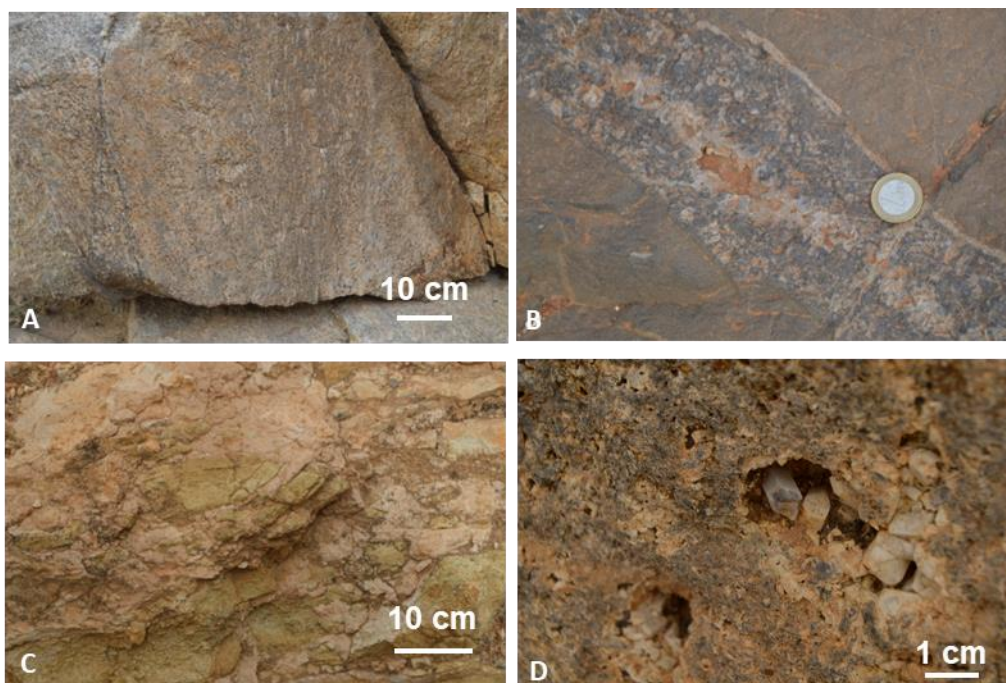
Fig. 33.- (a). Sienita nefelínica de El Sargento mostrando la orientación de los cristales de ortosa. (b). Diques de sienita nefelínica atravesando a las corneanas. (c). Gabros afectados por alteración hidrotermal en contacto con las sienitas de Las Peñitas. (d). Cristal de cuarzo junto a cristales de ortosa en cavidad miarolítica.

Si continuamos avanzando por el barranco (P-7.4), comprobamos cómo unos metros aguas abajo, éste se abre y cesan los berrocales a un lado y otro del barranco. En la margen derecha vemos una roca de color oscuro atravesado por venas de sienitas (Fig. 33b). La roca oscura es una brecha traquítica afectada por el metamorfismo de contacto provocado por la elevación de temperatura que sufrió esta roca en contacto con el magma que dio lugar al anillo interno de gabros próximo. Este calentamiento provocó la recristalización de la brecha

traquítica y dio lugar la corneana. Las venas de sienita proceden del mismo magma que dio lugar a las sienitas nefelínicas del anillo interno del Sargento que penetró en la corneana a través de fisuras existentes en la misma, de la misma manera que lo había hecho en la parada anterior a través de los gabros del anillo interno.

Poco más abajo, el este contemplamos el fuerte relieve que define el dique anular de traquita. Más adelante, por el mismo sendero, nos encontramos con los leucogabros de grano medio-grueso que forman parte de otro dique anular. En este punto, sobre los gabros se produce un curioso fenómeno de meteorización que da lugar a una "descamación en bolas" que llega a formar verdaderas esferas de roca.

Nos acercamos al tramo más espectacular del itinerario. Hacia el oeste aparece el paisaje impresionante que refleja la existencia del dique anular externo de sienitas de Las Peñitas que forma un espectacular "berrocal", único en las islas Canarias.

El dique anular se encuentra disectado por el Barranco de Río Palmas, dando lugar al Malpaso. Antes de entrar en el (Fig. 33c), nos encontramos con el contacto entre el dique anular externo de los leucogabros de grano medio-grueso y el dique anular de las sienitas de Las Peñitas. Este contacto viene marcado por la existencia de una traquita de grano fino que atraviesa y fragmenta los gabros, dando lugar a una brecha de intrusión en la que los fragmentos de gabros aparecen con un color verdoso-amarillento característico), debido a la transformación mineral que sufren los minerales del gabro al paso de aguas calientes procedentes de las sienitas.

Ya en el Malpaso, se nos descubre la sienita del dique anular de Las Peñitas (P-7.6). En esta zona cercana al contacto con los gabros, la sienita muestra un aspecto propio de un borde de enfriamiento: se trata de una roca de grano medio-grueso en el que destacan los fenocristales prismáticos de feldespato alcalino dando a la roca una textura porfídica. Los cristales de feldespato alcalino se orientan marcando una orientación heredera del flujo magmático, en este caso, vertical y de dirección norte-sur, que coincide con la dirección del contacto oriental del dique anular. A medida que atravesamos el Malpaso, y, alejarnos del

contacto oriental del dique anular, la sienita comienza a perder su carácter porfídico para convertirse en una roca de grano medio en la que los cristales prismáticos de feldespato alcalino forman un entramado entre los que hay cristales de color negro de piroxeno, anfíbol y biotita.

En algunas zonas la sienita muestra un aspecto muy particular: se encuentra salpicada por unas cavidades miarolíticas de 0,5 a 2 cm rodeadas de cristales de mayor tamaño entre los que son frecuentes los cristales prismáticos de cuarzo (Fig. 33d). En algunos casos, no existe la cavidad, pero los cristales de feldespato alcalino y de piroxeno y anfíbol adquieren tamaños de varios centímetros.

Más adelante, aparecen enclaves de esta sienita miarolítica incluidas en la sienita general de grano medio. Seguramente la sienita miarolítica cristalizó tempranamente desde el magma en las zonas más someras del anillo (la cúpula), a baja presión y con gran cantidad de fluido acuoso formando una plancha superior que, posteriormente el magma sienítico inferior, en movimiento y en proceso de cristalización, fracturó, fragmentó, incorporando estos fragmentos a la masa magmática en movimiento, trasladando y distribuyendo los enclaves de sienita miarolítica a lo largo de todo el dique anular.

El descenso del Malpaso resulta ser uno de los paseos más impresionantes de la isla majorera. A ambos lados del barranco nos llama la atención las formas del "berrocal" sienítico : "yelmos", "bolos", "tafonis". En el cauce del barranco aparecen numerosos charcos de agua que rellenan "pilancones" o "marmitas de gigantes".

Parada 8.

El metamorfismo de contacto asociado a los cuerpos plutónicos ultramáficos.

En el contacto entre las rocas plutónicas asociadas a la Dorsal Inicial y las rocas del Complejo Plutónico Ultra-alcalino se produce un intenso metamorfismo de contacto que es posible observar en el barranco de Pájara (punto P-8 en las Figuras 3 y 31).

En este punto, aparecen apófisis de piroxenitas olivínicas y werlhitas (Fig. 34b) que penetran a las rocas plutónicas ultra-alcalinas (piroxenitas, iolitas, pegmatitoides ijolíticos, sienitas), afectadas por importantes zonas de cizallas dúctiles, y los diques basálticos que las atraviesan (Fig.34a) dando lugar a intensas interdigitaciones. Las rocas de caja, especialmente los diques, generan un intenso bandeado anatectítico dando lugar a la aparición de "rocas cebradas" (Figs. 34c y 34d). Este bandeado anatéctico está muy condicionado en su orientación por la disposición de las zonas de cizalla conjugadas que afectan a las rocas ultra-alcalinas. El paleosoma restítico de color negro está constituido por un agregado granonematoblástico de clinopiroxeno, anfíbol, flogopita, ilmenita, magnetita y plagioclasa accesoria (Muñoz *et al.*, 2008). La composición del leucosoma varía entre sienita y sieno-diorita. El conjunto anatexítico también se encuentra atravesado por venas de gabros relacionados con las apófisis de piroxenitas. En algunos puntos aparecen diques basálticos posteriores que atraviesan tanto a las rocas de caja, como a las piroxenitas y wehrlitas.
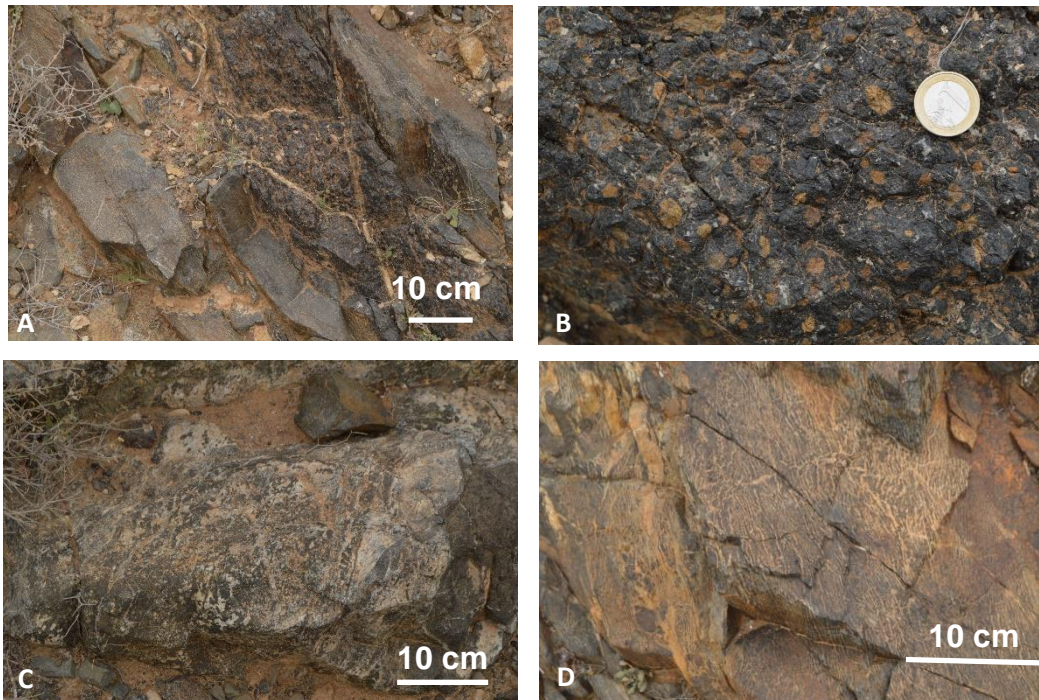
Fig. 34.- (a). Werhlita penetrando entre los diques anatatécticos. (b). Detalle de la wehrlita. (c). Pegmatitoides ijolíticos. (d). Anatexita (roca "cebrada") con el paleosoma y el leucosoma.

-C.4.- ITINERARIO 3.

Grandes deslizamientos gravitacionales en Fuerteventura: el deslizamiento del Puerto de Rosario Norte (Figs. 3 y 19).
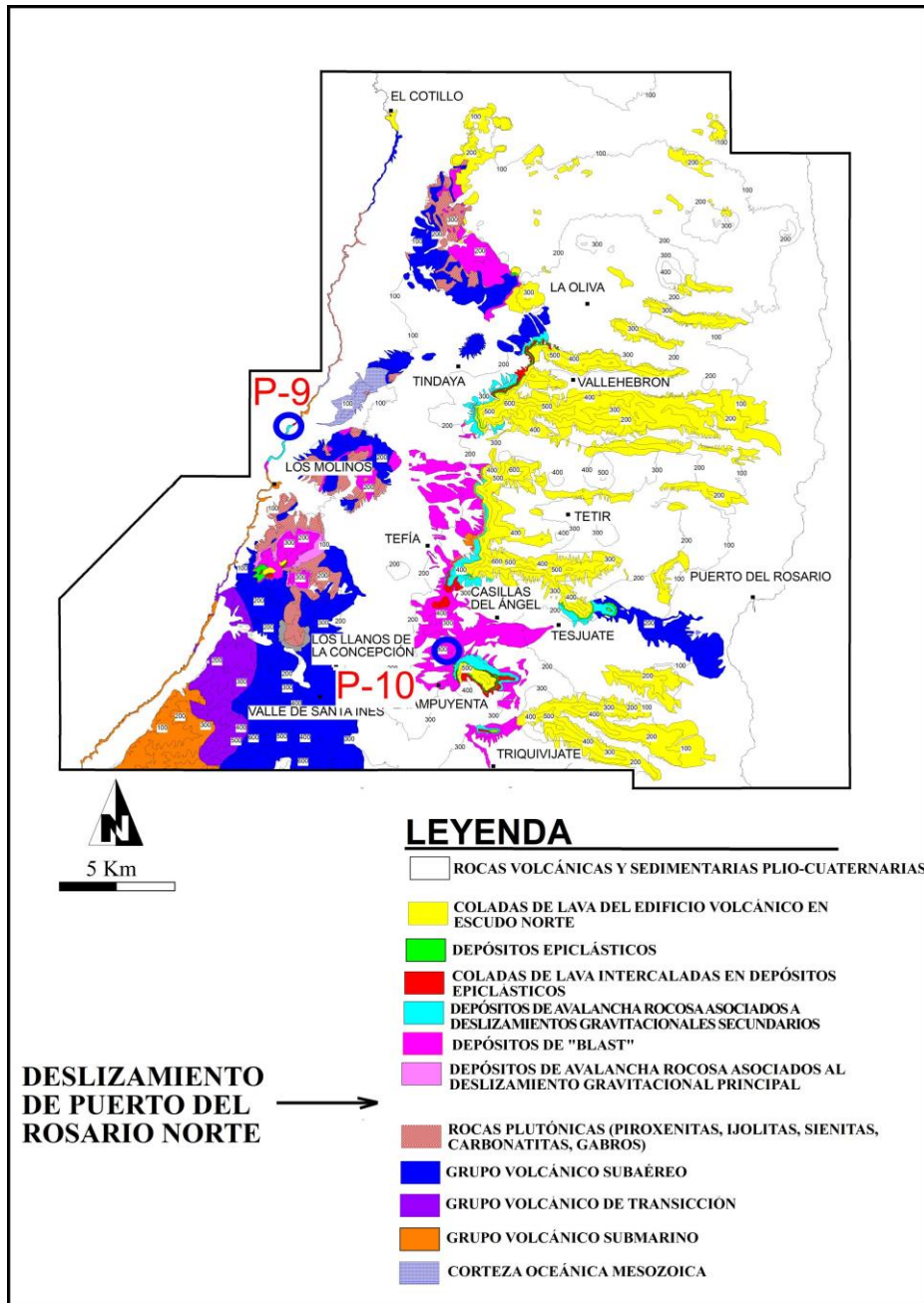
Fig. 35.- Mapa geológico de la parte norte de Fuerteventura. Se señalan los puntos del itinerario.

Parada 9.

Depósitos de avalancha de derrubios asociados al deslizamiento gravitacional del flanco occidental de la Dorsal Inicial en la costa de Los Molinos (deslizamiento gravitacional de Puerto del Rosario Norte).

Hace unos 14,5 Ma, el edificio Dorsal Inicial de la isla de Fuerteventura sufrió un deslizamiento gravitacional de toda la parte septentrional de su flanco occidental (Fig. 36). Los restos de la avalancha de derrubios producida tapizan el fondo del océano al oeste de la isla y también están presentes en el sector septentrional y central de la misma. La decapitación de la cámara magmática profunda del edificio volcánico por el deslizamiento produjo una explosión lateral dirigida (*blast*) que generó un flujo piroclástico denso estratificado (PDF) que cubrió los depósitos de avalancha previamente depositados. El deslizamiento produjo una enorme depresión abierta al oeste, que continuó rellenándose con materiales epiclásticos procedentes de deslizamientos menores y secundarios que afectaron a las paredes de la depresión, y del retrabajamiento erosivo de los propios depósitos del *blast* y de la avalancha principal. El proceso de relleno estuvo acompañado por la reanudación de la actividad volcánica en forma de erupciones subaéreas, algunas de ellas hidrovolcánicas.
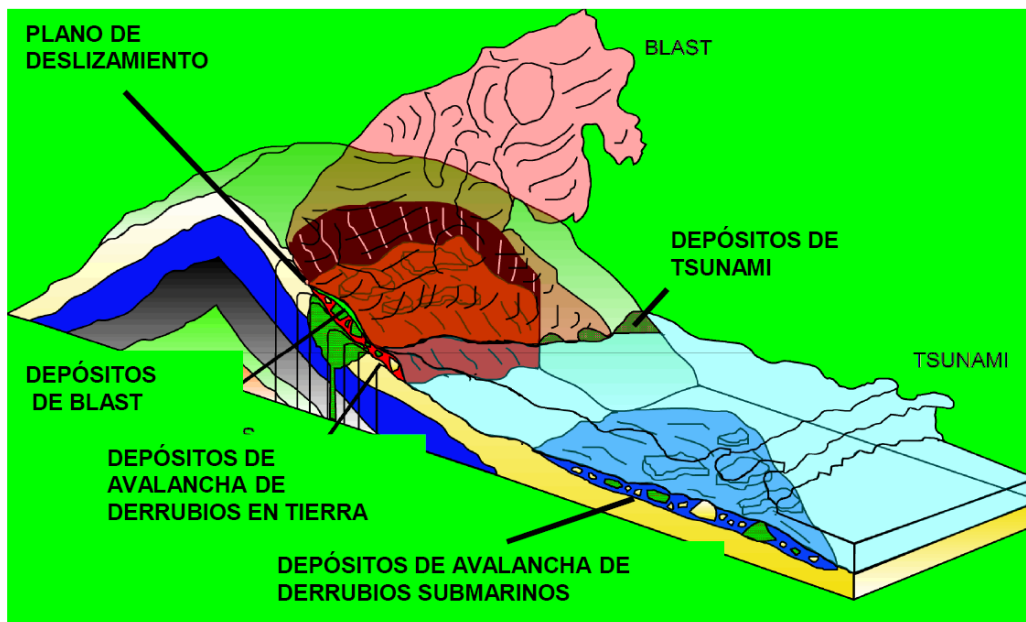
Fig. 36.- Recreación del deslizamiento gravitacional de Puerto del Rosario Norte.

En la costa occidental de Fuerteventura, al norte del Puertito de Los Molinos, aflora la superficie basal de deslizamiento de Puerto del Rosario Norte (DPRN).

Los materiales que asociamos al DPRN se disponen por encima de la superficie basal del deslizamiento sobre las rocas volcánicas submarinas de la Dorsal Inicial (Grupo Volcánico Submarino, GVS) (Fig. 37). Este conjunto está cubierto discordantemente por las coladas basálticas mio-pliocenas que truncan la superficie del deslizamiento (Fig. 37a). Bajo la superficie basal, los 4 m superiores del GVS están totalmente triturados y deformados en bandas adelgazadas y estiradas siguiendo planos paralelos a la superficie del deslizamiento. Estas bandas están integradas por brechas foliadas con clastos basálticos "supervivientes" (*survivor grains*) de 5 a 30 cm de diámetro, mayormente sub-redondeados y con poca evidencia de fracturación (Fig. 37b). En esta zona, con frecuencia, es posible reconocer los diferentes niveles de brechas de fragmentos de almohadillas y diques, a pesar de la intensa fracturación, que constituyen fragmentos de hasta 10-15 cm incluidos en una matriz cataclástica de grano fino. En las proximidades de la superficie del deslizamiento, las bandas estiradas dan lugar a una brecha granular foliada que a menudo muestra una intensa mezcla de los fragmentos, así como cambios abruptos en el espesor de las capas, pliegues, estructuras de flujo y otros signos de ductilidad mesoscópica. En todo este sector de la isla, los diques que atraviesan las rocas de la Dorsal Inicial (el Grupo Volcánico Submarino, el Grupo Volcánico Subaéreo, y las rocas plutónicas) se encuentran plegados bajo la superficie del deslizamiento.

Desde la superficie de deslizamiento, y a lo largo de la base del acantilado, se ha podido reconstruir la sección estratigráfica mostrada en la Fig. 38, integrada por una sucesión de aproximadamente 100 m de materiales epiclásticos (brechas, conglomerados y arenas), hialoclásticos y volcánicos. El estudio petrográfico y sedimentológico realizado en estos materiales nos ha permitido diferenciar cinco tipos de facies, cuyos caracteres más relevantes se han sintetizado en la Tabla I. La parte inferior de la sucesión (Fig. 38) está constituida por cinco niveles de brechas y/o, en menor medida, conglomerados (Fig. 37c, facies BS1) que se encuentran por debajo de un paquete de lavas almohadilladas (Fig. 37d, facies LS1). Su asociación con lavas almohadilladas (LS1) e hialoclastitas (BS2) sugiere que la sedimentación de estos cinco niveles tuvo lugar en zonas de pendiente submarina, relativamente poco profundas, por corrientes de turbidez de alta densidad producidos por la

transformación subacuática de flujos de gravedad (*debris flows*) desarrollados por la transformación subaérea de las avalanchas de derrubios (*debris-avalanches)* producidas por el deslizamiento basal principal y otros secundarios, del DPRN (Casillas *et al.,* 2012). Este tipo de transformaciones subacuáticas (Lowe, 1982; Mutti *et al.*, 1996; Sohn *et al.*, 1999) lleva aparejada la aparición de dos flujos asociados: uno inercial, basal y denso, de movimiento más rápido, donde la turbulencia se amortigua por una alta concentración de sedimentos; y otra superior, de un flujo turbulento y más diluido. Mientras que en zonas próximas a la costa se produjo la sedimentación de la mayor parte de los depósitos transportados por el flujo inercial, el flujo acompañante superior más diluido sobrepasó estos depósitos y, probablemente, pudo recorrer grandes distancias sobre el talud insular y la llanura abisal hasta llegar a zonas tan alejadas como la llanura abisal de Madeira, dando lugar a varias secuencias turbidíticas, similares a las que describen Wynn & Masson (2003) para el deslizamiento de El Golfo (El Hierro) y el de Icod-Las Cañadas (Tenerife) y en las secuencias de turbiditas volcanoclásticas del Mioceno medio estudiadas por Alibés *et al.* (1999) y Hunt *et al.* (2012). En el caso de Fuerteventura, los diferentes flujos diluidos acompañantes pudieron generar, al menos, cinco secuencias turbidíticas, sobre el fondo oceánico en muy poco tiempo. Otras facies epiclásticas presentes en la sucesión están formadas por arenas de grano grueso masivas o groseramente gradadas (facies SS1) y alternancias rítmicas granodecrecientes de arenas gruesas y finas (facies SS2). Las primeras se interpretan como un depósito a partir de una corriente turbidítica de alta densidad, similar a la división S3 de Lowe (1982) o las facies F5 de Mutti *et al.* (1999). La facies SS2 tiene caracteres similares a los depósitos de alfombra de tracción (*traction carpet*) descritos por Mutti (1992) y Sohn (1997). Por último, las lavas almohadilladas (Facies LS1) y las brechas de fragmentos de almohadillas (Facies BS2) se interpretan como el resultado del desarrollo y colapso de deltas de lava en la costa como consecuencia de la llegada a la misma de flujos lávicos procedentes de erupciones subaéreas. La aparición de estos materiales subacuáticos por encima del nivel del mar actual parece estar relacionada con un levantamiento generalizado de la parte occidental de Fuerteventura, posiblemente relacionado con el reajuste isostático sufrido por esta parte de la isla como consecuencia de la enorme liberación de masa provocado por el DPRN.
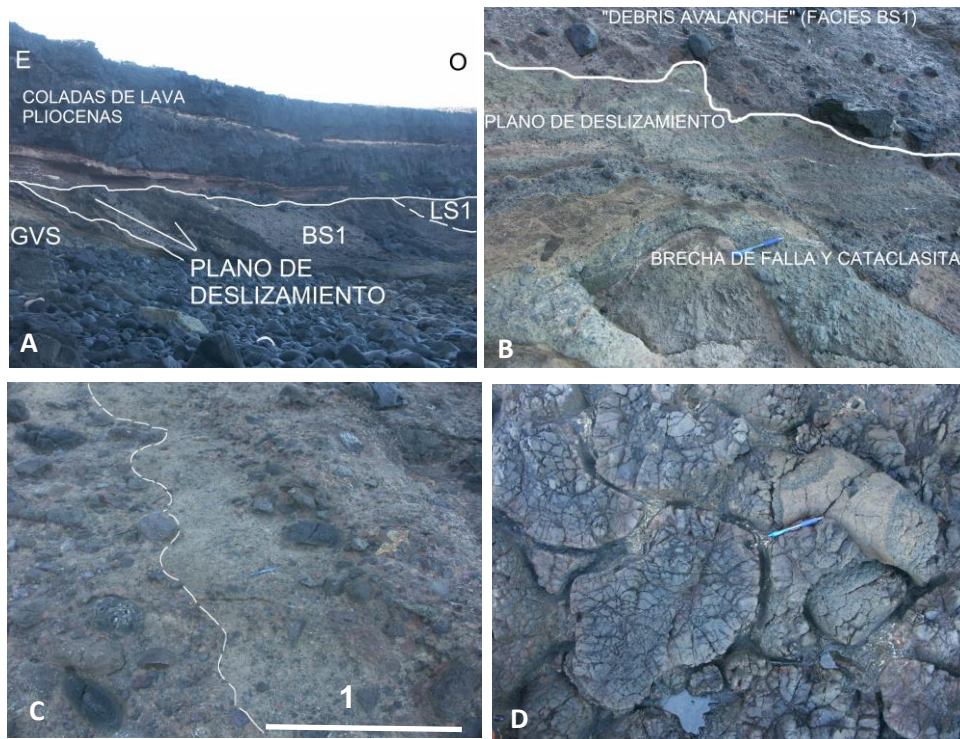
Fig. 37.- (a) Aspecto general del afloramiento. (b) Detalle del plano de deslizamiento. (c) Detalle de las facies BS1 (brechas/conglomerados) con gradación inverso-normal. (d) Facies LS1 (lavas almohadilladas).

Simbología

Nivel de concentración de cantos

Clastos plutónicos (gabros, piroxenitas, sienitas)

Clastos volcánicos (basaltos, traquitas, piroclastos basálticos, pómez)

Laminación cruzada de bajo ángulo

Laminación paralela

Plano de deslizamiento

Lavas almohadilladas. Facies LS1.

Brechas/Conglomerados. Facies BS1.

Brechas de fragmentos de almohadillas. Facies BS2A.

Brechas de fragmentos de almohadillas matriz-soportadas. Facies BS2B.

Arenas gruesas masivas. Facies SS1.

Alternancias de arenas de grano grueso y arenas de grano fino. Facies SS2.

Brecha de falla y cataclastitas.

10 metros

S P C B

Fig. 38.- Columna estratigráfica de la parada 9.

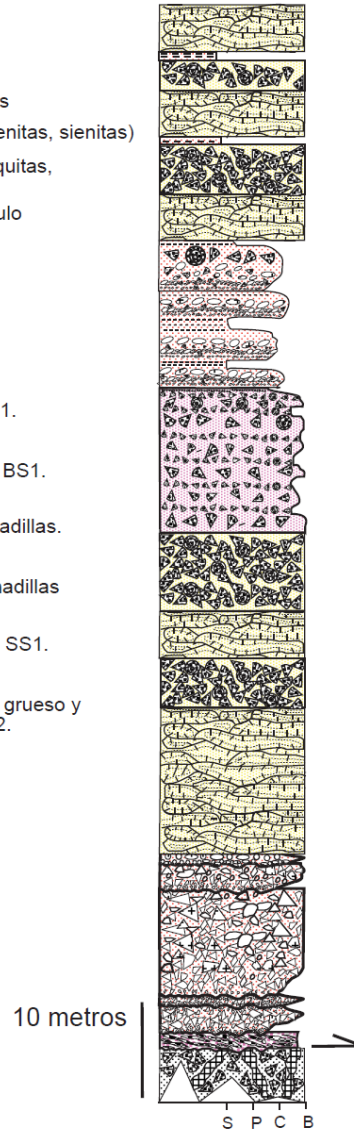| FACIES	LITOLOGÍA, TEXTURAS ESTRUCTURAS SEDIMENTARIAS Y ESTRATIFICACIÓN	APARICIÓN Y ESPESORES	INTERPRETACIÓN
(BS1) Brechas /Conglomerados.	Brechas (en menor medida conglomerados) clasto y matriz-soportadas, moderada a mal clasificadas. Clastos subangulosos a bien redondeados de basaltos vacuolares, diques basálticos, almagres, gabros, piroclastos basálticos, fragmentos de almohadillas y de traquitas. Contenido variable de matriz de arena a grava gruesa. Forman secuencias granocrecientes-granodecrecientes, con contactos netos y erosivos, con arenas gruesas y gravas de grano medio laminadas en la base, que evolucionan verticalmente a brechas con clastos de 5-10 cm de diámetro que hacia el techo pasan ser más arenosas y adquieren una distribución bimodal de los fragmentos con clastos dispersos de hasta 3 m de diámetro. En las capas más conglomeráticas los clastos son subredondeados y redondeados y se imbrican con el eje mayor hacia el O.	Aparecen sobre la superficie de deslizamiento principal o sobre las facies BS2. Forma secuencias granodecrecientes con las facies SS1 y SS2. Espesor entre 1-15 m.	Deposición a partir de flujos de derrubios y corrientes de turbidez de alta densidad (*"high density gravelly turbidity currents"* en el sentido de Lowe, 1982). Las facies observadas corresponderían a las divisiones R2 y R3 de Lowe (1982) o a la facies F3 de Mutti *et al.* (1999). Los niveles más brechoides corresponderían a la transformación submarina de las avalanchas de escombros generadas por el deslizamiento principal y otros secundarios. Los niveles más conglomeráticos y con fragmentos de almohadillas corresponderían a la transformación subacuática de los flujos hiperconcentrados subaéreos y del colapso de las lavas almohadilladas presentes en los deltas de lava.
(BS2) Brechas de fragmentos de almohadillas.	Brechas clasto (BS2A) y matriz-soportadas (BS2B) de fragmentos subangulosos de hasta 3 m de diámetro de lavas almohadilladas con la típica textura en "trozo de tarta". Matriz hialoclastítica de tamaño arena-grava fina, a veces, con una grosera laminación paralela.	Tramos de espesor variable entre 1 y 30 m alternando con o superpuestas a la facies LS1.	Depósitos de pendiente y base de deltas de lava generados por el colapso de los apilamientos de lavas almohadilladas (facies LS1) en las partes superiores de los deltas.
(SS1) Arenas gruesas masivas.	Arenas gruesas masivas o con grosera gradación normal.	Se encuentran superpuestas a la facies BS1. A techo suelen transitar a las facies SS2. Espesor variable entre 5-30 cm.	Sedimentación en masa desde una corriente de turbidez de alta densidad después de la zona de deposición de los flujos gravitatorios de gravas, brechas y conglomerados representados por las facies BS1. Equivalentes a la división S3 de Lowe (1982) o las facies F5 de Mutti *et al.* (1999).
(SS2) Alternancias rítmicas de arenas gruesas a finas.	Alternancias rítmicas de gravas finas-arenas gruesas-arenas finas (de milímetros hasta algún centímetro), constituyendo secuencias grano y estratodecrecientes.	Aparecen a techo de BS1 y SS1. Espesor 5-30 cm.	Depósitos de alfombra de tracción (*traction carpet*) generados por corrientes turbidíticas de alta densidad de tipo F7 de Mutti *et al.* (1999).
(LS1) Lavas almohadilladas.	Lavas almohadilladas poco vesiculadas en tubos continuos de hasta 75 cm de diámetro con gran cantidad de fracturas radiales y concéntricas. Entre los tubos hay escaso material hialoclastítico y algún hueco.	Se apoyan en las facies BS1 o BS2, formando 5 niveles de espesor variable entre 3 y 25 m.	Flujos lávicos procedentes de erupciones subaéreas que atraviesan la línea de costa formando deltas de lava.

Tabla I.- Descripción e interpretación de las principales litofacies submarinas relacionadas con el deslizamiento gravitacional de Puerto del Rosario Norte.

Parada 10.

Depósitos de avalancha de derrubios (debris avalanches) asociados al deslizamiento gravitacional del flanco occidental de la Dorsal Inicial en La Ampuyenta (deslizamiento gravitacional de Puerto del Rosario Norte).

En tierra, como consecuencia de este deslizamiento podemos encontrar toda una serie de materiales subaéreos relacionados con el mismo, diferenciando las facies epiclásticas de las piroclásticas y de las hidroclásticas. La Tabla II resume los caracteres y la interpretación de las facies epiclásticas subaéreas, diferenciadas. Las facies A y B1 corresponden a depósitos de avalancha de derrubios formados por los deslizamientos gravitacionales principal y secundarios. Las facies B2, B3, B4, C1, C2 y C3 representan depósitos formados por el retrabajamiento erosivo posterior de los niveles de avalancha mediante flujos hiperconcentrados cargados de clastos gruesos-muy gruesos, angulosos o redondeados. En el

caso de las facies C4 y C5 el mecanismo de transporte parece haber sido corrientes acuosas de alta energía. Las facies D y E se interpretan como pequeñas llanuras de inundación.

En esta parada podemos observar las características más significativas de las facies A (Megabloques) y B 1(Brechas matriz-soportadas) asociadas al deslizamiento principal (Figs. 37 y 38).
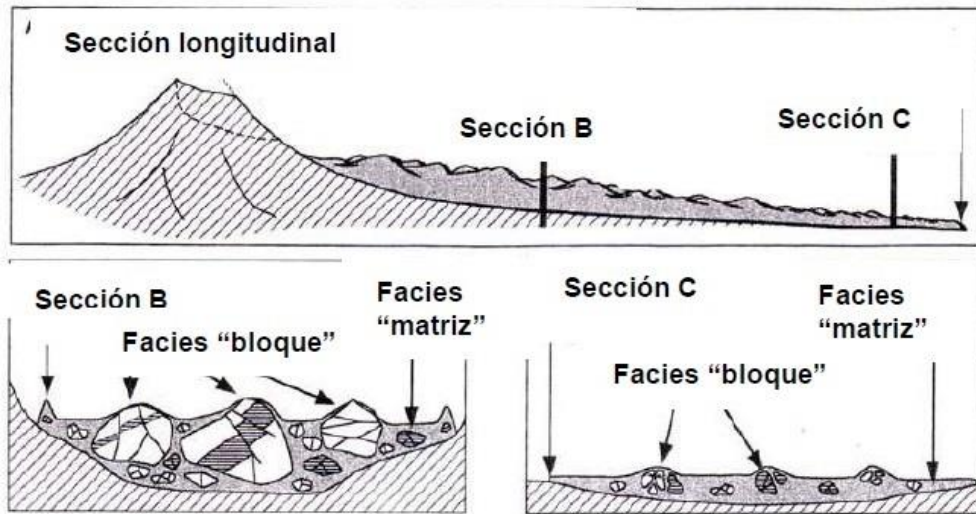

Fig. 39.- Esquema de un megadeslizamiento gravitacional y posición de las facies "bloque" y "matriz". Tomado de Oehler, (2005).

FACIES	LITOLOGÍA Y ESTRATIFICACIÓN	TEXTURAS Y ESTRUCTURAS SEDIMENTARIAS	INTERPRETACIÓN
A: MEGABLOQUES	Megabloques decamétricos y hectométricos muy pobremente clasificados.de basaltos plagioclásicos, diques y gabros. Matriz abundante de granulometría variable entre arcilla y canto. Espesor: 20->200 m	Fábrica desordenada y caótica; Abundantes diques clásticos arenosos y megabloques con *jigsaw cracks*	Facies de Megabloques de *debris avalanches* formada por un deslizamiento gravitacional "seco"
B1: BRECHAS MATRIZ-SOPORTADAS	Muy heterométricas. Bloques de hasta 1,5 m de diámetro, muy pobremente clasificados, de basaltos, traquitas, diques y gabros. Matriz muy abundante de grava fina-arena gruesa muy mal clasificada. Espesor: 2->100 m	Fábrica desordenada. Las capas tienen bases graduales e inversamente gradadas y los techos son netos o con gradación normal. Escasos clastos con *jigsaw-cracks*. Diques clásticos arcillosos	Facies de Matriz de *debris avalanches*
B2: BRECHAS CLASTO-SOPORTADAS	Muy heterométricas. Clastos de tamaño bloque y canto, menores que los de la facies B1. Matriz de arena gruesa-grava fina, escasa y bien a moderadamente clasificada. Espesor: 1,5-20 m	Fábrica desordenada o con gradación inversa a normal	*Flujos hiperconcentrados* generados por removilización del material del *debris avalanche*. La fábrica desordenada y escasa abrasión de los clastos indican un transporte muy reducido
B3: BRECHAS CLASTO-SOPORTADAS CON GRADACIÓN INVERSA	Clastos de 4,5 cm de tamaño medio y 70 cm de máximo, mal clasificados. Matriz escasa de arena gruesa-grava fina bien a moderadamente clasificada. Espesor: 0,7-2 m	Gradación inversa y base gradual o ligeramente erosiva; clastos groseramente ordenados paralelamente a la estratificación o imbricados con el eje a.	*Flujos hiperconcentrados* con transporte mayor que el de la facies B2. Soporte de los clastos principalmente por presión dispersiva
B4: BRECHAS CON INTERCALACIONES DE GRAVAS Y ARENAS	Las brechas son clasto y matriz-soportadas, muy heterométricas y con clastos <2 m; la matriz es abundante y de grava fina-arena gruesa, mal clasificada. Las gravas son finas y las arenas gruesas-muy gruesas, ambas con cantos y bloques dispersos. Los limos son escasos, con clastos de tamaño grava-canto. Capas irregulares <2 m, lateralmente discontinuas	Las brechas están desordenadas o con los clastos groseramente orientados o imbricados con el eje a; gradación inversa y normal. Las arenas y graveas muestran una grosera laminación paralela y cruzada de bajo ángulo. Los limos están laminados y tienen colores rojizos. Forman secuencias granodecrecientes groseras	*Flujos hiperconcentrados* probablemente canalizados con transición vertical a flujos acuosos arenosos
C1: CONGLOMERADOS MATRIZ-SOPORTADOS	Clastos de 20 cm tamaño medio y 1,20 de máximo, polimodales y bimodales, redondeados a subredondeados. Matriz abundante de arena gruesa-grava fina bien seleccionada	Fábrica desordenada	*Flujos hiperconcentrados* locales con clastos erosionados y retrabajados de zonas adyacentes. Escaso transporte y capacidad de selección. Idéntico a B2
C2: CONGLOMERADOS CLASTO-SOPORTADOS	Clastos de hasta 1,20 m de diámetro de basaltos y diques principalmente. Matriz: arena gruesa-grava fina, bien clasificada. Espesor:o,7-20 m	Masivos o groseramente estratificados; los clastos se hallan dispuestos con el eje a paralelo a la estratificación o imbricado. Pueden mostrar gradación inversa en la base y normal en el techo	*Flujos hiperconcentrados con gravas*, con fuerte interacción entre los clastos y rápida sedimentación. Soporte de los clastos principalmente por presión dispersiva, similar a B3
C3: CONGLOMERADOS, GRAVAS Y ARENAS INTERESTRATIFICADOS	Los conglomerados tienen diámetro medio de 10 cm y máximo de 30 cm, con bloques dispersos de hasta 2 m. Las gravas y arenas (gruesas a muy gruesas y mal clasificadas) forman capas irregulares y tienen cantos dispersos o en pequeñas lentes. Espesor: 10-30 m	Estratos irregulares y lenticulares con base erosiva y clastos orientados paralelamente a la estratificación o imbricados con el eje a. En ocasiones las litologías forman secuencias inversas y normales. Laminación paralela y cruzada planar y en surco en las arenas	*Flujos hiperconcentrados* probable-mente canalizados con transición vertical a flujos acuosos arenosos, similar a B4
C4: CONGLOMERADOS Y ARENAS EN SECUENCIAS CANALIFORMES	Conglomerados de cantos (15 cm de diámetro máximo) y gravas, en capas de 1-5 m. Arenas limosas en capas de 30-50 cm. Espesor: <35 m	Se ordenan formando secuencias granodecrecientes con base erosiva. Es frecuente la estratificación cruzada en surco de mediana-gran escala, la laminación paralela y la bioturbación figurativa	Flujos acuosos tractivos canalizados de energía decreciente de tipo *stream floods*
C5: GRAVAS FINAS Y ARENAS INTERESTRATIFICADAS	Arenas de grano muy grueso con cantos y bloques de hasta 1 m, dispersos u ordenados en láminas y lentes. Espesor: 0,5-3 m	Forman secuencias granodecrecientes con bases netas o ligeramente erosivas; las arenas muestran laminación paralela y cruzada de mediana–gran escala; imbricación del eje a en los clastos	Corrientes acuosas de tipo *stream* y *flash floods*. Posibles equivalentes distales de los flujos hiperconcentrados, que podrían llegar a estar representados en las lentes de cantos y bloques
D: ALTERNANCIA DE ARENAS Y LIMOS	Grano fino con clastos de 2-3 cm dispersos o formando lentes delgadas. Espesor: <2 m	Masivas o laminadas y con bioturbación vegetal	Débiles corrientes tractivas y desarrollo de paleosuelos inmaduros en llanuras de inundación efímeras
E: LIMOLITAS	Grano fino	Laminación paralela; color ocre	Llanuras de inundación efímeras

Tabla II.- Descripción e interpretación de las principales litofacies epiclásticas subaéreas relacionadas con el deslizamiento gravitacional de Puerto del Rosario Norte.
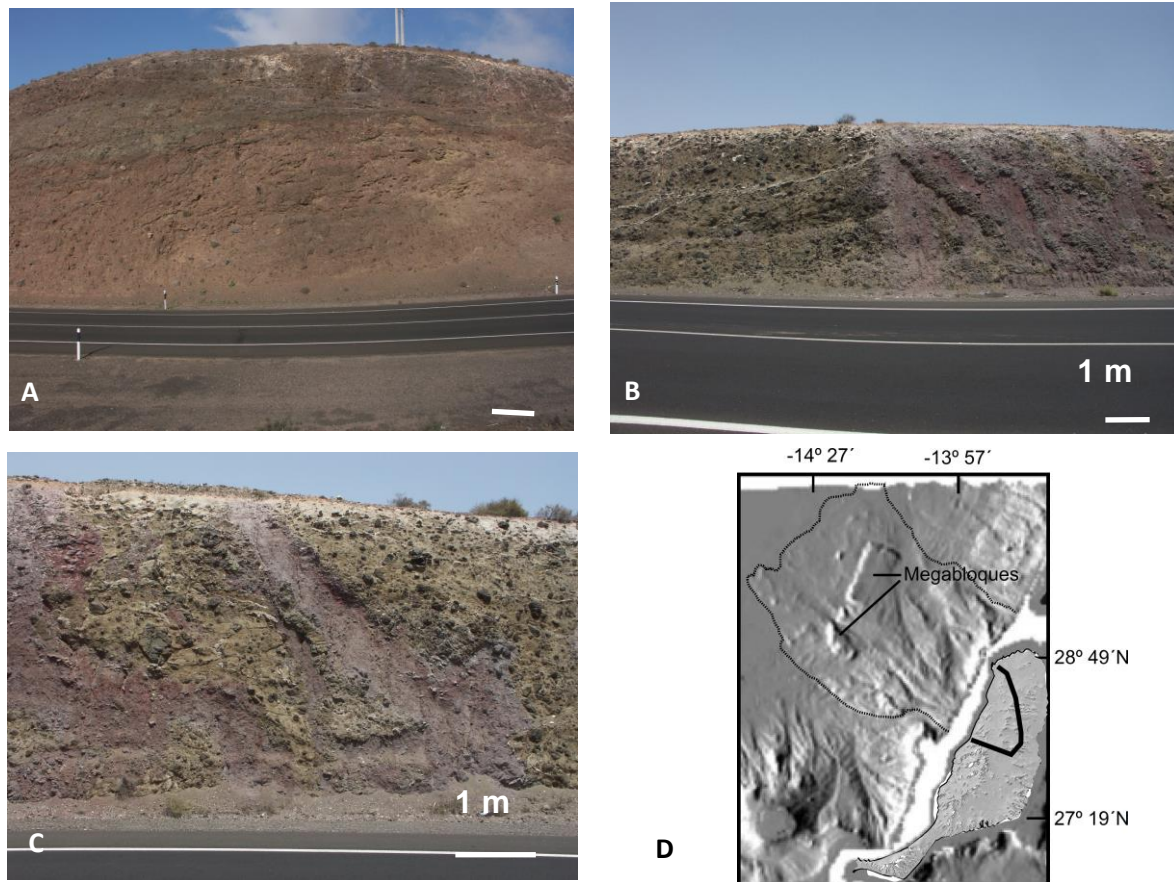
Fig. 40.- (a) Aspecto de las facies "Matriz". (b) Aspecto de las facies "Bloque". (c) Detalle de las facies "Bloque". (d) Extensión y alcance subaéreo y submarino del deslizamiento de Puerto del Rosario Norte. Nótese la aparición de megabloques submarinos a unos 50 kilómetros de Fuerteventura.

Transferencia de la ULL, a través de la financiación para la organización de congresos, reuniones científicas, jornadas o seminarios de carácter nacional e internacional durante el año 2023.

Referencias:

Abdel Monen, A., Watkins, N.D., & Gast, P.W. (1971). Potassium–argón ages, volcanic stratigraphy, and geomagnetic polarity history of the Canary Islands: Lanzarote, Fuerteventura, Gran Canaria and La Gomera. *Am. J. Sci.* 271, 490–521.

Acosta, J., Uchupi, E., Muñoz, A., Herranz, P., Palomo, C., Ballesteros, M. & ZEE Working Group, (2003). Geologic evolution of the Canarian Islands of Lanzarote, Fuerteventura, Gran Canaria and La Gomera and comparison of landslides at these islands with those at Tenerife, La Palma and El Hierro. *Marine Geophysical Researches*, 24, 1-40.

Ahijado, A. (1999). *Las intrusiones plutónicas e hipoabisales del sector meridional del Complejo Basal de Fuerteventura*. Tesis Doctoral. Universidad Complutense de Madrid, 392 p.

Ahijado, A. y Hernández-Pacheco, A. (1990). Las rocas ultramáficas alcalinas del Jable de Salinas, Fuerteventura, Islas Canarias. *Revista de la Sociedad Geológica de España*, 3, 275-287.

Ahijado, A. y Palacios, T. (1991). Synchysita en las carbonatitas de la Pta. del Peñón Blanco, Fuerteventura, Islas Canarias. *Geogaceta*, 10, 83-84.

Ahijado, A. y Hernández-Pacheco, A. (1992). El complejo ultramáfico-carbonatítico del Macizo de Amanay, Fuerteventura, Islas Canarias. *Actas del III Congreso Geológico de España y VIII Congreso Latinoamericano de Geología,* 1, 315-318.

Ahijado, A., Hernández-Pacheco, A. y Mata, J. (1992). Características geoquímicas de las carbonatitas de la Punta del Peñon Blanco. Fuerteventura. Canarias. *Geogaceta*, 11, 120-122.

Ahijado, A., Casillas, R., & Hernández-Pacheco, A. (2001). The dike swarms of the Amanay Massif, Fuerteventura, Canary Islands. *Journal of Asian Earth Science,* 19, 333-345.

Alibés, B., Rothwell, R., Canals, M., Weaver, P, & Alonso, B. (1999). Determination of sediment volumes, accumulation rates and turbidite emplacement frequencies on the Madeira Abyssal Plain (NE Atlantic): A correlation between seismic and borehole data. *Marine Geology*, 160(3), 225–250. 10.1016/S0025-3227(99)00026-2

Allibon, J., Bussy, F., Lewin, E. & Darbellay, B. (2011a). The tectonicallycontrolled emplacement of a vertically sheeted gabbro–pyroxenite intrusion: Feeder-zone of an ocean-islandvolcano (Fuerteventura, Canary Islands). *Tectonophysics* 500, 78–97.

Allibon, J., Ovtcharova, M., Bussy, F., Cosca, M., Schaltegger, U., Bussien, D. & Lewin, E. (2011b). Lifetime of an ocean island volcano feeder zone: constraints from U–Pb dating on coexisting zircon and baddeleyite, and Ar-40/Ar-39 age determinations, Fuerteventura, Canary Islands. *Canadian Journal of Earth Sciences* 48, 567–592.

Ancochea, E., Brandle, J.L., Cubas, C. R., Hernán, F. y Huertas, M. J. (1993). La Serie I de la Isla de Fuerteventura. *Memoria de la Real Acad. de Cien. Ex. Fís. y Nat. Serie de Ciencias Naturales,* 27, 151 pp.

Ancochea, E., Brändle, J.L., Cubas, C.R., Hernán, F. & Huertas, M.J. (1996). Volcanic complexes in the eastern ridge of the Canary Islands: the Miocene activity of the island of Fuerteventura*. Jour.Volcanol. Geoth. Res*., 70, 183-204.

Anderson, D.L., Tanllnoto, T., & Zhang, Y. (1992). Plate tectonics and hotspots: the third dimension. *Science* 256, 1645-1651.

Balcells, R., Barrera, J.L., Gómez, J.A., Cueto, L.A., Ancochea, E., Huertas, M. J., Ibarrola, E. y Snelling, N. (1994). Edades radiométricas en la Serie Miocena de Fuerteventura. (Islas Canarias). *Bol. Inst. Geol. Min. España,* 35, 450-470.

Balcells, R. J., Barrera, J. L. y Gómez Sainz de Aja, J. A. (2006). Mapa Geológico de España a escala 1: 100:000. Fuerteventura (92). Mapa y Memoria. Instituto Geológico y Minero de España. Madrid. 108 pp.

Balogh, K., Ahijado, A., Casillas, R. & Fernández, C. (1999). Contributions to the chronology of the Basal Complex of Fuerteventura, Canary Islands. *Jour.Volcanol. Geoth. Res.,* 90, 81-102.

Banda, E., Surinach, E., Udías, A., Dañobeitia, J.J., Mueller, S.T., Mézcua, J., Boloix, M., Ortiz, R. & Correig, A. (1980). Explosion seismology study of the Canary Inlands-first results. Abstracts. 7th EGS-ESC Meeting. Budapest, 5 pp.

Banda, E., Dañobeitia, J.J., Surinach, E. & Ansorge, J. (1981). Features of crustal structure under the Canary Islands.*Earth Planet. Sci. Letters,* 55, 11-24.

Barrera, J.L., Fernández Santín, S., Fúster, J.M. y Ibarrola, E. (1981). Ijolitas-Sienitas-Carbonatitas de los Macizos del Norte de Fuerteventura. *Bol. Inst. Geol. Min. España,* TXCII-IV, 309-321.

Bosshard, E. & Macfarlane, D. J. (1970). Crustal structure of the western Canary Islands from seismic refraction and gravity data. *Jour. Geophys. Res.,* 75, 901-4918.

Cantagrel, J.M., Fúster, J.M., Pin, C., Renaud, U. et Ibarrola, E. (1993). Age Miocène inférieur des carbonatites de Fuerteventura. *Compte Rendues de la Academie de Sciences de Paris*, 316, 1147-1153.

Caress, D.W., McNutt, M.K., Detrick, R.S. & Mutter, J.C. (1995). Seismic imaging of hotspot-related crustal underplating beneath the Marquesas Islands. *Nature*, 373, 600-603.

Carracedo, J.C. (1984). Marco geográfico. En L. Afonso (dir.), Geografía de Canarias. 1.Geografía física: 10-16. Editorial Interinsular Canaria, S.A. Santa Cruz de Tenerife.

Casillas, R., Ahijado, A. y Hernández-Pacheco, A. (1994). Zonas de cizalla dúctil en el Complejo Basal de Fuerteventura. *Geogaceta*, 15, 65-69.

Casillas, R. y Martín, G.M. (2021). Estructura y evolución del Edificio Volcánico Mioceno de Jandía (Fuerteventura, Islas Canarias). *Geogaceta* 69, 31-34.

Casillas, R., Nagy, G., Démeny, A., Ahijado, C. & Fernández, C. (2008). Cuspidine-niocalite-baghdadite solid solutions in the metacarbonatites of the Basal Complex of Fuerteventura (Canary Islands). *Lithos,* 105, 25-41.

Casillas, R., Démeny, A., Nagy, G., Ahijado, A. a& Fernández, C. (2011a). Metacarbonatites in the Basal Complex of Fuerteventura (Canary Islands). The role of fluid/rock interactions during contact metamorphism and anatexis. *Lithos*, 125 (1-2), 503-520.

Casillas, R., Colmenero, J.R. y Harani, S. (2012). Facies asociadas a deslizamientos gigantes en Fuerteventura (Islas Canarias). *Geotemas* 13, 345-349.

Casillas, R., Colmenero, J.R. y Harani, S. (2019). Depósitos submarinos asociados al deslizamiento gigante del Puerto del Rosario (norte de Fuerteventura, Islas Canarias). *Geogaceta* 66, 103-106.

Cendrero, A. (1966). Los volcanes recientes de Fuerteventura (Islas Canarias). *Estudios Geológicos,* 22, 201-226.

Coello, J., Cantagrel, J.M., Hernán, F., Fúster, J.M., Ibarrola, E., Ancochea, E., Casquet, C., Jamond, C., Díaz de Teran, J. R. &Cendrero, A. (1992). Evolution of the Eastern Volcanic Rigde of the Canary Islands Based on New K-Ar Data. *Jour. Volc. Geoth. Res.*, 53, 251-274.

Criado, C. (1991). *La evolución del relieve de Fuerteventura*. Servicio de Publicaciones del Excmo. Cabildo Insular de Fuerteventura, 318 p.

Cubas, C.R., Fernández Santín, S., Hernán, F., Hernández-Pacheco, A. y de la Nuez, J. (1989). Los domos sálicos de Fuerteventura. *Rev. Mat. y Proc.*, 6, 71-97.

De Ignacio, C., Muñoz, M., Sagredo, J., Fernández-Santín, S., & Johansson. (2006), A Isotope geochemistry and FOZO mantle component of the alkaline-carbonatitic association of Fuerteventura, Canary Islands, Spain. *Chem. Geol.,* 232, 99–113.

Demény, A., Ahijado, A., Casillas, R., & Vennemann, T.W. (1998). Crustal contamination and fluid/rock interaction in the carbonatites of Fuerteventura (Canary Islands, Spain): a C, O, H isotope study. *Lithos*, 44, 101–115.

Demény, A., Vennemann, T.W., Ahijado, A. & Casillas, R. (2004). Oxygen isotope thermometry in carbonatites, Fuerteventura, Canary Islands, Spain. Mineralogy and Petrology volume 80, 155–172.

Feraud, G., Giannerini, G., Campredon, R., & Stillman, C.J. (1985). Geochronology of some Canarian dike swarms: contribution to the volcano-tectonic evolution of the archipelago. *J. Volcanol. Geotherm. Res.* 25, 29–52.

Fernández, C., Casillas, R., Ahijado, A., Perelló, V. & Hernández-Pacheco, A. (1997). Shear zones as a result of intraplate tectonics in oceanic crust: the example of the Basal Complex of Fuerteventura (Canary Islands). *Jour. Struct. Geol.*, 19, 41-57.

Fernández, C., Casillas, R., García-Navarro, E., Gutiérrez, M., Camacho, M.A. & Ahijado, A. (2006). Miocene rifting of Fuerteventura (Canary Islands). *Tectonics*, 25. Doi:10.1029/2005TC001941.

Fúster, J.M. (1975). Las Islas Canarias: Un ejemplo de evolución temporal y espacial del vulcanismo oceánico. *Estudios Geológicos,* 31, 439–463.

Fúster, J.M., Cendrero, A., Gastesi, P., Ibarrola, E. y López Ruiz, J. (1968a). *Geología y Volcanología de las Islas Canarias: Fuerteventura*. Instituto Lucas Mallada. C.S.I.C, 239 p.

Fúster, J. M., Agostini, L., Aguilar, M., Bravo, T., Castañón, A., Cendrero, A., Hernández-Pacheco, A., López-Ruiz, J. y Sánchez-Cela, V. (1968b). *Mapa Geológico de España 1:50.000. La Oliva. IGME.*

Fúster, J.M., Muñoz, M., Sagredo, J., Yébenes, A., Bravo, T. y Hernández-Pacheco, A. (1980). Excursión nº 121 A + c del 26º I.G.C. a las Islas Canarias. *Bol. Inst. Geol. Min. España*, XCII-I, 351-390.

Fúster, J.M., Barrera, J.L., Muñoz, M., Sagredo, J. y Yébenes, A. (1984a). *Mapa y Memoria explicativa de la Hoja de Pájara del Mapa Geológico Nacional a escala 1:25.000.* IGME.

Fúster, J.M., Yébenes, A., Barrera, J.L., Muñoz, M. y Sagredo, J. (1984b). Mapa y *Memoria explicativa de la Hoja de Betancuria del Mapa Geológico Nacional a escala 1:25.000.* IGME.

Gastesi, P. (1969a). El Complejo básico y ultrabásico de Betancuria, Fuerteventura (Islas Canarias): estudio petrológico. *Estudios Geológicos*, 25, 1-51.

Gastesi, P. (1969b). Petrology of the ultramafic and basic rocks of Betancuria massif, Fuerteventura Island (Canarian Archipelago). *Bull. Volc.*, 33, 1008-1038.

Gastesi, P. (1973). Is the Betancuria massif of Fuerteventura Island, Canary Islands, a uplifted piece of oceanic crust? *Nature Physical Science*, 246 (155), 102-104.

Gutiérrez, M. (2000). *Estudio petrológico, geoquímico y estructural de la serie volcánica submarina del Complejo Basal de Fuerteventura (Islas Canarias): caracterización del crecimiento submarino y de la emersión de la Isla.* Tesis Doctoral. Universidad de La Laguna, 533 p.

Gutiérrez, M., Casillas, R., Fernández, C., Balogh, K., Ahijado, A., Castillo, C., Colmenero, J.R. & García Navarro, E. (2006). The submarine volcanic succession of the Basal Complex of Fuerteventura, Canary Islands: a model of submarine growth and emersion of some tectonic-volcanic Islands. *Geol. Soc. Amer. Bull.*, 118, 785-804.

Hobson, A., Bussy, F. & Hernández, J. (1998). Shallow-level migmatization of gabbros in a metamorphic contact aureole, Fuerteventura Basal Complex, Canary Islands. *Journal of Petrology* 39, 125-37.

Holloway, M. & Bussy, F. (2008). Trace element distribution among rock-forming minerals from metamorphosed to partially molten basic igneous rocks in a contact aureole (Fuerteventura, Canaries). *Lithos* 102, 616–639.

Holloway, M.I., Bussy, F. & Vennemann, T.W. (2008). Low-pressure, water-assisted anatexis of basic dykes in a contact metamorphic aureole, Fuerteventura (Canary Islands): oxygen isotope evidence for a meteoric fluid origin. *Contribution to Mineralogy and Petrolology*, 155, 111-121.

Hoernle, K. &Tilton, G. R. (1991). Sr-Nd-Pb isotope data for Fuerteventura Basal Complex and subaerial volcanics: application to magma genesis. *Schweiz. Mineral. Petrogr. Mitt.*, 71, 5-21.

Hoernle, K.A., Tilton, G., Le Bas, M.J., Duggen, S. & Garbe-Schönberg, D. (2002). Geochemistry of oceanic carbonatites compared with continental carbonatites: mantle recycling of oceanic crustal carbonate. *Contributions to Mineralogy and Petrology*, 142, 520-542.

Holik, J.S., Rabinowitz, P.D. & J.A. Austin (1991). Effects of Canary hotspot volcanism on structure of oceanic crust of Morocco, *J. Geophys. Res.,* 96, 12039–12067.

Hunt, J., Wynn, R., Masson, D., Talling, P. & Teagle, D.A.H. (2012). Turbidite record of frequency and source of large volume (>100 km3) Canary Island landslides in the last 1.5 Ma: Implications for landslide triggers and geohazards. *Geochemistry Geophysics Geosystems*, doi: 10.1029 / 2011gc003740.

Javoy, M., Stillman, C.J. & Pineau, F. (1986). Oxygen and hydrogen isotope studies on the basal complexes of the Canary Islands: implications on the conditions of their genesis *Contrib. Mineral Petrol.*, 92, 225-235.

Jenkyns, H.C. (1980). Cretaceous anoxic events: from continents to oceans. *Journal of the Geological Society*, 137(2),171-188.

Jiménez-Munt, I. & Negredo, A.M. (2003). Neotectonic modelling of the western part of the Africa–Eurasia plate boundary: from the Mid-Atlantic ridge to Algeria. *Earth Planet. Sci. Lett.*, 205, 257-271.

Le Bas, M.J., Rex, D.C. & Stillman, C.J. (1986). The early magmatic chronology of Fuerteventura. *Geol. Mag.*, 123, 287-298.

López Ruiz, L. (1970). Estudio petrográfico y geoquímico del Complejo filoniano de Fuerteventura (Islas Canarias). *Estudios Geológicos,* 26, 173-208.

Lowe, D.R. (1982). Sediment Gravity Flows: II Depositional Models with Special Reference to the Deposits of High-Density Turbidity Currents. *Journal of Sedimentary Petrology* 52, 279–297.

Mangas, J., Pérez Torrado, F.J., Reguilón, R.M. y Cabrera, M.C. (1992). Prospección radiométrica en rocas alcalinas y carbonatitas de la serie plutónica I de Fuerteventura (Islas Canarias). Resultados preliminares e implicaciones metalogénicas. *Actas del III Congreso Geológico de España y VIII Congreso Latinoamericano de Geología.* Salamanca. Tomo 3: 389-393.

Mangas, J., Pérez Torrado, F.J., Reguilón, R.M. & Martín-Izard, A. (1993). Alkaline and carbonatitic intrusive complexesfrom Fuerteventura (Canary Islands): radiometric exploration, chemical composition and stable isotope. En: *Int.Conf.Rare Earth Minerals : chemistry, origin and ore deposits.* London: 79-81.

Mangas, J., Pérez Torrado, F.J., Reguilón, R.M. y Martín-Izard, A. (1994). Mineralizaciones de tierras raras ligadas a los complejos intrusivos alcalino-carbonatíticos de Fuerteventura (Islas Canarias). *Bol. Inst. Geol. Min. España,* 17, 212-213.

Marinoni, L.B., a& G. Pasquarè (1994). Tectonic evolution of the emergent part of a volcanic ocean island: Lanzarote, Canary Islands. *Tectonophysics,* 239, 111-135.

Marrett, R. & Allmendinger, R.W. (1990). Kinematic analysis of fault-slip data. *J. Struct. Geol.*, 12, 973-986.

Meco, J. (1975). Los niveles con Strombus de Jandía (Fuerteventura, Islas Canarias). *Anuario de Estudios Atlánticos* 21, 643-660.

Meco, J. (1977). Paleontología de Canarias I: Los Strombus neógenos y cuaternarios del Atlántico euroafricano (taxonomía, biostratigrafía y paleoecología). Cabildo Insular de Gran Canaria. Las Palmas-Madrid.

Meco, J. (1993). Testimonios paleoclimáticos en Fuerteventura. *Revista El Geólogo*: 41-48.

Meco, J. & Pomel, R. S. (1985). Les formations marines et continentales intervolcaniques des Iles Canaries Orientales (Grande Canarie, Fuerteventura et Lanzarote): stratigraphie et signification paleoclimatique. *Estudios Geológicos*, 41: 223-227.

Meco, J. & Petit-Maire, N. (1986). El Cuaternario reciente de Canarias. Le Quaternarie recent des Canaries. Las Palmas- Marsaille. 94 pp.

Meco, J., Petit-Maire, N. & Reyss, J-L. (1992). Le Courant des Canaries pendant le stade isotopique 5, dápres lacomposition faunistique dún haut niveau marin a Fuerteventura (28º N). *C. R. Acad. Sci. Paris*, 314- Série 2, 203-208.

Muñoz, M. (1969). Estudio petrológico de las formaciones alcalinas de Fuerteventura (Islas Canarias). *Estudios Geológicos,* 25, 257-310.

Muñoz, M. y Sagredo, J. (1975). Existencia de metamorfismos superpuestos en el Complejo Basal de Fuerteventura (Canarias). *I Asamblea Nac. Geodesia y Geofísica,* 1287-1288.

Muñoz, M. y Sagredo, J. (1989). Características del metamorfismo térmico producido por los eventos plutónicos intrusivos más recientes del Complejo Basal de Fuerteventura. *Abst. ESF Meeting on Canarian Volcanism*. Lanzarote, 104-108.

Muñoz, M. y Sagredo, J., (1994). Reajustes mineralógicos y geoquímicos producidos durante el metamorfismo decontacto de diques basálticos (Fuerteventura, Islas Canarias). *Boletín de la Sociedad Española de Mineralogía*, 17, 86-87.

Muñoz, M., Sagredo, J., de Ignacio, C., Fernández-Suárez, F. & Jeffries, T.E. (2005). New data (U-Pb, K-Ar) on the geochronology of the alkaline-carbonatitic association of Fuerteventura, Canary Islands, Spain. *Lithos* 85, 140-153.

Mutti, E. (1992). Turbidite Sandstones. AGIPInst. Geologia Univ. Parma. San DonatoMilanese, 275 pp.

Mutti, E., Davoli, G., Tinterri R. y Zavala, C. (1996). Memorie di Scienze Geologiche, Universita di Padova 48, 233-291.

Mutti, E., Tinterri, R., Remacha, E., Mavilla, N., Angella, S. & Fava, L. (1999). An Introduction to the Analysis of Ancient Turbidite Basins from an Outcrop Perspective. *AAPG Course Notes*, 39, 93 pp.

Oehler, J.F. (2005). Les déstabilisations de flanc des volcens de l´Ille de La Réunion (Océan Indien): Mise en évidence, implications et origines. Tesis Doctoral, Universidad Blaise Pascal, Francia, 458 pp.

Pérez-Torrado, F. J., Carracedo, J.C., Guillou, H., Rodriguez-González, A. & Fernandez-Turiel, J.L. (2023). Age, duration, and spatial distribution of ocean shields

and rejuvenated volcanism: Fuerteventura and Lanzarote, Eastern Canaries. Journal of the Geological Society

Renz, O., Bernoulli, D. & Hottinger, L. (1992). Cretaceous ammonites from Fuerteventura, Canary Islands. *Geol. Mag*., 129, 763-769.

Robertson, A.H.F. & Bernouilli, D. (1982). *Stratigraphy, facies and significance of Late Mesozoic and Early Terciary Sedimentary rocks of Fuerteventura (Canary Islands) and Maio (Cape Verde Islans)*. En: Von Rad, Hiaz Sarnthein and Seibold. Geology of the Northwest African Continental Margin, 498-525.

Robertson, A. H. F. & Stillman, C.J. (1979a). Late Mesozoic sedimentary rocks of Fuerteventura, Canary Islands. Implications for West Africa continental margin evolution. *Jour. Geol. Soc. of London,* 136, 47-60.

Robertson, A. H. F. & Stillman, C.J. (1979b). Submarine volcanic and associated sedimentary rocks of the Fuerteventura Basal Complex, Canary Islands*. Geol. Mag*., 116, 203-214.

Rognon, P. et Coudé-Gaussen, G. (1987). Reconstitution paléoclimatique à partir des sédiments du Pleistocène supérieur et de l'Holocène du nord de Fuerteventura (Canaries). *Zeitschrift für Geomorphologie Neue Folge* 31(1), 1-19.

Rognon, P., Coudé-Gaussen, G., Le Coustumer, M. N., Balouet, J.C. ety Occhietti, S. (1989). Le massif dunaire de Jandia (Fuerteventura, Canaries): évolution des paléoenvironnements de 20 000 BP à l'actuel. *Bulletin de l'Association française pour l'étude du Quaternaire* 1, 31-37.

Rosendahl, B.R. (1987). Architecture of continental rifts with special reference to East Africa. *Ann. Rev. Earth Planet. Sci.,* 15, 445-503.

Rothe, P. (1968). Mesozoische Flysch-Ablagerugen auf der Kanaren insel Fuerteventura. G*eol. Rundschan*., 58, 314-332.

Sagredo, J., Ancochea, E., Brändle, J. L., Cubas, C. R., Fúster, J. M., Hernandez-Pacheco, A. y Muñoz, M. (1989). Magmatismo hipoabisal-subvolcánico y vulcanismo en un ámbito geodinámico distensivo (Fuerteventura, Islas Canarias). *Abst. Esf. Meeting on Canarian volcanism. Lanzarote*, 100-103.

Sagredo, J., Muñoz, M., y Galindo, C. (1996). Características petrológicas y edad K–Ar de las sienitas nefelínicas del Morro del Recogedero (Fuerteventura, Islas Canarias). *Geogaceta* 20, 506–509.

Sagan, M., Heaman, L.M., Pearson, D.G., Luo, & Stern, R. A. (2020). Removal of continental lithosphere beneath the Canary archipelago revealed from a U-Pb Age and Hf/O isotope study of modern sand detrital zircons. *Lithos,* 362-363. https://doi.org/10.1016/j.lithos.2020.105448.

Sohn, Y.K. (1997). On traction-carpet sedimentation. *Journal of Sedimentary Research* 67, 502-509.

Sohn, Y.K., Rhee, C.W. & Kim, B.C (1999). Debris Flow and Hyperconcentrated Flood-Flow Deposits in an Alluvial Fan, Northwestern Part of the Cretaceous Yongdong Basin, Central Korea. *Journal of Geology* 107, 111-132.

Steiner, C., Hobson, A., Favre, P., Stampfli, G.M. & Hernández, J. (1998). Early Jurassic sea-floor spreading in the central Atlantic, the Jurassic sequence of Fuerteventura (Canary Islands). *Geol. Soc. Amer. Bull*., 110, 1304-1317.

Stillman, C. J. (1987). *A Canary Islands Dyke Swarm: Implications for the formation of oceanic islands by extensional fissural volcanism.* En: Mafic Dyke Swarms. Halls, H. C. y Fahrig, W. F. Ed. Geol. Assoc. Canada Spec. paper, 34-54.

Stillman, C. J. (1999). Giant Miocene Landslides and the evolution of Fuerteventura, Canary Islands. *Jour. Volc. Geoth. Res., 94,* 89-104.

Stillman C.J., Fúster, J.M., Bennell-Baker, M.J., Muñoz, M., Smewing, J.D. & Sagredo, J. (1975). Basal Complex of Fuerteventura (Canary Islands) is an oceanic intrusive complex with rift-system affinities. *Nature,* 257, 469-471.

Stillman, C. J. & Robertson, A. H. F. (1977). The dyke swarm of the Fuerteventura Basal Complex, Canary Islans. Abstr. *Geol. Soc. Lond. Newsletter*, 6-8.

Tornare, E. Pilet, S. & Bussy, F. (2016). Magma Differentiation in Vertical conduits Revealed by the Complementary Study of Plutonic and Volcanic Rocks from Fuerteventura (Canary Islands). *Journal of Petrology* 57 (11-12), 2221–2250. DOI: 10.1093/petrology/egx004.

Wynn, R.B. & Masson, D.G. (2003). Canary Islands landslides and tsunami generation. En: *Submarine Mass Movements and Their Consequences* (J. Locat y J. Mienert, Eds.). Boston, London (Kluwer Academic Publ.), 325–332

Zazo, C., Hillarie-Marcel, CL., Goy, J.L., Ghaleb, B. & Hoyos, M. (1997). Cambios del nivel del mar-clima en los últimos 250 ka: (Canarias Orientales, España). *Bol. Geol. y Minero*, 108, 31-41.

ANEXO

Acompañamos esta memoria de cinco trabajos publicados por los investigadores del grupo responsable de esta excursión. Estimamos que las publicaciones anexadas ofrecen una visión general de las aportaciones realizadas por el grupo desde que comenzó a trabajar en Fuerteventura hace más de 25 años.

Fernández, C., Casillas, R., Ahijado, A., Perelló, V., Hernández-Pacheco, A. (1997). Shear zones a as result of intraplate tectonics in oceanic crust: the example of the Basal Complex of Fuerteventura (Canary Islands). *Journal of Structural Geology*, 19, 41-57.

Balogh, K., Ahijado, A., Casillas, R., Fernández, C. (1999). Contributions to the chronology of the Basal Complex of Fuerteventura, Canary Islands. *Journal of Volcanology and Geothermal Research*, 90, 81-101.

Gutiérrez, M., Casillas, R., Fernández, C., Balogh, K., Ahijado, A., Castillo, C., Colmenero, J.R., García-Navarro, E. (2006). The submarine volcanic succession of the basal complex of Fuerteventura, Canary Islands: A model of submarine growth and emergence of tectonic volcanic islands. *Geological Society of America Bulletin*, 118, 785-804.

Fernández, C., Casillas, R., García-Navarro, E., Gutiérrez, M., Camacho, M.A., Ahijado, A. (2006). Miocene rifting of Fuerteventura (Canary Islands). *Tectonics*, 25, TC6005, doi:10.1029/2005TC001941.

Casillas, R., Colmenero, J.R. y Harani, S. (2012). Facies asociadas a deslizamientos gigantes en Fuerteventura (Islas Canarias). *Geotemas* 13, 345-349.

Shear zones as a result of intraplate tectonics in oceanic crust: the example of the Basal Complex of Fuerteventura (Canary Islands)

CARLOS FERNANDEZ

Departamento de Geologia, Universidad de Huelva, E21819-Palos de la Frontera, Huelva, Spain

RAMON CASILLAS and AGUSTINA AHIJADO

Departamento de Edafología y Geología, Universidad de La Laguna, E38206-La Laguna Tenerife, Canary Islands, Spain

VIRGINIA PERELLO

Departamento de Geología, Universidad de Huelva, E21819-Palos de la Frontera, Huelva, Spain

and

ALFREDO HERNANDEZ-PACHECO

Departamento de Petrología y Geoquímica, Universidad Complutense de Madrid, E28040-Madrid, Spain

Abstract—Ductile shear zones affecting igneous rocks (pyroxenites, syenites, gabbros and carbonatites) belonging to the Basal Complex of the Island of Fuerteventura are described here. They develop typical mylonites with their cortege of structures and crystallographic fabrics. An evolution from brittle to ductile conditions has been recognized, and interpreted as being due to the ascent of alkaline magmas and related fluids and subsequent emplacement of weak rocks (carbonatites, syenites) along the shear zones. Local metamorphic changes favour the ductile behaviour *via* a reaction-enhanced softening mechanism. The shear zones are arranged in a nearly orthorhombic pattern. Kinematic criteria suggest an extensional tectonic scenario, with a bulk irrotational non-plane deformation. The long axis of the finite deformation ellipsoid is E–W and horizontal. The available data allow us to establish this deformation as being from the Late Oligocene to the Early Miocene. This is tentatively related to the plate-tectonics evolution and mantle anomalies in the northwestern corner of the African plate. © 1997 Elsevier Science Ltd. All rights reserved.

INTRODUCTION

Exploration of the oceanic crust is a powerful tool to understand the geometry and kinematics of the brittle and ductile structures within ocean ridges and transform faults, and therefore constitutes the key to knowledge of the tectonic evolution of plate boundaries. However, emerged portions of the oceanic crust are scarce and of small areal extent, making their importance invaluable. Fracture analyses carried out in selected areas, such as in Iceland (e.g. Gudmundsson, 1992; Fjäder *et al.*, 1994; Villemin *et al.*, 1994), can be cited as relevant examples of the study of the brittle behaviour in this context. Interesting data on the stretching of the deep crust at mid-ocean ridges have emerged from the study of the Deep Sea Drilling Project and the Ocean Drilling Program legs (e.g. Cannat *et al.*, 1991). A vast amount of structural data have been collected from the segments of oceanic lithosphere incorporated into continents during orogenies: the ophiolites. The Oman ophiolite (cf. Nicolas, 1989 for a review) and the Troodos Massif of Cyprus (Varga, 1991; Allerton and Vine, 1992; MacLeod and Murton, 1993) may be cited as two of the best-known cases in the world.

In contrast, little is known about intraplate tectonics in the oceanic lithosphere. From a petrologic point of view, the influence of the mantle hot spots in the oceanic crust is well established, and this has been used to deduce the position of euler poles and to compute relative velocities between plates (Minster and Jordan, 1978; Morgan, 1983; Müller *et al.*, 1993).

A complex tectonic scenario may be identified in the northwestern part of the African plate. At least from the Late Eocene, Africa converges towards the Eurasian plate. The Euler pole describing the relative motion of both plates is located to the southwest of the Canary Islands (e.g. Chase, 1978; Minster and Jordan, 1978; Argus *et al.*, 1989; Westaway, 1990). This causes a frontal convergence in the eastern and central Mediterranean, and a dextral, strike-slip transcurrent motion in the central-eastern Atlantic (the Gloria fault, Buforn *et al.*, 1988; Argus *et al.*, 1989). The presence of minor

42 C. FERNANDEZ, R. CASILLAS, A. AHIJADO, V. PERELLO and A. HERNANDEZ-PACHECO

continental blocks and ocean basins located between the continental masses of Africa and Eurasia led different authors to define this zone as a diffuse plate boundary (Vegas, 1985; Weijermars, 1988). Seismic evidence suggests that the African oceanic crust at the Central Atlantic may have been subjected to the same tectonic instability (Buforn *et al.*, 1988; Moreira, 1991). A further complexity results from the influence of a large region of upwelling in the upper mantle below the western Mediterranean and eastern Atlantic, which may account for some geochemical signatures of the Eastern Atlantic volcanic province (Hoernle *et al.*, 1995).

The Canary Islands belong to the Eastern Atlantic volcanic province, and are located within the African plate, not far from its diffuse boundary with the Eurasian plate. They represent an emerged area of intraplate oceanic crust (Stillman, 1987; Marinoni and Pasquarè, 1994; Neumann *et al.*, 1995). The archipelago lies close to the rifted north African continental margin, but it is considerably younger than the oceanic lithosphere in this area. The complex geological history may be partly a consequence of the plate tectonics scenario described above, and partly a result of a local intraplate tectonics (Marinoni and Pasquarè, 1994). In the present paper we describe two ductile–brittle shear zones affecting the older igneous series of the island of Fuerteventura. These shear zones accommodated important displacements (several hundred and perhaps even several thousand metres), and acted as ascent channels for mantle-derived magmas and fluids. The presence of ductile shear zones in Fuerteventura was first recognized and described by Casillas *et al.* (1994). The kinematic characterization of this deformation may be of relevance in the study of the recent tectonics of the African plate, and may contribute to a better knowledge of the behaviour of the oceanic crust in complex within-plate areas.

GEOLOGICAL SETTING

The Canary Islands are a group of volcanic islands and seamounts located on thick oceanic crust adjacent to the Atlantic-type continental margin of Africa (Fig. 1). From a geological perspective they constitute one of the more complex oceanic archipelagos in the world. Several successive magmatic periods led to the growth and emergence of these ocean islands, the process involving stages of partial destruction of the volcanic successions (Schmincke, 1982; Staudigel and Schmincke, 1984; Le Bas *et al.*, 1986; Coello *et al.*, 1991; Ancochea *et al.*, 1990, 1993, 1994).

Every island within the archipelago has its own geological history. The evolution process of Fuerteventura is the most complex and longest-lasting (Stillman *et al.*, 1975; Fúster *et al.*, 1980; Le Bas *et al.*, 1986; Coello *et al.*, 1991; Ancochea *et al.*, 1994). Fuerteventura forms part of the East Canary Ridge, together with Lanzarote

and the Conception Bank. It is located on thick (more than 11 km) and strongly reworked oceanic crust (Banda *et al.*, 1981). Three main lithological units can be distinguished in Fuerteventura (Fig. 1).

(1) *The Basal Complex* consists of sea-floor sediments overlain by submarine volcanic and volcaniclastic sequences. The exposed sediments, Cretaceous in age, are part of the overturned limb of a concentric recumbent fold (Rothe, 1968; Robertson and Stillman, 1979a; Fúster *et al.*, 1980; Robertson and Bernouilli, 1982; Renz *et al.*, 1992). The volcanic series comprise breccias, hyaloclastites and pillow-lavas of basaltic to trachybasaltic composition. Bioclastic and volcaniclastic sediments of Middle to Late Oligocene age appear intercalated within the volcanic series (Fúster and Aguilar, 1965; Robertson and Stillman, 1979b). Large plutonic, and hypabyssal bodies intruded the sediments and volcanics. Following Stillman *et al.* (1975), Fúster *et al.* (1980), Le Bas *et al.* (1986), Stillman (1987) and Sagredo *et al.* (1989), three magmatic episodes can be recognized, including (i) an initial ultra-alkaline series comprising pyroxenites, amphibole-rich ultramafic igneous rocks, amphibole-bearing gabbros and syenites, cross-cut by syenite and carbonatite dykes, (ii) elongate, NNE–SSW trending bodies of gabbro and pyroxenite, and (iii) concentric patterns of gabbro and syenite ring-dykes. A dense basaltic dyke-swarm traverses the various lithologies. These dykes may be considered as the feeder conduits for rocks that form the submarine and subaerial growth of Fuerteventura and, in places, constitute more than 90 % of the exposed rock (Stillman *et al.*, 1975; Fúster *et al.*, 1980; Le Bas *et al.*, 1986; Stillman, 1987; Sagredo *et al.*, 1989). This obscures the continuity of contacts and structures within the Basal Complex.

(2) *A subaerial volcanic succession* of Miocene age comprises three large shield volcanoes, reconstructed from the disposition of the partly-eroded volcanic sequences (Coello *et al.*, 1991; Ancochea *et al.*, 1994).

(3) *A later subaerial volcanic succession*, contains intercalated beach-sediments (Meco and Pomel, 1985).

The initial ultra-alkaline series of Unit (1) are the lithologies affected by the shear zones. The more recent plutonics and the subaerial volcanic successions cut the shear zones, imposing temporal constraints to their activity. No evidence of ductile shearing has been found as yet in the intruded Cretaceous to Oligocene sediments and submarine volcanics. Therefore, this study is devoted to the description of the deformation affecting the older plutonics of Unit (1), the Basal Complex.

GEOMETRY AND KINEMATICS OF THE SHEAR ZONES

The shear zones in the ultra-alkaline plutonic rocks of the Basal Complex are unevenly distributed. Basaltic
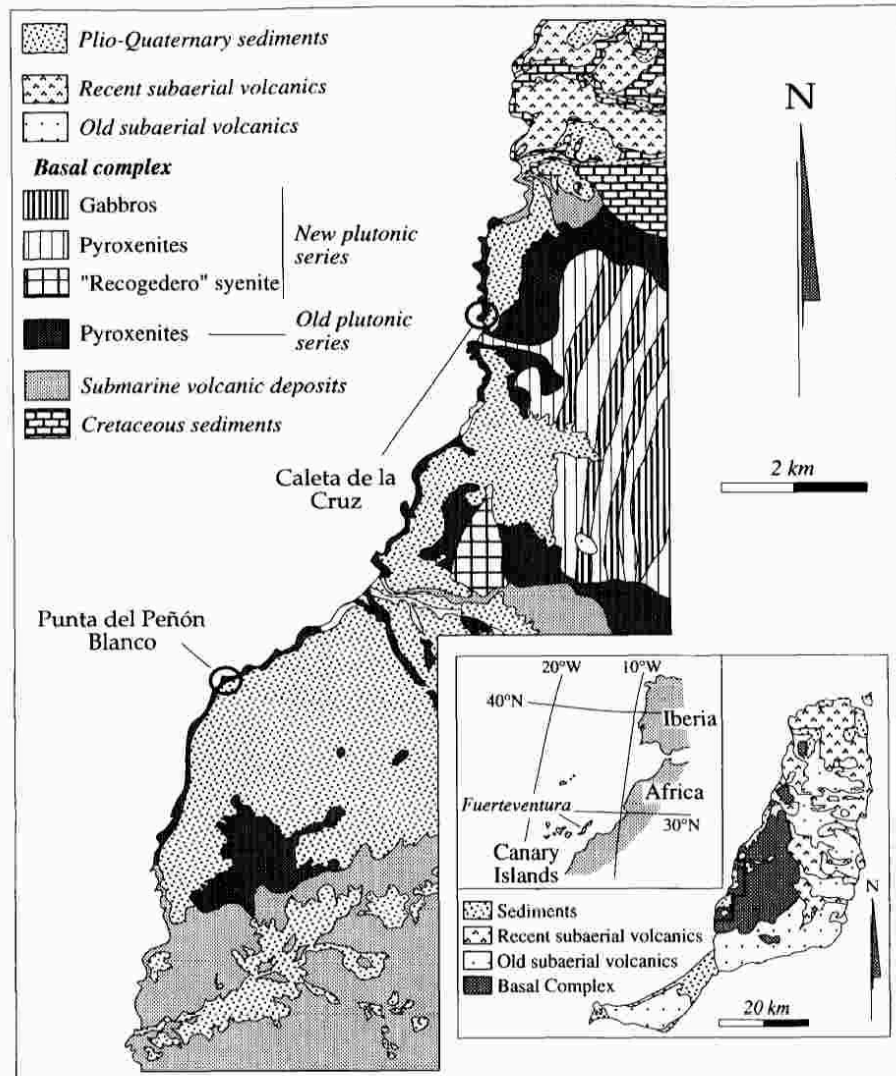
Fig. 1. Schematic geological map of western-central Fuerteventura, showing the lithologies of the Basal Complex and the location of the most important shear zones (Caleta de la Cruz and Punta del Peñón Blanco).

dykes disrupt the deformational structures and, in cases of large dyke densities, the shear zones are almost completely transposed. Exceptionally good exposures appear in the coastal cliffs and beaches, but the outcropping structures cannot be continued landwards due to the presence of the volcanic and sedimentary cover. In this work we describe the structures associated with two selected shear zones in the coastal section (Fig. 1): the Caleta de la Cruz and the Punta del Peñón Blanco shear zones. Here, the structures are clearly exposed and cleaned by sea-water abrasion and the density of the crosscutting dykes is moderate. The quality of the outcrops allowed the construction of orthogonal grids in the field with irregular, polygonal external contours. The side-length of the unit squares in the grids is 1 m. These grids were used as the reference frame for detailed geological mapping, a powerful tool to gain a complete geometric view of the shear zones. The analysis was

44   C. FERNANDEZ, R. CASILLAS, A. AHIJADO, V. PERELLO and A. HERNANDEZ-PACHECO

followed up by the use of conventional structural and petrologic techniques.

The Caleta de la Cruz shear zone (CCSZ)

This is a subvertical, NW–SE oriented shear zone (Fig. 2). A heterogeneous deformation affects a broad band (more than 10 m) of pyroxenites and syenites belonging to the initial ultra-alkaline series of the Basal Complex. The main structures originating in this shear zone are mylonitic foliation and lineation, curved-hinge folds, composite planar fabrics (C–S fabrics, Berthé *et al.*, 1979), lozenge-shaped blocks of undeformed pyroxenite, and minor discrete shear bands (Fig. 2). Apart from the heterogeneity of the deformation, the main characteristic of this zone is the brittle-to-ductile transition exhibited by the progressively developing structures. Near the external boundary of the shear zone, structures are brittle, with fractures fragmenting and displacing blocks of pyroxenite. This is observed also in the large lozenge-shaped blocks of pyroxenite within the CCSZ. The brittle structures are filled by carbonatite, whose appearance is strictly associated to the deformational structures. A complex metamorphic reaction (fenitization) between carbonatite and pyroxenite, which will be described in detail in the next section, results in an aggregate of phlogopite and diopside. Consequently, the ductility of the pyroxenite is highly enhanced locally, near the carbonatite intrusions. More continuous, straight and ductile shear bands appear in the inner part of the CCSZ. Here, a strongly foliated, fine-grained aggregate of

calcite, phlogopite and diopside embraces residual fragments of pyroxenite. A reaction-rim of phlogopite–diopside is always present around these fragments. Reaction-rims are often stretched on both sides of a fragment, defining asymmetric tails (Fig. 3a & b) that recall the σ- and δ-structures of the porphyroclast systems in quartz–feldspar mylonites (Passchier and Simpson, 1986).

The mylonitic lineation is defined by elongate mica aggregates and shows a low to moderate plunge (Fig. 2a). This points to an important strike-slip component of displacement for the CCSZ. Kinematic criteria used to infer the shear sense in the CCSZ include (i) the asymmetric attitude of the foliation embracing the pyroxenite fragments (Figs 3a & 4a), (ii) the asymmetric tails of elongate reaction-rims around the pyroxenite fragments (Fig. 3a & b), (iii) the orientation and sense of shear exhibited by the minor shear bands and faults, (iv) the composite planar fabrics, (v) the preferred orientation of the calcite *c*-axis fabric (see later), and (vi) the orientation and asymmetry of mesoscopic folds affecting the mylonitic foliation (Figs 2a & 3b). In this case, the flow direction and flow sense are obtained following the method of Hansen (1971). All these indicate a dextral shear component with a subordinate down-throw of the northeastern block.

A second shearing episode deforms the previous structures. The new shear zone, with a thickness of 1 m, cross-cuts the southern boundary of the CCSZ. Basic dykes that had intruded the foliated carbonatites of the CCSZ are displaced and disrupted by this second episode

Fig. 2. Detailed geological map of the Caleta de la Cruz shear zone. This represents the best subhorizontal outcrop of this shear zone. The inset shows a sketch obtained after eliminating the late basic dykes. Sample AJ6, used in the texture analysis, is also located in the map. This (and most of the following figures) refer to the magnetic north (MN) as the mean deviation from the geographical coordinates appears negligible (Marinori and Pasquarè, 1994). (a) Structural data of the first deformational stage (great circles: foliation; open squares: mineral and stretching lineations; ellipse: area covered by the lineation poles; black dots: fold axes and sense of fold asymmetry). (b) Structural data of the second deformational stage; symbols as in (a). Spherical projections are equal area, lower hemisphere.
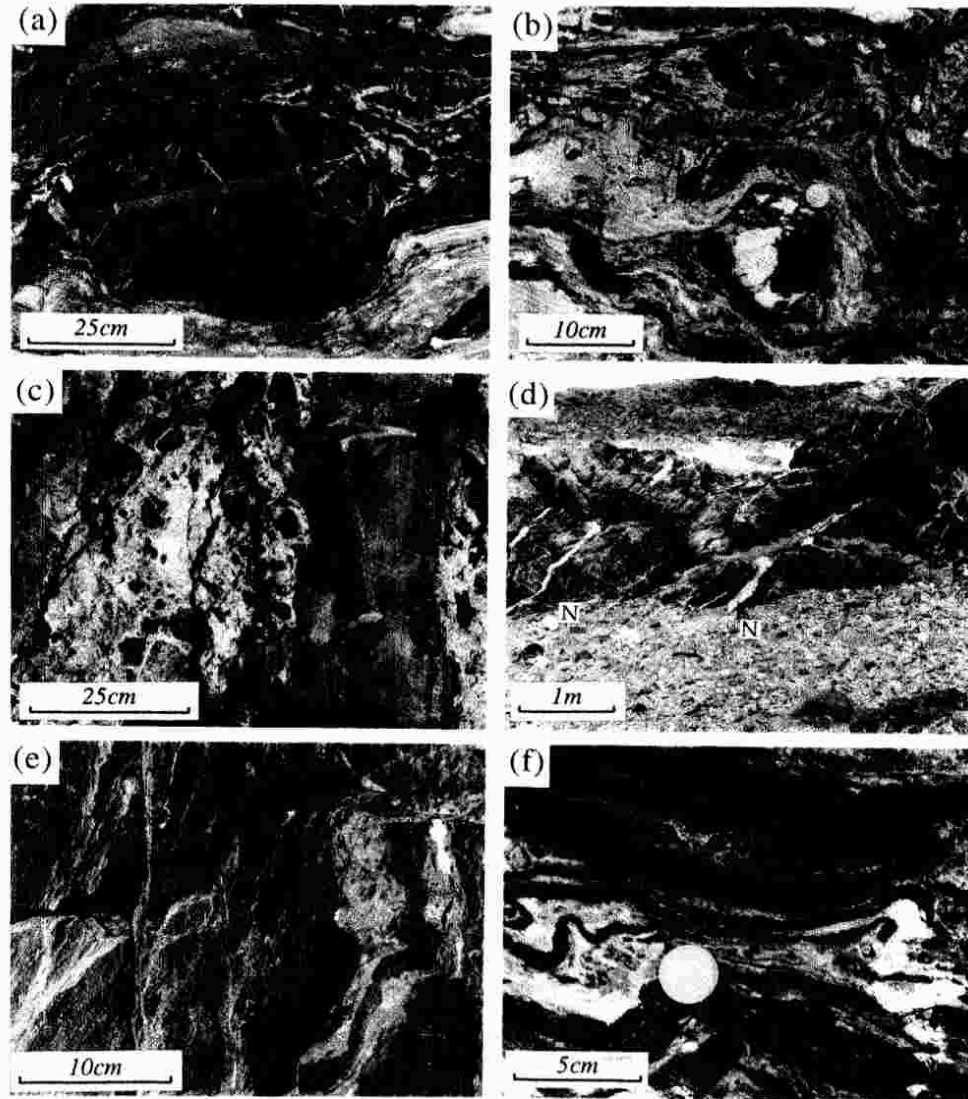
Fig. 3. (a) Pyroxenite block asymmetrically embraced by the mylonitic foliation composed of domains of recrystallized carbonatite (white) and domains of phlogopite ± diopside ± calcite (black). The pyroxenite block is contoured by a black reaction rim made of phlogopite and diopside. Caleta de la Cruz shear zone. ESE to the right of the photograph. (b) Folded mylonitic foliation with minor blocks of pyroxenite + syenite. Caleta de la Cruz shear zone. ESE to the right of the photograph. (c) Network of albitite in the Punta del Peñón Blanco area (type 1 veins). Hammer lies over a late, cross-cutting basic dike. (d) Pattern of type 2 and type 3 veins in the Punta del Peñón Blanco. Type 2 veins are filled by albitite and appear as thin and irregularly oriented veins. Type 3 veins are filled by white nepheline syenite (marked by N); they are thick and systematically dip to the left of the photograph (West). (e) Mylonitic lineation in the Punta del Peñón Blanco shear zone. ESE to the left of the photograph. (f) Curved-hinge fold in the Punta del Peñón Blanco shear zone. The folded layering is comprised of pre-and syn-kinematic basic dykes (black) and recrystallized carbonatite (white). ESE to the right of the photograph.

46   C. FERNANDEZ, R. CASILLAS, A. AHIJADO, V. PERELLO and A. HERNANDEZ-PACHECO
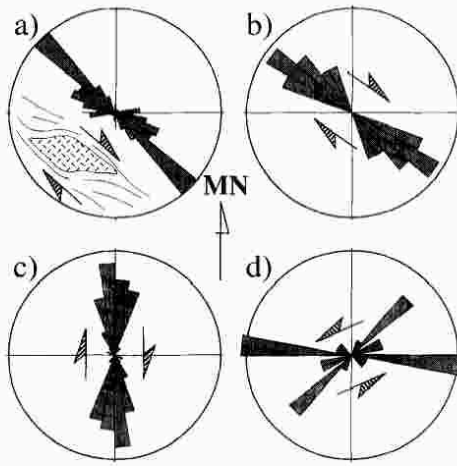
Fig. 4. Rose diagrams representing the traces of structural elements measured in the map of the Caleta de la Cruz shear zone. The frequency of the external perimeter is 30 %. (a) Traces of the first stage foliation ($n = 96$); the asymmetry of the diagram is explained as a consequence of the irregular distribution of the foliation embracing unstrained blocks in a dextral shear regime. (b) Traces of the second stage foliation ($n = 14$). (c) Traces of dextral shear bands ($n = 41$); (d) Traces of sinistral shear bands ($n = 22$).

(Fig. 5), indicating a horizontal displacement of more than 10 m in a dextral sense. The deformation associated with this shear zone caused a marked decrease in grain-size of the rock, as well as the elongation of the pyroxenite fragments. The kinematic pattern of this episode is not very different from that of the CCSZ, as deduced from the attitude of the mylonitic foliation and lineation and from the asymmetry of isoclinal intrafolial folds (Fig. 2b). Other kinematic criteria include the asymmetric shape of the disrupted basic-dyke fragments, the presence of tension gashes inclined with respect to the trend of the average foliation, the synthetic and antithetic shear bands, and the reorientation undergone by the earlier foliation in the vicinity of the newly-formed shear zone (Fig. 5).

The spatial association of both deformational episodes, together with the kinematic and metamorphic similarities between them, suggest a long-lived period of dextral ductile–brittle shearing with an intercalated stage of brittle behaviour and dyke intrusion.

The Punta del Peñón Blanco shear zone (PPBSZ)

This shear zone outcrops more than 7 km southwest of the Caleta de la Cruz (Fig. 1). A band of high ductile deformation with a thickness of around 40 m is located within a region of severely brecciated pyroxenite. A sudden decrease in the fracture intensity occurs on both sides of the brecciated area (Fig. 6a). Three types of veins fill the fractures in the brecciated pyroxenite:

Type 1. Irregularly impregnated areas which constitute a network of albitite (Fig. 3c).

Type 2. Albitite veins of cm-scale thickness, arranged in four systems with an approximate orthorhombic symmetry (Figs 3d & 6b).

Type 3. White nepheline syenite veins, with a marked unimodal preferred orientation (Figs 3d & 6c).

The PPBSZ is restricted to the ductile band located near the northern margin of the brecciated area, which becomes strongly deformed and even transposed (Fig. 7).

The albitite veins of the first two types described above are deformed by the ductile shear zone. However, the third type, of white syenite veins, systematically cross-cuts the ductile structures and appears only in the hanging-wall to the PPBSZ. They eventually affect the top of the main ductile band.

In Fig. 8, a selected region of the PPBSZ is shown in detail. As noted in the CCSZ with reference to the carbonatites, distinct lithological types are spatially related to the deformed area. These lithologies include carbonatite and dykes of grey nepheline syenite, which are scarce or absent in the ultra-alkaline unit outside the domains affected by the shear zones. Here we interpret these lithologies as intruded in relation to the activity of the shear zones. The dykes intrude the pyroxenite brecciated by the albitite network and veins. These dykes may extend by dozens of metres outside the boundaries of the PPBSZ (Fig. 7).

The mylonitic foliation has an average NW–SE trend. The plunge of the associated lineation approximates 40° to the SE (Figs 3e & 7c). Local places where the foliation trend departs from their average orientation are due to slight deflections around undeformed blocks of brecciated pyroxenite or nepheline syenite (Fig. 8). The mylonitic lineation is well developed in the grey nepheline syenites, where it is marked by the shape fabric of sanidine crystals and by the orientation of ribbons of sanidine and aggregates of aegirine–augite. Therefore, it constitutes a stretching lineation (Fig. 3e). In the carbonatites, which have an equigranular texture, the lineation is poorly defined, and the foliation is marked by occasional calc-silicate bands and alternating domains of fine- and coarse-grained carbonatite.

Kinematic criteria, some of which are clearly seen in the maps (Figs 7 & 8), are consistent with a dextral-normal sense of shear. These include: (i) the lateral displacement of the syenite and basic dykes, (ii) the asymmetric pattern of the mylonitic foliation around less deformed fragments, (iii) the asymmetric pressure-shadows around blocks of undeformed rock, (iv) the crystallographic preferred orientation of calcite (see later), and (v) the asymmetry of minor, curved-hinge folds (Fig. 3f), and their consistent spatial arrangement in relation to the mylonitic foliation and lineation (Fig. 7d), as deduced from the method of Hansen (1971).

To the south of the main ductile PPBSZ, several carbonatite bands deflect and displace grey syenite
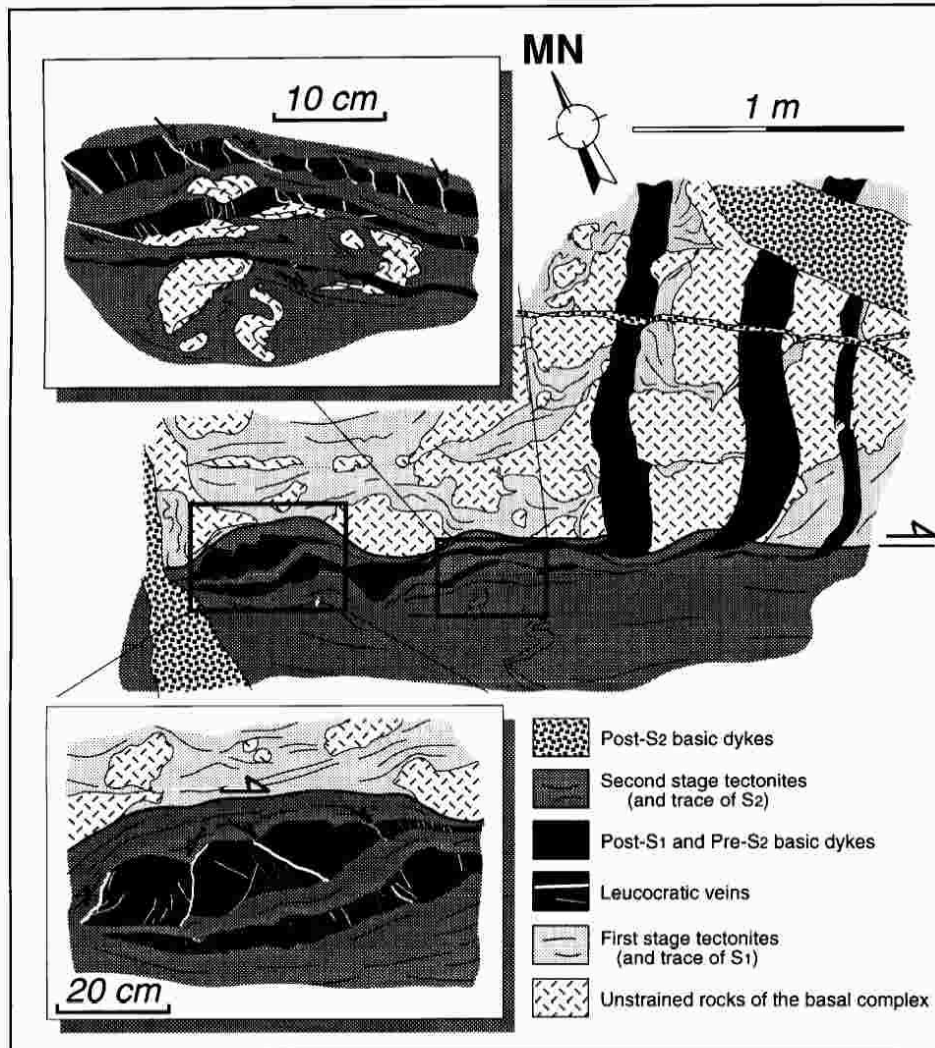
Fig. 5. Detailed sketch taken from field photographs, showing the effects of the second stage dextral shear zone on the basic dykes and first stage tectonites (Caleta de la Cruz shear zone). Insets depict the elongation of the basic dykes and their disruption by synthetic and antithetic fractures filled by leucocratic veins.

dykes (Fig. 7). The carbonatite within the bands is strongly foliated, and the syenite is more pervasively deformed when it approaches the bands. The strike-slip movement is dextral for the NW–SE and sinistral for the NE–SW oriented bands (Fig. 7a & b).

The large dykes of grey nepheline syenite located far from the main ductile shear zone are almost normal to the mylonitic lineation. As they approach the shear zone they become progressively rotated towards parallelism with the mylonitic foliation (Fig. 7e). The stretching and boudinage of the dykes generates a strongly developed planar–linear fabric.

The minimum displacement along the ductile band may be estimated according to the horizontal deviation of basic dykes in the margins of the shear zone (Fig. 8). A conservative extrapolation of this displacement to the

48   C. FERNANDEZ, R. CASILLAS, A. AHIJADO, V. PERELLO and A. HERNANDEZ-PACHECO
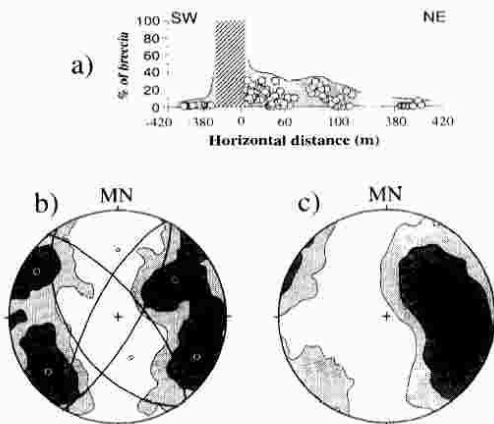
Fig. 6. Fracture intensity and orientation of the leucocratic veins in the Punta del Peñón Blanco area. (a) Linear percentage of brecciated areas with respect to the unstrained rock; the distance is measured in a direction normal to the boundaries of the ductile shear zone, the origin corresponding to the centre of the shear zone; the diagonal stripe pattern marks the area with 100 % breccia. (b) Contour diagram showing the orientation of the poles to the type 2, albitite veins; the maxima are the poles to the four great circles represented in the figure ($n = 339$). (c) Contour diagram showing the orientation of the poles to the type 3, nepheline syenite veins ($n \approx 72$). Contour diagrams are equal area, lower hemisphere projection, contoured after the Kamb method with $E = 3\sigma$, contour interval $= 2.0\sigma$.

entire band gives a net slip of more than 1 km. Considering the moderate thickness of the band (around 40 m), this is a quite large displacement, comparable to those measured in continental shear zones.

OPTICAL MICROSTRUCTURES, TEXTURES AND MINERAL CHANGES

The Caleta de la Cruz shear zone (CCSZ)

The pyroxenite blocks in contact with carbonatite develop a characteristic assemblage of phlogopite $\pm$ diopside $\pm$ magnetite $\pm$ apatite $\pm$ grossular/andradite garnet. Rocks in the deformed domains show unequivocal solid-state deformation microstructures, with a generalized reduction in the grain-size. The carbonatites filling fractures or located within pressure shadows around pyroxenitic blocks constitute unequant coarse-grained (2–3 mm) aggregates. Two conjugate sets of e-twins develop, although one set predominates over the other. Equant recrystallized grains (< 1 mm) appear at the

grain boundaries or are located within discrete bands parallel to the foliation. Towards the inner part of the ductile CCSZ the grain-size is reduced (200–400 μm). Here the calcite crystals exhibit undulatory extinction, but they are almost free of deformation twins. The grains are slightly flattened with their long axes aligned parallel to the foliation. A crystallographic preferred orientation (also referred to as texture or crystallographic fabric in this paper) has been measured in the more deformed carbonatite aggregates (sample AJ6, for location see Fig. 2). All the textures in this paper were measured using the optical U-stage. The c-axis of calcite was determined as the pole to the great circle connecting 5 individually measured slow vibration directions, in accordance with the method by Turner and Weiss (1963). The result is shown in Fig. 9(a), with a high-density area near the normal to the foliation. Two unequally populated submaxima are present (I and II in Fig. 9a). The stronger one (maximum I) is deflected from the normal to the foliation in a sense opposite to the sense of the imposed shear, as deduced from other independent kinematic criteria. This texture compares well with the CT5 sample experimentally deformed by Schmid *et al.* (1987) under low-temperature, simple shearing conditions. Schmid *et al.* (1987) interpret this texture as a consequence of the simultaneous activity of e-twinning and r-slip. The virtual absence of twins in our sample is difficult to explain in this way, although it is possible that twinning was completed in a majority of crystals, as shown by Schmid *et al.* (1987) for some of the grains within their specimen CT5.

The second deformation stage produces an ultramylonite. A characteristic mineral and textural change is suffered by the displaced basic dykes. Far from the second-stage shear zone, they cross the trend of the first-stage foliation, and preserve an igneous ophitic texture. They show prismatic crystals of pyroxene and red biotite, enclosed by poikilitic plagioclase. An important metamorphic–metasomatic process gives rise to an assemblage of green biotite + grossular/andradite garnet + sphene + magnetite + analcite + epidote/clinozoisite + calcite. As the dykes rotate towards parallelism with the second-stage shear zone margin, the garnet is fragmented and stretched to generate trails of porphyroclasts within a very fine-grained matrix composed of grossular/andradite garnet + green biotite + sphene + albite + analcite + carbonates + magnetite. As described above, tension gashes and discrete shear bands cross-cut the dyke fragments within the shear zone. The mineral assemblages filling the veins are similar to those described for the matrix of the deformed dykes, and include analcite + calcite +

Fig. 7. Geological map of the coastal outcrop of the Punta del Peñón Blanco shear zone. The basic dykes cutting the ductile structures are not represented in this figure. The marked area corresponds to the detailed map of Fig. 8. (a) Dextral and (b) sinistral shear bands to the west of the main ductile shear zone. (c) and (d) Structural data of the main ductile shear zone. The area with a grey pattern in (d) indicates the position of the mineral and stretching lineations. Legend for (a)–(d): great circles, mylonitic foliation; open squares, mineral and stretching lineation; black dots, fold axes and sense of fold asymmetry. (e) Nepheline syenite dykes to the west of the main ductile shear zone; the bold great circle represents their orientation in the centre of the map, and the dashed arrow marks their progressive reorientation towards the ductile shear zone. Spherical projections are equal area, lower hemisphere. Samples R1, 425 and 442, analyzed for crystallographic preferred orientation, are also located in the map.
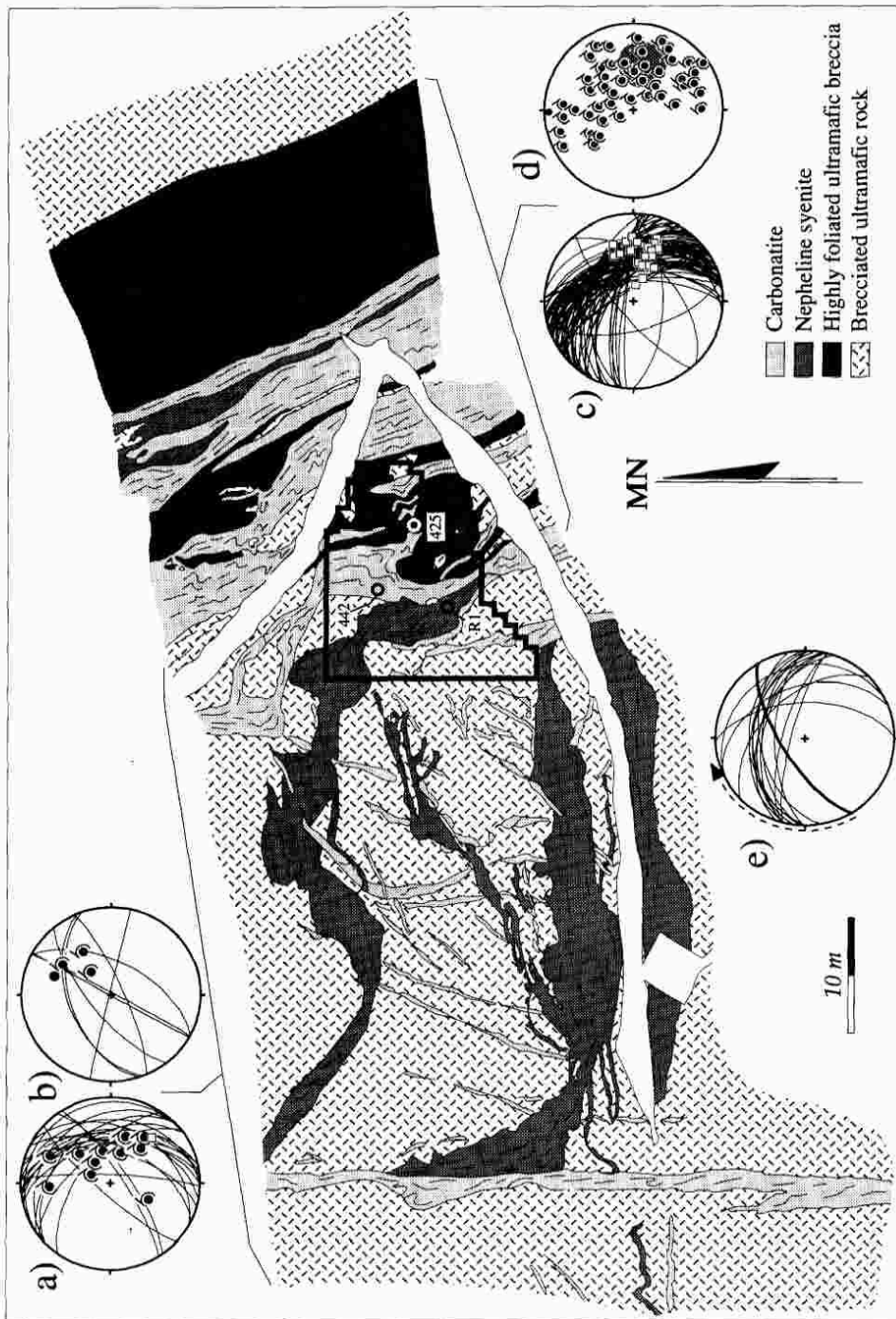
Fig. 7.

50   C. FERNANDEZ, R. CASILLAS, A. AHIJADO, V. PERELLO and A. HERNANDEZ-PACHECO
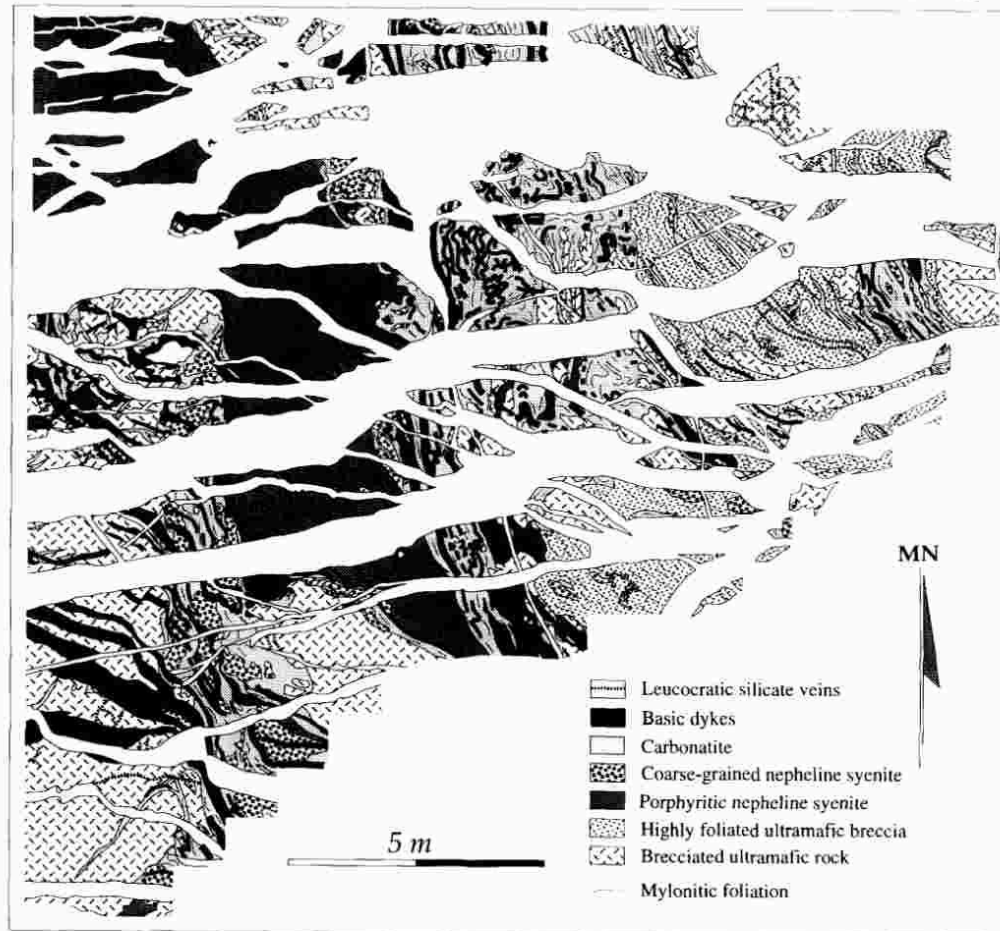
Fig. 8. Detailed geological map of the ductile shear zone in the Punta del Peñón Blanco (for location see Fig. 7).

garnet + green biotite. This strongly suggests a synchronous development of these structures with respect to the shear activity, and favours their use as kinematic criteria.

The fabrics of the first-stage deformation are heavily recrystallized within the second-stage shear zone. The metamorphic mineral assemblages are also changed to grossular/andradite garnet ± Sr-rich epidote/clinozoisite ± idocrase ± magnetite analcite ± Sr-rich allanite ± calcite.

The Punta del Peñón Blanco shear zone (CCSZ)

The microstructural study was focused on the grey nepheline syenite dykes, carbonatites and foliated pyroxenite breccias.

The nepheline syenite is essentially composed of sanidine, aegirine–augite and nepheline. When undeformed it presents an igneous porphyritic texture with prismatic sanidine and aegirine–augite phenocrysts in a matrix of nepheline, sanidine and aegirine–augite. The long axes of the sanidine phenocrysts have an average length of approximately 5 mm. With the increase in ductile deformation, the grain-size is reduced. Nepheline, with abundant undulatory extinction and subgrain boundaries, acquires a strong crystallographic preferred orientation (sample R1, for location see Fig. 7), with a single-maximum, *c*-axis fabric parallel to the mineral lineation (Fig. 9d). Recrystallization must proceed in an anhydrous environment as deduced from the mineralogy of the deformed rocks, devoid of hydrous minerals such as micas or amphiboles. Sanidine also shows subgrain boundaries and an interesting texture, with the α-axes of the optical indicatrix located in a single maximum close to the mineral lineation, the β-axes forming an incomplete girdle parallel to the foliation, with a maximum
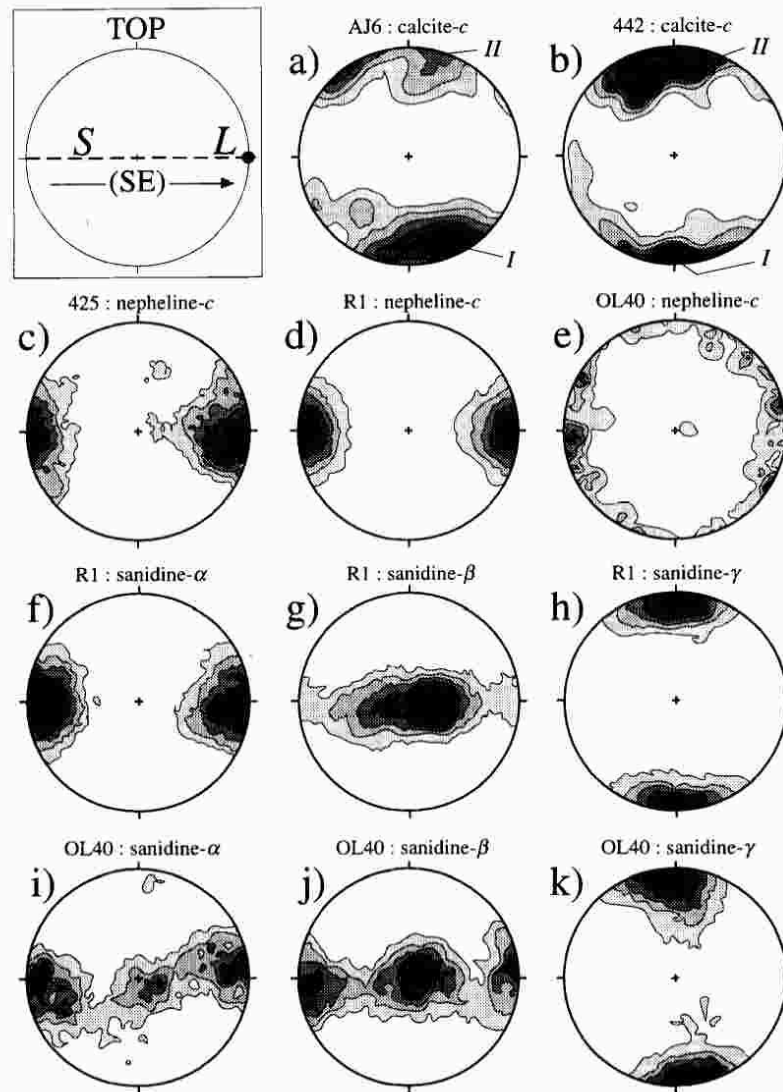
Fig. 9. Crystallographic preferred orientations in deformed rocks of the Basal Complex. The inset depicts the orientation of the structural co-ordinate system: foliation (*S*) and lineation (*L*). Shear sense is dextral for all diagrams. Equal area, lower hemisphere projection. Density calculation after the step-function, except for (a) and (b) where a spherical Gaussian function was used instead. Contouring after the Kamb method with $E = 3\sigma$. (a) *c*-axis fabric of calcite in a carbonatite from the CCSZ. Contour interval (c.i.) $= 1.2\sigma$. Number of measured crystals (n) $= 144$. (b) *c*-axis fabric of calcite in a carbonatite from the PPBSZ; c.i. $= 1.4\sigma$; $n = 232$. (c) *c*-axis fabric of nepheline in a deformed pyroxenite breccia from the PPBSZ; c.i. $= 1\sigma$; $n = 204$. (d) *c*-axis fabric of nepheline in a deformed syenite from the PPBSZ; c.i. $= 2.5\sigma$; $n = 120$. (e) *c*-axis fabric of nepheline in a deformed syenite from a shear zone to the north of the CCSZ; c.i. $= 4\sigma$; $n = 103$. (f) to (k) Sanidine fabrics showing the orientation of the optical indicatrix axes in syenites from the PPBSZ (f–h) and a shear zone to the north of the CCSZ (i–k). (f) c.i. $= 1\sigma$; $n = 134$. (g) c.i. $= 1.5\sigma$; $n = 134$. (h) c.i. $= 2.2\sigma$; $n = 134$. (i) c.i. $= 0.5\sigma$; $n = 120$. 0) c.i. $= 0.7\sigma$; $n = 120$. (k) c.i. $= 1\sigma$; $n = 120$.

52   C. FERNANDEZ, R. CASILLAS, A. AHIJADO, V. PERELLO and A. HERNANDEZ-PACHECO

normal to the lineation, and the γ-axes coinciding with the pole to the foliation (Fig. 9f–h). The prismatic phenocrysts of sanidine undergo a reorientation with their long-axis parallel to the trend of the mylonitic foliation. Kinematic criteria are abundant in these phenocrysts (now porphyroclasts), and include sheared and asymmetrically detached parts of crystals, bookshelf sliding, and the asymmetric pattern of the foliation embracing large sanidines. They typically show a core–mantle structure produced by dynamic recrystallization. The average size of the newly recrystallized crystals is 200 to 300 μm. As deformation increases, recrystallization pervades the whole crystal, which is stretched to give a polycrystalline ribbon. Phenocrysts of aegirine–augite are also transformed into elongate polycrystalline domains parallel to the mylonitic lineation, but no signs of plastic deformation can be observed within individual crystals.

The mineral composition of the undeformed carbonatite is seldom preserved and consists of an aggregate of large (up to 2 cm) crystals of calcite, phlogopite and sanidine. In areas of low to moderate deformation, the carbonatite changes to a heterogeneous aggregate of calcite (up to 1 cm in size) with a metamorphic microstructure characterized by straight grain boundaries meeting at 120°. Ore minerals are concentrated along grain boundaries and planes of cleavage. A slight bending of the phlogopite lattice is also clear. Within more deformed areas, the calcite crystals show a core–mantle microstructure, with the growth of newly-recrystallized, equant crystals (200–400 μm). The host crystals developed undulatory extinction and two conjugate sets of deformation twins. Progressively, the recrystallized grains pervade the host crystals, which remain as flattened relics with aspect ratios of 2–3:1 in a section normal to the foliation and parallel to the lineation. Eventually, the dynamic recrystallization affects the whole aggregate, resulting in an equigranular (400 μm) mosaic of calcite, with undulatory extinction, subgrain boundaries and deformation twins. The calcite-texture obtained in this strongly deformed rock (Fig. 9b: sample 442, see Fig. 7 for location) is asymmetric with respect to the structural co-ordinate system. As in the CCSZ, two sub-maxima develop (I and II in Fig. 9b), with the more populated one inclined to the foliation normal in a sense opposite to the external shear sense. Simultaneous activity of e-twinning and r-slip is again proposed to account for this texture (Schmid *et al.*, 1987). Within the pressure shadows or other protected regions, the calcite forms a polygonal mosaic of large crystals, with grain boundaries meeting at 90°.

The brecciated pyroxenite was severely deformed to give a foliated rock with a pervasive tectonic banding. This banding is composed of alternating white and dark bands. The heterogeneous character of the deformation in the PPBSZ is clearly seen since the banded domains often show clear-cut contacts with respect to undeformed blocks of brecciated pyroxenite (Fig. 8). An equigranular

aggregate of sanidine, albite and nepheline constitutes the white bands. It results from the transposition of the albitite veins and network. Some albitite veins exhibit isoclinal folds, with the tectonic banding as axial plane; other were stretched to generate pinch and swell structures and fish-mouth boudins. The crystallographic preferred orientation of nepheline is quite strong (sample 425, see Fig. 7 for location), with a single maximum of nepheline c-axes parallel to the mylonitic foliation (Fig. 9c). This strong fabric is due to the considerable solid-state deformation suffered by these bands. Similar nepheline c-axis fabrics were obtained by Fairbairn (1941) and Sturt (1961). The foliation in the dark bands is defined by the preferred orientation of biotite and diopside. Kinks and mica-fishes are the main microstructures in the biotite. The diopside shows no evidence of plastic intracrystalline deformation.

Textures in other minor shear zones

Nepheline syenites affected by other shear zones to the north of the CCSZ were also analyzed. The aim of this study is to show the homogeneity of the deformation mechanisms throughout the entire Basal Complex, with special reference to the textures in sanidine and nepheline.

Figure 9 (i–k) shows the axes of the optical indicatrix of sanidine composing more than 60 % of the matrix in a sample of a deformed syenite, 15 km to the north of the CCSZ (sample OL40). This shear zone is very heterogeneous and the deformation structures are not as strong as in the CCSZ or PPBSZ, suggesting lower strains. The α- and β-axis fabrics delineate a single girdle which is slightly oblique with respect to the foliation trace, the deflection being described by a counter-clockwise rotation around an axis normal to the stretching lineation and included within the mylonitic foliation. This counter-clockwise deflection is contrary to the imposed shear sense indicated by the meso- and microstructural criteria. Two maxima are discernible within both girdles, one of them normal to the mylonitic lineation, the other at 5–10° from it. The γ-axis fabric consists of a single maximum located at 5–10° counter-clockwise from the pole to the foliation plane. These results are similar to the fabrics of sanidine in the syenites of the PPBSZ (Fig. 9f–h). However, in the PPBSZ the fabrics are symmetrical with respect to the finite strain reference axes. Statistical measurement of the optic axial angles in sanidine, which is around 50° here and in the PPBSZ, indicates that it is high sanidine (e.g. Smith and Brown, 1988). In this case, the γ-axis maximum implies a strong disposition of the (001) planes near the foliation trace, with [001] normal to it. No accurate transmission electron microscopy analysis of the operative slip-systems was conducted in this work, and several problems are associated with the direct interpretation of fabric diagrams in terms of slip systems, as shown by Wenk and Christie (1991). In spite of these difficulties we suggest that (001) could have been an

important slip plane in the plastic behaviour of sanidines in the Basal Complex of Fuerteventura. This coincides with the results obtained by Willaime *et al.* (1979) and Scandale *et al.* (1983) on experimental grounds, and Sacerdoti *et al.* (1980) in the study of naturally deformed K-feldspar.

The nepheline constitutes a mere 10–15 % of the matrix. The nepheline *c*-axis fabric (Fig. 9e) is weaker compared to that exhibited by sanidine, and it shows a single girdle parallel to the plane containing the mylonitic lineation and the normal to the foliation. The main maximum within the girdle is deflected in a counter-clockwise sense from the stretching lineation. This fabric is weaker and quite different to the nepheline fabric in the PPBSZ (Fig. 9c & d).

Crystals of sanidine and nepheline in the matrix constitute an anhedral framework, and their microstructures are indicative of intracrystalline plasticity. Therefore, the systematic asymmetry between crystallographic axes of sanidine and nepheline and finite strain axes may be explained in the same manner as for quartz and calcite crystallographic fabrics; i.e. as being due to the presence of a rotational component in the flow (Law, 1990). Dextral simple shearing is deduced for this minor shear zone from other kinematic criteria. The physical process by which the sanidine and nepheline lattices rotate towards the pattern shown in Fig. 9 (e) and (i–k), under a component of dextral simple shear, is unknown and is beyond the scope of this work. However it seems reasonable to assume that with the increase in the shear strain, the textures become stronger and acquire a marked symmetry (Fig. 9c, d & f–h).

Deformation conditions

The mineral changes which took place within the carbonatites in contact with the other lithologies allow a preliminary estimation of the temperature conditions during the deformation. Two stages of skarn formation are involved in the process. The first stage resulted in metasomatic calc–silicate columns. Mineral assemblages are dominated by garnet + diopside. The pyroxenites and brecciated pyroxenites are transformed into aggregates of diopside ± garnet phlogopite ± apatite ± magnetite ± sulphides. The second stage is preferentially located along fractures, where a considerable change in the previous assemblages has occurred. The diopside is replaced by serpentine and green biotite, whereas the garnet is consumed to give another colorless garnet or an assemblage of epidote/clinozoisite ± albite ± calcite.

According to field and geochemical criteria, the thickness of volcanic materials overlying the ultra-alkaline series during activity of the shear zones can be estimated as 3 km (Javoy *et al.*, 1986). This implies a lithostatic pressure of around 1 kbar. If the fluid pressure is considered to be equal to the lithostatic pressure, the assemblage of diopside + phlogopite + grossular/andradite garnet, in the absence of wollastonite, suggests a
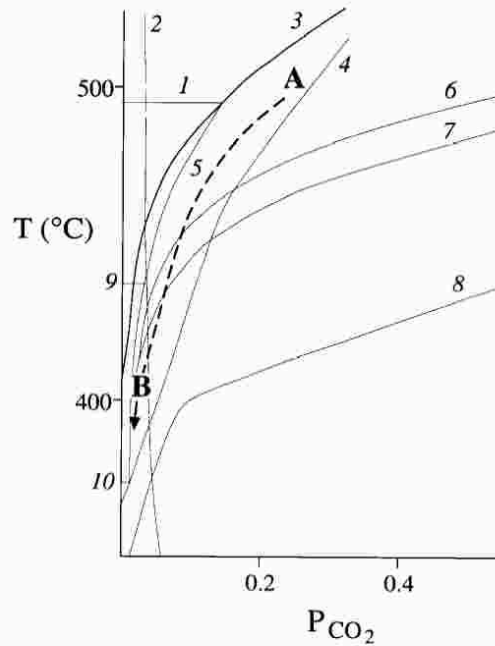
Fig. 10. T–P_{CO_2} diagram (lithostatic pressure = 1 kbar). The main reactions in the system KCMAS (H_2O–CO_2) and CAS (H_2O–CO_2) are represented (following Taylor and Liou, 1978). 1: Grossular + Quartz = Anorthite + Wollastonite; 2: Zoisite = Anorthite + Calcite; 3: Calcite + Quartz = Wollastonite; 4: Quartz + Calcite + Magnetite = Andradite; 5: Grossular = Anorthite + Calcite + Quartz; 6: Tremolite + Calcite + K-Feldspar = Diopside + Phlogopite; 7: Tremolite + Calcite + Quartz = Diopside; 8: Rutile + Calcite + Quartz = Sphene; 9: Zoisite + Quartz = Anorthite + Grossular; 10: Prehnite = Clinozoisite + Grossular + Quartz. Also shown are the interpreted conditions for the first (A) and for the second (B) metamorphic stages.

temperature of 500 °C for the first metasomatic stage (Fig. 10, point A). The assemblages of the second stage imply an evolution to lower temperature (around 400 °C) and P_{CO2} (Fig. 10, point B).

DISCUSSION

The shear zones affecting the Basal Complex of Fuerteventura show clearly the activity of plastic intracrystalline mechanisms (dislocation glide and creep and mechanical twinning). Calcite, nepheline and, to a lesser extent, sanidine and biotite/phlogopite, are the mineral phases where the microstructures and textures of plastic deformation are best developed. Pyroxene and amphibole do not exhibit unequivocal plastic intracrystalline features. This fact conditions the distinct rheological behaviour in the shear zones. A classification of rock types from least to most competent might be as follows: carbonatite, nepheline syenite, brecciated pyroxenite, basic rock of dykes, pyroxenite. The competence con-

trasts result in a wide variety of structures, as illustrated in this work. These structures demonstrate ductile or brittle–ductile behaviour. The temperature within the shear zones reaches 400–500 °C, and is probably higher than the temperature in the pyroxenite host rock. Carbonatite melts and related alkaline fluids were channelled through the shear zones and are the only local heat source available to generate the observed thermal anomaly. However, the increase in temperature cannot alone explain the ductile behaviour. The host rock is essentially composed of pyroxene and amphibole, and temperatures well above 500 °C are necessary to promote plastic deformation in these strong minerals (e.g. Mercier, 1985). A process of whole mineral transformation in the host rock, including reaction-enhanced softening (White and Knipe, 1978), is favoured here. Within the shear zones, weak plastic minerals, such as calcite, nepheline, sanidine, and phlogopite, replace strong pyroxene and amphibole. Therefore, the emplacement of carbonatite and syenite together with the metamorphic changes in the pyroxenite, which becomes a phlogopite-rich rock, is a convincing mechanism to account for the transition from the brittle to the ductile regime.

The syenites and carbonatites were emplaced between 21 and 30 Ma according to Le Bas *et al.* (1986) and Cantagrel *et al.* (1993). The complexes of gabbro and syenite ring-dykes, which were not affected by the shear zones, were emplaced at 14.6 to 20.8 Ma before present (Abdel-Monem *et al.*, 1971; Grunau *et al.*, 1975; Le Bas *et al.*, 1986; Cantagrel *et al.*, 1993). The lower part of the subaerial volcanic series, also unaffected by the ductile episode, has been dated at 22 Ma (Coello *et al.*, 1991; Ancochea *et al.*, 1993; Balcells *et al.*, 1994). Therefore, the age of the ductile deformational events may be established as Late Oligocene to Early Miocene.

Some relevant data for the interpretation of the tectonic regime that governed the activity of these shear zones have been obtained in the PPBSZ. As stated above, four sets of type 2 albitite veins are arranged in an almost orthorhombic pattern (Fig. 6b). Several authors proposed similar patterns to explain the kinematics of brittle fractures in a context of bulk non-plane deformation (e.g. Oertel, 1965; Reches, 1983; Reches and Dieterich, 1983). This concept is convincingly applied by Kirschner and Teyssier (1994) to coeval, orthorhombically arranged, en échelon vein arrays. The albitite veins in Punta del Peñón Blanco are not en échelon arrays. However, field criteria show that they accommodated some displacement parallel to the vein boundary, even though the main component is of vein-perpendicular extension. The cross-cutting relationships between the four sets suggest that they formed simultaneously. Furthermore, three lines of evidence reinforce the association between the type 2 veins and the ductile shear zones. First, the veins always appear in the immediate neighbourhood to the ductile shear zones. Second, representative orientation of the mylonitic foliation in the PPBSZ, coincide with one of the vein sets (Fig. 11a). Lastly, the orientation of minor
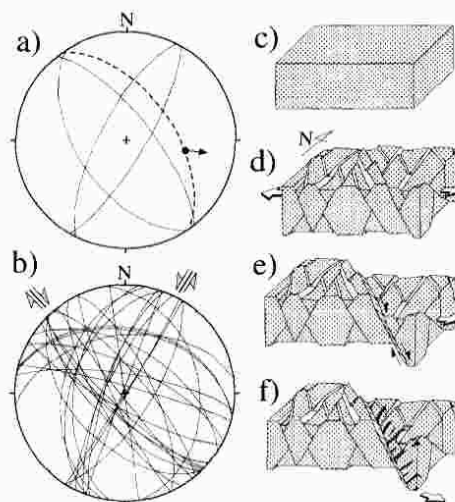
Fig. 11. (a) Equal area, lower hemisphere projection of the type 2 albitite veins of the Punta del Peñón Blanco fractured area (thin great circles); also shown are the average orientation of the foliation (dashed great circle) and stretching lineation (black dot, the arrow indicates the shear sense) in the ductile PPBSZ. (b) Equal area, lower hemisphere projection of dextral and sinistral ductile shear zones in the Basal Complex, excluding the Caleta de la Cruz and Punta del Peñón Blanco shear zones. (c) to (f) Hypothetical model for the tectonic evolution of the ductile–brittle shear zones in the Fuerteventura Basal Complex. Carbonatites and syenites are not distinguished.

ductile shear zones outside the CCSZ and PPBSZ show four sets that closely fit the pattern of the albitite veins (Fig. 11b). Interestingly, the NW-trending shear zones are consistently dextral to normal-dextral, and the NE-trending ones are sinistral to normal-sinistral. Furthermore, the minor shear zones related to the main PPBSZ present a similar configuration (Fig. 7a & b).

Accordingly, we propose the following kinematic scenario for the development of ductile shear zones in the Basal Complex of Fuerteventura (Fig. 11c–f).

(1) After the intrusion of large pyroxenite bodies and small syenite stocks (Fig. 11c) into a sedimentary and submarine volcanic series, a bulk extensional deformation began to affect these rocks. The finite deformation ellipsoid was of the general flattening type (Ramsay and Huber, 1983). The short axis of the ellipsoid was vertical, and the trend of the long and intermediate principal axes (both horizontal and implying positive elongation) was E–W and N–S, respectively. A high fluid-pressure (alkaline fluids) may have contributed to the brittle fracturing of the pyroxenite, first as a network of albitite, and then as a system of four sets of orthorhombically arranged veins (Fig. 11d). These alkaline fluids are derived through fenitization from ascending carbonatite magmas (Le Bas, 1984).

(2) Final intrusion of carbonatite magma and nepheline syenite dykes led to a rheological threshold, with the

onset of ductile deformation and large shear displacements along one or several of the previous four sets of fractures (Fig. 11e).

(3) Finally, during the waning stages of the tectonic activity, the deformation was concentrated in the hanging-wall block, with the development of tensional fractures normal to the slip vector (stretching lineation). The fluid pressure associated with the syenitic intrusions was high enough to collaborate in the development of these fractures, that became filled with the type 3 white syenite veins. They occasionally traversed the ductile fabrics at the top of the shear bands (Fig. 11f).

This model would account adequately for the observations in the Punta del Peñón Blanco area.

Giant submarine slides related to the gravitational collapse of large volcanoes have been described by Lipman *et al.* (1988) and Moore *et al.* (1995) on the west flank of the island of Hawaii. The collapse was associated to the activity of listric normal faults limiting large block-slumps in the breakaway area, and to dyke injection (Lipman *et al.*, 1988). Similarities between Fuerteventura and those collapse structures in Hawaii rely on the extensional character of the deformation. However, there are several important differences. First, the listric faults in Hawaii are thin-skinned gravity driven features that only affect the oversteepened accumulation of volcanic material (see Fig. 4 of Moore *et al.*, 1995). However, the mantle origin of the melts and alkaline fluids related to the tectonic activity of Fuerteventura, and the large displacements verified along the ductile shear zones suggest that these may be large structures of a lithosphere scale. Secondly, rapid (catastrophic) movement is advocated by Moore *et al.* (1995) to explain the characteristics of the Hawaiian slumps. The structures in the shear zones of Fuerteventura clearly need lower strain rates to develop. Thirdly, the extensional tectonics of Fuerteventura is not a local and episodic feature. The influence of this extensional regime is evident also in more recent structures, such as the dyke-swarm that traverses the Basal Complex in Fuerteventura (e.g. Stillman *et al.*, 1975; Stillman, 1987), the fracture systems in Lanzarote (Marinori and Pasquarè, 1994), or the structures recognized to the north and south of the Canary archipelago by Dañobeitia and Collette (1989). This implies similarly oriented structures covering an area with a length of several hundred of km. Furthermore, it is long-lived tectonics, lasting from at least the Upper Oligocene to the present. Fourthly, several local collapse features resembling the Hawaiian landslides have been proposed for the subaerial volcanoes of Fuerteventura by Ancochea *et al.* (1993). Current work is devoted to distinguishing the structures related to these local collapses. In brief, the explanation of the Fuerteventura tectonics must rely on a larger, lithospheric scale.

The upper mantle below the eastern Atlantic, and western and central Europe may be influenced by a large-scale mantle upwelling region, as suggested by Hoernle *et*

al. (1995). Furthermore, Neumann *et al.* (1995) proposed a thinned lithosphere beneath the eastern Canary Islands according to their study on mantle xenoliths from Lanzarote. The NE–SW elongate region of upwelling in the eastern Atlantic may be responsible for the uplift and rifting of the lithosphere, the shear zones acting as structures that accommodated vertical displacements and horizontal extension in an E–W to WNW–ESE direction (and also in a N–S direction). At the same time, these structures served as ascent channels for magmas of a deep origin in the mantle. This idea of a rifting in the Canary Islands is not new, having already been cited by Stillman *et al.* (1975).

Cannat *et al.* (1991) described similar structures in the Southwest Indian Ridge (ODP leg 118, site 735), with mylonitic shear zones and syntectonic magmatic intrusions. They relate these structures with the tectonics in slow-spreading oceanic ridges. Paleo-spreading centres in the Oman ophiolite are interpreted as the site of ascent of mantle diapirs emerging on the paleo-ridge axis (Ceuleneer, 1991), thus demonstrating the importance of the mantle upwellings in the tectonics of their overlying lithosphere. Clearly, the Fuerteventura case is one of intraplate tectonics, and the rifting process, slow and long-lasting, never produced the growth of oceanic crust with MORB signatures. However, the mechanism triggering the extension (large-scale mantle anomalies) and the structures developed are similar to those found in active or fossil ridge segments. Another important, although hitherto unexplained, issue is the relationship between this tectonic activity and the plate tectonics framework in the northwest corner of the African plate.

CONCLUSIONS

A system of ductile shear zones affected the Basal Complex of Fuerteventura from the Late Oligocene to the Early Miocene. Within the ultra-alkaline pyroxenites they began as brittle structures, associated with the ascent of alkaline magma and related fluids. These led to substantial mineral changes in the pyroxenites, which became rich in sheet-silicates and were traversed by carbonatites and syenites. Temperatures of around 500 °C were reached along these structures. A rheological change toward ductile deformation followed. This generated a large number of meso- and microstructures, as well as strong crystallographic fabrics. Two main ductile shear bands have been identified and described in this work: the Caleta de la Cruz and the Punta del Peñón Blanco shear zones.

Kinematically, these shear zones are high-angle extensional structures with variable strike-slip components. Displacements may well exceed 1 km in some cases. Both within individual fractured areas (Punta del Peñón Blanco) and as a geometrical feature of the deformed Basal Complex as a whole, the shear zones present a

nearly orthorhombic arrangement. In accordance with the interpretation given in the literature to other similar structures, a model of bulk irrotational, non-planar deformation is applied to these structures. Two principal axes of finite strain appear within the horizontal plane: the maximum positive elongation occurred in an E–W direction, with a minor extension along the N–S axis.

These geometrical and kinematical considerations, together with the magmatic context in which the shear zones were active, suggest a rifting scenario. The presence of large upwelling instability within the mantle under the African lithosphere may partly explain this tectonic activity. The complex plate-tectonics interplay between the Eurasian and African plates must be also considered, even if its influence seems more difficult to evaluate.

The development of major ductile shear zones is not exclusive to or characteristic of the continents; it may also be a conspicuous feature of the oceanic crust, not just at the plate boundaries but also in relation to intraplate tectonic activity.

REFERENCES

Abdel-Monem, A., Watkins, N. D. and Gast, P. W. (1971) Potassium–argon ages, volcanic stratigraphy, and geomagnetic polarity history of the Canary Islands: Lanzarote, Fuerteventura, Gran Canaria and La Gomera. *American Journal of Science* **271**, 490–521.

Allerton, S. and Vine, F. J. (1992) Deformation styles adjacent to transform faults: evidence from the Troodos ophiolite, Cyprus. In *Ophiolites and their Modern Oceanic Analogues* eds L. M. Parson, B. J. Murton, and P. Browning *Special Publications of the Geological Society London* **60**, 251–261.

Ancochea, E., Fúster, J. M., Ibarrola, E., Cendrero, A., Coello, L., Herndán, F., Cantagrel, J. M. and Jamond, C. (1990) Volcanic evolution of the Fuerteventura Island in the light of new K–Ar data. *Journal of Volcanology and Geothermal Research* **44**, 231–249.

Ancochea, E., Brändle, J. L., Cubas, C., Hernán, F. and Huertas, M. (1993). La Serie I de la isla de Fuerteventura. *Memorias de la Real Academia de Ciencas Exactes, Física y Naturales de Madrid* **27**, 1–151.

Ancochea, E., Hernán, F., Cendrero, A., Cantagrel, J. M., Fúster, J. M., Ibarrola, E. and Coello, J. (1994) Constructive and destructive episodes in the building of a young oceanic island, La Palma, Canary Islands and genesis of the Caldera de Taburiente. *Journal of Volcanology and Geothermal Research* **60**, 243–262.

Argus, D. F., Gordon, R. G., DeMets, C. and Stein, S. (1989) Closure of the Africa–Eurasia–North America plate motion circuit and tectonics of the Gloria fault. *Journal of Geophysical Research* **94**(B5), 5585–5602.

Balcells, R., Barrera, J. L., Gómez, J. A., Cueto, L. A., Ancochea, E., Huertas, M. L., Ibarrola, E. and Snelling, N. (1994) Edades radiométricas de los edificios miocenos de Fuerteventura (Islas Canarias). *Boletín geológico y minero* **105**, 50–56.

Banda, E., Dañobeitia, J. J., Suriñach, E. and Ansorge, J. (1981) Features of crustal structure under the Canary Islands. *Earth and Planetary Science Letters* **55**, 11–24.

Berthé, D., Choukroune, P. and Jegouzo, P. (1979) Orthogneiss, mylonite and non coaxial deformation of granites: the example of the South Armorican Shear Zone. *Journal of Structural Geology* **1**, 31–42.

Buforn, E., Udías, A. and Colombás, M. A. (1988) Seismicity, source mechanisms and tectonics of the Azores–Gibraltar plate boundary. *Tectonophysics* **152**, 89–118.

Cannat, M., Mével, C. and Stakes, D. (1991) Stretching of the deep crust at the slow-spreading Southwest Indian Ridge. *Tectonophysics* **190**, 73–94.

Cantagrel, J. M., Fúster, J. M., Pin, C., Renaud, U. and Ibarrola, E. (1993) Age Miocène inférieur des carbonatites de Fuerteventura. *Comptes Rendue de l'Académie des Sciences de Paris* **316**, 1147–1153.

Casillas, R., Ahijado, A. and Hernández-Pacheco, A. (1994) Zonas de cizalla dúctil en el Complejo Basal de Fuerteventura. *Geogaceta* **15**, 117–120.

Chase, C. G. (1978) Plate kinematics: The Americas, East Africa and the rest of the world. *Earth and Planetary Science Letters* **37**, 355–368.

Ceuleneer, G. (1991) Evidence for a paleo-spreading center in the Oman ophiolite: mantle structures in the Maqsad area. In *Ophiolite Genesis and Evolution of the Oceanic Lithosphere* eds. A. Peters, A. Nicolas and R. G. Coleman, pp. 147–173. Kluwer, Dordrecht.

Coello, L., Cantagrel, J. M., Hernán, F., Fúster, J. M., Ibarrola, E., Ancochea, E., Casquet, C. and Jamond, C. (1991) Evolution of the eastern volcanic ridge of the Canary Islands based on new K–Ar data. *Journal of Volcanology and Geothermal Research* **53**, 251–274.

Dañobeitia, J. J. and Collette, B. J. (1989) Estudio mediante sísmica de reflexión de un grupo de estructuras submarinas situadas al Norte y Sur del archipiélago Canario. *Acta Geologica Hisp.* **24**, 147–163.

Fairbairn, H. W. (1941) Petrofabric relations of nepheline and albite in litchfieldite from Blue Mountain, Ontario. *American Mineralogist* **26**, 316–320.

Fjäder, K., Gudmundsson, A. and Forslund, T. (1994) Dikes, minor faults and mineral veins associated with a transform fault in North Iceland. *Journal of Structural Geology* **16**, 109–119.

Fúster, J. M. and Aguilar, M. (1965) Nota previa sobre la geología del Macizo de Betancuria, Fuerteventura (Islas Canarias). *Estudios Geologicos* **21**, 181–197.

Fúster, J. M., Muñoz, M., Sagredo, L., Yébenes, A., Bravo, T. and Hernández-Pacheco, A. (1980) Excursión n° 121 A + c del 26° I. G. C. a las Islas Canarias. *Boletín Instituto geológico Minero España.* **92**, 351–390.

Grunau, H. R., Lehner, P., Cleintaur, M. R., Allenbach, P. and Bakker, G. (1975) New radiometric ages and seismic data from Fuerteventura (Canary Islands), Maio (Cape Verde Islands) and Sao Tomé (Gulf of Guinea). In *Progress in Geodynamics. Royal Soc. Neth. Acad. Arts Sci.* pp. 335–352. Amsterdam.

Gudmundsson, A. (1992) Formation and growth of normal faults at the divergent plate boundary in Iceland. *Terra Nova* **4**, 464–471.

Hansen, E. (1971) *Strain Facies.* Springer-Verlag, Berlin.

Hoernle, K., Zhang, Y.-S. and Graham, D. (1995) Seismic and geochemical evidence for large-scale mantle upwelling beneath the eastern Atlantic and western and central Europe. *Nature* **374**, 34–39.

Javoy, M., Stillman, C. J. and Pineau, F. (1986) Oxygen and Hydrogen isotope studies on the Basal Complexes of the Canary Islands. *Contributions to Mineralogy and Petrology* **92**, 225–235.

Kirschner, D. L. and Teyssier, C. (1994) Orthorhombically arranged vein arrays. *Journal of Structural Geology* **16**, 1129–1138.

Law, R. D. (1990) Crystallographic fabrics: a selective review of their applications to research in structural geology. In *Deformation Mechanisms, Rheology and Tectonics* eds R. J. Knipe and E. H. Rutter, *Special Publications of the geological Society London.* **54**, pp. 335–352

Le Bas, M. L. (1984) Oceanic carbonatites. In *Kimberlites and Related Rocks*, ed. L. Kornprobst, pp. 169–178. Elsevier, Amsterdam.

Le Bas, M. J., Rex, D. C. and Stillman, C. J. (1986) The early magmatic chronology of Fuerteventura. *Geological Magazine* **123**, 287–298.

Lipman, P. W., Normark, W. P., Moore, J. G., Wilson, J. B. and Gutmacher, C. E. (1988) The giant submarine Alika debris slide, Mauna Loa, Hawaii. *Journal of Geophysical Research* **93**, 4279–4299.

MacLeod, C. J. and Murton, B. J. (1993) Structure and tectonic evolution of the Southern Troodos Transform Fault Zone, Cyprus. In *Magmatic Processes and Plate Tectonics*, eds H. M. Prichard, T. Alabaster, N. B. W. Harris and C. R. Neary, *Special Publications of the Geological Society, London.* **76**, pp. 141–176.

Marinoni, L. B. and Pasquaré, G. (1994) Tectonic evolution of the emergent part of a volcanic ocean island: Lanzarote, Canary Islands. *Tectonophysics* **239**, 111–135.

Meco, J. and Pomel, R. (1985) Les formations marines et continentales intravolcaniques des Iles Canaries Orientales (Grande Canaria,

Shear zones in oceanic crust, Fuerteventura   57

Fuerteventura et Lanzarote): Stratigraphie et signification paléoclimatique. *Estudios Geológicos* **41**, 223–228.

Mercier, J.-C. C. (1985) Olivine and pyroxenes. In *Preferred Orientation in Deformed Metals and Rocks: an Introduction to Modern Texture Analysis*, ed. K.-R. Wenk, pp. 407–430. Academic Press, Orlando.

Minster, J. B. and Jordan, T. H. (1978) Present-day plate motions. *Journal of Geophysical Research* **83**(B11), 5331–5354.

Moore, J. G., Bryan, W. B., Beeson, M. H. and Normark, W. R. (1995) Giant blocks in the South Kona landslide, Hawaii. *Geology* **23**, 125–128.

Moreira, V. S. (1991) Historical seismicity and seismotectonics of the area situated between the Iberian Peninsula, Morocco, Selvagens and Azores Islands. In *Seismicity, Seismotectonics and Seismic Risk of the Ibero–Maghrebian Region*, ed. J. Mezcua and A. Udías, *Publicaciones del Instituto Geográfico Nacional*. Vol. **8**, pp. 213–225.

Morgan, W. J. (1983) Hotspot tracks and the early rifting fo the Atlantic. *Tectonophysics* **94**, 123–139.

Müller, R. D., Royer, J.-Y. and Lawver, L. A. (1993) Revised plate motions relative to the hotspots from combined Atlantic and Indian Ocean hotspot tracks. *Geology* **21**, 275–278.

Neumann, E.-R., Wulff-Pedersen, E., Johnsen, K., Andersen, T. and Krogh, E. (1995) Petrogenesis of spinel harzburgite and dunite suite xenoliths from Lanzarote, eastern Canary Islands: Implications for the upper mantle. *Lithos* **35**, 83–107.

Nicolas, A. (1989) *Structure of Ophiolites and Dynamics of Oceanic Lithosphere*. Kluwer, Dordrecht.

Oertel, G. (1965) The mechanism of faulting in clay experiments. *Tectonophysics* **2**, 343–393.

Passchier, C. W. and Simpson, C. (1986) Porphyroclast systems as kinematic indicators. *Journal of Structural Geology* **8**, 831–843.

Ramsay, J. G. and Huber, M. (1983) *The Techniques of Modern Structural Geology, Strain Analysis*, **Vol. 1**, Academic Press, London.

Reches, Z. (1983) Faulting of rocks in three-dimensional strain fields II; Theoretical analysis. *Tectonophysics* **95**, 133–156.

Reches, Z. and Dieterich, J. (1983) Faulting of rocks in three-dimensional strain fields I. Failure of rocks in polyaxial, servo-control experiments. *Tectonophysics* **95**, 111–132.

Renz, O., Bernouilli, D. and Hottinger, L. (1992) Cretaceous ammonites from Fuerteventura, Canary Islands. *Geological Magazine* **129**, 763–769.

Robertson, A. H. F. and Bernouilli, D. (1982) Stratigraphy, facies and significance of Late Mesozoic and Early Tertiary sedimentary rocks of Fuerteventura (Canary Islands) and Maio (Cape Verde Islands). In *Geology of the Northwest African Continental Margin*, eds U. Von Rad, K. Hinz, M. Sarnthein and E. Seibold, pp. 498–525. Springer-Verlag, Berlin.

Robertson, A. H. F. and Stillman, C. J. (1979) Late Mesozoic sedimentary rocks of Fuerteventura, Canary Islands. Implications for West Africa continental margin evolution. *Journal of Geological Society London* **136**, 47–60.

Robertson, A. H. F. and Stillman, C. J. (1979) Submarine volcanic and associated sedimentary rocks of the Fuerteventura Basal Complex, Canary Islands. *Geological Magazine* **116**, 203–214.

Rothe, P. (1968) Mesozoische Flysch-Alblagerugen auf der Kanareninsel Fuerteventura. *Geologische Rundschau* **58**, 314–332.

Sacerdoti, M., Labernadiere, H. and Gandais, M. (1980) Transmission electron microscope (TEM) study of geologically deformed potassic feldspars. *Bulletin Mineralogique* **103**, 155–158.

Sagredo, L, Ancochea, E., Brändle, J. L., Cubas, C. R., Fúster, J. M., Hernández-Pacheco, A. and Muñoz, M. (1989) Magmatismo hipoabisal-subvolánico y vulcanismo en un ámbito geodinámico distensivo (Fuerteventura, Islas Canarias). Meeting on Canarian Volcanism. Lanzarote Abstracts (European Science Foundation). pp. 100–103.

Scandale, E., Gandais, M. and Willaime, C. (1983) Transmission electron microscopy study of experimentally deformed K-feldspar single crystals. The (010)[001], (001)112[110], (110)1/2[112] and (111)1/2[110] slip systems. *Physics and Chemistry of Minerals* **9**, 182–187.

Schmid, S., Panozzo, R. and Batier, S. (1987) Simple shear experiments on calcite rocks: rheology and microfabric. *Journal of Structural Geology* **9**, 747–778.

Schmincke, H. U. (1982) Volcanic and chemical evolution of the Canary Islands. In *Geology of the Northwest African Continental Margin*, eds U. Von Rad, K. Hinz, M. Sarnthein and E. Seibold, pp. 274-306. Springer-Verlag, Berlin.

Smith, J. V. and Brown, W. L. (1988) *Feldspar Minerals*. Crystal Structures, Physical, Chemical and Microtextural Properties, **Vol 1**, Springer-Verlag, Berlin.

Staudigel, H. and Schmincke, H. U. (1984) The Pliocene seamount series of La Palma, Canary Islands. *Journal of Geophysical Research* **89**(B13), 11195–11215.

Stillman, C. J. (1987) A Canary Islands dyke swarm: Implications for the formation of oceanic islands by extensional fissural volcanism. In *Mafic Dyke Swarms*, eds H. C. Halls and W. R. Fahrig, *Geological Association of Canada Special Paper* **34**, pp. 243–255.

Stillman, C. J., Fúster, J. M., Bennell-Baker, M. J., Muñoz, M., Smewing, J. D. and Sagredo, J. (1975) Basal Complex of Fuerteventura (Canary Islands) as an oceanic intrusive complex with rift-system affinities. *Nature* **257**, 469–471.

Sturt, B. A. (1961) Preferred orientation of nepheline in deformed nepheline syenite gneisses from Sørøy, northern Norway. *Geological Magazine* **98**, 464–467.

Taylor, B. E. and Liou, J. G. (1978) The low-temperature stability of andradite in C–O–H fluids. *American Mineralogy* **63**, 378–393.

Turner, F. J. and Weiss, L. E. (1963) Structural Analysis of Metamorphic Tectonites. McGraw-Hill, New York.

Varga, R. J. (1991) Modes of extension at oceanic spreading centers: evidence from the Solea graben, Troodos ophiolite, Cyprus. *Journal of Structural Geology* **13**, 517–537.

Vegas, R. (1985) Tectónica del área Ibero-Mogrebí. In *Mecanismo de los terremotos y tectónica* eds A. Udías, D. Muñoz and E. Buforn, pp. 197-215. Universidad Complutense de Madrid.

Villemin, T., Bergerat, R., Angelier, J. and Lacasse, C. (1994) Brittle deformation and fracture patterns on oceanic rift shoulders: the Esja peninsula, SW Iceland. *Journal of Structural Geology* **16**, 1641–1654.

Weijermars, R. (1988) Where does Africa meet Europe? *Nature* **332**, 118.

Westaway, R. (1990) Present-day kinematics of the plate-boundary zone between Africa and Europe, from the Azores to the Aegean. *Earth and Planetary Science Letters* **96**, 393–406.

Wenk, H.-R. and Christie, J. M. (1991) Comments on the interpretation of deformation textures in rocks. *Journal of Structural Geology* **13**, 1091–1110.

White, S. H. and Knipe, R. P. (1978) Transformation-and reaction-enhanced ductility in rocks. *Journal of Geological Society London* **135**, 513–516.

Willaime, C., Christie, J. M. and Kovacs, M.-P. (1979) Experimental deformation of K-feldspar single crystals. *Bulletin Mineralogy* **102**, 168–177.

Contributions to the chronology of the Basal Complex of Fuerteventura, Canary Islands

K. Balogh [a], A. Ahijado [b,*], R. Casillas [b], C. Fernández [c]

[a] *Institute of Nuclear Research, Hungarian Academy of Sciences, H-4026 Debrecen, Hungary*
[b] *Depto. de Edafología y Geología, Universidad de La Laguna, 38206 Santa Cruz de Tenerife, Spain*
[c] *Depto. de Geología, Universidad de Huelva, 21819 Palos de la Frontera, Huelva, Spain*

Abstract

K–Ar and Ar–Ar analyses of the Basal Complex of Fuerteventura confirm the early start of magmatism in the Late Cretaceous. Plateau ages of 63.1 ± 0.8 Ma and 64.2 ± 1.0 Ma have been obtained for the oldest syenite intrusions indicating the minimum age of these plutonics. The emplacement of carbonatites and syenites along ductile shear zones took place during a relatively short period of time between 23.2 ± 1.0 and 22.1 ± 0.9 Ma. This episode is synchronous all over the island. Younger plutons were intruded around 21.1 ± 0.8 Ma ago and 20.7 ± 0.9 Ma and are probably related to the building of Miocene subaerial edifices. Almost all the minerals and rocks of the Basal Complex show a clear effect of excess argon. Some was acquired during the hydrothermal stage but also some excess argon was trapped during the early crystallization stage of the magma. Moreover, only a part of the radiogenic Ar which had accumulated in pre-Miocene rocks was released during the Miocene magmatism. © 1999 Elsevier Science B.V. All rights reserved.

Keywords: magmatism; carbonatites; syenites

1. Introduction

The Fuerteventura Basal Complex reveals a history of transition from normal ocean-floor sedimentation at the foot of the West African continental margin to the uplift and building of a discrete oceanic island (Stillman et al., 1975). Various attempts have been made to determine a chronostratigraphy for this Basal Complex. Most of the results have been obtained by the conventional K–Ar method. These studies have been partly frustrated by the combination of two problems: excess argon in the rocks; and a succession of thermal events bringing about resetting of the K–Ar clocks (Rona and Nalwalk, 1970; Abdel-Monem et al., 1971; Grunau et al., 1975; Feraud et al., 1985; Le Bas et al., 1986; Ibarrola et al., 1989; Cantagrel et al., 1993; Sagredo et al., 1996).

The age of the beginning of magmatic activity remains unclear and considerable controversy has surrounded some of the attempts to date the earliest magmatic events on Fuerteventura. On the basis of geological evidence, Le Bas et al. (1986) consider

* Corresponding author. Fax: +34-22-253344; E-mail: aahijado@ull.es

Fuerteventura as the result of a long period of magmatic activity that began around the time of the Cretaceous–Tertiary transition. The oldest K–Ar age presented by them is 48 Ma. They attribute the lack of older ages to resetting of K–Ar data by metamorphism. In contrast, Cantagrel et al. (1993) suggest a short eruptive history for this island, the Basal Complex having been developed between 30 and 20 Ma ago. This paper aims to contribute to the solution of these questions by additional determinations and an to attempt evaluate the effects of argon loss and excess argon.

2. Geological background

Two major geological units can be distinguished in the Canary Islands: the Basal Complex, and a younger subaerial volcanic series comprising Miocene series I and Pliocene–Quaternary series II, III and IV (Fúster et al., 1968; Coello et al., 1992). On Fuerteventura the Basal Complex is exposed in the western part of the island (Fig. 1), and consists of a group of sedimentary materials, submarine volcanic rocks, plutonic intrusions and dike swarms generated mainly during the stage of submarine
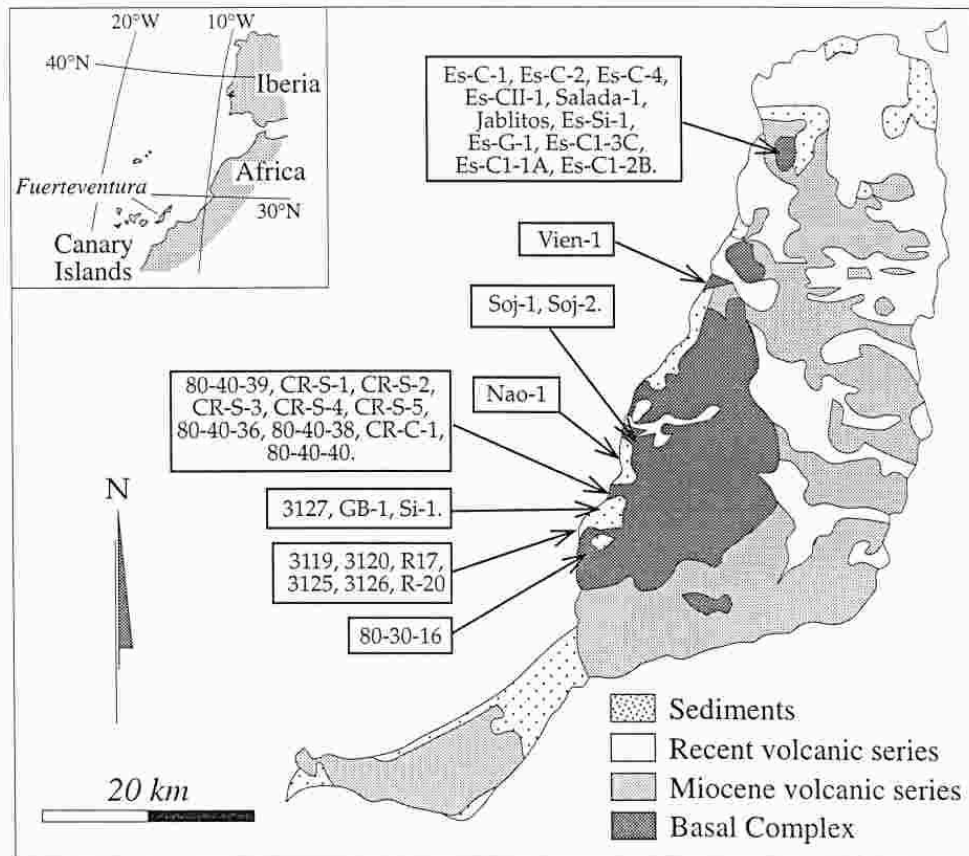
Fig. 1. Geological map of Fuerteventura with the location of samples. Inset: location of the Canary Islands.

growth of the island (Fúster et al., 1968; Stillman et al., 1975; Fúster et al., 1980; Le Bas et al., 1986; Stillman, 1987). This unit has been interpreted as an aborted oceanic rift (Stillman et al., 1975).

The Mesozoic deep-water sediments (Upper Jurassic to Lower–Middle Cretaceous) document more or less continuous hemipelagic and turbiditic deposition on the deep Atlantic sea floor adjacent to the African margin (Rothe, 1968; Robertson and Stillman, 1979a; Yebenes, 1980; Robertson and Bernouilli, 1982; Renz et al., 1992). The terrigenous material is thought to have been derived from the Precambrian crystalline rocks and folded Palaeozoic rocks of the Anti-Atlas located to the south of the South Atlas fault belt. The redeposited platform carbonate material was probably derived from disintegration of a carbonate platform recorded in deep seismic records about 50 km east of Fuerteventura (Robertson and Stillman, 1979a).

Submarine volcanic rocks form most of the Basal Complex and consist of basaltic volcanic breccias, hyaloclastites and pillow-lavas which are affected by an intense hydrothermal metamorphism in greenschist epidote–albite facies (Fúster et al., 1980; Ibarrola et al., 1989). The base of the volcanic formation is in apparent stratigraphic continuity with the Mesozoic sedimentary series. They form a part of the overturned limb of a recumbent fold (Robertson and Stillman, 1979a,b). Levels of bioclastic and volcanoclastic sediments appear locally within the submarine volcanic formation. These unstrained fossiliferous sediments (Middle to Late Oligocene) were formed in the shallow waters of a reef environment (Fúster and Aguilar, 1965; Robertson and Stillman, 1979a). In some areas of the Basal Complex, the submarine volcanic formation passes gradually to the basaltic subaereal lava flows of the basement of Miocene volcanic edifices (Ancochea et al., 1996).

The Mesozoic and Early Tertiary bedded succession is extensively intruded by numerous small plutonic and hypabbyssal intrusions. Four plutonic episodes can be recognized from cross-cutting relationships.

2.1. A1 rock group

The earliest event forming this group of rocks was the emplacement of a series of ultramafic and mafic rocks intruded by syenites (Le Bas et al., 1986; Ahijado and Hernández-Pacheco, 1990) which are exposed along the west coast of the island.

The oldest ultramafic and mafic rocks are composed of alkali pyroxenites, amphibololites and amphibole gabbros (Fúster et al., 1980; Ahijado and Hernández-Pacheco, 1990), and form large intrusive bodies of unknown geometry since they are covered by younger volcanic series and sedimentary formations. Their mineralogy is characterised by kaersutite, titanian diopside, apatite, magnetite and ilmenite.

The syenitic intrusions (Tierra Mala formation, Le Bas et al., 1986) are formed by hypersolvus alkaline feldspar, nepheline, aegirine augite, biotite, sphene, magnetite, apatite and zircon.

2.2. A2 rock group

A1 plutonic rocks are intruded by carbonatite, syenite dikes and ijolites. They form three complexes located from north to south at Esquinzo, Ajuí-Solapa and Punta del Peñón Blanco (Fúster et al., 1980; Le Bas, 1981; Barrera et al., 1986; Le Bas et al., 1986; Ahijado and Hernández-Pacheco, 1992). The emplacement of these rocks was simultaneous with the action of diverse brittle–ductile to ductile shear zones that represent important normal and strike–slip faults and affect especially the Caleta de la Cruz and Punta del Peñón Blanco outcrops (Casillas et al., 1994; Fernández et al., 1997).

The carbonatites are sövites composed of calcite, sanidine, phlogopite, aegirine, apatite, pyrochlore, magnetite and zircon. The syenites consist of several intrusions of nepheline syenites and are composed of sanidine, aegirine–augite, nepheline, biotite, magnetite, sphene and pyrochlore. In the ductile deformation structures, mineral changes took place within the carbonatites in contact with the other lithologies. The high temperature skarn stage resulted in metasomatic calc–silicate columns; the mineral assemblages are dominated by grossular–andradite garnet and diopside (Fernández et al., 1997).

2.3. A3 rock group

Cutting these early intrusions are various elongate NNE–SSW bodies of gabbro and pyroxenite that

produced high grade thermal metamorphic effects on the host-rocks. They form different plutons in the central and northern part of the Basal Complex (Gastesi, 1969; Muñoz and Sagredo, 1975; Stillman et al., 1975; Muñoz and Sagredo, 1989, 1994), and are characterised by variable amounts of olivine, titanian diopside, plagioclase, kaersutite, biotite, magnetite and apatite.

2.4. A4 rock group

The youngest plutons form concentric patterns of gabbro and syenite which constitute the Vega de Rio de Palmas Ring Complex (Muñoz, 1969). This is a high level permissive intrusion that sets a younger age limit to all these plutonic units.

Basaltic dike swarms traverses the various lithologies. The density of dike intrusion is extremely high in the Mesozoic sedimentary sequence, submarine volcanic rocks and the two first plutonic units (A1 and A2 rock groups), occupying more than 70% of the outcrops. From the detailed mapping of the Punta del Peñón Blanco and Caleta de la Cruz outcrops it has been determined that 70–80% of the dike intrusions are simultaneous with or younger than the shear zones (Fernández et al., 1997). The genesis of these dike swarms seems to have involved a crustal extension of more than 30 km (López Ruiz, 1970; Stillman and Robertson, 1977; Stillman, 1987).

3. Methods

3.1. K–Ar dating

Measurement of K–Ar ages was performed in the Institute of Nuclear Research of the Hungarian Academy of Sciences (ATOMKI), Debrecen. The samples were first crushed to 0.3–0.1 mm according to the grain sizes of minerals. Heavy liquids, magnetic separation and tapping on a paper sheet were used for mineral separation. Part of each sample was pulverized for K determination. An argon extraction line and a mass spectrometer, both designed and built in the ATOMKI, were used for the Ar measurement. The rock was degassed by high frequency induction heating, the usual getter materials (titanium sponge, getter pills of SAES St 707 type and cold

traps) were used for cleaning and transporting Ar. The ^{38}Ar spike was introduced to the system from a gas-pipette before the degassing was started. The purified Ar was directly introduced into the mass spectrometer. The mass spectrometer was a 90° magnetic sector type of 150 mm radius and was operated in the static regime. Recording and evaluation of the Ar spectrum was controlled by a microcomputer. Potassium was determined by flame photometry with a Li internal standard and Na buffer.

The interlaboratory standards Asia 1/65, HD-B1, LP-6 and GL-O as well as atmospheric Ar were used for controlling and calibration of the analyses. Details of the instruments, the applied methods and results of calibration have been described elsewhere (Odin et al., 1982; Balogh, 1985). K–Ar ages were calculated using the constants proposed by Steiger and Jäger (1977).

3.2. Ar–Ar dating

Samples were irradiated for 8 hours in the 229/3 position (out of the centre of the core) of the nuclear reactor of the Central Institute of Physics, Budapest, along with interlaboratory standard biotite LP-6. Distribution of fast neutron flux was monitored with Ni foils. The fast neutron flux was 1.46×10^{13} neutron/cm^2/s, and the total neutron dose was 4.2×10^{17} neutron/cm^2. Samples were wrapped in Al foil and placed in a cylindrical container made of 0.5 mm thick Cd. The Cd container was sealed hermetically in an Al canister.

Ar extraction was performed in a resistance heated molybdenum furnace. Temperature was controlled with a Pt–PtRd thermocouple. The furnace was connected to the Ar purification line used for K–Ar dating. Samples were heated for 50 min at each temperature step. Procedural system blanks (atmospheric composition) were measured before degassing at each temperature step (from 10^{-9} increasing to 10^{-8} cm^3 STP Ar at 1400°C).

4. Discussion of the results

4.1. Mesozoic sedimentary sequence

The age of the sedimentary sequence is well constrained by paleontological evidence (Rothe,

1968; Robertson and Stillman, 1979a; Yebenes, 1980; Robertson and Bernouilli, 1982; Renz et al., 1992). However, we have measured the K–Ar ages of these rocks to investigate the degree of radiogenic argon retention during regional metamorphism and/or the thermal effects of dike intrusion.

Three samples have been studied (Table 1). Vien-1 is a lutite from the northern outcrop of the sedimentary sequence and Soj-1 and Soj-2 are a sandstone and a lutite, respectively, from Barranco de Sojames in the southern outcrop (Unit D: Sandstone–Siltstone–Shale, Robertson and Stillman, 1979a) (Fig. 1). Vien-1 and Soj-1 samples give ages of 187 and 437 Ma, respectively, clearly reflecting argon-retaining detrital minerals. Sample SOJ-1 is particularly old, suggesting the presence of detrital minerals (feldspar and quartz) of African origin (Robertson and Stillman, 1979a).

Sample SOJ-2 may contain clays that seem to be generated during the folding stage of the sedimentary sequence. The age of 49 Ma may tentatively be assigned to the tectonic event which affected these rocks. Le Bas et al. (1986), in their chronology of Fuerteventura, suggest a similar age for this folding.

4.2. Early gabbro–pyroxenite–syenite intrusions (A1 rock group)

4.2.1. Ultramafic plutons

We have sampled the ultramafic plutonic bodies in the southernmost coastal outcrops near Punta del Peñón Blanco, where these rocks are less affected by younger intrusions (3119–3120) and have taken another sample (80-40-39) in the Caleta de la Cruz outcrop close to a syenitic–carbonatitic intrusion (A2 rock group) (Fig. 1). Their K–Ar ages (Table 1) increase with decreasing K content; this correlation, if it does not reflect the true age relations, may be caused by excess argon. The points representing the 3 samples from the ultramafic plutons define a straight line in the ^{40}Ar(rad)–K diagram (Fig. 2) and indicate an age of 21.9 ± 0.9 Ma. This age, defined only by three points, could be an artifact, but its similarity to the age obtained on the biotite from the carbonatite at Caleta de la Cruz (23.8 ± 1.0 Ma, Table 2) suggests that K–Ar ages on the ultramafic plutons are influenced by the incorporation of excess argon at the time of carbonatite intrusion. This implies that the geological reliability of the age of

Table 1
K–Ar analytical results of the sedimentary sequence and the Early gabbro–pyroxenite–syenite intrusions

Sample	Rock type	Locality	Source	%K	^{40}Ar(rad) cm^3 STP/g	^{40}Ar(rad)/ ^{40}Ar(tot)	Age, Ma $\pm \delta$
Sedimentary sequence							
VIEN-1	lutite	Punta del Viento	w.r.	1.83	1.405×10^{-5}	0.799	187.4 ± 7.1
SOJ-1	sandstone	Barranco de Sojames	w.r.	2.33	4.476×10^{-5}	0.936	437.0 ± 17.0
SOJ-2	lutite	Barranco de Sojames	w.r.	4.49	8.685×10^{-6}	0.692	49.1 ± 1.9
A1 group: Early gabbro–pyroxenite–syenite intrusions							
Ultramafic plutons							
3119	amphibololite	La Matanza	w.r.	0.70	8.607×10^{-7}	0.493	31.4 ± 1.4
3120	pyroxenite	La Matanza	w.r.	0.14	3.5475×10^{-7}	0.347	64.7 ± 3.2
80-40-39	amphibololite	Caleta Cruz	w.r.	2.95	2.7115×10^{-6}	0.517	23.5 ± 1.0
Syenite intrusions							
CR-S-1	syenite	Caleta Cruz	w.r.	6.58	9.947×10^{-6}	0.884	38.5 ± 1.5
CR-S-2	syenite	Caleta Cruz	w.r.	0.81	1.463×10^{-6}	0.595	45.7 ± 1.9
CR-S-3	syenite	Caleta Cruz	w.r.	4.86	1.1153×10^{-5}	0.915	60.0 ± 2.3
CR-S-3	syenite	Caleta Cruz	biotite	2.31	4.611×10^{-6}	0.172	50.6 ± 4.2
CR-S-4	syenite	Caleta Cruz	w.r.	3.56	6.176×10^{-6}	0.823	47.6 ± 1.8
80-40-36	syenite	Caleta Cruz	w.r.	0.59	1.648×10^{-6}	0.289	70.6 ± 3.9
80-40-38	syenite	Caleta Cruz	w.r.	5.89	1.048×10^{-5}	0.793	45.2 ± 1.7
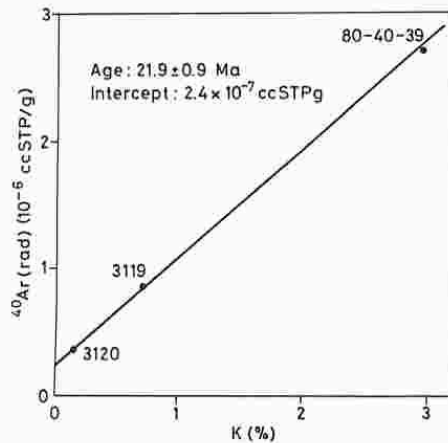
Fig. 2. Isochron diagram for the early ultramafic rocks.

64.7 ± 3.2 Ma (Table 1) on the pyroxenite from La Matanza (sample 3120) must be treated with caution, as it could be the result of incorporated excess argon.

Few data from this unit are available in the literature. Le Bas et al. (1986) measured a phlogopite concentrate from a phlogopitized pyroxenite of Caleta de la Cruz and obtained an age of 22.0 ± 1.0 Ma (Sample 75/199, Table 3), which they consider to be the result of thermal resetting produced by the youngest intrusions of this area (Vega-type syenites) since—following their argument—carbonatites are too old to generate this effect.

Our sample (80–40–39), from beside a carbonatite dike, has a similar location and composition and also gives an age of 23.5 ± 1 Ma. This result does not differ significantly from the age of the carbonatite intrusions in Fuerteventura (Cantagrel et al., 1993; this work). Thus, this syenite–carbonatite unit seems to be the best candidate to produce a thermal effect on the oldest formations in Caleta de la Cruz outcrop. Moreover, the rocks intruded by the carbonatites often recrystallize to grossularite. These metamorphic reactions have been interpreted as produced by a skarn event associate with the emplacement and deformation of the carbonatites (Fernández et al., 1997). Consequently, the problem of dating the oldest plutonic intrusions of Fuerteventura remains un-

Table 2
K–Ar analytical results of the syenite–carbonatite complexes

Sample	Rock type	Locality	Source	%K	^{40}Ar(rad) cm^3 STP/g	^{40}Ar(rad)/ ^{40}Ar(tot)	Age, Ma $\pm \delta$
A2 rock group: syenite–carbonatite complexes							
Esquinzo complex							
Es-C-1	carbonatite	Las Montañetas	feldspar	3.73	1.625×10^{-5}	0.777	109.0 ± 4.1
Es-C-2	carbonatite	Las Montañetas	feldspar	1.20	1.042×10^{-5}	0.480	211.0 ± 9.0
ES-C-4	carbonatite	Las Montañetas	feldspar	5.22	5.663×10^{-5}	0.483	27.7 ± 1.2
ES-CII-1	syenite	Los Jablitos	feldspar	12.22	1.480×10^{-5}	0.823	30.9 ± 1.2
Salada-1	carbonatite	Barranco del Agua Salada	phlogopite	7.60	8.008×10^{-6}	0.794	26.9 ± 1.0
Jablitos	carbonatite	Los Jablitos	phlogopite	4.05	4.459×10^{-6}	0.091	28.1 ± 4.3
Es-Si-1	syenite	Barranco de Esquinzo	feldspar	7.13	10.15×10^{-6}	0.404	36.3 ± 1.7
Ajui–Solapa complex							
NAO-1	carbonatite	Punta La Nao	feldspar	6.69	9.974×10^{-6}	0.900	38.0 ± 1.4
			magnetic minerals	1.02	2.285×10^{-6}	0.610	56.7 ± 2.2
CR-S-5	syenite	Caleta de la Cruz	w.r.	1.20	1.253×10^{-6}	0.575	26.7 ± 1.1
CR-C-1	carbonatite	Caleta de la Cruz	biotite	7.04	6.571×10^{-6}	0.692	23.8 ± 1.0
Punta del Peñón Blanco complex							
R-17	syenite	Punta Peñón Blanco	w.r.	1.60	1.384×10^{-6}	0.257	22.1 ± 1.3
3125	carbonatite	Punta Peñón Blanco	biotite	7.03	6.239×10^{-6}	0.585	22.7 ± 0.9
3126	carbonatite	Punta Peñón Blanco	feldspar	10.38	9.728×10^{-6}	0.747	24.0 ± 0.9

Table 4
Measured and calculated ages on fractions of CR-S-3 syenite

Fraction	Weight, g	K, %	^{40}Ar(rad) cm^3 STP/g	^{40}Ar(rad)/ ^{40}Ar(tot)	Age, Ma $\pm \delta$
D1 ($d < 2.58$ g/cm^3)	1.50	5.11	1.380×10^{-5}	0.905	68.2 ± 2.6
D1R (Residue of D1)	1.03	6.57	1.404×10^{-5}	0.921	54.2 ± 2.0
D1D*	0.47	1.91	1.327×10^{-5}		170.0
D2 (2.58 g/cm^3 $< d < 2.63$ g/cm^3)	1.5	4.93	1.156×10^{-5}	0.887	59.3 ± 2.2
D2R (Residue of D2)	1.00	5.59	1.070×10^{-5}	0.718	48.6 ± 1.9
D2D**	0.5	3.61	1.328×10^{-5}		92.2

* and **: D1D and D2D are the dissolved fractions of D1 and D2, the given values are calculated.

residues of 1.03 g for D1 and 1.00 g for D2. XRD analysis showed that residues did not contain nepheline. All four fractions were dated and ages were calculated for the dissolved parts of D1 and D2 (Table 4). Measured ages and the very old calculated ages for the dissolved fractions do not contradict the assumption that excess argon is in the nepheline. However, there is an alternative explanation, namely that excess argon is concentrated near to the mineral boundary of feldspars and nepheline, and is liberated during acid treatment. However, ages of the residue feldspars are still old and suggest that the older ages cannot be explained only by excess Ar in the nepheline and/or in sites near to the grain boundary of feldspar.

Ar–Ar measurements were performed on D1 (feldspar + nepheline) and D1R (feldspar) in order to compare the argon retentivity of nepheline and to observe the influence of this effect on ages (Table 3). The age spectrum of D1 starts with an old age of 171.3 Ma at 550°C; this is followed by younger ages (53.9–54.8 Ma) in the next two steps, and from 850°C a plateau is obtained for 66.5% of cumulative ^{39}Ar release (Fig. 3a). The age spectrum of D1R shows younger ages for steps until 790°C, and thereafter rises to a plateau of 64.2 ± 1.0 Ma, which is very close to the plateau of D1: 63.1 ± 0.8 Ma for steps from 937°C (Fig. 3b). The old first step age of fraction D1 is clearly caused by excess argon and this excess argon was mostly removed in D1R by the acid treatment.

Relatively few K–Ar ages have been reported on nepheline in the literature, but it appears quite retentive of radiogenic argon (e.g., MacIntyre et al., 1966). Therefore, considering also that the plateau ages of fraction D1 and the nepheline free D1R fraction are very similar, it is believed that excess argon is located near to the grain boundaries and not in the bulk of nepheline.

The age spectra of fractions D1 and D1R are interpreted (similar to Harrison and McDougall, 1982) as superposition of an argon loss profile formed from a flat spectrum that was retained partly in the plateau, and an incorporation profile of excess argon. The maximum age of argon loss is the youngest age of 24.5 Ma of fraction D1R at 670°C. Thereafter, at lower temperature, excess argon diffused in the near-boundary sites of mineral grains.

The coinciding plateau ages (63.1 ± 0.8 Ma and 64.2 ± 1.0 Ma) are accepted as the time of intrusion, i.e., the Ar–Ar spectra support the geological evidence of an old magmatic activity (Le Bas et al., 1986). The authors believe that the interpretation of saddle-shaped age spectra as followed by Zeitler and Fitz Gerald (1986) cannot be adopted here due to the plateaus. Explanation of the old plateau ages with excess Ar in the cooling syenite would be possible only by assuming a high (more than 1000) ^{40}Ar/^{36}Ar ratio for the incorporated argon. In the light of the K–Ar ages of the syenite intrusions (Table 1) and isotope data on the fractions of Cr-S-3 (Table 3) this assumption appears to be unrealistic.

Fig. 3. Ar–Ar spectra of separate fractions from a syenite from sample CR-S-3. (a) D1 fraction (feldspar + nepheline); (b) D1R fraction (feldspar).

(a)

CR-S-3, D1   K/Ar No. 3563

(b)

CR-S-3, D1R
K/Ar No. 3563

121
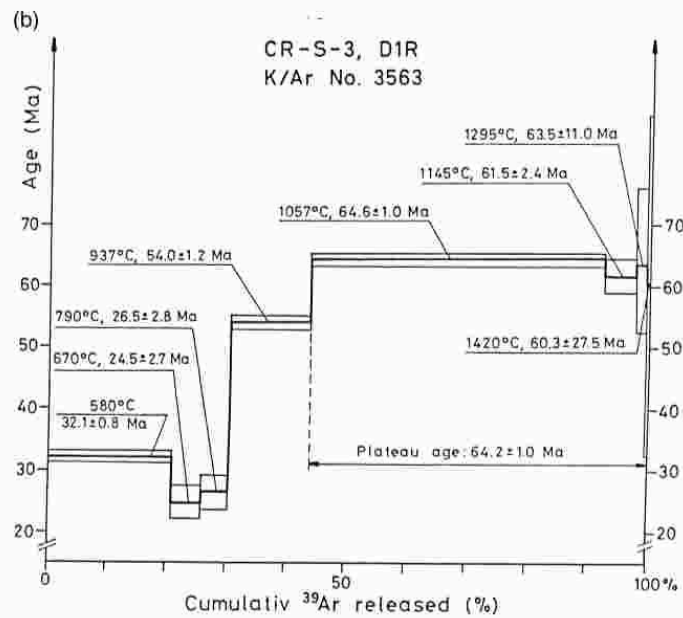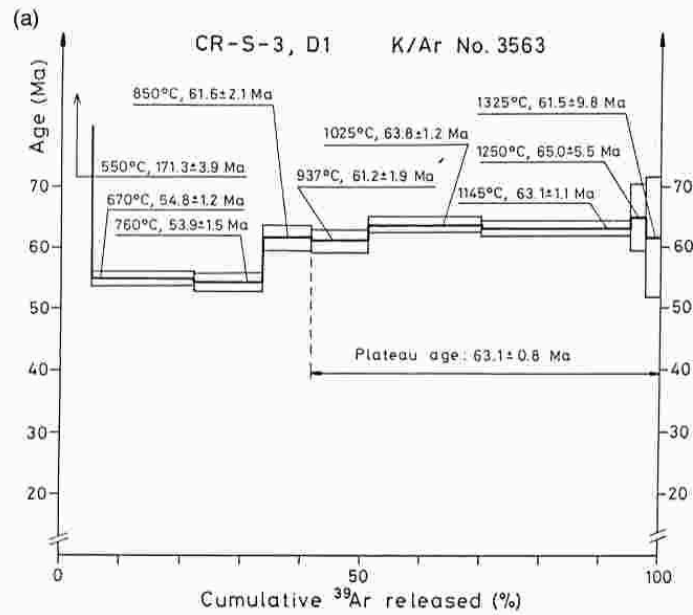
Diffusion parameters calculated from the fractional losses have been plotted in the Arrhenius diagram (Fig. 4) for the D1 and D1R fractions. A bend can be observed around 800°C; this is most likely caused by inhomogeneity of grain sizes, while the turning downward at 1100–1200°C is attributed to phase homogenization, as it has been shown by Harrison and McDougall (1981). An activation energy of 44.3 ± 1.2 kcal/mol has been obtained for the ^{39}Ar released in the 937–1145°C temperature range, where the more retentive part of argon is liberated. Calculated closure temperatures are 266°C to 293°C assuming cooling rates from 10°C/Ma to 100°C/Ma.

If part of the radiogenic argon was released during one or more short thermal pulses, then a part of radiogenic argon might have been retained at even higher temperature. The relatively high closure temperature of CR-S-3 feldspar supports the reality of the old plateau age. Additionally, the K/Ar age of an altered biotite from CR-S-3 gave 50.6 ± 4.2 Ma. (Table 1). This is regarded as an additional argument for old magmatism on the basis of the work by Zeitler and Fitz Gerald (1986). They studied K-feldspars with large amounts of excess argon and observed that coexisting biotite was free of excess argon. We attribute the bias of biotite age and feldspar plateau ages to the altered character of biotite.

4.3. Syenite–carbonatite complexes (A2 rock group)

4.3.1. Punta del Peñon Blanco

The K–Ar age of the carbonatite and syenite intrusions in this area varies between 22.1 Ma for a syenite dike (sample R17) and 22.7–24 Ma for mineral concentrates of a carbonatite (biotite and feldspar, samples 3125–3126) (Table 2). These results are similar to those previously obtained on biotite by Cantagrel et al. (1993): 21.6 ± 0.9 Ma for a syenite (sample F86) and 25 ± 0.9 Ma for a carbonatite (sample F78) from the same outcrop (Table 3).

The young and similar ages suggest that in this area the concentration of excess argon cannot be high. This is confirmed by the ^{40}Ar/^{36}Ar ratio and Ar(rad) concentration of calcite from a carbonatite (PPB-C-1, Table 6). Assuming an age of 22–23 Ma for the calcite, the measured ^{40}Ar/^{36}Ar ratio of 306.1 gives an initial ratio of 305.8. Using this value the corrected ages of 3125 and 3126 will be 22.1 Ma and 23.7 Ma. The oldest age on the feldspar suggests additional incorporation of some excess Ar. In view of our further results, the older age on sample F78 by Cantagrel et al. (1993) may be caused by excess Ar.

4.3.2. Ajui-Solapa complex

We have sampled carbonatites and syenites from the two main outcrops: Caleta de la Cruz and Punta de la Nao.

4.3.2.1. Caleta de la Cruz. Mica from a carbonatite (CR-C-1) gives an age of 23.8 ± 1.0 Ma while the associated syenite (CR-S-5) has an age of 26.7 ± 1.1 Ma (Table 2). We have studied the composition of the calcite from the carbonatite, a mineral phase very poor in K. It contained 5.7% 'radiogenic' argon, the extremely old 'age' shows that more than 98% of the 'radiogenic' argon is excess argon and the initial ^{40}Ar/^{36}Ar ratio of carbonatite appears to be about 313 (Table 6). Correcting the biotite age with this value has no significant effect (23.2 ± 1.0 Ma). This is the same as the U–Pb age of zircon (Table 3, sample X52) measured by Cantagrel et al. (1993) in the Esquinzo valley. Sagredo et al. (1996) reported
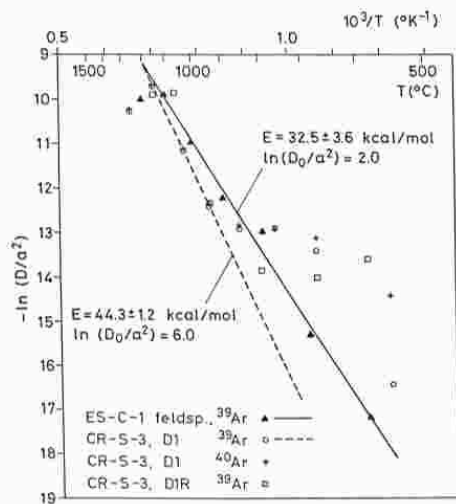
Fig. 4. Arrhenius diagrams.

an age of 25.2 ± 1 Ma for a nearby nepheline syenite intrusion (Morro del Recogedero) that has been included in this plutonic group (MR-363, Table 3).

4.3.2.2. Punta de la Nao. The data for the Punta de La Nao carbonatite intrusion (Nao-1) gives an age of 38.2 Ma on feldspar (Table 2). The high percentage of radiogenic argon in a calcite indicates that the original $^{40}Ar/^{36}Ar$ ratio was about 450, thus K/Ar ages are substantially increased by incorporated excess argon (Table 6). However, the relatively high K content (0.237%) of this calcite points to the contamination of this mineral by alkali feldspar inclusions.

Cantagrel et al. (1993) measured a biotite from an ijolite of this area (Sample X79, Table 3) and ob-

tained an age of 19.2 ± 0.9 Ma. This is not significantly different from the result of 20.1 ± 1 Ma given by Le Bas et al. (1986) from a metabasite xenolith in ijolite (sample F779, Table 3).

4.3.2.3. Esquinzo complex. The results obtained on feldspars from carbonatites that have suffered intense autometasomatism show very old ages between 109 and 211 Ma (Es-C-I and ES-C-2, Table 2). These results can clearly be attributed to considerable excess argon content.

Other feldspars (Es-C-4 and Es-CII-1, Table 2) have ages of 27.7 and 30.9 Ma from a carbonatite and a syenite respectively. Results on the 4 feldspar samples were plotted tentatively in the $^{40}Ar/^{36}Ar-$

Table 5
$^{40}Ar/^{39}Ar$ age spectrum results

T (°C)	$^{40}Ar*$	$^{40}Ar_{(atm)}$	$^{37}Ar_0$ 10^{-8} cm³ STP/g	^{36}Ar	$^{39}Ar_K$	Cumulative $^{39}Ar_{(\%)}$	$^{40}Ar*/$ $^{40}Ar(tot)$	$^{40}Ar*/$ $^{39}Ar_K$	Age, Ma $\pm \delta$	Ca/K
Sample Es-C-1, feldspar. Total fusion age: 110.8 ± 1.6 Ma; K/Ar age: 109 ± 4.1 Ma										
580	297	290	0.27	0.90	0.64	3.5	0.506	464	1506.0 ± 21	0.95
685	17.2	12.14	0.22	0.041	1.74	9.5	0.586	9.89	49.5 ± 3.0	0.28
790	13.7	6.07	0.22	0.021	2.78	28.0	0.692	4.93	24.8 ± 1.8	0.18
895	15.7	2.02	0.54	0.007	3.03	44.5	0.886	5.18	26.1 ± 1.7	0.40
1000	29.5	3.04	0.76	0.010	4.77	70.4	0.907	6.18	31.1 ± 1.2	0.36
1100	31.55	3.04	0.65	0.010	4.31	93.8	0.912	7.32	36.7 ± 1.2	0.34
1205	7.47	0.86	0.068	0.003	0.838	98.4	0.897	8.91	44.6 ± 6.2	0.18
1330	3.08	0.34	0.017	0.001	0.301	100.0	0.900	10.23	51.1 ± 17	0.13
Sample, CR-S-3, D1 fraction. Total fusion age: 66.2 ± 1.0 Ma; K/Ar age: 68.2 ± 2.6 Ma										
550	56.1	32.3	0.6	0.11	1.58	5.0	0.634	35.46	171.3 ± 3.9	0.85
670	58.7	11.1	0.65	0.038	5.35	22.0	0.841	10.97	54.8 ± 1.2	0.27
760	40.2	6.07	0.77	0.021	3.73	33.9	0.869	10.79	53.9 ± 1.5	0.46
850	31.7	12.5	0.22	0.041	2.48	41.8	0.740	12.36	61.6 ± 2.1	0.20
937	37.2	14.2	0.11	0.048	3.02	51.4	0.724	12.29	61.2 ± 1.9	0.08
1025	76.4	22.3	0.095	0.075	5.97	70.3	0.774	12.81	63.8 ± 1.2	0.04
1145	100.1	23.5	0.005	0.079	7.91	95.5	0.810	12.66	63.1 ± 1.1	0.02
1250	11.9	3.08	0.02	0.010	0.913	98.4	0.795	13.06	65.0 ± 5.5	
1325	6.3	2.26	0.02	0.080	0.510	100	0.736	12.35	61.5 ± 9.8	
Sample, CR-S-3, D1R fraction. Total fusion age: 52.5 ± 0.8 Ma; K/Ar age: 54.2 ± 2.0 Ma										
580	53.1	28.4		0.096	8.32	21.1	0.651	6.38	32.1 ± 0.8	
670	9.25	4.1		0.014	1.90	26.0	0.695	4.87	24.5 ± 2.7	
790	9.5	8.1		0.018	1.81	30.6	0.540	5.26	26.5 ± 2.8	
937	52.9	27.4		0.037	5.35	44.2	0.679	10.82	54.0 ± 1.2	
1057	248.4	53.9		0.182	19.5	92.8	0.822	12.97	64.6 ± 1.0	
1145	27.3	8.9		0.030	2.21	98.4	0.755	12.34	61.5 ± 2.4	
1299	5.8	2.26		0.008	0.455	99.6	0.720	12.75	63.5 ± 11.0	
1420	2.19	1.03		0.003	0.181	100.0	0.680	12.10	60.3 ± 27.5	

$J = 0.00281 \pm 1\%$, values are corrected for line blank, $^{37}A_0$ and $^{39}Ar_K$ for decay.

$K/^{36}Ar$ diagram, but the points are not arranged along a straight line, so isotopic equilibrium is not indicated.

Phlogopites from carbonatites were analysed from Salada-1 and Jablitos from the Esquinzo valley. The datum from Jablitos phlogopite is not precise enough due to alteration of the mica and it is not significantly older than the age of carbonatite found by Cantagrel et al. (1993). On the other hand, the age of 26.9 ± 1.0 Ma on Salada-1 is young, but significantly older than the most likely age of carbonatite intrusion around 23.2 Ma (Cantagrel et al., 1993; Table 3), and if we correct it with the $^{40}Ar/^{36}Ar$ ratio of the coexisting calcite, it will be reduced only to 26.6 Ma (Table 6). This shows that the assumption of equilibration of Ar isotopes in this carbonatite is insufficient to account for all excess Ar in the phlogopite. The origin and site of the additional excess argon is not clear.

Feldspar from Es-C-1 carbonatite was selected for Ar–Ar dating (Table 5). The 'saddle-shaped' age spectrum (Fig. 5) is similar to the ones obtained on feldspar with excess argon by Zeitler and Fitz Gerald (1986). Their interpretation appears to be appropriate for this spectrum since, in contrast to the feldspars from CR-S-3, at higher temperature steps there is no plateau, but ages increase with increasing temperature. According to these authors, excess argon is incorporated mostly into anion vacancies under hydrous conditions at low temperature. The high temperature release of excess argon that was incorporated at low temperature is explained by the dry environment of release in the laboratory. The minimum age of the spectrum (24.8 ± 2.7 Ma) does not differ significantly from the U–Pb age of 23.2 ± 0.2 Ma measured by Cantagrel et al. (1993) on zircon and the 25.0 ± 1.0 Ma age by Le Bas et al. (1986) from a biotitized ijolitic pyroxenite penetrated by carbonatite (Table 3).

An $^{40}Ar/^{36}Ar$ isotopic ratio of 598 is measured on the argon released at 580°C. If we correct the youngest age of 24.8 Ma with 598 as initial $^{40}Ar/^{36}Ar$, an age of 13.5 Ma would be obtained, which is unrealistic in view of earlier results. This shows that excess argon is not distributed throughout the bulk of the mineral, but it is restricted to near-boundary and/or low activation energy sites, and the $^{40}Ar/^{36}Ar$ ratio of argon trapped during cooling of the feldspar was remarkably less than 598.

$^{40}Ar/^{36}Ar$ ratios have been measured in the calcites from Esquinzo carbonatites (Table 6). Correcting for an estimated age of 22–23 Ma, the initial
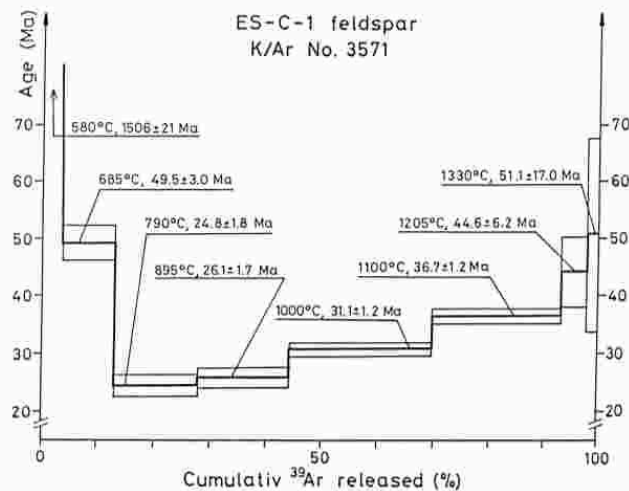
Fig. 5. Ar–Ar spectrum of feldspar from Esquinzo carbonatite (sample Es-C-1).

Table 6
Argon isotopic composition of carbonatite calcite

Sample	Locality	%K	^{40}Ar(excess + rad) STP/g	^{40}Ar/^{36}Ar	Formal age
Esquinzo complex					
Salada-1	Agua Salada	0.015	3.046×10^{-6}	308.7	2453
Es-C1-3(C)	Las Montañetas	0.033	1.503×10^{-6}	307.2	903
Es-C1-1(A)	Las Montañetas	0.038	1.944×10^{-6}	318.2	988
Es-C1-2(B)	Las Montañetas	0.035	1.266×10^{-6}	330.5	750
Jablitos	Los Jablitos	0.118	3.073×10^{-6}	305.5	570
Ajuí–Solapa complex					
Nao-1	Punta de la Nao	0.237	6.353×10^{-6}	456.7	584
Cr-C-1	Caleta de la Cruz	0.017	1.157×10^{-6}	313.4	1224
Punta del Peñón Blanco complex					
PPB-C-1	PPBlanco	0.023	8.346×10^{-7}	306.1	742

^{40}Ar/^{36}Ar ratios range from 305 to 330, and their excess argon content from 1.235×10^{-6} cm^3 STP/g to 2.967×10^{-6} cm^3 STP/g. It is difficult to decide if excess argon was incorporated into calcite during crystallization or was introduced later.

On the basis of fractional ^{39}Ar loss at the different temperature steps, diffusion parameters have been calculated for the feldspar from Es-C-1 carbonatite. Plotting them against the reciprocal absolute temperature in the Arrhenius diagram, 32.5 ± 3.6 kcal/mol activation energy is obtained for argon diffusion (Fig. 4). Using this value and the method of Dodson (1973), closure temperatures of 166°C to 193°C were calculated for 10°C/Ma to 100°C/Ma cooling rates.

In summary, the most likely age of the carbonatites in the Esquinzo valley is given by the U–Pb age of 23.2 ± 0.2 Ma by Cantagrel et al. (1993). It is demonstrated that older K–Ar and Ar–Ar ages presented here can be attributed to excess argon.

At Caleta de la Cruz, the age of carbonatite intrusion is best approximated by 23.2 ± 1.0 Ma (corrected age of biotite from sample CR-C-1, Table 2) and at Punta del Peñón del Blanco the corrected value of 22.1 ± 0.9 Ma on biotite from 3125 is accepted for the time of carbonatite intrusion. The youngest ages on syenites of the syenite–carbonatite complex (A2 group) are 21.6 Ma measured on biotite (F86) and on whole rock (MR-431) by Cantagrel et al. (1993). These data give a most likely interval from 23.2 Ma to 21.6 Ma for the carbonatite–syenite

intrusion and the shear tectonic episode of Fuerteventura.

4.4. Main dike swarm

Two basic dikes that cross-cut the shear zones in Punta del Peñón Blanco and Caleta de la Cruz (Fig. 1) give ages of 22.2 Ma and 22.7 Ma (sample 80-40-40 and R20, Table 7).

This upper margin is in accordance with the age obtained for the shear tectonic episode and the intrusion of syenites and carbonatites. Feraud et al. (1985) argue that by combining conventional K–Ar and Ar–Ar methods the main intrusion of dikes took place between 24 and 17 Ma.

Moreover, in the areas close to the younger plutonic bodies (A3 and A4 rock groups) the dike swarms have been affected by the thermal metamorphism produced by these intrusions. Feraud et al. (1985) find very disturbed argon–argon spectra in those dikes where significant excess argon is present.

4.5. A3 rock group

We have sampled a pyroxenite for one of the southernmost outcrops: Punta de Diego Diaz (Fig. 1). The age of 36 ± 4 Ma (3127, Table 7) is not geologically plausible when we consider that it cuts the dikes from the main dike swarms and the shear structures that have been dated around 23–22 Ma.

Table 7
K–Ar analytical results for the dike swarms and younger plutonic intrusions

Sample	Rock type	Locality	Source	%K	^{40}Ar(rad) cm^3 STP/g	^{40}Ar(rad)/ ^{40}Ar(tot)	Age, Ma $\pm$ δ
Dike swarm							
80-40-40	basalt	Caleta de la Cruz	w.r.	1.377	1.221×10^{-6}	0.324	22.7 ± 1.2
R20	basalt	Punta Peñón Blanco	w.r.	1.690	1.469×10^{-6}	0.376	22.2 ± 1.1
Younger plutonic intrusions							
A3 group							
3127	pyroxenite	Punta Diego Diaz	w.r.	0.184	2.598×10^{-7}	0.125	36.0 ± 4.0
Gb-1	gabbro	Punta Diego Diaz	w.r.	2.759	2.276×10^{-6}	0.592	21.1 ± 0.8
80-30-16	gabbro	Las Hendiduras	w.r.	0.404	4.141×10^{-7}	0.194	26.2 ± 2.0
ES-G-1	gabbro	Esquinzo	plagioclase	1.27	2.745×10^{-6}	0.416	54.8 ± 2.5
			pyroxene	0.144	2.170×10^{-7}	0.288	38.4 ± 2.6
A4 group							
Si-1	syenite	Punta Diego Diaz	w.r.	5.039	4.068×10^{-6}	0.448	20.7 ± 0.9

The old age is attributed to a small amount of excess argon that caused a great increase of age of the low K rock.

Anomalous results were also obtained from the northern outcrops of Esquinzo. Sample Es-G-1 (Table 7) gives an age of 54.8 Ma (plagioclase) and 38.4 Ma (pyroxene), again too old when compared with the age of the syenite–carbonatite complex and geological evidence. These ages are interpreted in terms of greater amounts of excess Ar incorporated under hydrothermal conditions in the plagioclase and some excess Ar of unspecified origin in the pyroxene.

In Punta de Diego Diaz, a gabbro intrusion is emplaced into the pyroxenite (Gb-1, Fig. 1). This gabbro has an age of 21.1 ± 0.8 Ma (Gb-1, Table 7). Another gabbro has been dated in Las Hendiduras, an area where the dike swarms occupy almost 100% of the outcrops (80-30-16, 3131, Table 7). It gives an age of 26.2 ± 2.0 Ma. The relatively low K content of this older gabbro would make its age sensitive to the presence of excess argon and the younger age of 21.1 ± 0.8 Ma is preferred as the maximum age of intrusion. In these plutons cross-cutting dikes are sparse, suggesting to us that the age of the gabbro from Punta de Diego Diaz could be the most representative of this plutonic episode.

Sagredo et al. (1996) indirectly date the age of these A3 plutonic rocks by determining the age of the contact metamorphism produced by these plutonic bodies on an older intrusion (Morro del Recogedero syenite). The result of 21.6 Ma (Sample 431; Table 3) is similar to the age of the gabbro from Punta de Diego Diaz.

4.6. A4 rock group

Some syenite dikes were emplaced into the gabbro of Punta de Diego Diaz around 20.7 Ma ago (Sample Si-1, Table 7, Fig. 1). These dikes can be correlated with the youngest plutonic intrusions of the Basal Complex: the syenites of the Vega de Rio Palmas Ring Complex with an age around 18.4 and 20.8 Ma (Table 3).

5. Origin, site and incorporation of excess argon

K–Ar and Ar–Ar ages measured for the majority of rocks and minerals of the Basal Complex of Fuerteventura are biased by excess Ar. The presence of excess Ar is indicated by the following observations:

(1) In the majority of rock and mineral samples, there is a negative correlation of K content and age.

(2) In the Ar–Ar spectra of feldspars of CR-S-3 and Es-C-1 very old ages are obtained in the first low temperature steps.

(3) Excess Ar is directly detected in calcites from carbonatites.

In principle, excess Ar may originate from the mantle or from older crustal material. Sr–Nd–Pb isotope data obtained by Hoernle and Tilton (1991) from Fuerteventura do not show crustal contamination, indicating that excess Ar may come from the mantle. We also note that Graham et al. (1996) detected a mantle component in the He fluid inclusions of Quaternary lavas in the Canary Islands.

Very old ages were measured for the low temperature step of Ar–Ar spectra of feldspars from Es-C-1 (Esquinzo carbonatite) and the D1 fraction of Cr-S-3 (Caleta de la Cruz syenite). This suggests that excess argon was incorporated in near-boundary and/or low activation energy sites of these minerals. Since this excess Ar is not uniformly distributed in the bulk of minerals, the temperature of incorporation must have been lower than the closure temperature for Ar (Zeitler and Fitz Gerald, 1986). The relatively good plateau ages obtained for feldspars of Cr-S-3 indicate near-boundary incorporation but this is not so certain for the feldspar of Es-C-1. For this latter sample, adopting the idea of Harrison and Mc-Dougall (1981) and Zeitler and Fitz Gerald (1986), excess Ar incorporation into anion vacancies is assumed. The isotopic composition of this component of excess Ar can be estimated from the $^{40}Ar/^{36}Ar$ ratio of Ar released at the first low temperature step of feldspar samples of Es-C-1 and the D1 fraction of Cr-S-3. This ratio is 598 for Es-C-1 and 781 for Cr-S-3.

Besides the demonstrated excess Ar component acquired during a hydrothermal stage, some excess Ar trapped during the early crystallization stage of the magma is also possible. This is indicated by the tendency towards older ages in unaltered low K rocks and also by the age (26.9 Ma) of phlogopite from Salada-1 carbonatite which is older than the carbonatite intrusion. This component should be distributed homogeneously in the minerals. The $^{40}Ar/^{36}$ Ar ratio of this 'initial' excess Ar component is uncertain. It is likely to be less than the ratio for the first steps of the Ar–Ar spectra of Es-C-1 and Cr-S-3 (D1), otherwise too young ages would be implied for the second and third steps of Es-C-1 and these cited values for the $^{40}Ar/^{36}Ar$ ratios would be minima for the rocks of the Basal Complex. Unfortunately, the similarity of $^{39}Ar/^{36}Ar$ ratios does not allow application of the isochron method.

Excess Ar is present in all calcite of the carbonatites, but its isotopic composition can be used for correcting ages of other minerals of the carbonatites only with variable success. For example, the phlogopite age of Salada-1 carbonatite remains older than the intrusion age of carbonatite (according to the U–Pb age by Cantagrel et al., 1993) when corrected with the calcite isotopic ratio. At the time of magmatic crystallization, homogenization of Ar isotopes can be assumed. The present complex isotopic distribution might have been caused by incorporation of excess Ar into the phlogopite under hydrothermal conditions, or by an isotopic exchange between the calcite and atmosphere after the hydrothermal process.

6. Geological evolution of Fuerteventura Island

The new geochronological data allow us to establish a long history of formation of the Island of Fuerteventura (Table 8). They agree with the idea of an onset of igneous activity in the Late Cretaceous proposed by Le Bas et al. (1986). In this long magmatic history, it is possible to distinguish a period of submarine growth represented by pillow lavas, breccias and hyaloclastites. They form submarine volcanic edifices associate with their respective subvolcanic and plutonic complexes. At least parts of these complexes correspond to the outcrops of the A1 rock unit: pyroxenites, amphibololites, amphibolic gabbros and syenites (Le Bas et al., 1986; Stillman, 1987).

The early stage of submarine growth embraces a long period from the Late Cretaceous (around 65 Ma ago) to Early Miocene (around 25 Ma). The emergence of the island and the beginning of the construction of large subaerial edifices coincide with the emplacement of the syenite–carbonatite intrusions (A2 unit) around 22–23 Ma ago. This emergence is probably related to differential uplift processes developed by the action of important ductile to brittle–ductile shear zones (Fernández et al., 1997).

After these first plutonic episodes the intrusion of the main dike swarms took place (between 24 and 20 Ma ago). Probably, this dense dike emplacement can be related to a regional crustal extension that accompanies the formation of the lower and intermediate

96   *K. Balogh et al. / Journal of Volcanology and Geothermal Research 90 (1999) 81–101*

Table 8
Geochronological evolution of the Basal Complex of Fuerteventura

M. a.		SEDIMENTARY SEQUENCE	PLUTONIC AND DIKE INTRUSIONS	TECTONIC PHASES	VOLCANIC SERIES
	PLIOCENE				
5,1					
	MIOCENE				
			A4 YOUNGER PLUTONICS [20 M. a.]		SUBAERIAL VOLCANIC EDIFICES
			A3		
			MAIN DIKE SWARM [22 M. a.]		
24,6			A2 SYENITE - CARBONATITE		
			COMPLEXES [22-23 M. a.]	BRITTLE-DUCTILE DEFORMATION [22-23 M. a.]	
	OLIGOCENE	BIOCLASTIC SEDIMENTS			UPPER SUBMARINE VOLCANIC SERIE
38					
	EOCENE				
				FOLDING [49 M. a.?]	LOWER SUBMARINE VOLCANIC SERIE
54,9					
	PALEOCENE				
65					
	Senonian		SYENITES [65 M. a.]		
			A1		
			ULTRAMAFIC ROCKS ?		
	UPPER CRETACEOUS				
100	Albian	PELAGIC CHALKS CARBONATE CLASTIC FAN SEDIMENTS			

levels of the volcanic subaerial edifices (Ancochea et al., 1996).

The building of the lower and middle levels of the central subaereal edifice located around Pajara (< 22 Ma to 20 Ma) seems to be related to the deep mafic and ultramafic plutonic complexes which constitute a coherent dike complex (Walker, 1992). It is similar to those described below the Ko'olau lava-shield volcano on O'ahu (Hawaiian Islands). The younger gabbro and pyroxenite intrusions (A3 Unit) consti-

tute this coherent dike complex, which crops out thanks to the uplift and intense erosion suffered by the subaereal edifice.

The temporal evolution in the basal zone of the subaereal volcanic edifice between the emplacement of the dike swarms to the appearance of the mafic–ultramafic plutonic complex can be explained with the model of Walker (1992). The ascent of the position of the neutral buoyancy level is the consequence of the growth of the cumulate prism and this also causes the ascent of the shallow magmatic chamber that feeds the edifice to keep pace with volcano growth.

The most recent plutonic intrusions of the Basal Complex (Ring Complexes of Vega de Rio de Palmas, Unit A4) are favoured by conic fractures with centripetic slopes. These intrusions are related to some central volcanic edifices, probably strato-volcanoes (Cantagrel et al., 1993). They are located in the axial zone of the domical extensional structure of the island.

The magmatic evolution of the Basal Complex of Fuerteventura has been accompanied by important tectonic events that have contributed to the emergence of the island. The folding and inversion of the sedimentary Mesozoic sequence and the lower volcanic submarine series has not yet been explained. It could have taken place around 50 Ma ago (Eocene, Le Bas et al., 1986; this work). The relationship of this tectonic phase either with the regional stress field in the African plate or with the evolution of the African northwestern margin (Atlas) is the object of discussion and controversy.

Around the Oligocene–Miocene boundary another tectonic episode produced the ductile–brittle shear zones and the simultaneous intrusion of the syenites and carbonatites (Unit A2). This episode was related to a lithospheric uplift probably produced by an asthenospheric ascent (Fernández et al., 1997). This event marked the beginning of a strong extensional period and produced dense dike intrusions, the emergence of the Island and the formation of the great Miocene volcanic edifices.

Relative movements of blocks have subsequently caused the uplift and erosion of the western part of the island. At present the rocks of the Basal Complex and the rest of the Miocene volcanic edifices appear at the same level (Ancochea et al., 1996).

7. Conclusions

(1) K–Ar and Ar–Ar dating was carried out on the Basal Complex of Fuerteventura. Many of the calculated ages are ambiguous due both to the presence of excess Ar and also to Ar loss caused by the thermal effect of younger magmatic activity. In order to estimate the Ar loss several sedimentary rocks were dated; the results demonstrated that only a part of radiogenic Ar was released during the Miocene magmatism.

(2) Three age data have been obtained on rocks from the oldest ultramafic pluton, ages ranging from 64.7 Ma to 23.5 Ma. However, the oldest age was measured on a pyroxenite of only 0.14% K content, and would be particularly sensitive to the presence of excess Ar. In the $^{40}Ar(rad)$–K diagram the points are arranged along a straight line and define a formal age of 21.9 Ma, which is interpreted as the time of incorporation of excess argon.

(3) Ages on the early syenite intrusions at Caleta de la Cruz range from 70.6 Ma to 38.5 Ma. The reason for these scattered ages was studied by dating a K-feldspar + nepheline concentrate from syenite, which was also dated after removing nepheline with acid treatment. Its Ar–Ar spectrum was explained as the superposition of two processes: (a) diffusional loss, probably at the time of Lower Miocene magmatism, and (b) later incorporation of excess Ar into near-boundary sites below the closure temperature of the K-feldspar. Plateau ages of 63.1 ± 0.8 Ma and 64.2 ± 1.0 Ma probably date the time of syenite intrusion. A relatively high closure temperature (293°C) was deduced for the feldspar at a 100°C/Ma cooling rate, this may explain why this alkali feldspar was not reset during the carbonatite intrusion. This is the first radiometric age indicating a Late Cretaceous–Early Tertiary start of magmatism.

(4) Autometasomatically altered feldspars from carbonatite of the Esquinzo complex yielded 109 Ma and 211 Ma ages. Ar–Ar measurements showed that a large amount of excess argon was incorporated into these minerals in a hydrothermal process below the closure temperature (193°C). The minimum age of the saddle shaped age spectrum (24.8 ± 2.7 Ma) is very near to the U–Pb age given by Cantagrel et al. (1993), i.e., Ar–Ar dating supports the Early Miocene age of carbonatite intrusion.

An age of 23.2 ± 1.0 Ma has been obtained for the carbonatite intrusion at Caleta de la Cruz. At Punta del Peñón Blanco, 22.7 ± 0.9 Ma was measured for carbonatite 3125 on biotite; this value is reduced to 22.1 ± 0.9 Ma when corrected with the initial Ar isotopic ratio of the carbonatite calcite.

(5) The youngest ages measured on younger plutonic intrusions (groups A3 and A4) are 21.1 ± 0.8 Ma and 20.7 ± 0.9 Ma on a gabbro and a syenite from Punta de Diego Diaz. Older ages of rocks from these groups are explained by excess Ar. In the case of the plagioclase of Es-G-1' excess Ar was incorporated under hydrothermal conditions, while samples 3127, 80-30-16 and the pyroxene of Es-G-1 retained their excess Ar content during crystallization and cooling.

(6) K–Ar and Ar–Ar age measurements on many rocks and minerals from the Basal Complex of Fuerteventura are biased by excess Ar. This excess argon has two sources. Some of it was acquired during an hydrothermal stage but some portion was probably trapped during the early crystallization stage of the magma.

(7) The new data obtained in this work confirm that the geological evolution of Fuerteventura took place during a long period of time from Late Cretaceous until Miocene. This long history is represented by different plutonic events. The oldest intrusions are probably related to the older submarine vulcanism whereas the youngest plutons are associated with the early formation stages of the Miocene subaereal edifices.

Appendix A. Sample site locations and rock descriptions

A.1. Sedimentary sequence

VIEN-1. Punta del Viento. 28°34′44″N, 14°2′36″W; 0 m. Lutite. Grains of quartz, alkali feldspar and muscovite. Clay matrix.

SOJ-1. Barranco de Sojames. 28°24′44″N; 14°8′36″W; 60 m. Sandstone. Grains of quartz, alkali feldspar and muscovite. Clay matrix.

SOJ-2. Barranco de Sojames. 28°24′44″N; 14°8′36″W; 60 m. Sandstone. Grains of quartz and moscovite. Clay matrix.

A.1.1. A1 rock group: Early gabbro–pyroxenite–syenite intrusions

3119. La Matanza. 28°19′56″N; 14ø11′46″W; 0 m. Amphibololite intrusion. Kaersutite cumulate with interstitial titanian diopside, apatite, ilmenite and magnetite.

3120. La Matanza. 28°19′56″N; 14°11′46″W; 0 m. Pyroxenite intrusion. Titanian diopside cumulate with minor kaersutite. Apatite, magnetite and ilmenite as accessories.

80-40-39. Caleta de la Cruz. 28°22′47″N; 14°9′42″W; 0 m. Amphibololite intrusion. Kaersutite cumulate with titanian diopside, magnetite and apatite. Secondary minerals: phlogopite and epidote. Albite in veins.

CR-S-1. Caleta de la Cruz. 28°22′47″N; 14°9′42″W; 0 m. Sodalite–nepheline syenite intrusion. Hypersolvus alkaline feldspar, cancrinitized nepheline, sodalite and biotite. Magnetite, zircon, sphene and apatite as accessories. Calcite in veins.

CR-S-2. Caleta de la Cruz. 28°22′47″N; 14°9′42″W; 0 m. Nepheline syenite intrusion. Albite, cancrinitized nepheline and biotite. Magnetite, zircon, sphene and apatite as accessories. Secondary minerals: biotite and garnet. Calcite in veins.

CR-S-3. Caleta de la Cruz. 28°22′47″N; 14°9′42″W; 0 m. Nepheline syenite. Hypersolvus

alkaline feldspar, nepheline partly cancrinitized, aegirine augite, biotite. Magnetite, zircon, sphene and apatite as accessories.

CR-S-4 Caleta de la Cruz. 28°22′47″N; 14°9′42″W; 0 m. Sodalite–nepheline syenite. Hypersolvus alkaline feldspar, nepheline, sodalite, aegirine augite and biotite. Magnetite, zircon, sphene and apatite as accessories.

80-40-36 Caleta de la Cruz. 28°22′47″N; 14°9′42″W; 0 m. Syenite intrusion. Hypersolvus alkaline feldspar perthite-rich aggregate with nepheline, aegirine augite and biotite. Magnetite, zircon, sphene and apatite as accessories. Nepheline is usually transformed to cancrinite.

80-40-38 Caleta de la Cruz. 28°22′47″N; 14°9′42″W; 0 m. Syenite intrusion. Hypersolvus alkaline feldspar full of perthites partly albitized, cancrinitized nepheline, aegirine augite and biotite. Other phases are: magnetite, zircon, sphene, apatite and melanite. Zeolites in cavities. Calcite veins.

A.1.2. A2 rock group: syenite–carbonatite complexes

A.1.2.1. Esquinzo complex. Es-C-1. Las Montañetas. 28°38′12″N; 15°59′2″W; 160 m. Carbonatite dike. Calcite, aegirine augite, albitized alkali feldspar, magnetite and apatite.

Es-C-2. Las Montañetas. 28°38′12″N; 15°59′2″W; 160 m. Carbonatite dike. Calcite, aegirine augite, albitized alkali feldspar, magnetite and apatite. Secondary minerals: analcime, epidote and sericite.

Es-C-3 Las Montañetas. 28°38′12″N; 15°59′2″W; 160 m. Carbonatite vein. Calcite and alkali feldspar.

Es-C-4 Las Montañetas. 28°38′12″N; 15°59′2″W; 160 m. Carbonatite dike. Calcite, aegirine augite, albitized alkali feldspar, magnetite and apatite.

Es-CII-1 Los Jablitos. 28°37′56″N; 13°59′20″W; 130 m. Syenite dike. Alkali feldspar, magnetite and apatite. Calcite in veins.

Salada-1. Barranco del Agua Salada. 28°37′39″N; 13°59′13″W; 155 m. Carbonatite vein. Calcite and phlogopite.

Jablitos. Los Jablitos. 28°37′56″N; 13°59′20″W; 130 m. Carbonatite vein. Calcite and phlogopite.

Es-Si-1. Barranco de Esquinzo. 28°37′56″N; 13°59′30″W; 120 m. Nepheline syenite. Hypersolvus

alkaline feldspar, cancrinitized nepheline, aegirine augite, magnetite, zircon, sphene and apatite.

A.1.2.2. Ajui-solapa complex. Nao-1 Punta de la Nao. 28°23′22″N; 14°9′39″W; 0 m. Carbonatite dike. Calcite, alkali feldspar, biotite, aegirine augite, magnetite and apatite. The alkali feldspar is partly albitized.

CR-S-5. Caleta de la Cruz. 28°22′47″N; 14°9′42″W; 0 m. Foliated nepheline syenite. Albite and cancrinitized nepheline. Magnetite, zircon, sphene and apatite as accessories.

CR-C-1. Caleta de la Cruz. 28°22′47″N; 14°9′42″W; 0 m. Foliated carbonatite. Calcite, biotite, magnetite and apatite. Metamorphic minerals: diopside and biotite.

A.1.2.3. Punta del Peñón Blanco complex. R-17. Punta del Peñón Blanco. 28°19′51″N; 14°11′46″W; 0 m. Porhyritic syenite dyke. Alkaline feldspar, nepheline and aegirine augite in a groundmass with a similar composition and magnetite, zircon, sphene and apatite. Secondary minerals: albite, cancrinite, biotite, hornblende, epidote and sphene.

3125. Punta del Peñón Blanco. 28°19′51″N; 14°11′46″W; 0 m. Carbonatite. Calcite, alkali feldspar, phlogopite, magnetite and apatite. Secondary minerals: albite and diopside.

3126. Punta del Peñón Blanco. 28°19′51″N; 14°11′46″W; 0 m. Carbonatite. Calcite, alkali feldspar, phlogopite, magnetite and apatite. Secondary minerals: albite and diopside.

A.1.2.4. Main dike swarm. 80-40-40 Caleta de la Cruz. 28°22′47″N; 14°9′42″W; 0 m. Basalt dike. Plagioclase and dioside phenocrysts in a groundmass with plagioclase, diopside, kaersutite, magnetite and apatite.

R20 Punta del Peñón Blanco. 28°19′51″N; 14°11′46″W; 0 m. Porphyritic basalt dike. Titanian diopside, olivine and plagioclase phenocrysts in a groundmass composed of diopside, plagioclase and magnetite. Minor calcite and clorite.

A.1.3. A3 rock group

3127. Punta de Diego Diaz. 28°20′8″N; 14°11′17″W; 0 m. Olivine pyroxenite. Plagioclase, olivine, titanian diopside, kaersutite, biotite, mag-

netite and apatite. Minor amounts of epidote and albite.

Gb-1 Punta de Diego Diaz. 28°20′8″N; 14°11′17″W; 0 m. Gabbro stock. Plagioclase, titanian diopside, kaersutite, biotite, apatite and magnetite. Minor amounts of epidote, clorite and zeolites as secondary minerals.

80-30-16 Las Hendiduras. 28°16′37″N; 14°12′5″W; 300 m. Olivine Gabbro. Plagioclase, titanian diopside, serpentinized olivine, magnetite and apatite.

Es-G-1 Barranco de Esquinzo. 28°37′56″N; 13°59′30″W; 120 m. Olivine gabbro. Olivine, titanian diopside, kaersutite, plagioclase, magnetite, ilmenite and apatite.

A.1.4. A4 rock group

Si-1 Punta de Diego Diaz. 28°20′8″N; 14°11′17″W; 0 m. Syenite dike. Hypersolvus alkaline feldspar, biotite, amphibole with minor sphene, magnetite, zircon and apatite.

References

Abdel-Monem, A., Watkins, N.D., Gast, W., 1971. Potassium–argon ages, volcanic stratigraphy and geomagnetic polarity history of the Canary Islands: Lanzarote, Fuerteventura and La Gomera. Am. J. Sci. 271, 490–521.

Ahijado, A., Hernández-Pacheco, A., 1990. Las rocas ultramáficas alcalinas del Jable de Salinas, Fuerteventura, Islas Canarias. Rev. Soc. Geol. Esp. 3, 275–287.

Ahijado, A., Hernández-Pacheco, A., 1992. El complejo ultramáfico–carbonatítico del Macizo de Amanay, Fuerteventura, Islas Canarias. II Congreso Geológico de España, Salamanca 1, 315–318.

Ancochea, E., Brändle, J.L., Cubas, C.R., Hernán, F., Huertas, M.J., 1996. Volcanic complexes in the eastern ridge of the Canary Islands. J. Volcanol. Geotherm. Res. 70, 183–204.

Balogh, K., 1985. K/Ar dating of Neogene volcanic activity in Hungary: experimental technique, experiences and methods of chronologic studies. ATOMKI Rep. D/1. pp. 277–288.

Barrera, J.L., Fernández Santín, S., Fúster, J.M., Ibarrola, E., 1986. Ijolitas–sienitas–carbonatitas de los Macizos del Norte de Fuerteventura. Bol. Geol. Min. 92–94, 309–321.

Cantagrel, J.M., Fúster, J.M., Pin, C., Renaud, U., Ibarrola, E., 1993. Age Miocène inférieur des carbonatites de Fuerteventura. C.R. Acad. Sci. Paris 316, 1147–1153.

Casillas, R., Ahijado, A., Hernández-Pacheco, A., 1994. Zonas de cizalla déctil en el Complejo Basal de Fuerteventura. Geogaceta 15, 117–120.

Coello, J., Cantagrel, J.M., Ibarrola, E., Jamond, C., Hern n, F., Fúster, J.M., Ancochea, E., Casquet, C., Diaz de Teran, J.R., Cendrero, A., 1992. Evolution of the eastern volcanic ridge of the Canary Islands based on new K–Ar data. J. Volcanol. Geotherm. Res. 53, 251–274.

Dodson, M.H., 1973. Closure temperature in cooling geochronological and petrological systems. Contrib. Mineral. Petrol. 40, 259–274.

Feraud, G., Giannerini, G., Campredon, R., Stillman, C.J., 1985. Geochronology of some canarian dyke swarms: contribution to the tectonic evolution of the archipelago. J. Volcanol. Geotherm. Res. 25, 29–52.

Fernández, C., Casillas, R., Ahijado, A., Perelló, V., Hernández-Pacheco, A., 1997. Shear zones as a result of intraplate tectonics in oceanic crust: the example of the Basal Complex of Fuerteventura (Canary Island). J. Struct. Geol. 18, 1–17.

Fúster, J.M., Aguilar, M., 1965. Nota previa sobre la geología del Macizo de Betancuria, Fuerteventura (Islas Canarias). Estud. Geol. 21, 181–197.

Fúster, J.M., Cendrero, A., Gastesi, P., Ibarrola, E., Lopez Ruiz, J., 1968. Geología y volcanología de las Islas Canarias-Fuerteventura. Instituto 'Lucas Mallada'. Consejo Superior de Investigaciones Científicas, Madrid. 239 pp.

Fúster, J.M., Muñoz, M., Sagredo, J., Yébenes, A., Bravo, T., Hernández-Pacheco, A., 1980. Excursión no. 121 A+c del 26° I.G.C. a las Islas Canarias. Bol. Inst. Geol. Min. España 92 (2), 351–390.

Gastesi, P., 1969. El complejo plutónico básico y ultrabásico de Betancuria, Fuerteventura (Islas Canarias). Estudio Petrológico. Estud. Geol. 25, 1–51.

Graham, D.H., Hoernle, K.A., Lupton, J.E., Schmincke, H.U., 1996. Helium isotope variations in volcanic rocks from the Canary Islands and Madeira (Abstract) Shallow Level Processes in Ocean Island Magmatism: Distinguishing Mantle and Crustal Signatures, Chapman Conference, Tenerife.

Grunau, H.R., Lehner, P., Cleintor, M.R., Allenbach, P., Baker, G., 1975. New radiometric ages and seismic data from Fuerteventura (Canary Islands), Maio (Cape Verde Islands) and Sao Tomé (Gukf of Guinea). In: Borradaile, G.J., Ritsema, A.R., Rondeel, H.E., Simon, O.J. (Eds.), Progress in Geodynamics. R. Neth. Acad. Arts. Sci. North Holland, Amsterdam, pp. 90–118.

Harrison, T.M., McDougall, J., 1981. Excess ^{40}Ar in metamorphic rocks from Broken Hill, New South Wales: implications for ^{40}Ar/^{39}Ar age spectra and the thermal history of the region. Earth Planet. Sci. Lett. 55, 123–149.

Harrison, T.M., McDougall, J., 1982. The thermal significance of potassium feldspar K–Ar ages inferred from ^{40}Ar/^{36}Ar age spectrum results. Geochim. Cosmochim. Acta 46, 1811–1820.

Hoernle, K., Tilton, G.R., 1991. Sr–Nd–Pb isotope data for Fuerteventura Basal Complex and subaerial volcanics: application to magma genesis. Schweiz. Mineral. Petrogr. Mitt. 71, 5–21.

Ibarrola, E., Fúster, J.M., Cantagrel, J.M., 1989. Edades K–Ar de las rocas volcánicas submarinas en el sector norte del Complejo Basal de Fuerteventura. ESF Meeting on Canarian Volcanism, pp. 124–128.

Le Bas, M.J., 1981. The pyroxenite–ijolite–carbonatite intrusive igneous complexes of Fuerteventura, Canary Islands. J. Geol. Soc. London 138, 496.

Le Bas, M.J., Rex, D.C., Stillman, C.J., 1986. The early magmatic chronology of Fuerteventura. Geol. Mag. 123, 287–298.

López Ruiz, L., 1970. Estudio petrográfico y geoquímico del Complejo filoniano de Fuerteventura (Islas Canarias). Estud. Geol. 26, 173–208.

MacIntyre, R.M., York, D., Gittins, J., 1966. Argon retentivity of nephelines. Nature 209, 702–703.

Muñoz, M., 1969. Estudio petrológico de las formaciones alcalinas de Fuerteventura (Islas Canarias). Estud. Geol. 25, 257–310.

Muñoz, M., Sagredo, J., 1975. Existencia de metamorfismos superpuestos en el complejo basal de Fuerteventura (Canarias). I Asamblea Nac. Geodesia y Geofísica, pp. 1287–1288.

Muñoz, M., Sagredo, J., 1989. Características del metamorfismo térmico producido por los eventos plutónicos intrusivos más recientes del Complejo Basal de Fuerteventura. Abst. ESF Meeting on Canarian Volcanism, pp. 104–108.

Muñoz, M., Sagredo, J., 1994. Reajustes mineralógicos y geoquímicos producidos durante el metamorfismo de contacto de diques basálticos (Fuerteventura, Islas Canarias). Bol. Soc. Esp. Min. 17 (1), 86–87.

Odin, G.S., 35 collaborators (C.J. Adams, R.L. Armstrong, G.P. Bagdasaryan, A.K. Baksi, K. Balogh, I.L. Barnes, N.A.I.M. Boelrijk, F.P. Bonadonna, M.G. Bonhomme, C. Cassignol, L. Chanin, P.Y. Gillot, A. Gledhill, K. Govindaraju, R. Harakal, W. Harre, E.H. Hebeda, J.C. Hunziker, C.O. Ingamells, K. Kawashita, E. Kiss, H. Kreuzer, L.E. Long, I. McDougall, F. Mcdowell, H. Mehnert, R. Montigny, P. Pasteels, F. Radicati, D.C. Rex, C.C. Rundle, C. Savelli, J. Sonet, E. Welin, J.L. Zimmermann), 1982. Interlaboratory standars for dating purposes. In: Odin, G.S. (Ed.), Numerical Dating in Stratigraphy. Wiley, Chichester, pp. 123–150.

Renz, O., Bernoulli, D., Hottinger, L., 1992. Cretaceous ammonites from Fuerteventura, Canary Islands. Geol. Mag. 129 (6), 763–769.

Rona, P.A., Nalwalk, A.J., 1970. Post-early pliocene unconformity on Fuerteventura, Canary Islands. Geol. Soc. Am. Bull. 81, 2117–2122.

Robertson, A.H.F., Bernouilli, D., 1982. Stratigraphy, facies and significance of late mesozoic and early tertiary sedimentary rocks of Fuerteventura (Canary Islands) and Maio (Cape Verde Islands). In: Rad, V., Sarnthein, H., Seibold (Eds.), Geology of the Northwest African Continental Margin, pp. 498–525.

Robertson, A.H.F., Stillman, C.J., 1979a. Late mesozoic sedimentary rocks of Fuerteventura, Canary Islands. Implications for west Africa continental margin evolution. J. Geol. Soc. London 136, 47–60.

Robertson, A.H.F., Stillman, C.J., 1979b. Submarine volcanic and associated sedimentary rocks of the Fuerteventura Basal Complex, Canary Islands. Geol. Mag. 116, 203–214.

Rothe, P., 1968. Mesozoische Flysch-Ablagerugen auf der Kanareninsel Fuerteventura. Geol. Rundsch 58, 314–332.

Sagredo, J., Muñoz, M., Galindo, C., 1996. Características petrológicas y edad K/Ar de las sienitas nefelínicas del Morro del Recogedero (Fuerteventura, Islas Canarias). Geogaceta 20 (2), 506–509.

Steiger, R.H., Jäger, E., 1977. Subcommission on geochronology: convention on the use of decay constants in geo and cosmochronology. Earth Planet. Sci. Lett. 12, 359–362.

Stillman, C.J., 1987. A Canary Islands dyke swarm: implications for the formation of oceanic islands by extensional fissural volcanism. In: Halls, H.C., Fahrig, W.F. (Eds.), Mafic Dyke Swarms. Geol. Assoc. Can. Spec. Pap., Vol. 34., pp. 243–255.

Stillman, C.J., Fúster, J.M., Bennell-Baker, M.J., Muñoz, M., Smewing, J.D., Sagredo, J., 1975. Basal Complex of Fuerteventura (Canary Islands) is an oceanic intrusive complex with rift-system affinities. Nature 257, 469–471.

Stillman, C.J., Robertson, A.H.F., 1977. The dyke swarm of the Fuerteventura Basal Complex, Canary Islands. Abstr. Geol. Soc. London Newsletter 6, 8.

Walker, G.P.L., 1992. Coherent intrusion complexes in large basaltic volcanoes, a new structural model. J. Volcanol. Geotherm. Res. 50, 41–54.

Yebenes, A., 1980. Fuerteventura: evolución sedimentológica de una isla volcánica. IX Congreso Nacional de Sedimentología. Resumenes y Comunicaciones. Ediciones Universidad de Salamanca, Vol. 1, pp. 98–99.

Zeitler, P.K., Fitz Gerald, J.D., 1986. Saddle-shaped $^{40}Ar/^{39}Ar$ age spectra from young microstructurally complex potassium feldspars. Geochim. Cosmochim. Acta 50, 1185–1199.

The submarine volcanic succession of the basal complex of Fuerteventura, Canary Islands: A model of submarine growth and emergence of tectonic volcanic islands

Margarita Gutiérrez[‡]
Estudios del Terreno S.L., C/España no. 21, locales 13 y 14, 38390 Santa Úrsula, Santa Cruz de Tenerife, Canary Islands, Spain

Ramón Casillas[‡]
Departamento de Edafología y Geología, Facultad de Biología, Universidad de La Laguna, C/Astrofísico Sánchez, s/n, 38206 La Laguna, Santa Cruz de Tenerife, Canary Islands, Spain

Carlos Fernández[§]
Departamento de Geodinámica y Paleontología, Universidad de Huelva, Campus de El Carmen, 21071 Huelva, Spain

Kadosa Balogh[#]
Institute of Nuclear Research, Hungarian Academy of Sciences, P.O. Box 51, H-4001 Debrecen, Hungary

Agustina Ahijado[††]
Departamento de Edafología y Geología, Facultad de Biología, Universidad de La Laguna, C/Astrofísico Sánchez, s/n, 38206 La Laguna, Santa Cruz de Tenerife, Canary Islands, Spain

Carolina Castillo[‡‡]
Departamento de Biología Animal, Facultad de Biología, Universidad de La Laguna, C/Astrofísico Sánchez, s/n, 38206 La Laguna, Santa Cruz de Tenerife, Canary Islands, Spain

Juan Ramón Colmenero[§§]
Facultad de Ciencias, Universidad de Salamanca, Plaza de la Merced, s/n, 37008 Salamanca, Spain

Encarnación García-Navarro[##]
Departamento de Geodinámica y Paleontología, Universidad de Huelva, Campus de El Carmen, 21071 Huelva, Spain

ABSTRACT

Three lithostratigraphic units have been distinguished in the volcanic succession of the basal complex of Fuerteventura Island. These units are, from bottom to top: the submarine volcanic group, the transitional volcanic group, and the subaerial volcanic group. These three groups record the submarine growth and emergence of the island. The volcanism is represented by ultra-alkaline and strongly alkaline igneous series. The igneous activity was due to the presence of an anomalous zone in the sublithospheric mantle, the low density of which also caused uplift of the Mesozoic oceanic crust. Two extensional phases and an intervening contractional phase developed coeval to the generation of the volcanic succession. The submarine volcanic group was deposited in the hanging wall basin of a large listric extensional detachment directed toward the SSW. The transitional volcanic group was syntectonic with respect to a late inversion of the listric detachment. Finally, the subaerial volcanic group resulted from a second episode of WNW extension. This study of the evolution of the basal complex of Fuerteventura serves as the basis for a tectonic model of submarine growth and emergence of volcanic islands.

Keywords: basal complex, submarine volcanism, emergence of volcanic islands, Fuerteventura, Canary Islands.

INTRODUCTION

Submarine growth of intraplate oceanic islands and volcanic seamounts has received a large amount of research attention in the last decades. Much information about seamount distribution, morphology, size, structure, and growth has been acquired through the use of surface and subsurface analytical techniques (e.g., Cotton, 1969; Batiza et al., 1984), dredging or drilling of seamount material or volcaniclastic aprons (e.g., Moore and Fiske, 1969; Schmincke and Segschneider, 1998), visual observations using submersibles (e.g., Fornari et al., 1978), and study of subaerially exposed uplifted seamounts (e.g., Jones, 1969a; McPherson, 1983; Staudigel and Schmincke, 1984). Intraplate basaltic seamounts commonly have a summit crater or small caldera, a high-density core, and one or more rift zones (e.g., Cotton, 1969; Batiza et al., 1984; Hildebrand et

[‡]E-mail: margarita@estudiosdelterreno.com.
[‡]E-mail: rcasilla@ull.es.
[§]E-mail: fcarlos@uhu.es.
[#]E-mail: balogh@moon.atomki.hu.
[††]E-mail: aahijado@ull.es.
[‡‡]E-mail: ccruiz@ull.es.
[§§]E-mail: colme@usal.es.
[##]E-mail: navarro@uhu.es.

785

al., 1989; Binard et al., 1992). The geological studies and the facies analysis of subaerially exposed, uplifted seamounts (e.g., Jones, 1969a; McPherson, 1983; Staudigel and Schmincke, 1984; McPhie, 1995) and volcaniclastic aprons surrounding oceanic islands (e.g., Schmincke and Segschneider, 1998) have led to the definition of two overlapping stages in the submarine evolution of oceanic islands: an initial deep-water stage and a second shallow-water, shield stage (Staudigel and Schmincke, 1984). Little is known in general about the geochemical evolution in these submarine stages of oceanic island volcano formation, but the Loihi seamount in Hawaii (e.g., Moore et al., 1982; Craig, 1983; Smith et al., 2002) and the Jasper seamount (NE Pacific, offshore California) (e.g., Gee and Staudigel, 1988; Gee et al., 1991) have been

studied in some detail. The geochemical evolution of these two seamounts is very different. In the Loihi seamount, the alkalinity of the lavas decreases with time, whereas in the Jasper seamount, the alkalinity increases.

As a result of locally extreme tectonic uplift of some units, the stage of submarine growth can be directly studied on some of the islands of the Canary Archipelago (Staudigel and Schmincke, 1984). This growth stage is mainly represented by the exhumed basal complexes of the islands of La Gomera, La Palma, and Fuerteventura (e.g., Fúster et al., 1968; Stillman et al., 1975), and it can be deduced from the analysis of samples from a deep well in Lanzarote (Sánchez-Guzmán and Abad, 1986). In particular, the study of the Fuerteventura Island bears a special interest because a complete submarine volcanic

sequence crops out at the western part of the island (Robertson and Stillman, 1979b). This sequence, representing the submarine-growth stage of the island, was deposited on the floor of the Atlantic Ocean, which is also exposed at the basal complex of Fuerteventura (Steiner et al., 1998). The aim of this paper is to describe and interpret the volcanic facies, the internal structure, the growth, and the geochemical evolution of the submarine volcanic complex of the Fuerteventura Island. We suggest that processes of uplift of a buoyant mantle accompanied by lithosphere extension through diking and faulting continued throughout the submarine growth of the island. This uplift may be partially responsible for the emergence of the submarine sequence and of the ocean floor. We also discuss the tectonic evolution of the zone during the early Cenozoic, with reference to the tectonics of nearby regions, like the Atlas Mountains.

GEOLOGICAL SETTING

The geological history of Fuerteventura is the most complex and longest lasting of the Canary Islands (e.g., Fúster et al., 1968; Stillman et al., 1975; Fúster et al., 1980; Le Bas et al., 1986; Coello et al., 1992; Ancochea et al., 1996; Steiner et al., 1998; Balogh et al., 1999). Fuerteventura was formed on the Atlantic oceanic crust (Banda et al., 1981; Steiner et al., 1998). According to the available seismic information, the thickness of the crust beneath the eastern Canaries, including Fuerteventura, is ~15–20 km (e.g., Dañobeitia and Canales, 2000). A 2–4-km-thick layer with seismic velocities of 4.2–4.3 km s^{-1} defines the upper crust. The middle crust appears as a 5–6-km-thick layer with velocities of 6.1–6.6 km s^{-1}. An 8–10-km-thick layer with an average seismic velocity of 7.4 km s^{-1} appears at the base of the crust in Fuerteventura and Lanzarote. This layer has been interpreted as oceanic crust intruded by mantle-derived material (Watts, 1994). This thick crust overlies an anomalous upper mantle with velocities of 7.6–7.8 km s^{-1} (Dañobeitia and Canales, 2000).

Four main geological units can be distinguished in the island (Figs. 1 and 2). These are, from older to younger, the exposed Mesozoic oceanic crust, the submarine and transitional volcanic complexes, the Miocene subaerial volcanic complexes, and the Pliocene-Quaternary sedimentary and volcanic rocks. The Mesozoic oceanic crust, the submarine volcanic complex, and the plutonic bodies and dike swarms associated with the submarine volcanic complex and with the Miocene subaerial volcanic complexes, form a heterogeneous lithostratigraphic unit known as the basal complex of Fuerteventura (Fúster et al., 1968; Stillman et al., 1975).
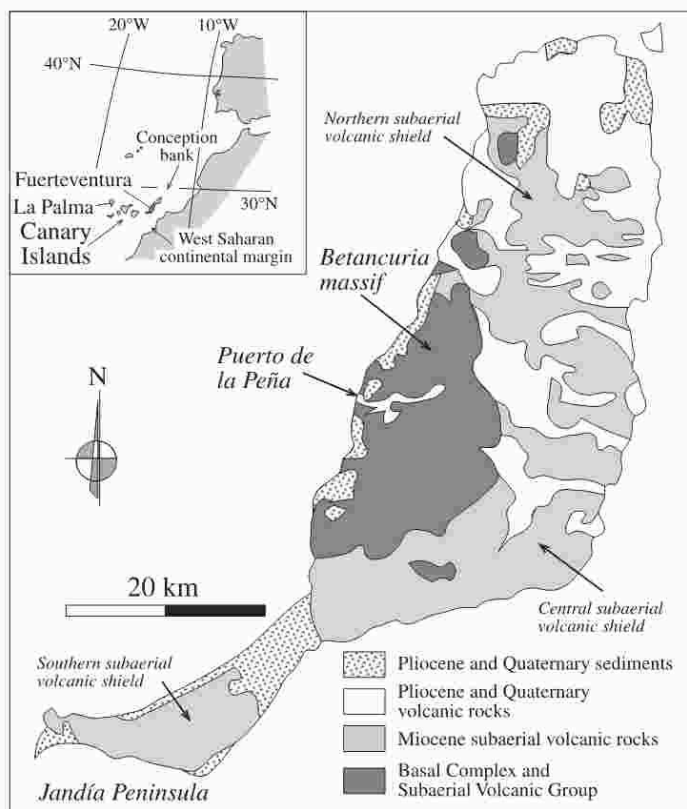
Figure 1. Schematic geological map of Fuerteventura. The inset shows the location of Fuerteventura in the Canary Archipelago. Map was modified from Ancochea et al. (1993).

Former studies have included subaerial volcanic rocks into the submarine and transitional complexes (e.g., Fúster et al., 1984a, 1984b). Gutiérrez (2000) assigned these rocks to the subaerial volcanic complexes, excluding them from the basal complex. This is the approach followed in this contribution.

Exposed Mesozoic Oceanic Crust

This fragment of Mesozoic oceanic crust comprises tholeiitic normal mid-ocean-ridge basalts (N-MORBs) of Early Jurassic age (e.g., Robertson and Stillman, 1979a; Steiner et al., 1998) overlain by a thick sedimentary sequence. Terrigenous quartzose clastics, black shales, redeposited limestones, marls and chalks with chert nodules form the Mesozoic sedimentary sequence, which spans from the Early Jurassic to the Late Cretaceous. The presence of the bivalvia fossil *Bositra buchi* is typical of the lower unit. The ammonite *Partschiceras* cf. *witeavesi* and the association of planktonic foraminifers *Schakoina galdolfii* Reichel, *Rotalipora* sp.,

Hedbergella sp., and *Gabonella* sp. characterize the upper sedimentary unit (Steiner et al., 1998). This succession is part of a deep-sea fan derived from the West African continental margin (e.g., Fúster et al., 1968; Robertson and Stillman, 1979a; Steiner et al., 1998). The thickness of this succession attained 1600 m (Steiner et al., 1998). The approximate water depth was more than 3000 m for the units previous to the Albian, although lower depths have been estimated for the deposition of the Albian units (Fúster et al., 1980). The N-MORBs crop out at a height of around 200 m above sea level. Therefore, Fuerteventura has undergone an uplift of between 1800 m (the thickness of the Mesozoic sediments plus the present-day height of the outcropping MORBs) and more than 3000 m since Albian times.

Submarine Volcanic Complex

The Mesozoic oceanic crust is covered by a submarine volcanic sequence constituted by a thick pile of pillow lavas and hyaloclastites of

basaltic and trachybasaltic composition (Robertson and Stillman, 1979b; Fúster et al., 1984a, 1984b; Le Bas et al., 1986; Stillman, 1987, 1999; Gutiérrez, 2000). The basal contact of the submarine volcanic sequence is a slight erosional unconformity over the Mesozoic rocks, implying a small difference of around 20° in bedding dips. The earliest submarine volcanic rocks were extruded after a hiatus, the duration of which will be discussed later in the Geochronology section. The description of this submarine sequence is the primary objective of this work. Plutonic activity coeval with the generation of the submarine volcanic sequence yielded ultra-alkaline rocks. These intrusives crop out along the western coast of the island, to the north and south of the exposed Mesozoic oceanic crust. Most of these intrusive rocks are mica- or amphibole-bearing pyroxenites (kaersutitites of Wagner et al., 2003), melteigites, ijolites-urtites, amphibole-bearing gabbros, nepheline syenites, nephelinites, and carbonatites (e.g., Fúster et al., 1980; Le Bas et al., 1986; Ahijado, 1999). The nepheline syenites and carbonatites
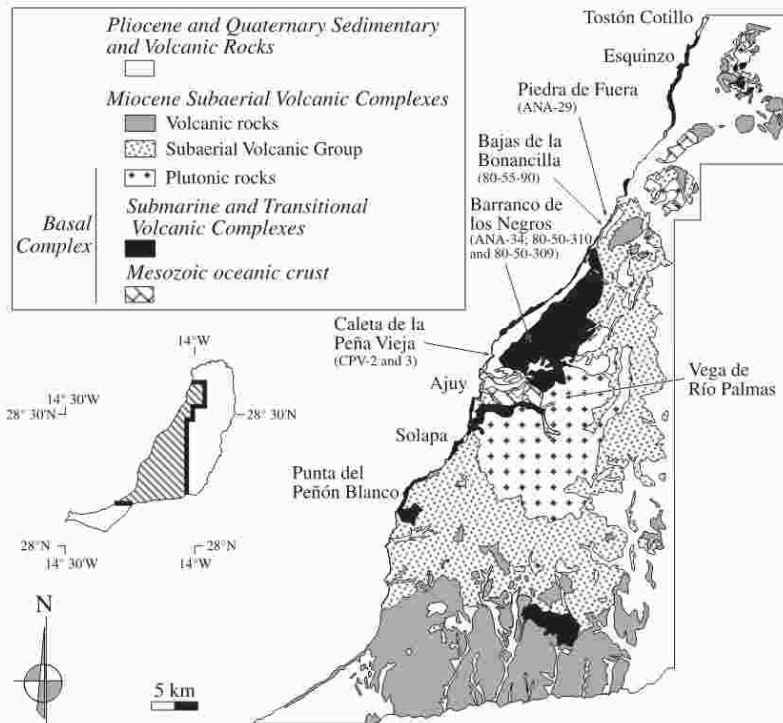
Figure 2. Geological map of the western part of Fuerteventura. Relevant sites mentioned in the text are shown, as well as the location of samples for the geochronological analyses (Table 1).

are predominantly exposed at Esquinzo, Ajuy, Solapa, and Punta del Peñon Blanco (Fig. 2) (e.g., Fúster et al., 1980; Le Bas et al., 1986; Ahijado, 1999; Balogh et al., 1999). The emplacement of these rocks at around 25 Ma (Le Bas et al., 1986; Cantagrel et al., 1993; Sagredo et al., 1996; Ahijado, 1999; Balogh et al., 1999) was coeval with movement along several brittle-ductile to ductile shear zones, as shown by the structural studies of Casillas et al. (1994) and Fernández et al. (1997).

Miocene Subaerial Volcanic Complexes

The main stages of subaerial growth of the island are the result of the formation of three adjacent huge basaltic volcanic complexes: the southern, central, and northern edifices (Fig. 1) (Ancochea et al., 1996). Each Miocene volcanic complex grew over a long period of probably >10 m.y. During that time, several episodes of effusive volcanic activity were separated by periods of quiescence accompanied by deep erosion and giant landslides (Ancochea et al., 1996; Stillman, 1999). The ages of these volcanic complexes (Ancochea et al., 1996, K-Ar method) differ slightly. The central edifice is the oldest, with the main stage of building occurring between 22.49 ± 0.79 and 14.05 ± 0.4 Ma, followed by a significant pause and a late smaller building stage at 13 ± 0.3 Ma. In the northern edifice, the main activity took place between 17 ± 0.85 and 12.8 ± 0.3 Ma, and in the southern edifice, between 20.7 ± 0.4 and 14.2 ± 04 Ma. The remnants of these volcanic complexes, deeply eroded, appear in the eastern part of the island and in the Jandía Peninsula (Figs. 1 and 2). A cortege of plutonic rocks (pyroxenites, gabbros, and syenites) and a dike swarm crop out in the core of the northern and central edifices (e.g., Gastesi, 1969). These rocks represent the hypabyssal roots of the successive episodes of growth of the subaerial volcanic complexes (Ancochea et al., 1996; Balogh et al., 1999). The density of the dike swarms associated with the subaerial volcanic complexes is extremely high, attaining average values of 50%–90% of sheeted dikes in the center of the basal complex, although these values decrease toward its eastern and western limits (e.g., Stillman and Robertson, 1977; Stillman, 1987; Ahijado, 1999; Ahijado et al., 2001). Accordingly, the generation of these dike swarms seems to have involved a crustal extension of around 30 km (e.g., López Ruiz, 1970; Stillman, 1987; Ahijado et al., 2001). The most frequent strike of these dikes is NNE-SSW, but some of them exhibit NE-SW and NW-SE azimuths. Their composition is mainly basaltic or trachybasaltic.

The basal complex thus comprises the Mesozoic oceanic crust, the submarine volcanic complex (excluding the basal part of the subaerial volcanic complexes, i.e., the subaerial volcanic group), and the plutonic bodies and dike swarms associated with the submarine volcanic complex and with the Miocene subaerial volcanic complexes (Fig. 1) (Fúster et al., 1968; Stillman et al., 1975). Metamorphism affected most of the rocks forming the basal complex. An intense hydrothermal metamorphism of epidote-albite greenschist facies took place, probably as a result of the massive intrusion of dike swarms (e.g., Fúster et al., 1968; Muñoz and Sagredo, 1994; Stillman et al., 1975; Stillman and Robertson, 1977; Robertson and Stillman, 1979b; Fúster et al., 1984a; Gutiérrez, 2000). Two metamorphic zones can be distinguished: a low-temperature (actinolite) and a high-temperature (hornblende) zone. The high-temperature zone geographically coincides with the maximum density of basic dike intrusion (Gutiérrez, 2000). Therefore, it can be deduced that dikes acted as preferred pathways for fluid circulation and constituted the thermal source for the observed mineral transformations. A contact metamorphism has also affected the host rocks of the plutons related to the subaerial volcanic complexes (e.g., Muñoz and Sagredo, 1994; Hobson et al., 1998).

Pliocene-Quaternary Sedimentary and Volcanic Rocks

After the Miocene volcanic activity, the island was affected by an erosive period. During that period of volcanic quiescence, the Miocene edifices were deeply eroded. During the Pliocene, volcanic activity restarted with the formation of several small basaltic volcanoes and associated lava fields. This activity has continued up to prehistoric times (Cendrero, 1966). Littoral and shallow-water marine deposits were formed in the Pliocene-Quaternary (e.g., Martín González et al., 2001; Meco et al., 2002). Eolian complexes with intercalations of alluvial fan and paleosol deposits overlie these sediments (e.g., Meco and Pomel, 1985; Meco et al., 1997).

DESCRIPTION OF THE SUBMARINE VOLCANIC COMPLEX

Stratigraphy

The submarine volcanic complex of Fuerteventura, exposed along the western coast of the island, is composed of two lithostratigraphic units: the submarine volcanic group, representing the period of submarine growth, and the transitional volcanic group, corresponding to the

emergence of the island (Fig. 3). Subaerial volcanic rocks (the subaerial volcanic group) overlie these units. This subaerial volcanic group can be tentatively assigned to the lowest part of the central and northern subaerial edifices.

The submarine and transitional volcanic groups have been subdivided into six and five lithostratigraphic formations, respectively (Gutiérrez, 2000). The distinct volcanic sequences were named and classified according to the nomenclature established by McPhie et al. (1993). Gutiérrez (2000) established the basis for the stratigraphical division and characterization of these units. The definitions and nomenclature follow the North American Stratigraphic Code (North American Commission on Stratigraphic Nomenclature, 1983). A detailed description of the distinguished formations appears in the GSA Data Repository item[1] accompanying this work. The most important volcano-stratigraphical characteristics of these formations can be observed in Figure 4, which shows representative stratigraphical columns, although some lateral facies variations are to be expected within a given formation.

Six formations have been distinguished in the submarine volcanic group (Fig. 4), from the Barranco del Tarajalito Formation (base, unit A) to the El Valle Formation (top, unit F). The average thickness of this group is 2000–2100 m. Volcanogenic facies (Fig. 5A) appear interbedded with primary volcanic facies (Fig. 5B). Here, volcanogenic deposits are defined as the result of surface processes operating on pre-existing volcanic series (McPhie et al., 1993). Indicators of lava flow directions include the orientations of individual pillows and the arrangement and elongation of vesicles (Gutiérrez, 2000). Results point to a NNE-SSW direction of lava flows in the Barranco del Tarajalito, La Herradura, and Los Negros Formations. The average vesicularity index of pillow lavas in the basal formations (e.g., La Herradura Formation) is of around 50% (Fig. 5B). Assuming that vesicularity is due to exsolution of water, this proportion indicates low water depths during the emission of these pillow lavas (Jones, 1969b), which are in accordance with other water-depth indicators of this sequence. The silty levels of the Toscano Formation show abundant bioturbation, with both horizontal and vertical burrows (Fig. 5C). The grain size and thickness of deposits in the Toscano Formation increase toward the north and east, indicating a source to the east. In some levels at the top of this group, coral specimens

Figure 3. Geological map showing the different formations of the submarine volcanic group and the transitional volcanic group: Unit A—Barranco del Tarajalito Formation, unit B—La Herradura Formation, unit C—Los Negros Formation, unit D—La Gatera Formation, unit E—Toscano Formation, unit F—El Valle Formation, units G1 and G2—Caleta del Barco Formation, unit G3—Piedra de Fuera Formation, unit G4—Janey Formation, unit G5—Barranco de la Fuente Blanca Formation.
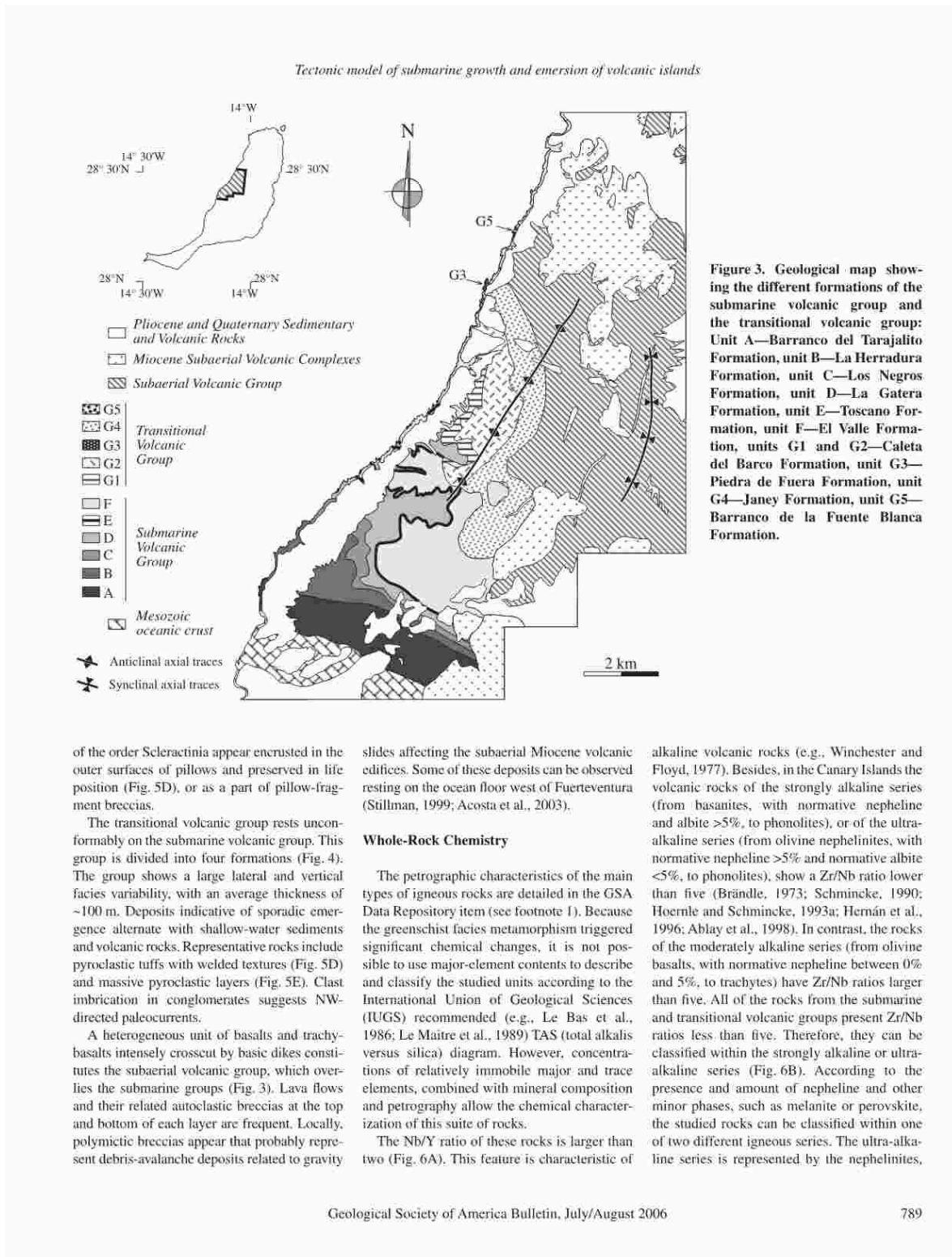
of the order Scleractinia appear encrusted in the outer surfaces of pillows and preserved in life position (Fig. 5D), or as a part of pillow-fragment breccias.

The transitional volcanic group rests unconformably on the submarine volcanic group. This group is divided into four formations (Fig. 4). The group shows a large lateral and vertical facies variability, with an average thickness of ~100 m. Deposits indicative of sporadic emergence alternate with shallow-water sediments and volcanic rocks. Representative rocks include pyroclastic tuffs with welded textures (Fig. 5D) and massive pyroclastic layers (Fig. 5E). Clast imbrication in conglomerates suggests NW-directed paleocurrents.

A heterogeneous unit of basalts and trachybasalts intensely crosscut by basic dikes constitutes the subaerial volcanic group, which overlies the submarine groups (Fig. 3). Lava flows and their related autoclastic breccias at the top and bottom of each layer are frequent. Locally, polymictic breccias appear that probably represent debris-avalanche deposits related to gravity

slides affecting the subaerial Miocene volcanic edifices. Some of these deposits can be observed resting on the ocean floor west of Fuerteventura (Stillman, 1999; Acosta et al., 2003).

Whole-Rock Chemistry

The petrographic characteristics of the main types of igneous rocks are detailed in the GSA Data Repository item (see footnote 1). Because the greenschist facies metamorphism triggered significant chemical changes, it is not possible to use major-element contents to describe and classify the studied units according to the International Union of Geological Sciences (IUGS) recommended (e.g., Le Bas et al., 1986; Le Maitre et al., 1989) TAS (total alkalis versus silica) diagram. However, concentrations of relatively immobile major and trace elements, combined with mineral composition and petrography allow the chemical characterization of this suite of rocks.

The Nb/Y ratio of these rocks is larger than two (Fig. 6A). This feature is characteristic of

alkaline volcanic rocks (e.g., Winchester and Floyd, 1977). Besides, in the Canary Islands the volcanic rocks of the strongly alkaline series (from basanites, with normative nepheline and albite >5%, to phonolites), or of the ultra-alkaline series (from olivine nephelinites, with normative nepheline >5% and normative albite <5%, to phonolites), show a Zr/Nb ratio lower than five (Brändle, 1973; Schmincke, 1990; Hoernle and Schmincke, 1993a; Hernán et al., 1996; Ablay et al., 1998). In contrast, the rocks of the moderately alkaline series (from olivine basalts, with normative nepheline between 0% and 5%, to trachytes) have Zr/Nb ratios larger than five. All of the rocks from the submarine and transitional volcanic groups present Zr/Nb ratios less than five. Therefore, they can be classified within the strongly alkaline or ultra-alkaline series (Fig. 6B). According to the presence and amount of nepheline and other minor phases, such as melanite or perovskite, the studied rocks can be classified within one of two different igneous series. The ultra-alkaline series is represented by the nephelinites,

143
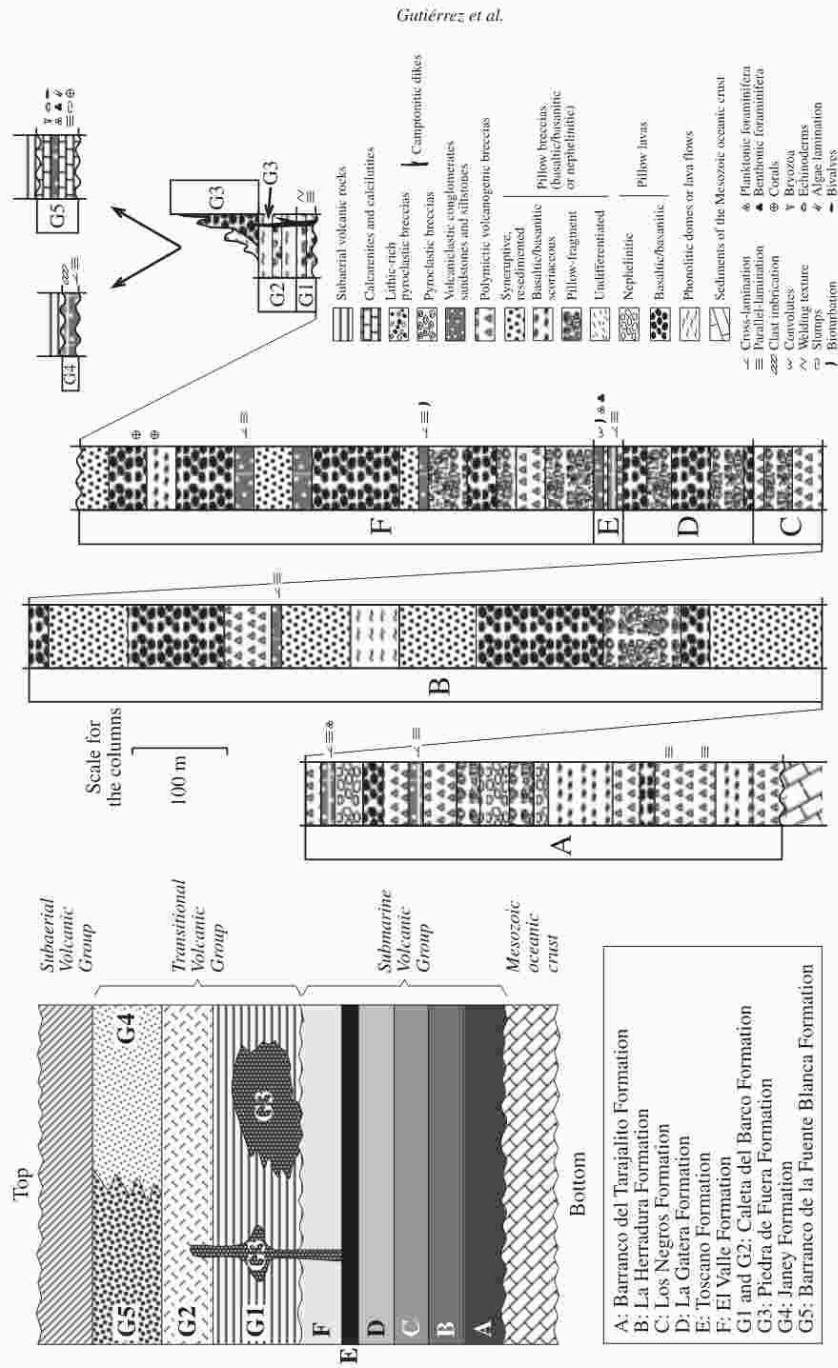
Figure 4. Stratigraphic relationships between the different lithological units (left) and synthetic stratigraphic columns (center and right).

144
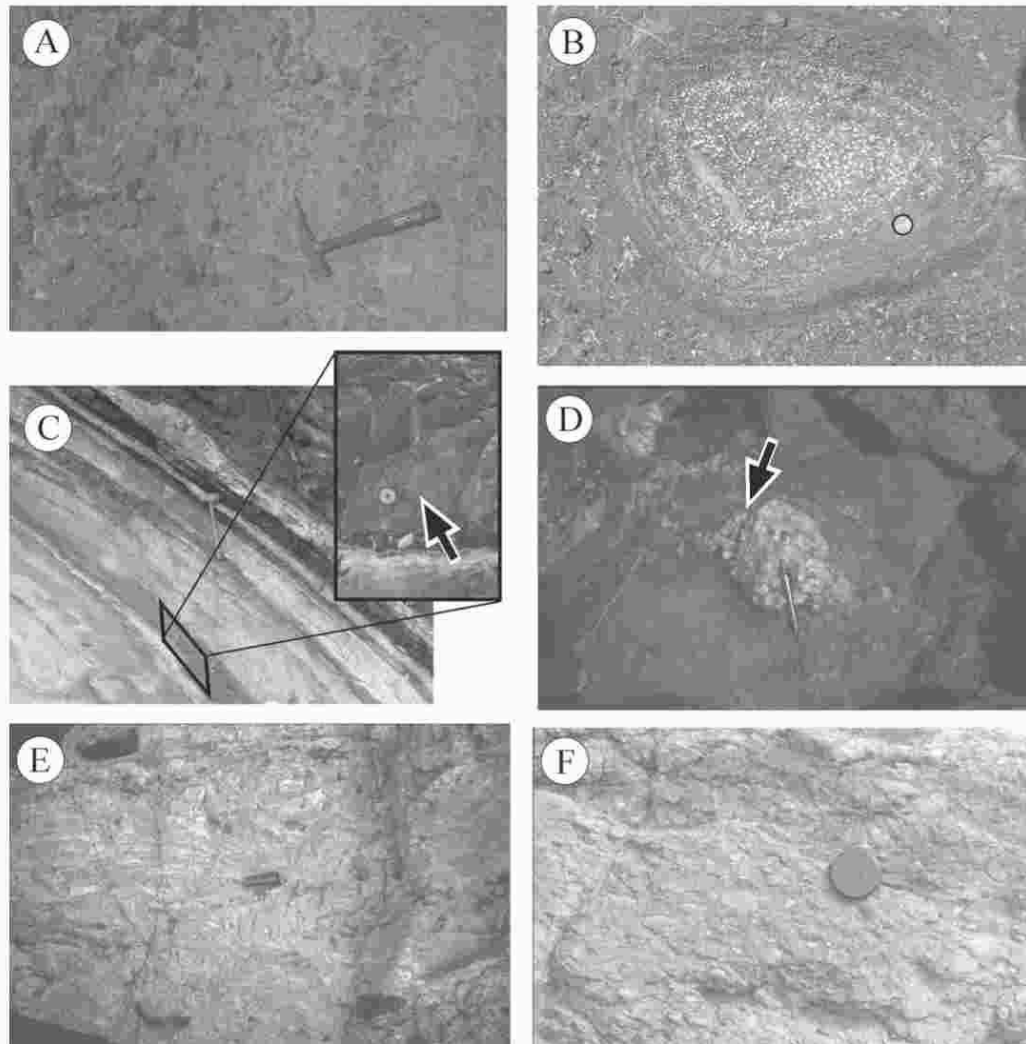
Figure 5. Field photographs showing representative structures of the studied units. (A) Matrix-supported, volcanic polymictic breccias. Clasts are fragments of basaltic/basanitic pillows (unit A, Barranco del Tarajalito Formation). (B) Pillow-lava fragment included in the resedimented pillow-fragment breccias. Note the presence of abundant, concentric vesicles (unit B, La Herradura Formation). (C) Alternating volcanic sandstones and siltstones. The inset shows horizontal bioturbation in a siltstone layer (unit E, Toscano Formation). (D) Scleractinia corals, preserved in life position, encrusted in the outer surface of a pillow (unit F, El Valle Formation). (E) Coarse-grained pyroclastic tuffs with strongly flow-foliated trachyte pumice fragments (welded structure) (unit G1, Caleta del Barco Formation). (F) Polymictic matrix-supported conglomerates. Rock fragments are rounded and imbricate, showing a high sphericity index (unit G4, Janey Formation).

Gutiérrez et al.
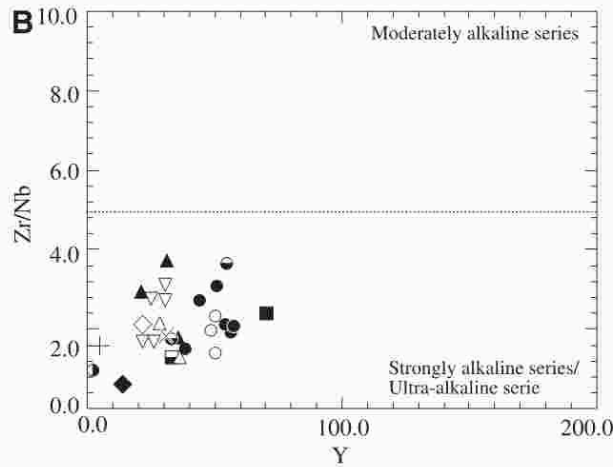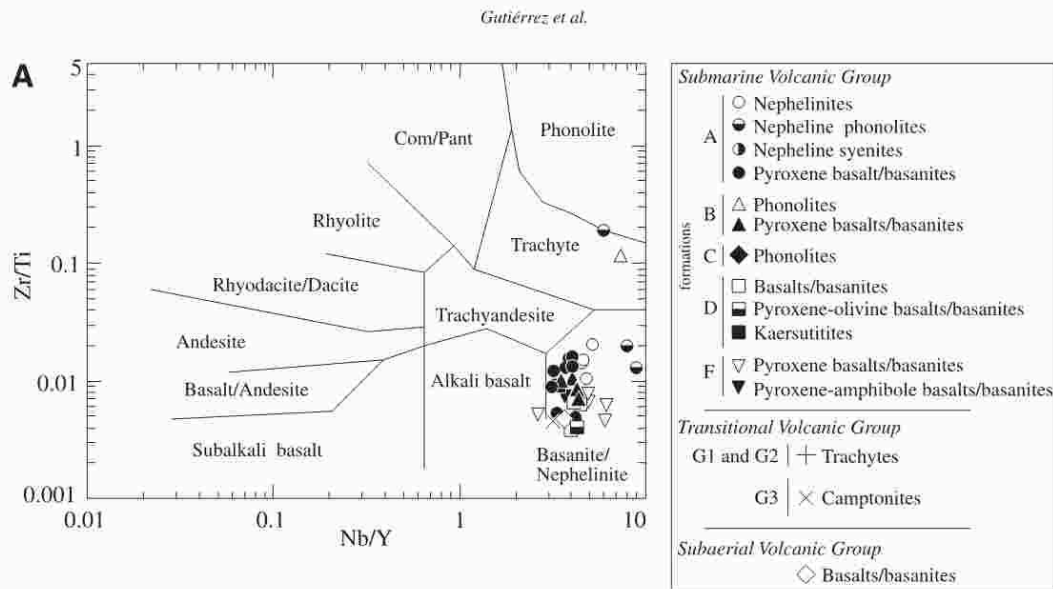
Figure 6. (A) Plot of the studied samples in the Zr–Ti-Nb–Y discrimination diagram of Winchester and Floyd (1977). (B) Representation of the analyzed samples in the Zr–Nb-Y discrimination diagram. The horizontal straight line separates the fields of the different alkaline series of the Canarian rocks (Schmincke, 1990; Brändle, 1973; Hoernle and Schmincke, 1993a; Hoernle and Schmincke, 1993b; Ablay et al., 1998; Hernán et al., 1996). Moderately alkaline series range from olivine basalts (normative Ne = 0%–5%) to trachytes. Strongly alkaline series vary from basanites (normative Ne > 5% and Ab > 5%) to phonolites. Ultra-alkaline series include rocks from olivine nephelinites (normative Ne > 5%, Ab < 5%) to phonolites. See Figures 3 and 4 for the nomenclature of the units.

TABLE 1. RADIOMETRIC DATA

Sample	Formation	Location	Mineral	K (%)	^{40}Ar (rad) ccSTP/g	^{40}Ar (rad) (%)	K/Ar age (Ma)		Ar/Ar age (Ma)		Rb/Sr age (Ma)	
CPV-2	Barranco del Tarajalito (unit A)	Caleta de la Peña Vieja	Biotite	7.20	7.447×10^{-6}	70	26.4	1.1	25.1	0.4	–	
CPV-3	Barranco del Tarajalito (unit A)	Caleta de la Peña Vieja	Biotite	5.92	6.884×10^{-6}	75.6	29.7	1.2	–		–	
ANA-34	La Gatera (unit D)	Barranco de Los Negros	Amphibole	0.804	9.847×10^{-7}	22.0	31.2	2.2	–		–	
80–50–310	La Gatera (unit D)	Barranco de Los Negros	Phlogopite	5.01	5.578×10^{-6}	61.0	28.4	1.1	–		–	
80–50–309	El Valle (unit F)	Barranco de Los Negros	Amphibole	2.30	2.086×10^{-6}	62.7	23.2	0.9	–		–	
ANA-29	Piedra de Fuera (unit G3)	Piedra de Fuera	Phlogopite	5.79	5.766×10^{-6}	65.7	25.3	1.0	–		22.5	0.2
80–55–90	Piedra de Fuera (unit G3)	Bajas de la Bonancilla	Phlogopite	6.53	5.966×10^{-6}	74.0	23.4	0.9	–		–	

Note: Radiometric ages for the different units are listed here. Locations of samples are in Figure 2. K/Ar and Ar/Ar radiometric ages are new. Rb/Sr determinations are from Demeny et al. (2004). Uncertainties represent errors given at the 1σ level.

146

Tectonic model of submarine growth and emersion of volcanic islands

nephelinite phonolites, pyroxenites, kaersu-titites, melteigites, ijolites-urtites, and neph-elinite syenites appearing in the Barranco del Tarajalito and Barranco de Los Negros For-mations. The modal amount of nepheline is often larger than 40% in these rocks, and they commonly contain melanite and perovskite. The camptonites of the transitional volcanic group show clear ultra-alkaline affinities. The strongly alkaline series is represented by the basanites, phonolites, trachytes, and syenites from the remaining formations of the subma-rine and transitional volcanic groups.

Geochronology

Five new K/Ar ages and one new Ar/Ar age of rocks from the submarine volcanic group and two K/Ar ages of samples from the transitional volcanic group are shown in Table 1, as well as one published Rb/Sr isochron age (Demény et al., 2004). The evidence of hydrothermal meta-morphism (greenschist facies) in some samples and the frequent presence of excess argon (Feraud et al., 1985; Cantagrel et al., 1993; Balogh et al., 1999) imply that the radiometric ages may be biased (either older or younger), and must be treated with caution. Because of these uncertainties, only rocks dated by differ-ent methods will be discussed here.

In the submarine volcanic group, biotite and phlogopite ages range from 29.7 1.2 Ma to 25.1 0.4 Ma, while 31.2 2.2 Ma and 23.2 0.9 Ma have been measured on the amphiboles. In the transitional volcanic group, phlogopite ages are 25.3 1.0 Ma and 23.4 0.9 Ma, while the Rb/Sr isochron is younger (22.5 0.2 Ma). All errors herein are given at the 1σ level. There is no significant difference between the K/Ar and Ar/Ar ages for the biotite from sample CPV-2. The Ar/Ar age spectrum does not show argon loss at the low-temperature steps, and the inverse isochron (Figs. 7 and 8) gives 24.7 1.1 Ma, and 310.5 6.8 Ma for the initial $^{40}Ar/^{36}Ar$ ratio. The small difference between the K/Ar and Ar/Ar ages is most likely caused by a small amount of excess argon, and the plateau age of 25.1 0.4 Ma, defined for 97.6% of the spectrum, is regarded as the age of volcanic activity. K-Ar ages from rocks of the transitional volcanic group in this work are similar to the K-Ar ages obtained by Ibarrola et al. (1989) of around 24.0 2 Ma. Also, the ages obtained here for CPV-2 and CPV-3 fall within the range of ages (19.2 0.9–30.9 1.2 Ma) proposed by previous authors (Fig. 9) for the rocks of the plutonic ultra-alkaline complexes (Esquinzo, Ajuy-Solapa, and Punta del Peñón Blanco areas: Le Bas et al., 1986; Cantagrel et al., 1993; Sagredo et al., 1996; Ahijado, 1999;
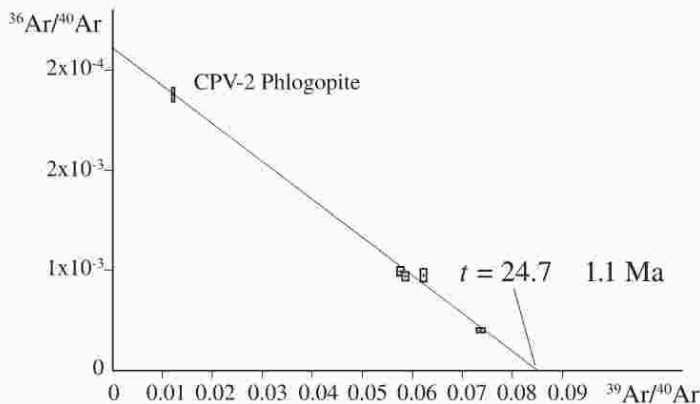
Figure 7. $^{36}Ar/^{40}Ar$ vs. $^{39}Ar/^{40}Ar$ isochron diagram for the CPV-2 sample.
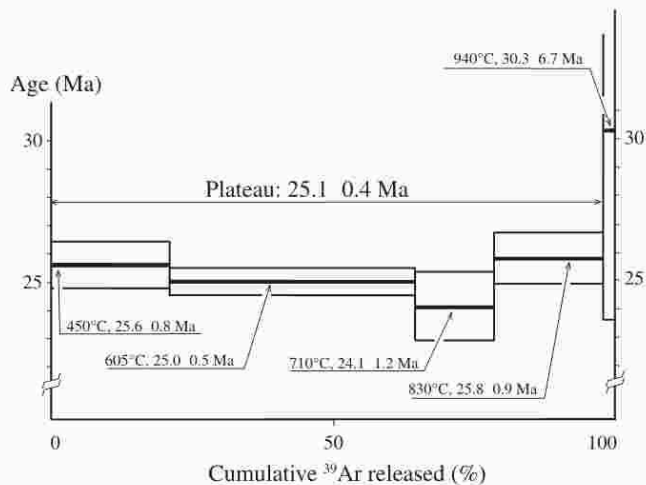
Figure 8. Ar-Ar emission spectra of phlogopite from the CPV-2 sample.

Balogh et al., 1999), based on the use of the K-Ar, Ar-Ar, and U-Pb methods.

The results obtained here indicate an Oligo-cene to early Miocene age for the submarine building and later emergence of the Fuerteven-tura Island (submarine and transitional volcanic groups, Fig. 9). The submarine volcanic build-ing of this island was broadly coeval with the formation of the plutonic ultra-alkaline com-plex of Esquinzo. Also, the transitional vol-canic group overlaps the age of the plutonic

complexes of Ajuy-Solapa and Punta del Peñón Blanco (Fig. 9). The subaerial volcanic group, which overlies the transitional volcanic group, must correspond to the large subaerial shield volcanoes studied by Ancochea et al. (1996).

Structure

Very few detailed structural studies of the Mesozoic sediments and submarine volcanic series of Fuerteventura have been presented

147
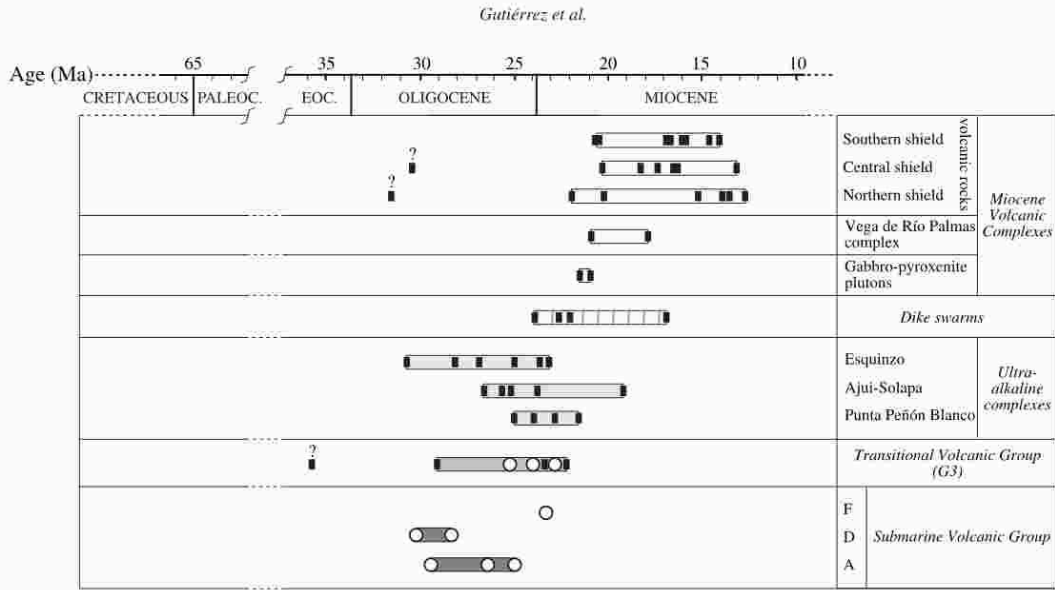
Figure 9. Chronological diagram of different geological units of Fuerteventura. Data marked with black rectangles are from Feraud et al. (1985), Feraud (1981), Le Bas et al. (1986), Ibarrola et al. (1989), Coello et al. (1992), Cantagrel et al. (1993), Balcells et al. (1994), Ancochea et al. (1996), Ahijado (1999), and Balogh et al. (1999). Data marked with open circles are from Gutiérrez (2000). See Figures 3 and 4 for the nomenclature of the formations.

until now. The work of Robertson and Stillman (1979a) is the main, and virtually only, source of structural data for these rocks. More recent studies discuss the tectonic evolution of the basal complex, but they do not present significant new structural information about the Mesozoic or submarine volcanic series. Here, detailed mapping and new structural data are presented (Fig. 10) that allow a more complete understanding of the geometry of the Mesozoic crust and its overlying submarine rocks. This geometrical description, together with the vol-

cano-stratigraphic information, is essential to any model that attempts to describe the tectonic evolution of this zone.

The Mesozoic sediments are almost invariably vertical to overturned, and they are systematically older southwards (Robertson and Stillman, 1979a), where a block of MORB oceanic basement is exposed (Fig. 2 of Steiner et al., 1998). Variation in bedding orientation is compatible with a large-wavelength fold with a WNW-ESE–oriented, nearly horizontal fold axis (Fig. 10A). Dispersion around the best-fit

large circle is a consequence of later deformation phases. These new data confirm the previous observations of Robertson and Stillman (1979a), who interpreted the systematic cleavage-bedding relationships and the orientation of minor folds appearing in these sediments as indicative of the presence of a major NE-facing reclined fold. In summary, the Mesozoic sequence forms part of the locally inverted limb of a reclined, N-verging major fold, with a block of oceanic basement cropping out at its core. Unfortunately, the younger Miocene subaerial

Figure 10. Structural map of the submarine, transitional, and subaerial volcanic groups and equal-area, lower-hemisphere projections of poles to bedding (So) for the Mesozoic sedimentary rocks and the submarine and transitional volcanic groups; *n* is number of data. See Figure 3 for the nomenclature of the formations. Great circles represent the cylindrical best fit to the measured data, and gray squares mark the pole to these great circles, i.e., the location of the statistically determined fold axes (f_1 and f_2). (A) Mesozoic sediments (f_1: statistically determined fold axis); (B) unit A (f_1: statistically determined fold axis); (C) unit B; (D) units C to G5 (f_2: statistically determined fold axis). (E) Rose diagram of lava flow directions measured in the Barranco del Tarajalito, La Herradura, and La Gatera Formations (units A, B, D), restored after eliminating the effects of the two folding phases (f_1: here represents axial trace of the first-phase folds); the arrow indicates increasing distance from the source region for unit E. (F) Orientation of paleocurrents measured in the Janey Formation (unit G4) of the transitional volcanic group, restored after eliminating the effects of the second phase of folding (f_2: approximate axial trace of the second-phase folds); the arrow marks the average direction of the paleocurrent obtained at 16 sites with clast imbrication measurements; the shaded interval around the arrow corresponds to the 95% confidence interval (statistics based on the von Mises distribution, Mardia, 1972). (G) Cross section across the studied area (see A for location); a.s.l.—above sea level. Units A to G correspond to the formations of the submarine and transitional volcanic groups defined in this work (see Figures 3 and 4 for the nomenclature).

149

Tectonic model of submarine growth and emersion of volcanic islands

150

Gutiérrez et al.

volcanic complexes to the east and the massive, intrusive rocks of the basal complex to the south obscure the full extent of the fold. The submarine volcanic group shows a quite complex orientation of layering. The basal unit (Barranco del Tarajalito Formation) also shows subvertical layering, folded comparably with the Mesozoic sediments (Fig. 10B). However, the bedding orientation of La Herradura Formation is highly variable (Fig. 10C). The remaining units of the subaerial and transitional volcanic groups tend to show more subhorizontal bedding, with WNW- and ESE-directed dips (Fig. 10D). Near the coast, these units predominantly dip to the WNW (Robertson and Stillman, 1979a). This dip sense changes inland, defining a large open anticline with a NNE-SSW–trending, subvertical axial plane, and an axis with a shallow plunge to the NNE (Fig. 10D). A similar open syncline can be observed to the east (map in Fig. 10). Dispersion of bedding data around the best-fit great circles can be explained by differences in depositional dips (especially for units B to G5), in accordance with the observed steep dips (20°–30°) of basaltic talus slopes (Mitchell et al., 2000).

Accordingly, the bedding dip data demonstrate a folding about a NW-SE axis followed by folding about a NNE-SSW axis. The axes of both fold generations are subhorizontal and almost perpendicular. The axial surfaces, however, are oblique due to the N-verging orientation of the fold deduced from the analysis of the Mesozoic sediments and Barranco del Tarajalito Formation of the submarine volcanic group. Therefore, an interference pattern intermediate between the types 1 (dome-basin pattern) and 2 (dome-crescent-mushroom pattern) of the Ramsay (1967) classification scheme describes the structure. The swarm of basic dikes cuts across the axial plane of the WNW-ESE fold deduced from the study of the Mesozoic sediments. Therefore, the dikes are not affected by this folding episode. However, the NNE-SSE–oriented folds tilted these dikes (Gutiérrez, 2000). Accordingly, the WNW-ESE folds are older than the NNE-SSW folds. In Figure 10, these structures have been labeled f_1 and f_2, respectively.

Figure 10G shows a cross section normal to the axial trace of the f_1 folds and parallel to the axial trace of the f_2 folds, running along the hinge of the f_2 anticline. The most striking feature in this cross section is the fan-shape geometry defined by the units of the submarine volcanic group (units A to F). The transitional volcanic group (units G1 to G5) discordantly overlies the submarine volcanic group, onlapping from the Caleta del Barco Formation (units G1 and G2) to the Janey Formation (unit G4) (Fig. 3). Although not shown in Figure 10G, the

subaerial volcanic group, which lies on the submarine volcanic group (El Valle Formation) at the SE part of the studied region (Fig. 3), overlies the rest of the units separated by an erosional unconformity. These features are interpreted in terms of the submarine growth of the island in the next section.

DISCUSSION

Volcanological Interpretation of the Submarine and Transitional Volcanic Groups

The interpretation of the studied units will be presented from bottom to top. The formations of the submarine volcanic group were deposited under low water depths, as indicated by the vesicularity index of pillow lavas (e.g., Fig. 5B) and other water-depth indicators. The changing orientation of layering in breccia levels, without relation to the general structure of the sequence described above, suggests that these deposits were generated in small overlapping volcanic cones.

The volcanic facies of the Barranco del Tarajalito Formation (unit A) are proximal with respect to the eruption centers. The association of pillow lavas, pillow breccias, resedimented pillow-fragment breccias, and scoria pillow breccias indicates that the volcanic activity was focused along small submarine cones with an essentially effusive activity. There were also periods with predominantly submarine lava fountain activity that generated the layers of scoria pillow breccias in shallow waters (around 650 m; Wright, 1996), as illustrated in the paleogeographic reconstruction of this unit (Fig. 11A). Density-modified grain flows, cohesionless debris flows, or hyperconcentrated flows were the cause of the volcanic breccias from the volcanogenic facies association. Interbedded sandstones and siltstones can be assigned to the deposition of hyperconcentrated flows, tractive currents, or suspensions probably related to those high-density gravity flows. The composition and textures observed in the fragments of these deposits indicate the partial destruction of ultra-alkaline volcanic edifices constituted by pillow lavas, domes, phonolite-nephelinite flows, and related autoclastic breccias. The presence of plutonic fragments is indicative of the erosion of exposed ultra-alkaline plutons. During their motion, gravity flows enclosed contemporary fragments of basalt/basanite and clasts from the Mesozoic sedimentary sequence.

In La Herradura Formation (unit B), abrupt lateral facies changes suggest that eruption of basaltic/basanitic lavas took place through small cones (Fig. 11B), with overlapping of pillow-lava units and different breccia types related to

the destruction of those pillow-lava units. Lava fountains were also common. Effusive emission of phonolitic flows and domes and generation of autoclastic breccias and resedimented autoclastic breccias periodically accompanied this basaltic/basanitic activity.

The bimodal basaltic/basanitic-phonolitic volcanic activity continued during the generation of Los Negros Formation (unit C). However, the primary facies are scarce and they probably can be related to the activity of small basaltic/basanitic cones or edifices formed by pillow lavas and pillow-fragment breccias. The abundance of volcanogenic deposits must be related to gravity flows (debris flows, density-modified grain flows) and turbiditic currents on the flanks of volcanic edifices (Fig. 11C). The abundance of this type of facies could also indicate a migration of emission centers away from the deposition basin, or a hiatus in volcanic activity that favored the destruction of the previous submarine volcanic edifices through gravity-driven landslides. Tectonic and seismic instabilities inside the basin would also favor these processes. Cones that have erupted through debris-avalanche deposits of El Hierro island (western Canaries) (Gee et al., 2001) might be modern analogues to this unit.

Primary facies in La Gatera Formation (unit D) indicate an effusive character of volcanic activity (Fig. 11D). Bimodal (basaltic/basanitic and phonolitic) volcanic activity continued during the deposition of the Toscano Formation (unit E). However, the sedimentological characteristics of these deposits indicate that they were formed predominantly from turbidity currents in submarine fans surrounding the margins of the basin (Fig. 11E). Distal parts of these fans were located in the southwestern area, were the most fine-grained materials are found.

Effusive volcanic activity prevailed during the generation of the El Valle Formation (unit F) (Fig. 11F). Basaltic/basanitic volcanic cones emitted pillow lavas, which in turn generated pillow breccias and pillow-fragment breccias, sometimes resedimented by density-modified grain flows. This activity alternated with that of lava fountains, which produced scoria pillow breccias. The presence of colonial scleractinians, subrounded clasts in the breccias, and low-angle planar cross-lamination suggests that this volcanic activity and resedimentation processes took place below shallow waters. Debris-flows in submarine fans surrounding the volcanic cones and the margins of the basin generated volcanic breccias, sandstones, and siltstones.

The transitional volcanic group is thinner and more heterogeneous than the submarine volcanic group. The rocks of this transitional group record the first stages of emergence of the island.

151

Figure 11. Depositional models of the different geological formations of the submarine volcanic group. (A) Barranco del Tarajalito Formation; (B) La Herradura Formation; (C) Los Negros Formation; (D) La Gatera Formation; (E) Toscano Formation; (F) El Valle Formation. Depositional models of the different geological formations of the transitional volcanic group. (G) Caleta del Barco Formation; (H) Piedra de Fuera Formation; the block diagram is a sketch of facies generated in lava deltas; (I) Janey Formation; (J) Barranco de la Fuente Blanca Formation. Vertical scales are exaggerated to illustrate the volcano-stratigraphic characteristics of each unit. Marine animals are not to scale.

152

Textures, structures, and composition of rocks in the Caleta del Barco Formation (units G1 and G2) indicate that it consists of pyroclastic flow and fall deposits due to explosive Plinian subaerial eruptions (Fig. 11G). These pyroclastic flows included a large amount of lithic fragments coming from blocks dragged from the host rocks during flow in the magma conduit that later disintegrated due to the dynamics of explosive eruptions. Composition of phonolitic and trachytic flows is similar to that of pyroclastic layers. Therefore, it is probable that both were emitted during the same volcanic cycle.

The Piedra de Fuera Formation (unit G3) is extremely heterogeneous. The arrangement and alternation of pillow lavas and breccias suggest that they formed a flow-foot breccia (Jones and Nelson, 1970) inside a lava delta (Fig. 11H), generated after a subaerial flow entered into the sea (Jones and Nelson, 1970; Furnes and Fridleifsson, 1974). Pillow lavas, pillow-fragment breccias, and scoria pillow breccias were generated during subaquatic effusive eruptions and in lava fountains in shallow waters. These materials form small volcanic edifices. Camptonitic dikes represent the hypabyssal counterparts to the other rocks described in this unit.

The occurrence of matrix-supported conglomerates with imbricate clasts and a low sphericity index in the Janey Formation (unit G4) suggests a subtidal depositional environment with a continuous clast supply from the foreshore. This supply should have resulted from gravity flows, as debris flows (Fig. 11I). The faunal associations and sedimentological characteristics observed in the Barranco de la Fuente Blanca Formation (unit G5) indicate that these sediments were formed in shallow water reefs and that they were later resedimented by gravity flows (Fig. 11J).

In summary, the submarine and transitional volcanic groups in Fuerteventura do not clearly define a single large central edifice. Resedimentation of previously deposited materials through massive gravity flows is common, and these sedimentary deposits predominate in places over proximal volcanic facies. In particular, the volcanogenic deposits attain a volume percentage of 30% in the submarine volcanic group and 40% in the transitional volcanic group (Fig. 4). Volume percentages exceeding 50% can be obtained in both groups after adding the syneruptive resedimented deposits to the volcanogenic deposits. Therefore, the most accurate image of the depositional setting for both lithostratigraphic groups is a large basin infilled by abundant volcanogenic deposits (Fig. 10G). Geochemically, basaltic/basanitic magmatic activity was dominant, with only sporadic episodes of phonolitic activity. The first stages of

filling of the basin reveal the activity of a predominantly ultra-alkaline volcanism, which switched to strongly alkaline with time. The distinct periods of volcanism led to the formation of small overlapping volcanic cones constituted by pillow lavas and autoclastic levels and scoria pillow-fragment breccias due to the activity of lava fountains. NNE-SSW lava flow directions, which predominated during the formation of the submarine volcanic group, switched to the NW paleocurrent directions prevalent at least during the last stages of the transitional volcanic group (Janey Formation). The source region was located to the NNE or NE of the basin for the Toscano Formation (unit E), and to the SE of the basin for the Janey Formation (unit G4).

Model of Tectonic Evolution of the Submarine and Transitional Volcanic Groups

A lively debate persists about the origin of the Canary Archipelago. Hotspot models (e.g., Morgan, 1971; Hoernle and Schmincke, 1993b; Carracedo et al., 1998) rival with theories based on displacement along large fractures associated with the tectonic evolution of the northwestern African plate (e.g., Anguita and Hernán, 1975; Araña and Ortiz, 1991). Checking out these or other models needs an accurate understanding of the tectonic evolution of the submarine stage at each island. Unfortunately, basal complexes only crop out in three islands of the archipelago (Fuerteventura, La Gomera, and La Palma), and, as explained before, published structural data are still scarce. With respect to Fuerteventura, two main stages of tectonic evolution have been identified. The first stage involved the generation and deformation of the submarine sedimentary and volcanic rocks. Given the age of these series (Fig. 9), this first stage took place in the Oligocene. The only published tectonic model of this period is that of Robertson and Stillman (1979a), who explained the tectonic structures of the Mesozoic sediments and submarine volcanic rocks as a result of successive phases of uplift, compression, and extension. More recently, Fernández et al. (1997) described an extensional episode dated as late Oligocene or early Miocene that marks a transition to the second stage of tectonic evolution, which is essentially Miocene. The second stage coincides with the subaerial building of the island. Several deformation phases, extensional and transpressional, have been proposed for this second, Miocene stage (e.g., Ancochea et al., 1996; Muñoz et al., 1997; Hobson et al. 1998). The purpose of this section is to use the new volcano-stratigraphical and structural information gathered here to contribute to the knowledge of the first stage (Oligocene) of evolution of the basal complex

of Fuerteventura. The results are of interest in the debate about the origin of the Canary Archipelago, and the general models of submarine evolution and emergence of ocean islands.

To decipher the tectonic evolution of the submarine rocks of Fuerteventura, it is necessary to carefully analyze the observed pattern of superposed folding. The cross section of Figure 10G shows a clear fanning in the submarine volcanic complex. The available structural information allows us to discard that this fanning could be the result of the complex geometry of the interference pattern. The half-wavelength of the f_1 fold, although unknown, must exceed 5 km. This makes it quite improbable that the fanning could be entirely a consequence of the geometry of the f_1 folds. It can be concluded that this fanning is in part a primary feature of the submarine volcanic group. The axis of this fan coincides with the f_1 axis, suggesting that the submarine volcanic group can be considered as a syntectonic series with respect to the f_1 folding phase. Interestingly, the lava flow directions measured in the submarine volcanic group are almost normal to the f_1 axial traces (Fig. 11E), suggesting again a structural control on the deposition of the volcanic and sedimentary sequences. In other words, the depocenter was located immediately to the north of the inverted limb of the f_1 anticline as defined by the pretectonic Mesozoic sediments.

Fanning of growth strata is best described as a progressive unconformity. Similar, although not identical, fanning of growth strata has been described in Iceland's rift zone, where it has been interpreted as a result of subsidence due to the weight of syntectonic lavas (Palmason, 1980). Patterns similar to those of Iceland have been imaged by seismic reflection at the southern flank of the Azores Platform (Alves et al., 2004). However, the geometry of the syntectonic series in the Icelandic rifts or in the Azores differs in detail from that of Fuerteventura. In particular, the dip of the lavas rarely attains the large values measured in units A to D, and overturned beds have not been described (e.g., Bull et al., 2003). Continuous fanning of growth strata from subhorizontal to nearly vertical or even overturned beds has been identified in two contrasting continental settings: that associated with listric extensional growth faults subjected to a late inversion (e.g., McClay et al., 2004), or as a consequence of the progressive evolution of fault-related folds in contractional regimes (e.g., Hardy and Poblet, 1994; Hardy et al., 1996). It seems reasonable to cast some doubts about the applicability of these models to analyze the tectonic evolution of intraplate oceanic lithospheres. However, flat detachments, listric extensional faults, and oceanic core complexes similar to those of extended continental regions

Tectonic model of submarine growth and emersion of volcanic islands

are being widely recognized in the study of the seafloor (e.g., Karson, 1998). Some of these listric faults affect the oceanic crust and converge toward the Moho, which coincides with a major ductile shear zone. Certainly, displacement along these structures takes place beneath the ridge axes (MacLeod et al., 2002), but these faults can be seen in the oceanic crust far from the active ridges, as revealed through the study of major faulted scarpments (Karson, 1998). A Jurassic oceanic crust, like that of Fuerteventura, subjected to renewed uplift is probably able to reactivate these old faults, or to generate new structures of a similar geometry. Therefore, we suggest that the models of deformation of the continental crust cited before can be used as a first approximation to qualitatively describe the tectonic evolution of a similarly deformed oceanic crust. In fact, the oceanic structures imaged by Karson (1998) and MacLeod et al. (2002) are indistinguishable from those observed in comparable continental extensional settings.

The location of Fuerteventura above a wide zone of anomalous hot mantle (Hoernle et al., 1995) and the amount of uplift experienced by the oceanic crust since the Albian (a minimum of 1800 m, and perhaps more than 3000 m) favor the interpretation of an extensional regime against the contractional hypothesis. As mentioned before, an extensional kinematic regime has also been proposed for the subsequent stage of Miocene deformation of Fuerteventura (Casillas et al., 1994; Fernández et al., 1997; Muñoz et al., 1997). Besides, some evidence of contractional structures has been found (Hobson et al., 1998; Gutiérrez et al., 2002). The main proof of a contractional phase is the overturned Mesozoic series. Robertson and Stillman (1979a) suggested that the fold affecting the Mesozoic sedimentary rocks (f_1) could have been generated by dextral motion along a N–S–oriented transcurrent shear zone. Nevertheless, pretectonic and early syntectonic series can be rotated up to quite large dip angles through displacement at the hanging wall of a listric extensional fault (e.g., McClay et al., 2004). Only moderate contractional deformation is needed to overturn these highly dipping series. Therefore, the hypothesis favored in this work involves displacement along a listric extensional detachment that experienced a late inversion as a thrust or transpression shear zone. Gravity and bathymetric studies in and around Fuerteventura provide support for the presence of such a WNW-ESE–directed structure (González Montesinos, 2002; Acosta et al., 2003). We contend that the submarine volcanic group was deposited at the hanging wall of this fault, which was active during the Oligocene. The strike of this fault is WNW-ESE, and the hanging wall was displaced toward the SSW. The Mesozoic oce-

anic crust was displaced and folded in the hanging wall, generating a roll-over geometry (fold f_1). The uplifted footwall, located to the north of the studied area, coincides with the exposures of Mesozoic rocks south of Esquinzo (Fig. 2). At the Esquinzo area, the Mesozoic sediments strike WNW-ESE and dip gently to the SSW, although in the southern part of this area, Mesozoic beds dip steeply to the SSW. The original fault trace is covered with Neogene and Quaternary subaerial volcanic rocks and sediments. The available data don't allow an accurate reconstruction of the fault geometry by section balancing. However, this structure is a large extensional fault in the sense of Roberts and Yielding (1994), because it affects the sedimentary rocks and the tholeiitic N-MORBs of the Mesozoic oceanic crust. The thickness of the synextensional growth wedge (>5 km, Fig. 10G) is also indicative of the crustal-scale size of this structure. The contractional phase responsible for the overturned position of the Mesozoic series and the basal part of the submarine volcanic group probably took place in the late Oligocene, perhaps coincident with deposition of the transitional volcanic group, which lies unconformably above the submarine volcanic group. This contractional phase represented the end of the first stage of tectonic evolution of Fuerteventura, mostly accomplished while the zone was below the waters of the Atlantic Ocean.

Finally, the last units of the transitional volcanic group (Janey and Barranco de la Fuente Blanca Formations) represent shallow-water depositional and eruption environments, and predominantly NW paleocurrents, at high angles to the f_3 axial trace (Fig. 10F). The age of this upper part of the transitional volcanic group is probably early Miocene (Fig. 9) and coincides with a part of the syenite-carbonatite complex of Punta del Peñón Blanco. This complex intruded during an extensional episode characterized by WNW extension directions (Fernández et al., 1997). According to its structural and cartographic characteristics, Gutiérrez (2000) interpreted the f_3 fold as a large roll-over fold associated with WNW-ESE extension. The uplifted footwall should be located to the east of the present-day exposure of the basal complex. This can explain the paleocurrents in the Janey Formation (unit G4). The subsiding block was filled first with shallow-water sediments (Janey and Barranco de la Fuente Blanca Formations, units G4 and G5) and finally with a thick series of volcanic rocks (the subaerial volcanic group). During this stage, Fuerteventura emerged definitely from the waters of the Atlantic Ocean. This could be a consequence of magma production rate exceeding the subsidence rate or, alternatively, a result of renewed uplift of the complex due to isostatic

uplift linked to the extension (e.g., Wernicke, 1985), or of the influence of a thermally anomalous mantle. This phase corresponds to the inception of the second stage of tectonic evolution of the already emerged Fuerteventura Island.

Submarine Growth of Fuerteventura: Tectonic Controls on Emergence of an Intraplate Volcanic Island

The model of seamount growth by Staudigel and Schmincke (1984) (inset of Fig. 12) is based on the interpretation of the exposed submarine series at La Palma (western Canary Islands, Fig. 1). Its first stage of evolution consists of deep-water (1000–5000 m) volcanic facies on top of the sediment layer of the oceanic crust. Intrusion of dikes and sills caused deformation and doming of the unconsolidated sediments. Redepositional processes affected the sediments of the growing seamount, which was massively intruded by later sills. The second stage was characterized by explosive volcanic activity below intermediate-water and shoaling depths. Deposits were more vesicular than in the first stage, and debris-flow breccias were deposited on flanks and aprons of the seamount. The emergence stage was characterized by tuff cones and associated pyroclastic deposits. The transition to the island stage was marked by the emission of voluminous subaerial lava flows forming a resistant lava cap on the easily eroding pyroclasts.

Fuerteventura differs in many ways from this classical model. The initial submarine volcanic rocks resting over the Mesozoic sediments are highly vesicular, and emission depths could not have exceeded 700 m. Therefore, no signs of deep-water volcanic facies are found in Fuerteventura. The high proportions of clastic rocks and the virtual absence of sills of the submarine volcanic group are similar to the characteristics of the intermediate-water or shoaling stage of the classical model. The transitional volcanic group can be compared with the emergent stage. In Fuerteventura, the submarine volcanic rocks and their oceanic basement are tectonically tilted. The submarine volcanic group defines a progressive unconformity, and it can be considered as a syntectonic unit, related to the evolution of the hanging wall basin of a listric detachment. The transitional volcanic group onlaps the submarine volcanic rocks, and it probably marks the evolution from an extensional to a contractional and back to an extensional regime.

Based on our interpretations of the Fuerteventura submarine evolution, we propose an alternative model of submarine growth of volcanic islands (Fig. 12A–D). This model is not opposite but complementary to that of Staudigel and Schmincke (1984). In this new model, the

Gutiérrez et al.
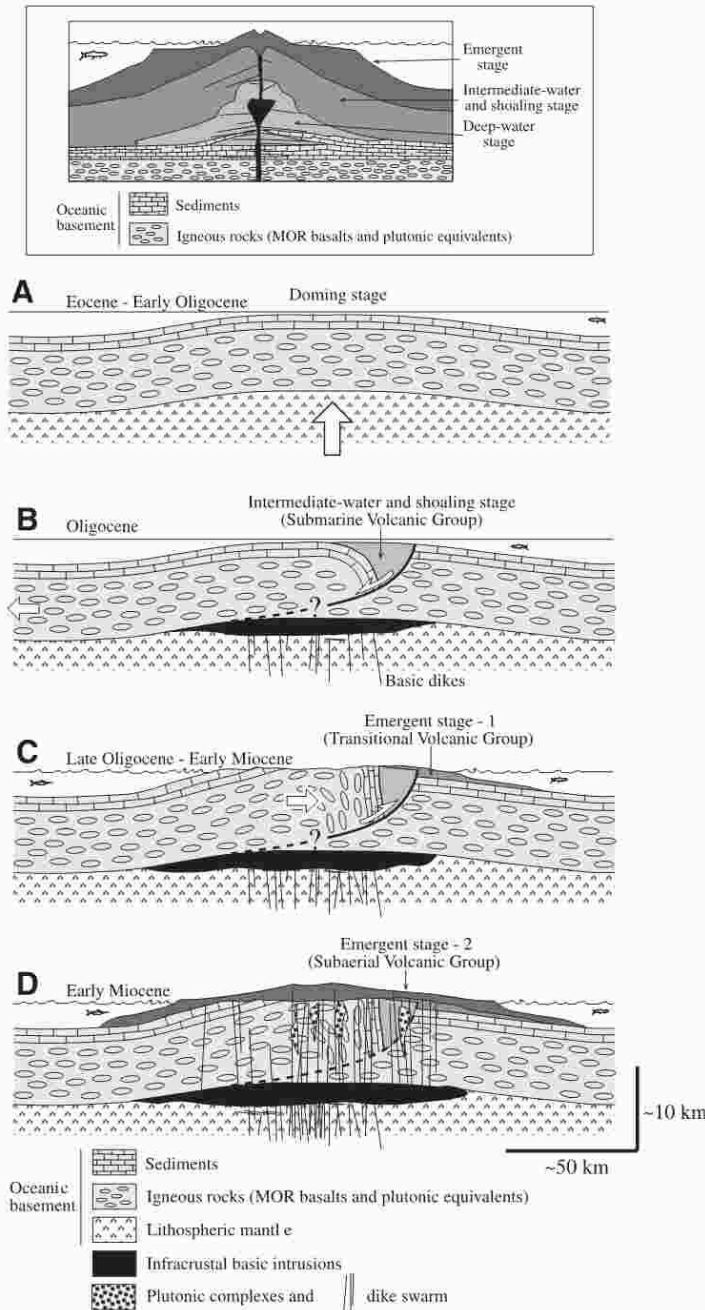
Figure 12. Top: Simplified sketch showing the model of evolution of a seamount growth of Staudigel and Schmincke (1984). Black represents intrusive rocks. See text for further explanation. (A–D) Model of submarine growth and emergence of volcanic islands in tectonically active settings, exemplified by the basal complex of Fuerteventura. Note the difference between the vertical and horizontal scales. (A) First stage: broad arching of the oceanic crust, probably caused by sublithospheric forces. (B) Second stage: collapse of the domal uplifted area by large extensional faults and generation of intermediate- and shallow-water submarine volcanic rocks in the hanging wall basins. (C) Third stage: inversion of the extensional detachments as reverse faults, triggering a transient emergence of the basin and its basement; generation of an onlapping transitional volcanic unit with subaerial and shallow-water facies. (D) Fourth stage: renewal of extensional displacements (orthogonal with respect to that of the second stage in Fuerteventura) with massive emission of predominantly subaerial lava flows; definitive emergence of the island. MOR—mid-ocean ridge.

155

tectonic evolution of the oceanic basement plays a fundamental role in the growth and emergence of the island. It is, therefore, more dynamic than the classical model, which considers a static ocean floor. The oceanic basement must be uplifted before the first stage of submarine volcanism. Uplifts of between 1500 m and 3500 m have been cited for the ocean crust at Fuerteventura (Watts, 1994; Martínez del Olmo and Buitrago Borrás, 2002), where the original water depth may have been greater than 2500 m (Martínez del Olmo and Buitrago Borrás, 2002). Given the intermediate-water volcanic facies of the submarine volcanic group, a broad doming of the ocean floor is assumed in this model for the early Oligocene (Fig. 12A), albeit the shape and extent of this uplifted area is unknown. During a second phase, the domal area locally collapsed, and a large extensional fault was generated. The volcanic activity was focused along this large structure, volcanic material filled the hanging wall basin of the fault (Fig. 12B). The shallow-water bathymetry of this basin experienced few changes during the second phase. However, more than 2 km of volcanic growth strata were deposited and progressively tilted in the basin due to the asymmetric subsidence and rotation of its floor. Inversion of the extensional fault during the late Oligocene triggered a first episode of transient, tectonic emergence of the basin. This represents the third phase of evolution, with deposition of pyroclastic and sedimentary rock series onlapping the previous submarine sequence (Fig. 12C). Renewed volcanic activity during the early Miocene was favored by a new extensional episode (fourth phase), the subaerial volcanic series (Fig. 12D), which unconformably covered the basin and its margins with voluminous lava flows. This stage heralded the growth of the Miocene large shield volcanoes (Ancochea et al., 1996) and the generation of a stable island.

The origin of the doming must have been located below the lithosphere, as the fate of an old oceanic lithosphere (of Toarcian age in Fuerteventura, according to Steiner et al., 1998) is to continuously subside (e.g., Stein and Stein, 1992). A mantle plume (e.g., Holik et al., 1991; Carracedo et al., 1998) or a large anomalous zone in the upper sublithospheric mantle (e.g., Hoernle et al., 1995) has been reported in the literature to account for the origin of the Canary Archipelago. These hypotheses and those considering the tectonic influence of the nearby Atlas region (e.g., Anguita and Hernán, 1975) can now be evaluated according to the results of our work. Convergence between the African and Eurasian plates began in the Late Cretaceous and continued until the present day with only minor modifications (e.g., Dewey et al., 1989).

A first contractional episode has been identified in the Atlas domain during the late Eocene (e.g., Brede et al., 1992). However, as shown by Frizon de Lamotte et al. (2000), the Oligocene to early Miocene Africa-Eurasia convergence was mainly absorbed across the ALKAPECA (Alborán, Kabylies, Peloritan, and Calabria) domain and the Iberian-Balearic margin. The Atlas system experienced the main contractional deformation phase late in the Miocene and more clearly during the Pleistocene and early Quaternary (Frizon de Lamotte et al., 2000). Therefore, the link between the Atlas tectonics and the early evolution of Fuerteventura seems weak. Also, the Anti-Atlas Mountains do not continue westward onto the African continental shelf (Dillon, 1974). The western Mediterranean region and the Atlas system have been considered as a diffuse plate boundary (Gómez et al., 1996) with very heterogeneous, heterochronous, and varied deformation. However, the West Saharan continental margin, next to the Canary Archipelago (Fig. 1), does not show any record of contractional deformation (Von Rad and Wissmann, 1982; Martínez del Olmo and Buitrago Borrás, 2002). Oligocene erosion, due to a global sea-level fall, was important along this margin, and especially in the northern coastal basin, nearby Fuerteventura (Ranke et al., 1982), where the doming could have intensified the effect of the eustatic regression. Therefore, the tectonic setting of the submarine and transitional volcanism in Fuerteventura was probably linked more to a regional sublithospheric cause than to the plate-tectonic evolution of the northwest African plate.

An alternative interpretation considers that emplacement of high-level plutonic complexes (ultra-alkaline complexes, Vega de Río Palmas complex, and gabbro-pyroxenite plutons) may have had some effect in lifting their envelope (e.g., Le Bas et al., 1986). Uplifts probably exceeding 1500 m and near-vertical dips of bedding seem too high of values to be attributed to emplacement of basic magmas alone, although collaboration of plutons in this uplift cannot be discarded. Most of these plutons occurred later and crosscut the submarine and transitional volcanic groups (e.g., the Vega de Río Palma complex, Figs. 2 and 9). Therefore, they cannot be responsible for the syntectonic tilting of the submarine series. Also, the subcylindrical style of the f_1 and f_2 folds seems at odds with the irregular geometry of the plutons.

Independent of the origin of the doming, this process and the subsequent tectonic phases provided the uplift necessary to bring the Mesozoic oceanic basement above sea level. Lithosphere doming followed by large-scale faulting and massive emission of volcanic rocks is a typical sequence of many rift settings in the continental lithosphere (mantle-activated rifts of Condie, 1982). The orthogonal arrangement of the two extensional episodes (Oligocene and Miocene) is remarkable. Furthermore, the Miocene extension involved WNW predominant stretching along with NNE subordinate extension (Fernández et al., 1997). Similar orthogonal arrangements of faults and joints have been described in the evolution of elongate continental intraplate basins subjected to successive cycles of uplifting and subsidence (Price and Cosgrove, 1990). In Fuerteventura, this evolution could be tentatively explained as due to the elongate geometry of the uplifted region. In fact, a broad crustal arching has been observed in the Conception Bank (Fig. 1), to the north of Fuerteventura (Martínez del Olmo and Buitrago Borrás, 2002). A recent gravity survey has shown the presence of a positive Bouguer anomaly coinciding with the exposure of the basal complex (González Montesinos, 2002). Interestingly, González Montesinos (2002) has modeled the anomaly as a high-density body that can be followed from the surface down to at least 15 km below sea level. This high-density body shows two main trends: NNE-SSW and WNW-ESE. The NNE-SSW trend extends along the western coast of Fuerteventura toward the north. The WNW-ESE trend coincides with the outcropping Mesozoic oceanic crust, in the area studied in this work, and it continues offshore the east and west coasts of Fuerteventura, reaching the boundaries of the surveyed area. The geometry and size of the WNW-ESE branch of the modeled body support the hypothesis of crustal or lithosphere scale for the main fault associated with the generation of the submarine volcanic complex. This branch is also outlined by a spur-like feature, localized by Acosta et al. (2003), which divides the northwest margin of Fuerteventura in two. The orthogonal arrangement of both trends of gravity anomalies coincides with the pattern and location of the superposed structures due to the two main deformation phases in Fuerteventura. Finally, the origin and importance of the intervening contractional episode are debatable. It is tempting to investigate the link between this contractional episode and the tectonics resulting from the Cenozoic convergence between Africa and Eurasia, although a local rather than regional origin is more likely, considering the low deformation intensity and the reduced areal extension shown by this episode.

CONCLUSIONS

The period of submarine growth and emergence of the intraplate island of Fuerteventura (Canary Islands) is recorded in three main lithostratigraphic units: the submarine volcanic

Gutiérrez *et al.*

group, the transitional volcanic group, and the subaerial volcanic group. The submarine volcanic group consists of more than 2 km of intermediate- to shallow-water primary volcanic facies, with abundant interlayered volcanogenic deposits. The different lithostratigraphic units of this group fill a syntectonic wedge-shaped basin. The oceanic basement (sediments and MORBs) forms the substratum of this basin. The margins of the basin are oriented WNW-ESE, the strike of paleocurrents is NNE-SSW, and the source region is located to the NNE. The transitional volcanic group marks a first stage of emergence of the SSW margin of the basin. Coastal and shallow-water sediments cover subaerial lavas and pyroclastic flows. During the last stages of deposition of the transitional volcanic group, the paleocurrents changed to WNW-ESE. Massive subaerial lava flows of the subaerial volcanic group lie indistinctly over the oceanic basement and the submarine and transitional groups. This episode marks the beginning of the formation of the main shield volcanoes of the island. The structural characteristics of these units show a complex pattern of superposed folding. The older folding stage (f_1) developed coeval with the deposition of the submarine volcanic group and the lower part of the transitional volcanic group. It is here interpreted that this fold was originally generated as a roll-over fold over a large listric extensional detachment with WNW-ESE strike. The syntectonic basin is considered as a hanging wall half-graben filled with the submarine group (growth strata). Inversion of the detachment as a reverse fault generated the local overturning of the oceanic basement, and it is responsible for the onlapping character of the transitional volcanic group. Late during the generation of the transitional volcanic group, the detachment became blocked, and a new WNW-ESE–directed extension affected the zone. Emission of huge volumes of lava flows (subaerial volcanic group) was associated with this deformation phase. A dense swarm of NNE-SSW–oriented basic dikes traversed the crust in response to this deformation stage, acting as feeders of the subaerial lava flows. Generation of a new roll-over (f_2) fold took place, causing deformation of the pretectonic and syntectonic sequences and development of complex folding interference patterns. The image resulting from the study of the Fuerteventura basal complex is quite different to that of the classical model of seamount growth. We suggest that some intraplate oceanic islands can evolve under tectonically active settings, similar to that of continental rifting scenarios. A possible mechanism is the multistage collapse of a broad uplift of the oceanic basement associated with the presence of a large zone of anomalous sublithospheric mantle.

REFERENCES CITED

Ablay, G.J., Carroll, M.R., Palmer, M.R., Martí, J., and Sparks, R.S.J., 1998, Basanite-phonolite lineages of the Teide-Pico Viejo volcanic complex, Tenerife, Canary Islands: Journal of Petrology, v. 39, no. 5, p. 905–936, doi: 10.1093/petrology/39.5.905.

Acosta, J., Uchupi, E., Muñoz, A., Herranz, P., Palomo, C., Ballesteros, M., and ZEE Working Group, 2003, Geologic evolution of the Canarian Islands of Lanzarote, Fuerteventura, Gran Canaria and La Gomera and comparison of landslides at these islands with those at Tenerife, La Palma and El Hierro: Marine Geophysical Researches, v. 24, p. 1–40, doi: 10.1007/s11001-004-1513-3.

Ahijado, A., 1999, Las intrusiones plutónicas e hipoabisales del sector meridional del complejo basal de Fuerteventura [Ph.D. thesis]: Madrid, Universidad Complutense de Madrid, 392 p.

Ahijado, A., Casillas, R., and Hernández-Pacheco, A., 2001, The dike swarms of the Amanay Massif, Fuerteventura, Canary Islands: Journal of Asian Earth Sciences, v. 19, p. 333–345, doi: 10.1016/S1367-9120(99)00066-8.

Alves, T.M., Cunha, T., Bouriak, S., Volkonskaya, A., Monteiro, J.H., and Ivanov, M., 2004, Surveying the flanks of the Mid-Atlantic Ridge: The Atlantis Basin, North Atlantic Ocean (36°N): Marine Geology, v. 209, p. 199–222, doi: 10.1016/j.margeo.2004.06.002.

Ancochea, E., Brändle, J.L., Cubas, C.R., Hernán, F., and Huertas, M.J., 1993, La Serie I de la Isla de Fuerteventura: Memorias de la Real Academia de Ciencias Exactas, Físicas y Naturales, v. 27, 151 p.

Ancochea, E., Brändle, J.L., Cubas, C.R., Hernán, F., and Huertas, M.J., 1996, Volcanic complexes in the eastern ridge of the Canary Islands: The Miocene activity of the island of Fuerteventura: Journal of Volcanology and Geothermal Research, v. 70, p. 183–204, doi: 10.1016/0377-0273(95)00051-8.

Anguita, F., and Hernán, F., 1975, A propagating fracture model versus a hotspot origin for the Canary Islands: Earth and Planetary Science Letters, v. 27, p. 11–19, doi: 10.1016/0012-821X(75)90155-7.

Araña, V., and Ortiz, R., 1991, The Canary Islands: Tectonics, magmatism and geodynamic framework, *in* Kampunzu, A.B., and Lubala, R.T., eds., Magmatism in extensional structural settings: The Phanerozoic African plate: New York, Springer, p. 209–249.

Balcells, R., Barrera, J.L., Gómez, J.A., Cueto, L.A., Ancochea, E., Huertas, M.J., Ibarrola, E., and Snelling, N., 1994, Edades radiométricas de los edificios Miocenos de Fuerteventura (Islas Canarias): Boletín Geológico y Minero, v. 105, no. 1, p. 50–56.

Balogh, K., Ahijado, A., Casillas, R., and Fernández, C., 1999, Contributions to the chronology of the basal complex of Fuerteventura, Canary Islands: Journal of Volcanology and Geothermal Research, v. 90, p. 81–102, doi: 10.1016/S0377-0273(99)00008-6.

Banda, E., Dañobeitia, J.J., Suriñach, E., and Ansorge, J., 1981, Features of crustal structure under the Canary Islands: Earth and Planetary Science Letters, v. 55, p. 11–24, doi: 10.1016/0012-821X(81)90082-0.

Batiza, R., Fornari, D.J., Vanko, D.A., and Lonsdale, P., 1984, Craters, calderas and hyaloclastites on young Pacific seamounts: Journal of Geophysical Research, v. 89, p. 8371–8390.

Binard, N., Hekinian, R., Cheminee, J.L., and Stoffers, P., 1992, Styles of eruptive activity on intraplate volcanoes in the Society and Austral hot-spot regions—Bathymetry, petrology, and submersible observations: Journal of Geophysical Research, v. 97, p. 13,999–14,015.

Brändle, J.L., 1973, Evolución geoquímica de los materiales volcánicos sálicos y alcalinos de la Isla de Tenerife: Estudios Geológicos, v. 29, p. 5–51.

Brede, R., Hauptmann, M., and Herbig, H.G., 1992, Plate tectonics and intracratonic mountain ranges in Morocco: The Mesozoic-Cenozoic development of the Central High Atlas and the Middle Atlas: Geologische Rundschau, v. 81, p. 127–141, doi: 10.1007/BF01764544.

Bull, J.M., Minshull, T.A., Mitchell, N.C., Thors, K., Dix, J.K., and Best, A.I., 2003, Fault and magmatic interaction within Iceland's western rift over the last 9 kyr: Geophysical Journal International, v. 154, p. F1–F8, doi: 10.1046/j.1365-246X.2003.01990.x.

Cantagrel, J.M., Fúster, J.M., Pin, C., Renaud, U., and Ibarrola, E., 1993, Age Miocène inférieur des carbonatites de Fuerteventura: Compte Rendues de l'Academie de Sciences de Paris, v. 316, p. 1147–1153.

Carracedo, J.C., Day, S., Guillou, H., Rodríguez, E., Canas, J.A., and Pérez, F.J., 1998, Hotspot volcanism close to a passive continental margin: Geological Magazine, v. 135, p. 591–604, doi: 10.1017/S0016756898001447.

Casillas, R., Ahijado, A., and Hernández-Pacheco, A., 1994, Zonas de cizalla dúctil en el complejo basal de Fuerteventura: Geogaceta, v. 15, p. 117–120.

Cendrero, A., 1966, Los volcanes recientes de Fuerteventura (Islas Canarias): Estudios Geológicos, v. 22, p. 201–226.

Coello, J., Cantagrel, J.M., Hernán, F., Fúster, J.M., Ibarrola, E., Ancochea, E., Casquet, C., Jamond, J.R., and Cendrero, A., 1992, Evolution of the eastern volcanic ridge of the Canary Islands based on new K-Ar data: Journal of Volcanology and Geothermal Research, v. 53, p. 251–274.

Condie, K.C., 1982, Plate tectonics and continental drift: Elmsford, New York, Pergamon Press, 310 p.

Cotton, C.A., 1969, The pedestals of oceanic islands: Geological Society of America Bulletin, v. 80, p. 749–760.

Craig, H., 1983, Loihi seamount—Collected papers—Introduction: Earth and Planetary Science Letters, v. 66, no. 1–3, p. 334–336, doi: 10.1016/0012-821X(83)90149-8.

Dañobeitia, J.J., and Canales, J.O., 2000, Magmatic underplating in the Canary Archipelago: Journal of Volcanology and Geothermal Research, v. 103, p. 27–41, doi: 10.1016/S0377-0273(00)00214-6.

Demény, A., Vennemann, T.W., Hegner, E., Ahijado, A., Casillas, R., Nagy, G., Homonnay, Z., Gutierrez, M., and Szabo, C., 2004, H, O, Sr, Nd and Pb isotopic evidence for recycled oceanic crust in the transitional volcanic group of Fuerteventura, Canary Islands. Spain: Chemical Geology, v. 205, p. 37–54.

Dewey, J.F., Helman, M.L., Turco, E., Hutton, D.H.W., and Knott, S.D., 1989, Kinematics of the western Mediterranean, *in* Coward, M.P., Dietrich, D., and Park, R.G., eds., Alpine tectonics: Geological Society [London] Special Publication 45, p. 265–283.

Dillon, W.P., 1974, Structure and development of the southern Moroccan continental shelf: Marine Geology, v. 16, p. 121–143, doi: 10.1016/0025-3227(74)90004-8.

Fernández, C., Casillas, R., Ahijado, A., Perelló, V., and Hernández-Pacheco, A., 1997, Shear zones as result of intraplate tectonics in oceanic crust: An example of the basal complex of Fuerteventura (Canary Islands): Journal of Structural Geology, v. 19, p. 41–57, doi: 10.1016/S0191-8141(96)00074-0.

Feraud, G., 1981, Datation de reseaux de dykes et de roches volcaniques sous-marines par les méthodes K-Ar et ⁴⁰Ar-³⁹Ar: Utilisation des dykes comme marqueurs de paleocontraintes [Ph.D. thesis]: Nice, Université de Nice, 130 p.

Feraud, G., Giannérini, G., Campredon, R., and Stillman, C.J., 1985, Geochronology of some Canarian dike swarms: Contribution to the volcano-tectonic evolution of the archipelago: Journal of Volcanology

157

Tectonic model of submarine growth and emersion of volcanic islands

and Geothermal Research, v. 25, p. 29–52, doi: 10.1016/0377-0273(85)90003-4.

Fornari, D.J., Malahoff, A., and Heezen, B.C., 1978, Volcanic structure of the crest of the Puna Ridge, Hawaii: Geophysical implications of submarine volcanic terrain: Geological Society of America Bulletin, v. 89, p. 605–616, doi: 10.1130/0016-7606(1978)89<605: VSOTCO>2.0.CO;2.

Frizon de Lamotte, D., Saint Bezar, B., and Bracène, R., 2000, The two main steps of the Atlas building and geodynamics of the western Mediterranean: Tectonics, v. 19, p. 740–761, doi: 10.1029/2000TC900003.

Furnes, H., and Fridleifsson, I.B., 1974, Tidal effects on the formation of pillow lava/ hyaloclastite deltas: Geology, v. 2, no. 8, p. 381–384.

Fúster, J.M., Cendrero, A., Gastesi, P., Ibarrola, E., and Lopez Ruiz, J., 1968, Geología y volcanología de las Islas Canarias, Fuerteventura: Madrid, Instituto "Lucas Mallada," Consejo Superior de Investigaciones Científicas, 239 p.

Fúster, J.M., Muñoz, M., Sagredo, J., Yébenes, A., Bravo, T., and Hernández-Pacheco, A., 1980, Excursión n° 121 A + c del 26° I.G.C. a las Islas Canarias: Boletín del Instituto Geológico y Minero de España, v. 92, p. 351–390.

Fúster, J.M., Barrera, J.L., Muñoz, M., Sagredo, J., and Yébenes, A., 1984a, Mapa y memoria explicativa de la hoja de Pájara (1106 IV) del Mapa Geológico Nacional: Madrid, Instituto Geológico y Minero de España, scale 1:25,000, 1 sheet.

Fúster, J.M., Yébenes, A., Barrera, J.L., Muñoz, M., and Sagredo, J., 1984b, Mapa y memoria explicativa de la hoja de Betancuria (1106 II) del Mapa Geológico Nacional: Madrid, Instituto Geológico y Minero de España, scale 1:25,000, 1 sheet.

Gastesi, P., 1969, Petrology of the ultramafic and basic rocks of Betancuria massif, Fuerteventura Island (Canarian Archipelago): Bulletin of Volcanology, v. 33, p. 1008–1038.

Gee, J., and Staudigel, H., 1988, Geological and geochemical evolution of Jasper Seamount (abs.): Eos (Transactions, American Geophysical Union), v. 69, p. 1503.

Gee, J., Staudigel, H., and Natland, J.H., 1991, Geology and petrology of Jasper Seamount: Journal of Geophysical Research, v. 96, p. 4083–4105.

Gee, M.J.R., Watts, A.B., Masson, D.G., and Mitchell, N.C., 2001, Landslides and the evolution of El Hierro in the Canary Islands: Marine Geology, v. 177, p. 271–293, doi: 10.1016/S0025-3227(01)00153-0.

Gómez, F., Barazangi, M., and Bensaid, M., 1996, Active tectonism in the intracontinental Middle Atlas Mountains of Morocco: Simultaneous crustal shortening and extension: Journal of the Geological Society of London, v. 153, p. 389–402.

González Montesinos, F., 2002, Inversión gravimétrica 3D por técnicas de evolución: Aplicación a la isla de Fuerteventura: Puerto del Rosario, Cabildo de Fuerteventura, Servicio de Publicaciones, 209 p.

Gutiérrez, M., 2000, Estudio petrológico, geoquímico y estructural de la serie volcánica submarina del complejo basal de Fuerteventura (Islas Canarias): Caracterización del crecimiento submarino y de la emersión de la isla [Ph.D. thesis]: La Laguna, Universidad de La Laguna, 533 p.

Gutiérrez, M., Casillas, R., Fernández, C., Balogh, K., Ahijado, A., and Castillo, C., 2002, La serie volcánica submarina del complejo basal de Fuerteventura: Crecimiento submarino y emersion de la isla: Geogaceta, v. 32, p. 57–60.

Hardy, S., and Poblet, J., 1994, Geometric and numerical model of progressive limb rotation in detachment folds: Geology, v. 22, p. 371–374, doi: 10.1130/0091-7613(1994)022<0371:GANMOP>2.3.CO;2.

Hardy, S., Poblet, J., McClay, K., and Waltham, D., 1996, Mathematical modelling of growth strata associated with fault-related fold structures, *in* Buchanan, P.G., and Nieuwland, D.A., eds., Modern developments in structural interpretation, validation and modelling: Geological Society [London] Special Publication 99, p. 265–282.

Hernán, F., Cubas, C.R., Ancochea, E., Bründle, J.L., and Huertas, M.J., 1996, Características composicionales y procesos de evolución magmática en el complejo volcánico sur-III de Fuerteventura (Islas Canarias): Geogaceta, v. 20, no. 3, p. 550–553.

Hildebrand, J.A., Dorman, L.M., Hammer, P.T.C., Schreiner, A.E., and Corneuille, B.D., 1989, Seismic tomography of Jasper Seamount: Geophysical Research Letters, v. 16, p. 1355–1358.

Hobson, A., Bussy, F., and Hernández, J., 1998, Shallow-level migmatization of gabbros in a metamorphic contact aureole, Fuerteventura basal complex, Canary Islands: Journal of Petrology, v. 39, p. 1025–1037, doi: 10.1093/petrology/39.5.1025.

Hoernle, K.A.J., and Schmincke, H.U., 1993a, The petrology of tholeiites trough melilite nephelinites on Gran Canaria, Canary Islands: Crystal fractionation, accumulation and depths of melting: Journal of Petrology, v. 34, p. 573–597.

Hoernle, K.A.J., and Schmincke, H.U., 1993b, The role of partial melting in the 15 Ma geochemical evolution of Gran Canaria: A blob model for Canary hotspot: Journal of Petrology, v. 34, p. 599–626.

Hoernle, K.A.J., Zhang, Y.S., and Graham, D., 1995, Seismic and geochemical evidence for large-scale mantle upwelling beneath the eastern Atlantic and western and central Europe: Nature, v. 374, p. 34–39, doi: 10.1038/374034a0.

Holik, J.S., Rabinowitz, P.D., and Austin, J.A., 1991, Effects of Canary hot spot volcanism on structure of oceanic crust off Morocco: Journal of Geophysical Research, v. 96, p. 12,039–12,067.

Ibarrola, E., Fúster, J.M., and Cantagrel, J.M., 1989, Edades K-Ar de las rocas volcánicas submarinas del sector norte del complejo basal de Fuerteventura, *in* Proceedings, European Science Foundation Meeting on Canarian Volcanism, Lanzarote, p. 124–128.

Jones, J.G., 1969a, Intraglacial volcanoes of the Langarvatn region, south-west Iceland. I.Q.J.: Journal of the Geological Society of London, v. 124, p. 197–211.

Jones, J.G., 1969b, Pillow lavas as depth indicators: American Journal of Science, v. 267, p. 181–195.

Jones, J.G., and Nelson, P.H., 1970, The flow of basalt lava from air into water—Its structural expression and stratigraphic significance: Geological Magazine, v. 107, no. 1, p. 13–16.

Karson, J.A., 1998, Internal structure of oceanic lithosphere: A perspective from tectonic windows, *in* Buck, W.R., Delaney, P.T., Karson, J.A., and Lagabrielle, Y., eds., Faulting and magmatism at mid-ocean ridges: Washington, D.C., American Geophysical Union Geophysical Monograph 106, p. 177–218.

Le Bas, M.J., Rex, D.C., and Stillman, C.J., 1986, The early magmatic chronology of Fuerteventura: Geological Magazine, v. 123, p. 287–298.

Le Maitre, R.W., Bateman, P., Dudek, A., Keller, J., Le Bas, M.J., Sabine, P.A., Schmid, R., Sørensen, H., Streckeisen, A., Wooley, A.R., and Zanettin, B., 1989, A classification of igneous rocks and glossary of terms: Oxford, Blackwell Scientific Publications, 193 p.

López Ruiz, L., 1970, Estudio petrográfico y geoquímico del complejo filoniano de Fuerteventura (Islas Canarias): Estudios Geológicos, v. 26, p. 173–208.

MacLeod, C.J., Escartín, J., Banerji, D., Banks, G.J., Gleeson, M., Irving, D.H.B., Lilly, R.M., McCaig, A.M., Niu, Y., Allerton, S., and Smith, D.K., 2002, Direct geological evidence for oceanic detachment faulting: The Mid-Atlantic Ridge, 15°45'N: Geology, v. 30, p. 879–882, doi: 10.1130/0091-7613(2002)030<0879: DGEFOD>2.0.CO;2.

Mardia, K.V., 1972, Statistics of directional data: London, Academic Press, 357 p.

Martínez del Olmo, W., and Buitrago Borrás, J., 2002, Sedimentación y volcanismo al este de las islas de Fuerteventura y Lanzarote (Surco de Fúster Casas): Geogaceta, v. 32, p. 51–54.

Martín González, C., Castillo, C., Gutiérrez González, M., and Aguirre, J., 2001, Estudio paleoambiental de los depósitos litorales someros del Plioceno inferior de Fuerteventura (Islas Canarias): Revista Española de Paleontología, v. 16 (número extraordinario), p. 47–57.

McClay, K., Muñoz, J.A., and García-Senz, J., 2004, Extensional salt tectonics in a contractional orogen: A newly identified tectonic event in the Spanish Pyrenees: Geology, v. 32, p. 737–740, doi: 10.1130/G20565.1.

McPherson, G.J., 1983, The Snow Mountain volcanic complex: An on land seamount in the Franciscan terrain, California: The Journal of Geology, v. 91, p. 73–92.

McPhie, J., 1995, A Pliocene shoaling basaltic seamount: Ba volcanic group at Rakiraki, Fiji: Journal of Volcanology and Geothermal Research, v. 64, p. 193–210, doi: 10.1016/0377-0273(94)00050-Q.

McPhie, J., Doyle, M., and Allen, R., 1993, Volcanic textures: A guide to the interpretation of textures in volcanic rocks: Hobart, Centre for Ore Deposit and Exploration Studies, University of Tasmania, Tasmanian Government Printing Office, 198 p.

Meco, J., and Pomel, R.S., 1985, Les formations marines et continentales intervolcaniques des Iles Canaries Orientales (Grande Canarie, Fuerteventura et Lanzarote): Stratigraphie et signification paleoclimatique: Estudios Geológicos, v. 41, p. 223–227.

Meco, J., Petit-Maire, N., Fontugne, M., Shimmield, G., and Ramos, A.J., 1997, The Quaternary deposits in Lanzarote and Fuerteventura (Eastern Canary Islands, Spain): An overview, *in* Meco, J., and Petit-Maire, N., eds., Climates of the past: Proceedings Clip Meeting, Lanzarote and Fuerteventura: Las Palmas, University of Las Palmas de Gran Canaria, p. 123–136.

Meco, J., Guillou, H., Carracedo, J.C., Lomoschitz, A., Ramos, A.J.G., and Rodríguez-Yánez, J.J., 2002, The maximum warmings of the Pleistocene world climate recorded in the Canary Islands: Palaeogeography, Palaeoclimatology, Palaeoecology, v. 185, p. 197–210, doi: 10.1016/S0031-0182(02)00300-0.

Mitchell, N.C., Tivey, M.A., and Gente, P., 2000, Slopes of mid-ocean ridge fault scarps from submersible observations: Earth and Planetary Science Letters, v. 183, p. 543–555, doi: 10.1016/S0012-821X(00)00270-3.

Moore, J.G., and Fiske, R.S., 1969, Volcanic substructure inferred from dredge samples and ocean-bottom photographs, Hawaii: Geological Society of America Bulletin, v. 80, p. 1191–1202.

Moore, J.G., Clague, D.A., and Normark, W.R., 1982, Diverse basalt types from Loihi seamount, Hawaii: Geology, v. 10, p. 88–92, doi: 10.1130/0091-7613(1982)10<88: DBTFLS>2.0.CO;2.

Morgan, W.J., 1971, Convection plumes in the lower mantle: Nature, v. 230, p. 42–43, doi: 10.1038/230042a0.

Muñoz, M., and Sagredo, J., 1994, Reajustes mineralógicos y geoquímicos producidos durante el metamorfismo de contacto de diques basálticos (Fuerteventura, Islas Canarias): Boletín de la Sociedad Española de Mineralogía, v. 17, p. 86–87.

Muñoz, M., Sagredo, J., Rincón-Calero, P.J., and Vegas, R., 1997, Emplazamiento en una zona de cizalla ductil-frágil transtensiva para el plutón de Pájara, Fuerteventura: Islas Canarias: Geogaceta, v. 21, p. 171–174.

North American Commission on Stratigraphic Nomenclature, 1983, North American Stratigraphic Code: American Association of Petroleum Geologists Bulletin, v. 67, p. 841–875.

Palmason, G., 1980, A continuum model of crustal generation in Iceland: Kinematic aspects: Journal of Geophysics, v. 47, p. 7–18.

Price, N.J., and Cosgrove, J.W., 1990, Analysis of geological structures: New York, Cambridge University Press, 502 p.

Ramsay, J.G., 1967, Folding and fracturing of rocks: New York, McGraw-Hill, 568 p.

Ranke, U., von Rad, U., and Wissmann, G., 1982, Stratigraphy, facies and tectonic development of the on- and offshore Aaiun-Tarfaya basin: A review, *in* Von Rad, U., Hinz, K., Sarnthein, M., and Seibold, E., eds., Geology of the northwest African continental margin: Berlin, Springer, p. 86–105.

Roberts, A., and Yielding, G., 1994, Continental extensional tectonics, *in* Hancock, P.L., ed., Continental deformation: Oxford, Pergamon Press, p. 223–250.

Robertson, A.H.F., and Stillman, C.J., 1979a, Late Mesozoic sedimentary rocks of Fuerteventura, Canary Islands: Implications for West Africa continental margin evolution: Journal of the Geological Society of London, v. 36, p. 47–60.

Robertson, A.H.F., and Stillman, C.J., 1979b, Submarine volcanic and associated sedimentary rocks of the Fuerteventura basal complex, Canary Islands: Geological Magazine, v. 116, p. 203–214.

Sagredo, J., Muñoz, M., and Galindo, C., 1996, Características petrológicas y edad K-Ar de las sienitas nefelínicas del Morro del Recogedero (Fuerteventura, Islas Canarias): Geogaceta, v. 20, p. 506–509.

158

Gutiérrez et al.

Sánchez-Guzmán, J., and Abad, J., 1986, Sondeo geotérmico Lanzarote-1: Significado geológico y geotérmico: Anales de Física, serie B, v. 82, p. 102–109.

Schmincke, H.-U., 1990, Gran Canaria: Geological field guide: Witten, Pluto Press, 212 p.

Schmincke, H.-U., and Segschneider, B., 1998, Shallow submarine to emergent basaltic shield volcanism of Gran Canaria: Evidence from drilling into the volcanic apron, *in* Weaver, P.P.E., Schmincke, H.-U., Firth, J.V., and Duffield, W., Proceedings of the Ocean Drilling Program, Scientific Results, Volume 157: College Station, Texas, Ocean Drilling Program, p. 141–181.

Smith, D.K., Kong, L.S.L., Johnson, K.T.M., and Reynolds, J.R., 2002, Volcanic morphology of the submarine Puna Ridge, Kilauea volcano, *in* Takahashi, E., Lipman, P.W., Garcia, M.J., Naka, J., and Aramaki, S., eds., Hawaiian volcanoes, deep underwater perspectives: Washington, D.C., American Geophysical Union Geophysical Monograph 128, p. 125–142.

Staudigel, H., and Schmincke, H.-U., 1984, The Pliocene seamount series of La Palma, Canary Islands: Journal of Geophysical Research, v. 89, p. 11,195–11,215.

Stein, C.A., and Stein, S., 1992, A model for the global variation in oceanic depth and heat flow with lithospheric age: Nature, v. 359, p. 123–129, doi: 10.1038/359123a0.

Steiner, C., Hobson, A., Favre, P., and Stampli, G.M., 1998, Early Jurassic sea-floor spreading in the central Atlantic—The Jurassic sequence of Fuerteventura (Canary Islands): Geological Society of America Bulletin, v. 110, p. 1304–1317, doi: 10.1130/0016-7606(1998)110<1304:MSOFCI>2.3.CO;2.

Stillman, C.J., 1987, A Canary Islands dyke swarm: Implications for the formation of oceanic islands by extensional fissural volcanism, *in* Halls, H.C., and Fahrig, W.F., eds., Mafic dyke swarms: Geological Association of Canada Special Paper 34, p. 243–255.

Stillman, C.J., 1999, Giant Miocene landslides and the evolution of Fuerteventura, Canary Islands: Journal of Volcanology and Geothermal Research, v. 94, p. 89–104, doi: 10.1016/S0377-0273(99)00099-2.

Stillman, C.J., and Robertson, A.H.F., 1977, The dyke swarm of the Fuerteventura basal complex, Canary Islands [abs.]: Geological Society of London Newsletter, v. 6, p. 8.

Stillman, C.J., Fuster, J.M., Bennell-Baker, M.J., Muñoz, M., Smewing, J.D., and Sagredo, J., 1975, Basal complex of Fuerteventura (Canary Islands) is an oceanic intrusive complex with rift-system affinities: Nature, v. 257, p. 469–471, doi: 10.1038/257469a0.

Von Rad, U., and Wissmann, G., 1982, Cretaceous-Cenozoic history of the West Saharan continental margin (NW Africa): Development, destruction and gravitational sedimentation, *in* Von Rad, U., Hinz, K., Sarnthein, M., and Seibold, E., eds., Geology of the northwest African continental margin: Berlin, Springer, p. 106–131.

Wagner, C., Mokhtari, A., Deloule, E., and Chabaux, F., 2003, Carbonatite and alkaline magmatism in Taourirt (Morocco): Petrological, geochemical and Sr-Nd isotope characteristics: Journal of Petrology, v. 44, no. 5, p. 937–965, doi: 10.1093/petrology/44.5.937.

Watts, A.B., 1994, Crustal structure, gravity anomalies and flexure of the lithosphere in the vicinity of the Canary Islands: Geophysical Journal, v. 119, p. 648–666.

Wernicke, B., 1985, Uniform normal-sense simple shear of the continental lithosphere: Canadian Journal of Earth Sciences, v. 22, p. 108–125.

Winchester, J.A., and Floyd, P.A., 1977, Geochemical discrimination of different magma series and their differentiation products using immobile elements: Chemical Geology, v. 20, p. 325–343, doi: 10.1016/0009-2541(77)90057-2.

Wright, I.C., 1996, Volcaniclastic processes on modern submarine arc stratovolcanoes: Sidescan and photographic evidence from the Rumble IV and V volcanoes, southern Kermadec Arc (SW Pacific): Marine Geology, v. 136, p. 21–39, doi: 10.1016/S0025-3227(96)00054-0.

159

Miocene rifting of Fuerteventura (Canary Islands)

Carlos Fernández,[1] Ramón Casillas,[2] Encarnación García Navarro,[1] Margarita Gutiérrez,[3] Manuel A. Camacho,[1] and Agustina Ahijado[2]

[1]   The older geological units of the volcanic island of Fuerteventura (Canary Islands), i.e., the so-called basal complex and the lower part of the subaerial volcanic rocks, show abundant structures indicative of a long-lived period of Miocene tectonic activity. These structures include faults, dike swarms, kilometer-scale folds, tilted sequences, and fissural and central volcanic edifices. A detailed structural study, based on geological mapping and the use of fault slip inversion techniques and statistical analysis of dike orientation, has allowed the identification of three separated Miocene deformation phases: M-D$_1$, M-D$_2$, and M-D$_3$. The average extension directions determined for these phases are NW-SE, NNE-SSW, and ENE-WSW, respectively. A model of oceanic lithosphere rifting is proposed to account for this deformation history. A buoyant, anomalous sublithosphere mantle triggered the extension in the lithosphere beneath Fuerteventura, isolating it during the early and middle Miocene from the plate-scale collision regime predominant in the NW corner of the African plate. **Citation:** Fernández, C., R. Casillas, E. García Navarro, M. Gutiérrez, M. A. Camacho, and A. Ahijado (2006), Miocene rifting of Fuerteventura (Canary Islands), *Tectonics, 25,* TC6005, doi:10.1029/2005TC001941.

1. Introduction

[2]   Volcanic edifices in oceanic intraplate islands have been extensively studied during the last decades due to both academic and economic interests. Volcanic islands mostly lie above hot spots and their analysis is essential to test alternative models on how the lithosphere and the sublithosphere mantle contribute to the kinematics and dynamics of plates [e.g., *Foulger et al.*, 2005]. Active volcanoes are highly dynamical structures with intervening episodes of growth and structural failure [e.g., *McGuire et al.*, 1996]. Understanding this complex evolution is the best tool for risk mitigation and to guarantee safety of populations. Modern research is focused in the study of the relationships between regional and local stress fields, and geometrical, kinematic and rheological evolution of volcanic edifices and their substratum. Methodology includes numerical and analogue modeling [e.g., *van Wyk de Vries and Matela*, 1998; *Cecchi et al.*, 2005] and field studies [e.g., *van Wyk de Vries et al.*, 2001]. A considerable effort has been recently devoted to the analysis of the role of regional tectonics on the evolution of oceanic islands. Apart from the cases of obvious association of oceanic volcanoes with diverging plate boundaries (Iceland, Azores) [e.g., *Searle*, 1980; *Bull et al.*, 2003], a lively debate is going on about the origin of oceanic intraplate islands and island chains as a result of plume- or nonplume-related magmatism (interesting material on this topic can be found at http://www.mantleplumes.org/). Unfortunately, very few works have addressed the problem of analyzing deformation structures in a regionally stressed shield-volcano substratum. This is the main goal of this contribution, devoted to the study of the structures associated with the growth of the large Miocene shield volcanoes in the Fuerteventura Island (Canary Archipelago).

[3]   The Canary Islands are a volcanic archipelago located at the eastern Atlantic Ocean, not far from the NW Africa coast. Several hypotheses concerning the origin of the Canary Islands have been presented. These include the mantle plume hypothesis [*Morgan*, 1971; *Holik et al.*, 1991; *Hoernle and Schmincke*, 1993; *Hoernle et al.*, 1995; *Carracedo et al.*, 1998], the propagating fracture hypothesis [*Anguita and Hernán*, 1975], the local extensional ridge [*Fúster*, 1975], and the uplifted tectonic blocks [*Araña and Ortiz*, 1991]. Unfortunately, most of these models have been elaborated with a scarce knowledge of the main structural features and tectonic evolution of the archipelago. This lack of structural information is especially important for the lower units that, in the Fuerteventura Island, include the uplifted oceanic crust, the rocks of the submarine stage of growth, and the plutonic roots of the subaerial volcanic successions. Significant advances have been made in the last years, and an increasing number of structural data have been gathered in the distinct islands of the archipelago [e.g., *Casillas et al.*, 1994; *Marinoni and Pasquarè*, 1994; *Fernández et al.*, 1997; *Marinoni and Gudmundsson*, 2000; *Fernández et al.*, 2002]. The structural evolution of the Lanzarote Island (Figure 1, inset) has been polyphasic, as shown by *Marinoni and Pasquarè* [1994] for the posterosional evolution stage of that island. *Marinoni and Pasquarè* [1994] recognized at least two recent (<6 Ma) deformation phases that generated predominantly strike-slip faults, a tectonic regime that fits the predictions of numerical models for the northwestern African plate [*Jiménez-Munt and Negredo*, 2003]. Ductile-

[1]Departamento de Geodinámica y Paleontología, Universidad de Huelva, Huelva, Spain.
[2]Departamento de Edafología y Geología, Universidad de La Laguna, La Laguna, Tenerife, Canary Islands, Spain.
[3]Estudios del Terreno S.L., Santa Úrsula, Santa Cruz de Tenerife, Canary Islands, Spain.
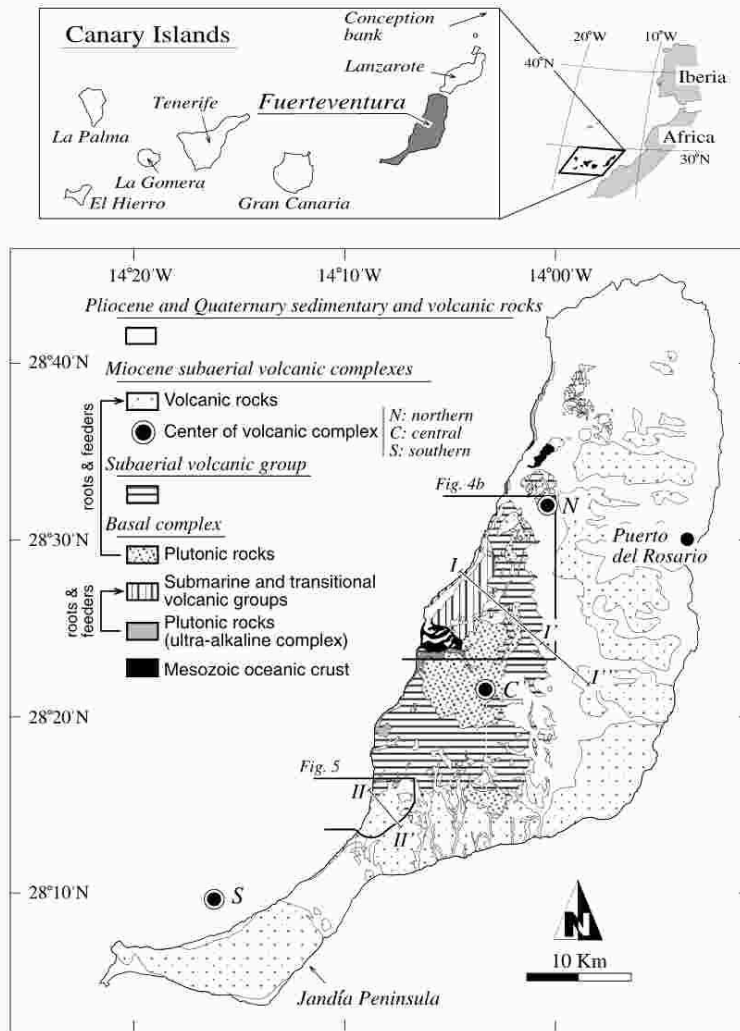
Figure 1. Location of the Fuerteventura Island in the Canary Archipelago and simplified geological map of the island. Modified from *Ancochea et al.* [1993]. The outlined areas correspond to the regions mapped in detail and shown in Figures 4b and 5. Cross sections I-I'-I" and II-II' are also shown. S, C and N refer to the centers of the large volcanoes described by *Ancochea et al.* [1993].

brittle shear zones have been described in Fuerteventura [*Casillas et al.*, 1994; *Fernández et al.*, 1997]. These shear zones generated during an old extensional episode (~25 Ma), contemporary with the transition from submarine to subaerial growth of Fuerteventura [*Gutiérrez et al.*, 2006]. Polyphase brittle deformations have also been described for the shield-building stage of Tenerife (<8 to >3 Ma) [*Marinoni and Gudmundsson*, 2000] and La Palma (<2 Ma) [*Fernández et al.*, 2002]. However, the structural information is scarce and irregularly distributed

across the archipelago, and much more work remains to be done in this field. These data are fundamental to any comprehensive model attempting to explain the origin of the Canary Islands.

[4] New information concerning the Miocene tectonic evolution of the Fuerteventura Island is presented in this work. The Oligocene tectonic history of Fuerteventura, coeval with its submarine stage of growth, has been presented elsewhere [*Gutiérrez*, 2000; *Gutiérrez et al.*, 2006]. This work is primarily focused on the study of the Miocene deformation stages, which coincided with the main episodes of the subaerial volcanic evolution of the island. Section 5 includes some ideas about the implications of the results of this work to unravel the tectonic origin of the archipelago, and to contribute to the understanding of the structural evolution of some volcanic edifices in oceanic islands associated with hot spots. Current discussion on plumes, plates and magmatism [e.g., *Foulger et al.*, 2005] can also benefit from the results of this work.

2. Geological Setting

[5] Fuerteventura is located at the eastern Canary ridge [*Coello et al.*, 1992], defined by a NNE-SSW trending volcanic province comprising the Fuerteventura and Lanzarote Islands, and their submerged prolongation at the Conception Bank [*Weigel et al.*, 1978; *Dañobeitia*, 1988] (Figure 1). The geological history of Fuerteventura is long and complex [*Fúster et al.*, 1968; *Stillman et al.*, 1975; *Fúster et al.*, 1980; *Le Bas et al.*, 1986; *Sagredo et al.*, 1989; *Coello et al.*, 1992; *Ancochea et al.*, 1996; *Steiner et al.*, 1998; *Balogh et al.*, 1999; *Muñoz et al.*, 2005], and the island lies on the Atlantic oceanic crust, Early Jurassic in age [*Banda et al.*, 1981; *Steiner et al.*, 1998]. Depth to the Moho beneath Fuerteventura is of 15–20 km [e.g., *Dañobeitia and Canales*, 2000]. A layer 2–4 km thick with seismic velocities of 4.2–4.3 km s^{-1} characterizes the upper crust. This layer overlies the middle crust, with a thickness of 5–6 km and seismic velocities of 6.1–6.6 km s^{-1}. Finally, the basal part of the crust coincides with a 7.4 km s^{-1} velocity layer, 8–10 km thick, interpreted as oceanic crust intruded by mantle-derived material [*Watts*, 1994]. The upper mantle shows seismic velocities of 7.6–7.8 km s^{-1} above Fuerteventura [*Dañobeitia and Canales*, 2000].

[6] For the purposes of this work, four main units can be distinguished in the island (Figure 1). These are, from mostly older to younger, the basal complex [*Fúster et al.*, 1968; *Stillman et al.*, 1975], the subaerial volcanic group [*Gutiérrez*, 2000], the Miocene subaerial volcanic complexes, and the Pliocene and Quaternary sedimentary and volcanic rocks. These units are described with detail in this section previous to the analysis of their structural characteristics.

2.1. Basal Complex

[7] In this work, the basal complex includes the exposures of the Mesozoic oceanic crust, the submarine and transitional volcanic groups, and the plutonic bodies and dike swarms associated with these groups and with the subaerial volcanic

units. Former studies considered the subaerial volcanic group as a part of the basal complex [e.g., *Fúster et al.*, 1968; *Stillman et al.*, 1975]. However, the work of *Gutiérrez* [2000] has shown the distinctive characteristics of this subaerial volcanic group and, given its tectonic relevance, it has been distinguished here from the basal complex.

[8] The outcropping fragment of Mesozoic oceanic crust consists of a thick sedimentary sequence (around 1600 m) overlying tholeiitic normal mid-ocean ridge basalts [*Robertson and Stillman*, 1979a; *Robertson and Bernouilli*, 1982; *Steiner et al.*, 1998]. The terrigenous and pelagic sedimentary succession spans from the Early Jurassic to the Late Cretaceous [*Steiner et al.*, 1998], and it was deposited at a deep-sea fan derived from the West African continental margin [*Fúster et al.*, 1968; *Robertson and Stillman*, 1979a; *Robertson and Bernouilli*, 1982; *Steiner et al.*, 1998].

[9] Resting unconformably on the Mesozoic oceanic crust is the submarine volcanic group [*Robertson and Stillman*, 1979b; *Fúster et al.*, 1984a, 1984b; *Le Bas et al.*, 1986; *Stillman*, 1987, 1999; *Gutiérrez*, 2000; *Gutiérrez et al.*, 2006]. This unit is composed of primary volcanic facies and volcanogenic facies (nomenclature after *McPhie et al.* [1993]), which are characterized by the presence of rocks with ultra-alkaline affinity and strongly alkaline rocks. The age of the submarine volcanic group is Oligocene, and it has been interpreted as a syntectonic unit with respect to a NNE-SSW directed extension [*Gutiérrez*, 2000; *Gutiérrez et al.*, 2006].

[10] Onlapping the submarine volcanic group is the transitional volcanic group. This is a lithostratigraphic unit, late Oligocene in age, which has been interpreted as a result of explosive plinian subaerial eruptions, lava deltas, shallow water effusive eruptions, gravity flows, and shallow water reefs [*Gutiérrez*, 2000; *Gutiérrez et al.*, 2006]. Late during the deposition of the transitional volcanic group started the ESE-WNW directed extensional episode characterizing the Neogene subaerial building of the island, whose study is the main objective of this contribution.

[11] Plutonic and hypabyssal rocks, probably associated with the submarine and transitional volcanic groups, form the ultra-alkaline complex [*Fúster et al.*, 1980; *Le Bas et al.*, 1986; *Ahijado and Hernández-Pacheco*, 1990; *Muñoz et al.*, 2005]. The younger of these rocks became emplaced contemporary with displacement along brittle and ductile extensional shear zones [*Casillas et al.*, 1994; *Fernández et al.*, 1997]. These zones were active during the late Oligocene, around 25 Myr ago [*Le Bas et al.*, 1986; *Cantagrel et al.*, 1993; *Sagredo et al.*, 1996; *Ahijado*, 1999; *Balogh et al.*, 1999], therefore heralding the Neogene extensional episodes that are described in this work.

[12] A cortege of plutonic rocks (pyroxenites, gabbros and syenites) and a dike swarm crosscut the whole of the previously described units in the basal complex [*Gastesi*, 1969, *Muñoz*, 1969] as well as the rocks of the subaerial volcanic group. These rocks are mostly Miocene, and they have been interpreted as the hypabyssal roots of the successive episodes of growth of the subaerial volcanic edifices [*Ancochea et al.*, 1996; *Balogh et al.*, 1999; *Muñoz et al.*, 2005].

2.2. Subaerial Volcanic Group

[13] The subaerial volcanic group rests unconformably on the units forming the basal complex (Figure 1). A very heterogeneous unit of basalts, trachybasalts, debris-avalanche breccias and debris-flow breccias form this group, which is intensely crosscut by the previously mentioned basic dikes and plutons. The density of the dike swarm has obliterated many of the original features of these rocks, although lava flows, sometimes of pahoehoe type, and their related autoclastic breccias are commonly observed. This group has been originally defined by *Gutiérrez* [2000], who first described its subaerial character, thus separating it from the clearly submarine and transitional rocks of the basal complex. The age of this group has not been determined, but it must be comprised between the last stages of deposition of the transitional volcanic group [23 Ma after *Gutiérrez*, 2000] and the oldest episodes of the Miocene subaerial volcanic complexes (20–22 Ma according to *Ancochea et al.* [1996]).

[14] The rocks forming the basal complex and the subaerial volcanic group suffered a locally intense hydrothermal metamorphism of greenschist facies. The origin of this metamorphism is the massive intrusion of dike swarms and plutons related to the subaerial volcanic rocks [*Fúster et al.*, 1968; *Stillman et al.*, 1975; *Robertson and Stillman*, 1979b; *Fúster et al.*, 1984a; *Javoy et al.*, 1986; *Muñoz and Sagredo*, 1994; *Hobson et al.*, 1998; *Gutiérrez*, 2000].

2.3. Miocene Subaerial Volcanic Complexes

[15] Three huge basaltic volcanic constructs were generated during the Miocene in Fuerteventura: the southern, central, and northern edifices (Figure 1) [*Ancochea et al.*, 1996]. The growth of each edifice was punctuated by periods of volcanic quiescence associated with erosion and development of giant landslides [*Ancochea et al.*, 1996; *Stillman*, 1999]. The southern edifice (the SVC of *Ancochea et al.* [1996]) crops out in the Jandía Península (Figure 1), and it was built by three successive constructive episodes, SVC-I, SVC-II, and SVC-III. The bottom of the series (SVC-I, 20.7–19.3 Ma [*Ancochea et al.*, 1996]) is mostly composed of pahoehoe basaltic lava flows, hydromagmatic pyroclasts and quartz-trachytic plugs and tuffs. Locally, resting unconformably on this pahoehoe unit is a level of polymictic breccias, of variable thickness, that is covered by a series of ankaramite lava flows. The SVC-II episode (17.2–15.4 Ma [*Ancochea et al.*, 1996]), formed by lava flows and pyroclasts of basaltic and trachybasaltic composition, lies unconformably above the SVC-I, filling an important paleorelief [*Ancochea et al.*, 1996]. Finally, ankaramite flows, olivine-pyroxene basalts and, to a lesser extent, trachybasalt flows of the SVC-III episode (15.2–14.2 Ma [*Ancochea et al.*, 1996]) lie indistinctly above SVC-I or SVC-II. On the basis of structural and topographic criteria, *Ancochea et al.* [1996] proposed the existence of a large central volcano for SVC-II and SVC-III, with its center located offshore, to the north of the Jandía Península (Figure 1).

[16] Three constructive episodes have been distinguished in the central volcanic complex (the CVC) according to *Ancochea et al.* [1996]. The CVC-I presents a lower unit of polymictic breccias that rest above the lava flows of the subaerial volcanic group. These breccias probably represent debris-avalanche deposits related to gravity slides of unknown dimensions, and they could be correlated with those appearing at the top of the SVC-I. In that case, the subaerial volcanic group and the pahoehoe lavas of the basal SVC-I could correspond to the same volcanic episode. Above the polymictic breccias there appears a thick (>1000 m) sequence of basaltic, mainly ankaramitic, flows, tilted and crosscut by abundant dikes, that will be studied with detail in this work. Thin basaltic flows and pyroclast levels, as well as trachyte flows, plugs and dikes, constitute the CVC-II (22.5–20 Ma [*Ancochea et al.*, 1996]). A polymictic breccia seals the unconformity between CVC-I and CVC-II. Thick flows of basalt and trachybasalt of the CVC-III episode (15.6–14.5 Ma [*Ancochea et al.*, 1996]) lie above CVC-I, CVC-II, or even above the subaerial volcanic group. Again, a central volcanic edifice has been deduced for the CVC (center in Figure 1), with different centers depending on the considered constructive episode.

[17] The northern edifice (NVC) includes two constructive episodes (NVC-I and NVC-II) separated by a volcanic agglomerate unit (Ampuyenta Formation) witnessing the collapse of the NVC-I edifice. Basalts, picritic basalts, oceanitic basalts, trachybasalts and trachytes predominate in NVC-I (22(?)–15.3 Ma [*Ancochea et al.*, 1996]). Basaltic lava flows constitute the NVC-II episode (14.3–12.8 Ma [*Ancochea et al.*, 1996]) that rests unconformably on the Ampuyenta Formation. The available data suggest a central volcanic edifice for NVC-II whose focus has been located at the northern half of Fuerteventura (Figure 1).

[18] It cannot be excluded that a part of the exposure of the subaerial volcanic group, especially the top of this unit in areas densely traversed by dikes, could correspond to rocks of the CVC-I and NVC-I episodes.

2.4. Pliocene and Quaternary Sedimentary and Volcanic Rocks

[19] A period of quiescence followed the Miocene subaerial volcanic activity, and the edifices were deeply eroded. Small basaltic volcanoes and associated lava fields resulted from a renewed activity during the Pliocene that has continued up to prehistoric times. Littoral and shallow water marine deposits, eolian and alluvial complexes and paleosoil deposits were generated in the Pliocene and Quaternary [*Meco and Stearns*, 1981; *Meco and Pomel*, 1985; *Zazo et al.*, 2002].

3. Structural Description

[20] The extensional deformation events that started in the late Oligocene left a structural imprint in the materials of the basal complex, the subaerial volcanic group and the Miocene subaerial volcanic complexes. Three types of structures are studied in this work: dikes, folds and faults.

[21] A dense dike swarm crops out in the western half of Fuerteventura (Figures 2a–2c), essentially affecting the basal complex and the subaerial volcanic group. The impressive spectacle of this dike swarm has attired the attention of a large number of authors [*Fúster et al.*, 1968; *López Ruiz*, 1970; *Stillman and Robertson*, 1977; *Stillman*, 1987; *Ahijado*, 1999; *Ahijado et al.*, 2001]. The composition of these dikes is mainly basaltic or trachybasaltic, though trachyte and phonolite dikes are also found. The emplacement of this dike swarm should have involved a large crustal stretch [*López Ruiz*, 1970; *Stillman and Robertson*, 1977; *Stillman*, 1987; *Ahijado et al.*, 2001]. Measurement of dike orientation in this work has included data of almost 3000 dikes (see section 4). Field analysis of the observed systematic crosscut relationships (Figures 2b and 2c) at each measurement site allows proposing separation into three main dike systems. We have labeled them as system 1, 2 and 3. Dikes of system 1 crosscut the basal complex, the subaerial volcanic group, and the rocks of the lower episode (I) of the Miocene volcanic edifices. Around an 82% of the measured dikes correspond to system 1, and probably more if relative volume proportions were considered (Figure 2b). Dikes of system 2 also affect the rocks of the intermediate episode (II) of the large Miocene volcanoes. Finally, dikes of system 3 also crosscut the rocks of the most recent episode (III) of the Miocene volcanic edifices. A more detailed analysis of dikes, taking into account their kinematic implications, will be done in section 4. Here, only the main features of the geometrical arrangement of dikes will be described. The trends of the distinct dike systems are NE-SW, E-W, and NNW-SSE for systems 1, 2, and 3, respectively (Figure 3), with significant local variations that will be presented and discussed in sections 3 and 4. It must be indicated that these average trends are essentially obtained from dike measurement in the basal complex, the subaerial volcanic group and the lower part of the Miocene subaerial edifices. More complex, radial patterns have been described by *Ancochea et al.* [1996] for dikes of our systems 2 and 3, based on their study of the middle and upper sequences of the Miocene edifices. Instead, our work is focused on the more constant trends shown by dikes in the substratum to these large edifices.

[22] The most relevant geometric feature of system 1 dikes is the spatial arrangement of their average dip senses (Figure 3a). Although the dikes show in general steep dip angles (around 92% of the measured dikes exceed 70°, a value that is similar for the three dike systems), systematic spatial patterns with large areas of constant dip sense can be observed for the dikes of system 1. This feature is illustrated in Figure 3a, which show the statistical average orientation at each site (for a location of the measurement sites, see section 4). Of particular relevance here is the indication of dip sense. In sites with steeply dipping dikes, sampling hazards and measurement errors yield rather erratic average dip direction. Therefore, to show truly representative dip direction results, Figure 3a depicts exclusively the orientation of system 1 dikes in measurement sites with average dips of less than 80°, which is considered as a reasonable limit to exclude the effects of sampling and measurement

error. Predominantly east dipping system 1 dikes characterize the central and northern western coast of Fuerteventura. Instead, the central and southern part of the island shows west dipping system 1 dikes with only local deviations. Accordingly, lines marking the change between both dip senses can be traced that represent vertical axial surfaces of large fans defined by downward or upward converging dikes (Figure 3a). By contrast, no systematic spatial arrangement of dip senses can be observed for the dikes of systems 2 and 3 (Figures 3b and 3c). The geometry of the dike density contours will be described below.

[23] Most of the subaerial volcanic rocks and several units of the basal complex show well-defined bedding, of volcanic or sedimentary origin (Figures 2d, 2e, and 2f). The bedding appears partially transposed in zones of high dike density, although it is often possible to measure its trend and dip. Figure 4a shows a summary of the bedding attitude measurements in the submarine, transitional and subaerial volcanic groups, and in the successions of the older constructive episodes of the northern and central volcanic complexes. The most striking feature of this map, apart from the predominant NE-SW trending directions, is the presence of large-scale folds affecting the bedding surfaces. An anticline can be observed in the northwestern part of the island. A close-up view of this structure, which affects the submarine, transitional and subaerial volcanic groups, reveals that it is an open fold, slightly west vergent (Figure 4b). The statistical axis of this fold dips 14° toward the NNE. The dikes of system 1 are mostly normal to the bedding. However, the axial surface of the anticline is not strictly coincident with the surface marking the change in dip sense of dikes (Figure 4b, cross section I-I'). Other folds appear to the east of the anticline, including an open syncline that coincides with the location of the plutonic rocks associated with the Miocene volcanic complexes (Figure 4b).

[24] Steep dipping bedding can be observed at the southern part of the exposure of the basal complex and the subaerial volcanic group (Figures 2d and 4a). This zone (Las Hermosas area) is a part of the eastern limb of the anticline described before in the central part of the island. Detailed mapping of this zone shows a close geometrical association between variations in the bedding dip and a system of NE-SW trending normal faults (Figure 5). The system 1 dikes in this zone are consistently normal to the bedding (Figure 5, cross section II-II', and Figure 6), and subparallel to the main NW dipping normal faults. Assuming that changes in the bedding dip are related to major curvatures in the fault surfaces, and applying the constant heave Chevron construction [*Williams and Vann*, 1987], a basal detachment can be obtained for the Las Hermosas and La Pared faults (Figure 5, map and cross section II-II'). The cross section is parallel to the average slip sense on the fault surfaces (e.g., Figure 6 and fault data in section 4). The main faults in Las Hermosas area converge toward this basal detachment, which shows a gentle dip to the NW. This hypothetical basal detachment lies at a depth of around 2.5 km below the present-day surface. Other faults can be
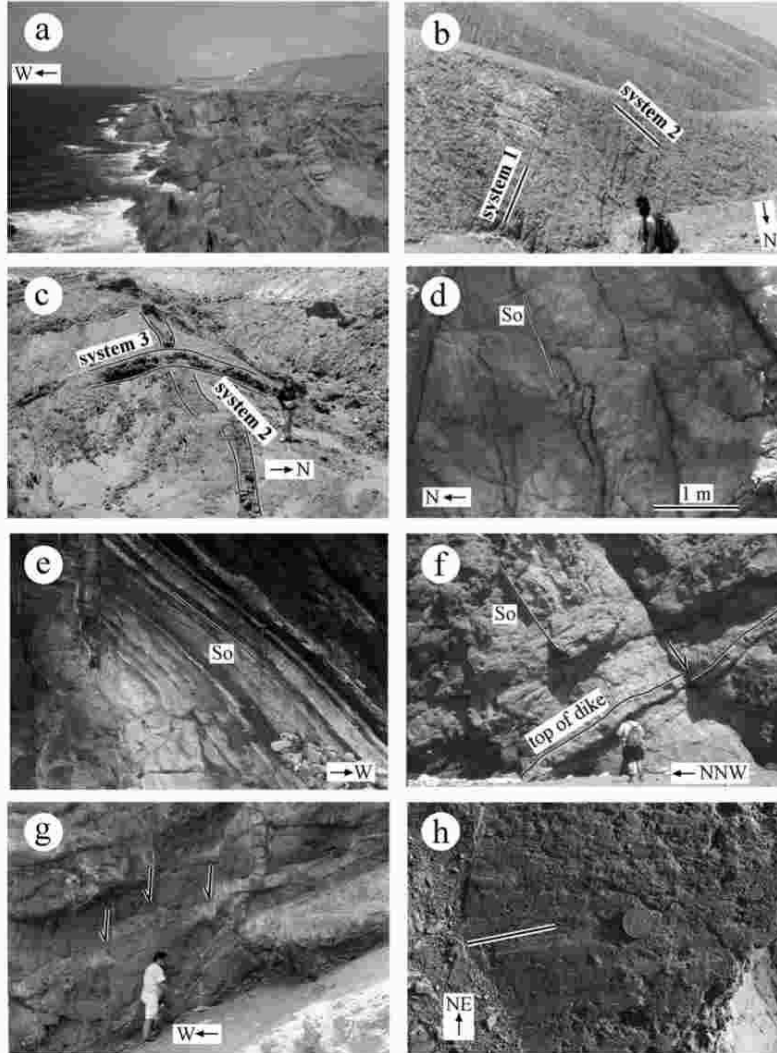
Figure 2. (a) View of the dike swarm that cuts the basal complex in the western coast of Fuerteventura. (b) Dike swarm in the basal complex; dike density larger than 90%. Dikes of system 2 (WNW-ESE) crosscut dikes of system 1 (NNE-SSW). (c) Crosscut relationship between a dike of system 3 (N-S) and a dike of system 2 (E-W) in the Jandía Peninsula. (d) Subvertical bedding shown by the subaerial volcanic rocks in the southwestern coast (Las Hermosas area). (e) Moderately dipping bedding of the submarine volcanic rocks (central western coast of Fuerteventura). (f) Normal fault displacing dikes in the southwestern coast (Las Hermosas area). (g) Normal faults displacing subhorizontal dikes in the west coast, to the north of Las Hermosas area. (h) Slickenside striation (continuous line) in a fault plane affecting the subaerial volcanic group (southwestern coast, Las Hermosas area).
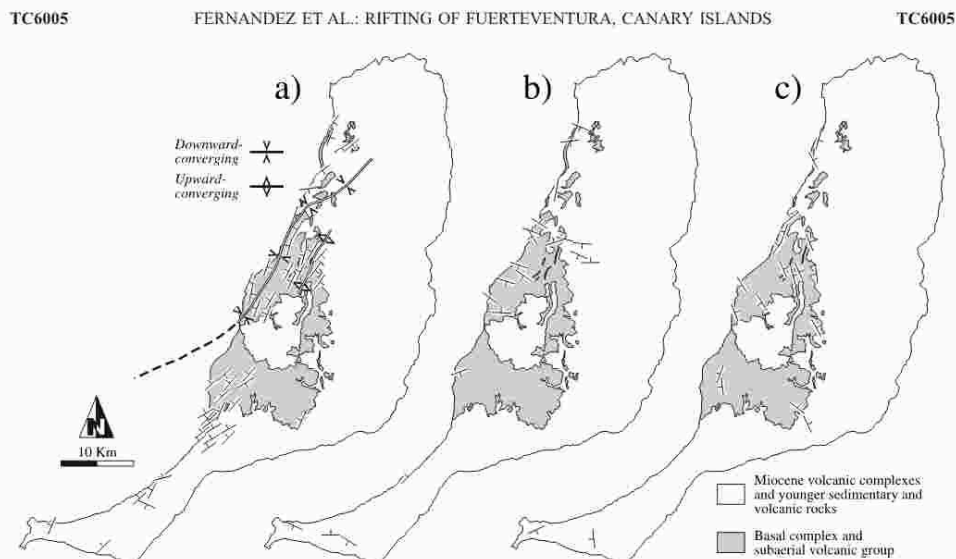
Figure 3. Average orientation (trend and dip direction) of dikes traversing the basal complex, the subaerial volcanic group and the basal episodes of the Miocene volcanic complexes. Only sites with average dips lower than 80° are represented. (a) Dikes of system 1. The traces of the surface with downward converging or upward converging dikes are shown. (b) Dikes of system 2. (c) Dikes of system 3. See text for further explanation.

observed to the SE of Las Hermosas fault, suggesting that the basal detachment must continue in that direction.

[25] The structural data presented in this work are summarized in Figure 7. The axial traces of the bedding folds are parallel and almost coincident with the traces of the axial surfaces to the dike fans (Figure 7a). The traces of these large structures are not straight and two main curvatures can be observed. The NNE-SSW trends predominant in the central area pass to NE-SW trends to the north. The Atlantic Ocean covers the prolongation of these structures to the south, but the NE-SW trends observed in Las Hermosas area seem to indicate that a similar curvature exists in the southern half of the island. Therefore the described structures delineate a huge sigmoid at the scale of the Fuerteventura Island.

[26] Significantly, the density peaks of system 1 dike swarm closely fit the geometry of the sigmoid structures defined by dike and bedding orientation (Figures 7b and 7c). The dike density map nearly coincides with that presented by *Stillman* [1987] in the basal complex. Density of system 1 dikes is partly dependent on the age of their host rocks. Generally speaking, the rocks of the Mesozoic crust show dike densities larger than the subaerial volcanic group, which is contemporary with these dikes (Figure 7c). However, dike densities larger than 90% have been found in rocks ranging in age from the Mesozoic to the Miocene (Figure 7c). On the other side, densities between 20% and 30% are also observed in the Mesozoic oceanic crust.

Therefore it must be concluded that dike density is also structurally controlled, with elongate, NNE-SSE to NE-SW trending areas of high dike densities bounded laterally by low dike density bands (Figure 7c). Planimetry of the dike density map (Figure 7b) reveals that the elongation (change in length/initial length) in the studied area is of 0.7–1.0 (70–100%) due to dike intrusion. This large value of elongation is heterogeneously distributed, ranging from 3 at cross section I-I′-I″, to less than 0.5 at cross section II-II′ (location of cross sections in Figure 1). The extension within cross section I-I′-I″ yields a net crustal lengthening of 8 km. Dike densities in the Jandía Peninsula have not been represented in Figure 7 because they are noticeably lower than in the north, rarely exceeding 10%.

4. Kinematic Analysis of Faults and Dikes

[27] A detailed analysis of the structures indicative of brittle deformation has been performed in Fuerteventura to obtain a better understanding of the Miocene tectonic evolution of this island. This study includes inversion of fault slip data and statistical analysis of dike orientation. The data have been obtained in the field, in different measurement sites covering the exposures of the basal complex and Miocene rocks (Figure 8). The rocks of constructive episodes II and III of the three distinct Miocene volcanic complexes are virtually devoid of faults with reliable kinematic indicators. Accordingly, the sites of fault
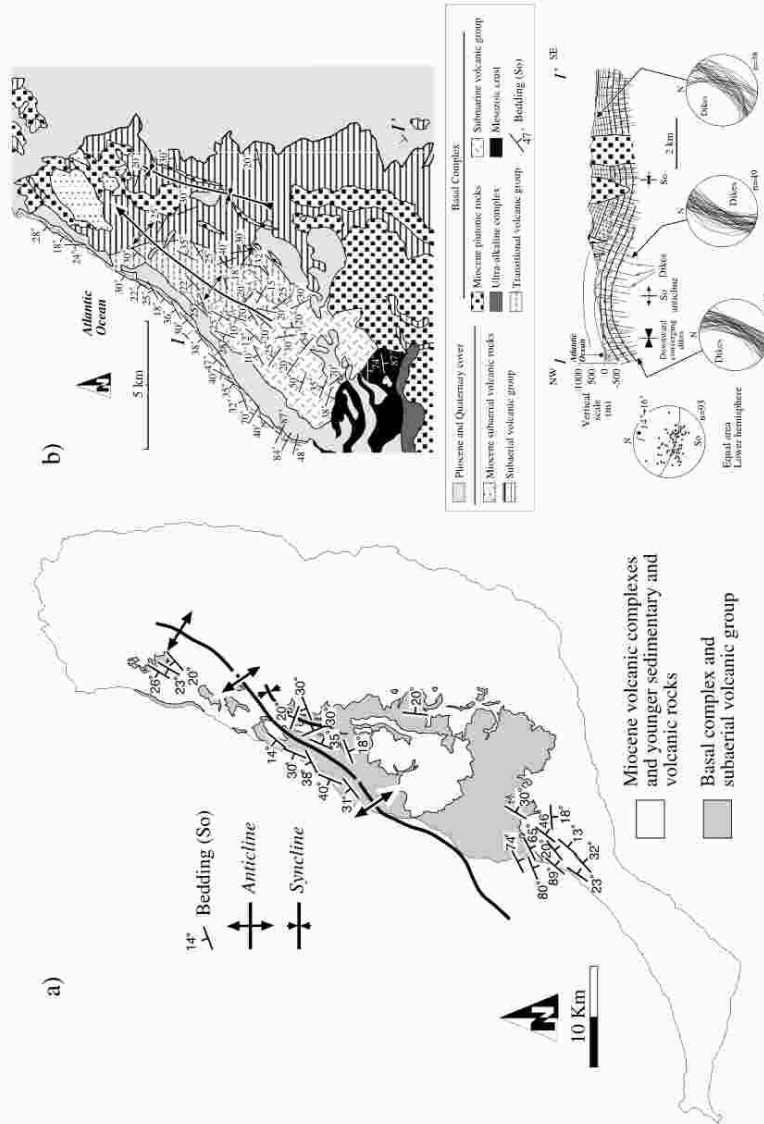
Figure 4. (a) Spatial variation of the bedding orientation in the submarine, transitional, and volcanic groups and in the basal episodes of the Miocene volcanic complexes. A large anticline can be traced near the western coast of Fuerteventura. (b) Detailed geological map of the submarine, transitional, and subaerial volcanic group in central west Fuerteventura (for a location, see Figure 1). The cross section I-I′ shows the main structures. The stereograms show the variation in the dike dip along the cross section, and the poles to the bedding (So) with location of the statistical best fit fold axis (*f*).
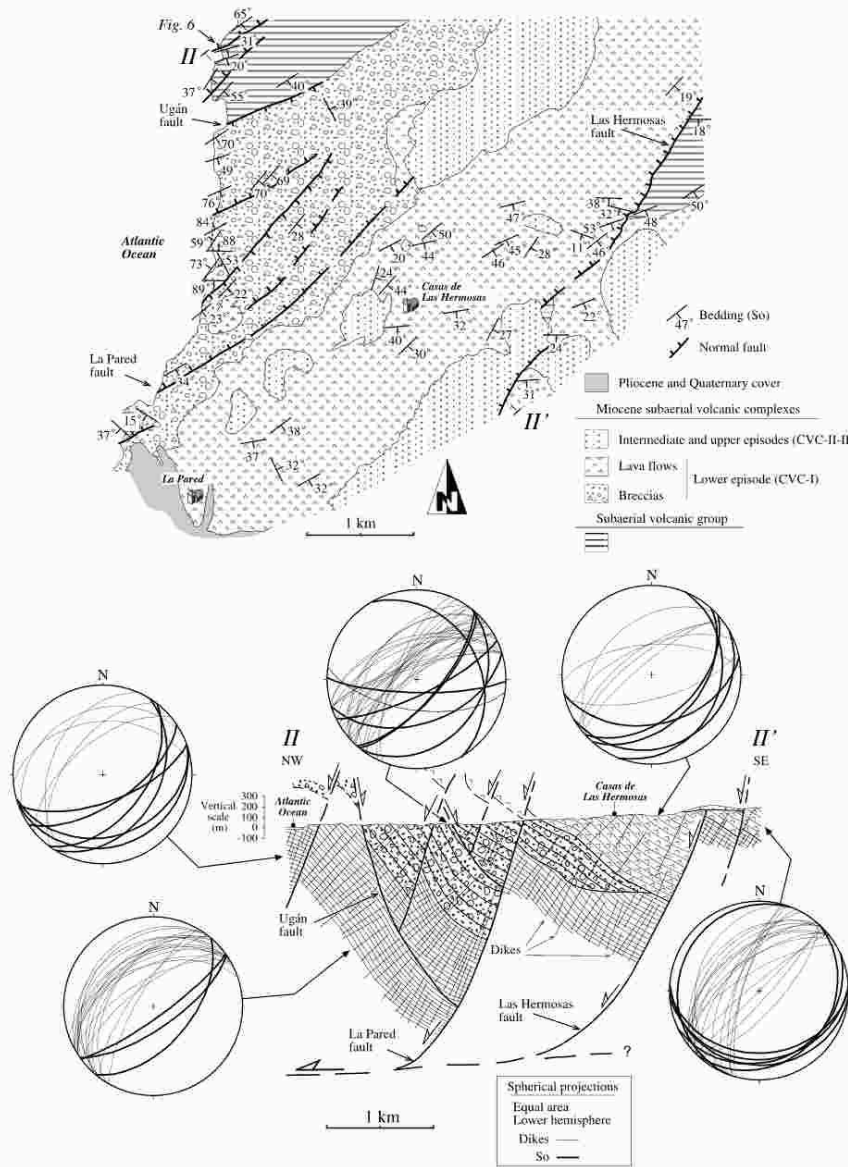
Figure 5. Detailed geological map of the Las Hermosas area (for a location, see Figure 1). Cross section II-II' shows the reconstruction of the fault geometry at depth. The stereograms include data from bedding (So) and dike orientations. Note the statistically normal arrangement of both types of structures and the distinct tilting angle distinguishable at each block.

9 of 27
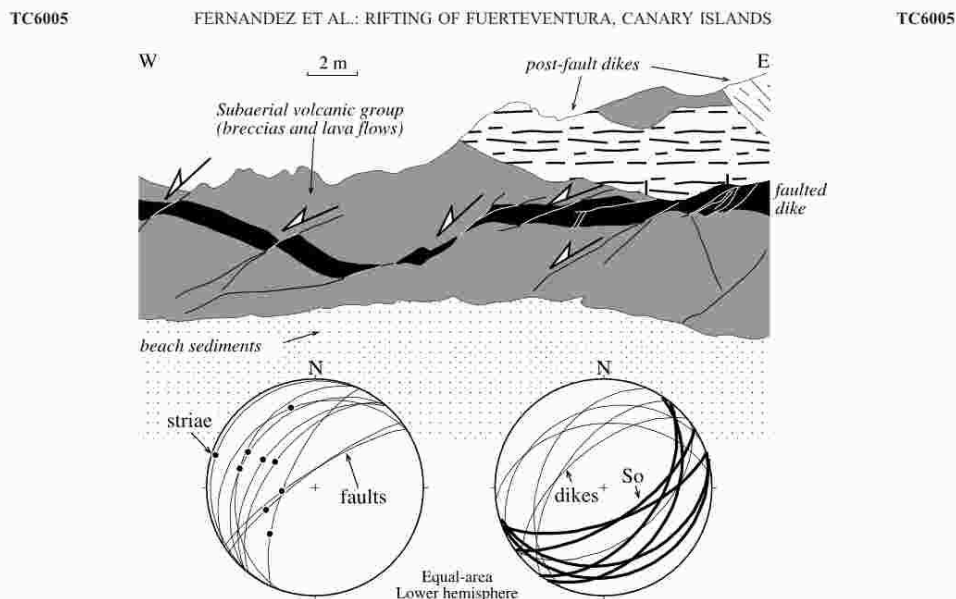
Figure 6. Detailed geometry of the system 1 normal faults displacing subhorizontal dikes in the western coast of Las Hermosas area, near the point II of cross section II-II' (see Figure 5 for location).

slip measurement are concentrated in the rocks of the basal complex, the subaerial volcanic group and the episode I of the Miocene volcanic complexes. Most of the dike measurement sites are also located in these same rock units, and therefore the discussion of the dike results will also consider the data of the younger episodes (II and III) of the Miocene volcanism given by other authors [e.g., *Ancochea et al.*, 1996].

4.1. Methodology

[28] Fault slip data have been observed in 55 sites (Figure 8a and Table 1) adding together 1780 measured faults. Typically, each data consists of trend, dip and dip sense of the fault surface, pitch of the slickenside striation (Figure 2h), and sense of displacement along the fault. The kinematic analysis of the distinct fault systems has followed the method of *Marret and Allmendinger* [1990]. This is a graphical technique that allows estimating the orientation of the P (infinitesimal principal shortening) and T (infinitesimal principal extension) axes of the incremental deformation tensor for each fault. Once determined the P and T axes for the totality of faults of a given system, the tensor summation for this system is achieved by computing the orientation tensor of these kinematic axes (for a definition of the orientation tensor, see *Scheidegger* [1965] and *Mardia* [1972]). The eigenvectors of the orientation tensor give the orientation of the P and T axes for the entire fault system at each site.

[29] The study of dike orientation includes 2996 measurements of trend, dip and dip sense of dikes determined in 96 sites (Figure 8b and Table 2). Assuming that dikes were generated as fractures of mode I [*Lawn and Wilshaw*, 1975; *Pollard and Segall*, 1987], the maximum extension direction must lie normal to their boundaries [*Walker*, 1987; *Marinoni*, 2001]. As explained before, three dike systems have been distinguished according to the relative crosscutting relationships among them (Figures 2b and 2c). Again, the orientation tensor has been calculated for each system and site. The eigenvector associated with the largest eigenvalue of this matrix gives the orientation of the principal extension direction.

[30] Finally, maps of trajectories of maximum extension have been traced from the results of the statistical analysis fault and dike data at each site. Tracing of trajectories has used the algorithm of *Lee and Angelier* [1994], which takes into account variations in parameters like data dispersion and local gridding effects.

4.2. Results

[31] The results obtained in the studied area are presented in Tables 1 and 2 and in Figures 9, 10, and 11. Stereograms of faults and dikes and determination of principal deformation axes for selected sites are shown in Figures 9a (left) and 10a. The entire set of stereograms is available in the auxiliary material[1].
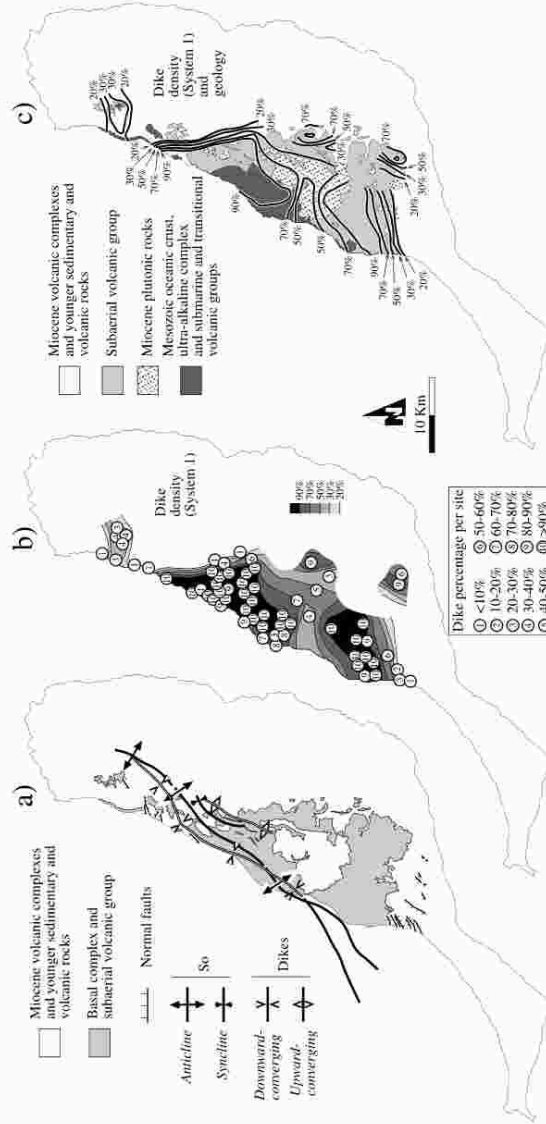
Figure 7. Summary of the main structural data of the basal complex, the subaerial volcanic group and the Miocene volcanic complexes of Fuerteventura. (a) Comparison of the main structures defined from the study of bedding (So) and dike orientation. (b) Dike density contours (system 1) obtained from data of *Gutiérrez* [2000] and this work. At each measurement site the dike percentage has been determined measuring the linear percentage of system 1 dikes versus host rock and excluding younger dikes. (c) Dike density contours (system 1) traced on a geological sketch of Fuerteventura.
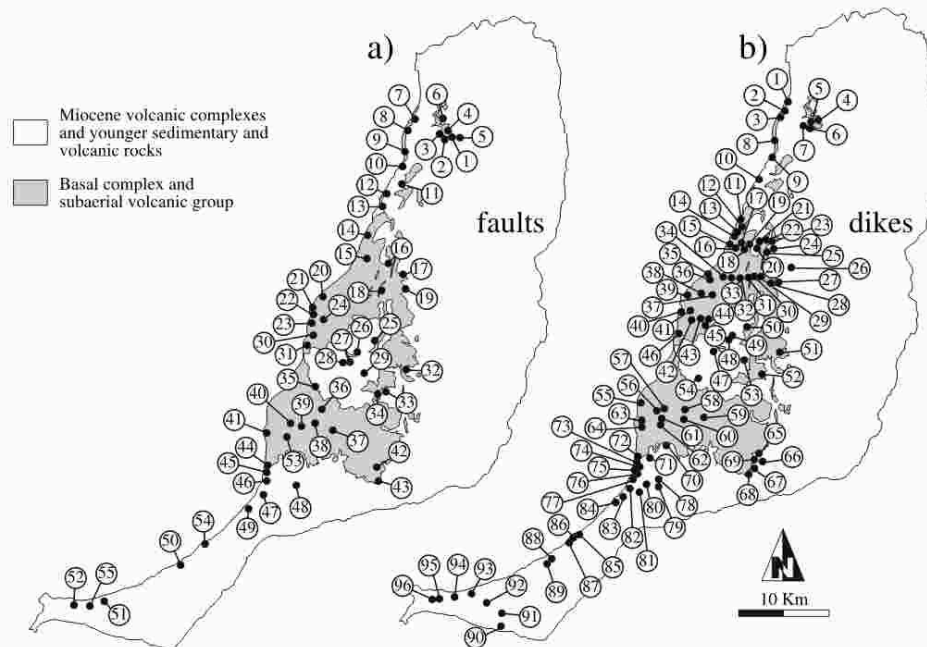
Figure 8. Location of (a) fault, and (b) dike measurement sites. Numbers refer to the sites listed in Tables 1 and 2.

[32] The fault sample obtained at each site has been separated into different systems according to field observations like crosscut relationships and relative age criteria. This technique is probably the most reliable to discriminate among the distinct faulting episodes affecting a given rock volume [*Homberg et al.*, 2004]. In some cases, these discriminating field criteria are not available, and the fault separation has been done by comparison with the results obtained from the study of dikes in the same site or from fault crosscutting in nearby measurement sites. Three fault systems (1, 2, and 3, from older to younger) have been distinguished at the scale of the studied area. System 1 faults are the most abundant, constituting almost a 60% of the measured faults. Systems 2 and 3 represent the 13% and 27% of the measured faults, respectively. All the measured faults are normal (Figures 2f and 2g and Table 1), albeit a strike-slip component is commonly present (Figure 9a). Accordingly, the principal extension axis (T) is subhorizontal in all cases, while P is subvertical (Table 1). The three fault systems distinguished in this work correspond to three distinct tectonic episodes with contrasted orientations of their kinematic axes. The T axes trajectories are NW-SE oriented for fault system 1 (Figures 9b and 11a), although they rotate toward NNW-SSE trends in the Jandía Peninsula. The horizontal extension trajectories for fault system 2 are NNE-SSW oriented, at a high angle, though not normal, to the extension trajectories of fault system 1 (Figures 9b and 11a). Fault system 3 shows E-W extension trajectories. However, NE-SW trends are also common in the northern and southern parts of the island. The trends of the faults of the three systems are statistically normal to those of their corresponding horizontal extension trajectories (Figures 9 and 11a).

[33] The three distinct dike systems (1, 2, and 3, form older to younger) coincide in age and kinematics with the systems defined in the fault study. Also the maps of the horizontal extension trajectories obtained from the dike study (Figure 11b) are very similar to those of faults. Dikes of system 1 are the most abundant. They probably represent more than 90% in volume of the dike swarm, and around 82% of the total number of measured dikes (Table 2). Systems 2 and 3 include the 8% and 10% of the measured dikes, respectively. The dikes in Fuerteventura are mostly subvertical (Figure 10a), although some significant deviations to this rule are important to define the large-scale structure in the basal complex, as explained before. Apart from this, the pole to the average dike boundary, coinciding with the principal extension axis, is subhorizontal in most

Table 1. Results of the Fault Slip Inversion Data Obtained From the Method of *Marret and Allmendinger* [1990][a]

Site	FS	Unit	Nt	P and T Axes (Dip/Strike) P	T
1	1	SaVG	54	79/322	10/128
	3	SaVG	18	86/237	4/51
2	1	SaVG	31	79/337	6/98
	2	SaVG	7	82/141	5/14
3	1	UC	44	67/292	21/132
4	2	UC	15	71/323	13/190
5	1	SaVG	4	77/218	4/111
	2	SaVG	12	80/358	8/212
6	1	UC	38	77/345	6/104
7	1	UC	19	84/242	3/127
	3	UC	5	70/312	6/59
8	3	UC	43	60/330	5/232
9	1	UC	15	74/140	16/318
10	1	UC	13	69/341	19/138
	3	UC	21	75/170	3/70
11	1	MS	34	80/148	10/309
12	3	SmVG	26	79/300	10/95
13	1	SmVG	34	87/94	2/309
14	3	SmVG	9	86/304	4/90
15	1	SmVG	33	83/223	2/115
16	1	SaVG	6	53/59	21/298
17	1	SaVG	23	77/252	11/110
	2	SaVG	17	73/252	8/12
18	1	SaVG	48	67/206	5/104
19	1	SaVG	44	83/258	4/132
20	1	SmVG	19	68/192	12/314
	3	SmVG	19	62/206	10/98
21	3	MS	10	76/131	12/284
22	1	MS	26	86/42	1/295
	2	MS	23	76/28	12/181
23	1	MS	15	69/337	14/107
	2	MS	15	79/351	10/193
24	1	SmVG	16	83/281	7/105
25	2	PS	28	79/147	5/34
26	1	PS	35	87/88	3/290
27	1	PS	8	79/147	11/309
	3	PS	6	20/350	18/87
28	1	PS	7	65/199	8/307
29	2	PS	7	84/172	6/349
	3	PS	33	69/245	17/99
30	2	MS	3	57/208	27/350
	3	MS	41	78/101	11/292
31	1	MS	7	65/248	19/112
	2	MS	3	44/328	20/217
32	3	SaVG	55	71/105	19/278
33	2	SaVG	26	76/7	14/198
	3	SaVG	7	53/3	4/267
34	1	SaVG	23	73/53	4/314
	2	SaVG	12	7/138	2/48
35	1	SaVG	7	81/132	9/315
36	1	SaVG	26	66/122	23/309
37	1	SaVG	51	77/274	11/129
38	3	SaVG	42	72/197	5/93
39	3	SaVG	21	62/170	13/285
40	1	SaVG	25	74/172	11/303
	2	SaVG	7	24/65	4/333
41	1	SaVG	19	76/7	4/113
	2	SaVG	22	83/308	4/178
42	3	UC	52	76/298	11/81
43	3	UC	15	80/67	9/270
44	1	MVS	98	81/256	5/135
45	3	MVS	25	81/31	3/282
46	1	MVS	15	80/320	10/131
47	1	MVS	34	86/277	4/130
48	1	MVS	29	77/102	10/321

Table 1. (continued)

Site	FS	Unit	Nt	P and T Axes (Dip/Strike) P	T
	2	MVS	10	78/104	2/205
49	2	MVS	12	76/156	13/353
50	1	MVS	23	81/83	6/309
	3	MVS	25	78/227	12/56
51	1	MVS	44	85/188	5/348
	3	MVS	17	73/238	10/112
52	1	MVS	24	77/87	2/349
53	1	SaVG	42	74/162	13/310
54	2	MVS	13	76/111	1/203
55	1	MVS	23	70/214	16/357

[a]Definitions are FS, fault system; MS, Mesozoic sediments; SmVG, Submarine and transitional volcanic groups; UC, Ultra-alkaline complex; SaVG, Subaerial volcanic group; PS, Miocene plutonic rocks; MVS, Miocene volcanic rocks (episodes SVC-I, CVC-I, and NVC-I); Nt, total number of faults measured and separated in subsets. P and T are kinematic shortening and extension axes.

cases (Table 2). As stated in the structural description, the azimuths of the distinct dike systems are very different (Figures 2b and 2c), therefore suggesting a succession of tectonic stages with contrasted kinematic patterns. Dikes of system 1 bear consistently a NE-SW to NNE-SSW average trend. Contemporary and late to these dikes is the intrusion of banded plutons with alternating bands of pyroxenite and gabbro (Pajara pluton [*Muñoz et al.*, 1997; *Hobson et al.*, 1998]). These alternating bands are NNE-SSW oriented, which coincides with the average trend of system 1 dikes. The map of horizontal extension trajectories for these dikes and plutons shows quite parallel NW-SE trends (Figures 10b and 11b). As in the case of the fault analysis, a change toward a NNW-SSE extension direction can be observed in the Jandía Peninsula. The dikes of system 1 do not affect the episodes II and III of the Miocene volcanic complexes, and are the main responsible for the high dike densities affecting large zones of the basal complex and the subaerial volcanic group (Figures 2a, 2b, 7b, and 7c). The trend of the dikes of system 2 is E-W, with slight variations from NW-SE to NE-SW (Figure 10a). Accordingly, the horizontal extension trajectories are NNE-SSW oriented, although N-S and NNW-SSE trends are observed in the southern part of the island (Figures 10b and 11b). The dikes of system 3 show more variable trends, which rotate from NNW-SSE to NNE-SSW, although even larger variations can be observed in the Jandía Peninsula (Figure 10). Therefore the horizontal extension trajectories obtained for dike system 3 are less constant in strike than for systems 1 and 2 (Figures 10b and 11b). Apart from this variability, an average ENE-WSW trend predominates for system 3.

5. Discussion

[34] The structural data presented in this work are indicative of an extensional tectonic activity affecting Fuerteventura from the end of the Oligocene (25 Ma) to, at least, the middle Miocene (~12 Ma), which is the age of the

Table 2. Fisher Statistical Results of the Dikes Poles[a]   **Table 2.** (continued)

Site	DS	Unit	Nt	t_3 (Dip/Strike)	Site	DS	Unit	Nt	t_3 (Dip/Strike)
1	1	UC	11	23/308	36	1	SmVG	45	14/291
	2		3	12/22		2		3	39/18
2	1	UC	5	16/288	37	1	SmVG	49	7/109
	2		2	6/16	38	1	SmVG	48	4/292
3	2	UC	10	13/353		2		2	24/14
	3		3	15/286	39	1	SmVG	47	21/296
4	1	MVS	9	3/321		2		2	1/195
	3		10	9/63		3		2	23/57
5	1	UC	27	2/317	40	1	MS	46	3/109
	3		2	1/259		2		2	34/36
6	1	MVS	21	10/316	41	1	MS	66	15/281
	2		1	0/194		2		1	7/348
7	1	MVS	22	10/329	42	1	MS	120	10/107
	3		1	0/254	43	1	SmVG	45	4/116
8	1	UC	16	4/104		2		5	18/183
	2		2	8/157	44	1	SmVG	48	10/120
	3		3	28/243		2		1	9/170
9	1	MS	8	33/322		3		1	14/60
	3		10	8/109	45	1	MS	13	10/110
10	1	SmVG	9	63/352		2		3	6/346
	2		8	61/282	46	1	MS	23	6/300
11	1	SaVG	44	16/289		3		11	18/249
	2		2	12/212	47	1	PS	50	4/129
	3		35	35/137	48	1	PS	21	4/293
12	1	SaVG	8	22/119		2		14	7/160
13	2	SaVG	6	25/200		3		14	6/242
	3		38	12/112	49	1	PS	35	1/105
14	1	SaVG	18	4/298		2		3	17/154
	2		3	19/55	50	1	PS	12	2/106
	3		30	34/122		2		8	5/345
15	1	SmVG	40	80/106		3		5	2/64
16	1	SmVG	43	7/299	51	1	SaVG	36	1/128
17	1	SaVG	40	5/96		2		5	7/352
18	1	SaVG	32	0/100		3		9	16/242
	2		4	8/194	52	1	SaVG	18	8/120
19	1	SaVG	42	5/93		2		10	1/158
	2		2	24/163	53	1	PS	17	3/112
20	1	SaVG	47	7/300		2		1	1/154
	2		3	7/191		3		7	1/254
21	1	SaVG	48	3/302	54	1	PS	32	10/138
	2		2	44/193	55	2	UC	4	18/340
22	1	SaVG	49	12/107	56	1	SaVG	20	3/317
	3		2	7/62		3		3	12/111
23	1	SaVG	8	7/129	57	1	SaVG	30	6/131
	3		8	22/247	58	1	SaVG	50	17/130
24	1	SaVG	29	12/121	59	1	SaVG	28	6/123
	2		2	32/4	60	1	SaVG	17	22/325
25	1	SaVG	28	11/313	61	1	SaVG	33	20/128
	2		1	24/29	62	1	SaVG	19	32/134
	3		3	2/72		3		4	33/89
26	1	MVS	6	9/125	63	1	SaVG	27	12/136
	2		1	29/180	64	1	SaVG	26	2/154
27	1	SaVG	38	16/304		3		1	3/99
	3		4	18/82	65	1	SaVG	20	4/125
28	1	SaVG	42	12/306		3		15	11/217
	3		8	2/264	66	1	MVS	1	20/320
29	1	SaVG	45	4/114		3		3	12/244
30	1	SaVG	47	14/117	67	1	MVS	24	2/98
	3		3	15/233	68	3	MVS	2	7/218
31	1	SaVG	48	11/110	69	1	UC	20	16/117
	3		2	22/256	70	1	SaVG	16	11/132
32	1		24	14/120	71	1	SaVG	12	14/112
	3		5	22/245	72	1	SaVG	4	14/152
33	1	SmVG	49	3/115	73	1	SaVG	9	19/133
	2		1	0/170	74	1	SaVG	28	40/141
	3		2	0/235	75	1	MVS	4	40/137
34	1	SmVG	37	3/298	76	1	MVS	36	17/149
35	1	SmVG	49	2/115	77	1	MVS	2	22/141
	2		1	11/33	78	1	MVS	16	22/150

Table 2. (continued)

Site	DS	Unit	Nt	t_3 (Dip/Strike)
79	1	MVS	2	22/138
80	1	MVS	7	22/151
81	1	MVS	4	24/147
82	1	MVS	38	1/328
83	1	MVS	4	6/138
84	1	MVS	10	7/94
	2		4	5/334
85	1	MVS	12	1/143
86	1	MVS	4	11/165
	2		23	12/134
	3		3	2/33
87	1	MVS	13	12/115
	2		12	8/152
88	1	MVS	78	18/137
	3		2	6/42
89	1	MVS	5	19/21
	2		11	6/1
	3		17	4/277
90	1	MVS	17	20/135
91	2	MVS	5	23/31
	3		1	20/85
92	1	MVS	1	6/300
	2		5	12/41
93	2	MVS	36	9/4
	3		12	3/274
94	1	MVS	3	6/222
	2		15	9/4
	3		10	1/112
95	1	MVS	7	14/112
	2		5	20/29
	3		21	18/347
96	1	MVS	38	1/317

[a]Definitions are DS, dike system; MS, Mesozoic sediments; SmVG, Submarine and transitional volcanic groups; UC, ultra-alkaline complex; SaVG, Subaerial volcanic group; PS, Miocene plutonic rocks; MVS, Miocene volcanic rocks (episodes SVC-I, CVC-I, and NVC-I); Nt, total number of dikes measured and separated in subsets; t_3, eigenvector associated with the least eigenvalue of the orientation matrix [*Scheidegger*, 1965], which coincides with the extension direction.

youngest constructive episodes and dikes of the Miocene volcanic complexes. This tectonic activity followed the previous Oligocene extensional event that was followed by a contractional episode during the late Oligocene [*Gutiérrez et al.*, 2006]. The distinct structures generated during the Miocene events (folds, faults, dikes, plutons, volcanic edifices) show a remarkable geometrical and kinematic coherence. Accordingly, the three defined fault systems can be correlated with the corresponding dike systems, taking into account not only kinematic considerations, but also relative age relationships. Therefore three deformation phases are proposed here, and defined as M-D$_1$, M-D$_2$, and M-D$_3$, to distinguish them from the Oligocene deformation phases (O-D).

5.1. Phase M-D$_1$

[35] Dikes and faults of system 1 (Figures 3a, 4b, 5, 6, 9, 10, and 11), as well as the large-scale folds of the bedding surfaces (Figure 4) and most of the mapped NE-SW trending faults (Figure 5), affect the same rock units and are assigned to the M-D$_1$ phase. Dike and fault analysis

indicates that an extensional tectonic regime prevailed during M-D$_1$. The kinematic indicators show a NW-SE to WNW-ESE extension direction (Figures 7a, 9, 10, and 11). A large-scale folding of the crust was developed in this stage, with a sigmoid pattern in plan view (Figure 7a). Most of dikes were intruded during M-D$_1$, with the areas of higher dike density almost matching the fold culminations or the highly fractured areas (Figures 7b and 7c). The brittle-ductile shear zones described by *Fernández et al.* [1997] affecting the ultra-alkaline complexes show kinematic characteristics identical to those of M-D$_1$, and it is proposed here that these shear zones represent the early stages of extension associated with the M-D$_1$ phase. Therefore the inception of the M-D$_1$ structures can be extended back to 25 Ma (Figure 12). Faults of system 1 affect part of the Miocene plutonic rocks that have been dated at around 20 Ma [*Sagredo et al.*, 1996; *Muñoz et al.*, 1997; *Balogh et al.*, 1999]. Similarly, *Feraud* [1981] and *Feraud et al.* [1985] have dated dikes of system 1, which yielded ages ranging from 20.3 to 19.9 Ma. Therefore it is proposed that the M-D$_1$ phase lasted from 25 Ma to around 20 Ma. The Mesozoic oceanic crust, the submarine volcanic group, and the older rocks of the ultra-alkaline complexes and of the transitional volcanic group are pretectonic rocks (Figure 12). Instead, the younger rocks of the ultra-alkaline complexes and of the transitional volcanic group, the subaerial volcanic group, a part of the Miocene plutonic rocks, most of the basic dike swarm and the early episodes of the Miocene volcanic complexes are syntectonic with M-D$_1$ (Figure 12). *Ancochea et al.* [1996] identified several deformation phases according with the distinct unconformities separating the episodes of the Miocene volcanic complexes. The M-D$_1$ phase approximately coincides with phase F$_1$ of *Ancochea et al.* [1996].

[36] With respect to the tectonic interpretation of M-D$_1$, there are several possible explanations of the observed structures. A contractional event could be proposed for the large-scale folding. However, the geometrical association between folds and tilted bedding, dikes and normal faults seems to discard that possibility. Emplacement of magma at depth can induce doming at surface [e.g., *Jackson and Pollard*, 1990] and it can also explain the intrusion of the dike swarm. However, bedding plane reverse faults, and normal and reverse faults at high angle to bedding are predicted to develop at the overburden [*Jackson and Pollard*, 1990]. Furthermore, the geometry of the exposed plutonic rocks in the basal complex (Figures 1 and 4) does not correlate with the shape and location of the large-scale anticline (Figure 4). In particular, most of the mapped plutons coincide with the axial trace of large-scale synclines. Therefore the available geological data dismiss the interpretation of the M-D$_1$ structures in terms of intrusion-controlled doming. However, this mechanism could have played an active role in the generation of some local structures, like the southern periclinal closure of the syncline mapped in Figure 4b. Concentric flexural folds and thrusts are structures normally developed at the ductile substratum of large volcanoes as a consequence of gravitational spreading [*Merle and Borgia*, 1996; *van Wyk de*
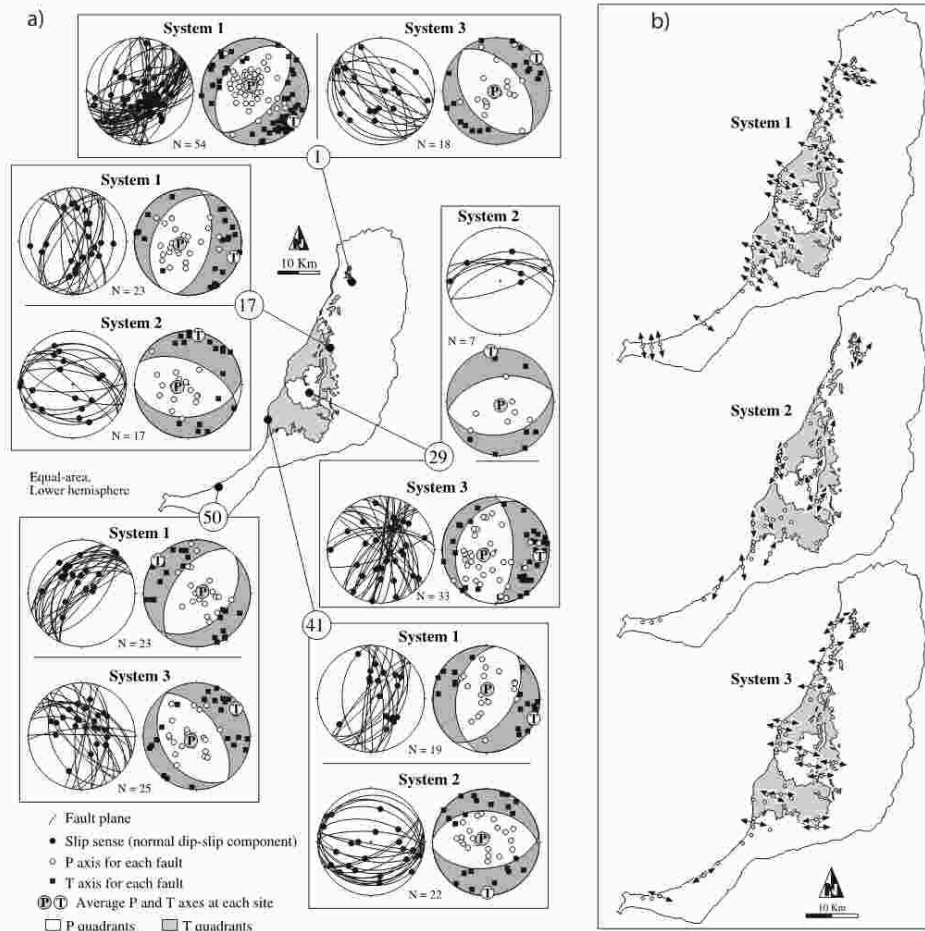
Figure 9. (a) Selected examples of fault measurement sites representing (left/top) great circles of fault planes and slickenside striations; all the faults are normal (black dots) with variable component of strike-slip displacement and (right/bottom) results of the PT method of *Marret and Allmendinger* [1990]. Open circles and solid squares mark the location of the maximum shortening (P) and maximum extension (T) axes for each fault, respectively; the white and gray quadrants represent the regions of the projection with predominance of P and T axes, respectively; the large circles labeled P and T show the location of the average deformation axes for each site and fault system. Numbers refer to the chosen measurement sites located in Figure 8. (b) Spatial distribution of azimuths of the T (maximum extension) axes for fault systems 1, 2, and 3.

Vries et al., 2001; *Oehler et al.*, 2005]. This interpretation faces several problems. First, compressive structures do not normally appear at the base of the volcano, but they are generally located about 20 km from its base [*Oehler et* *al.*, 2005]. Comparison of our Figures 1 and 4a indicates that the folds are located less than 10 km from the center of the central edifice of Fuerteventura, at a location where numerical models predict subvertical maximum compres-
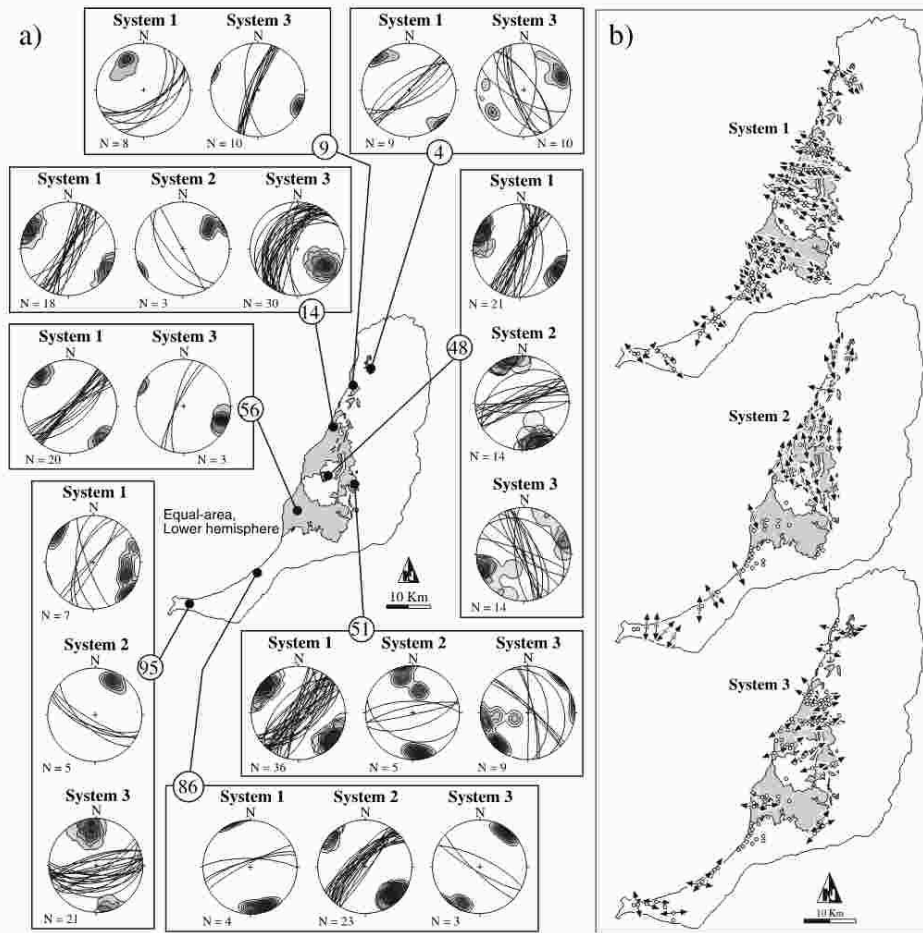
Figure 10. (a) Selected examples of dike measurement sites. The stereograms show cyclographic projections of the measured dikes at each site. Dike separation into systems has been performed by field crosscut relationships. Density contours of the poles to the dikes are also shown. Density diagrams after the *Kamb* [1959] method with the number of expected values under uniform distribution equal to 5 times the standard deviation. Numbers refer to the chosen measurement sites located in Figure 8. (b) Spatial distribution of azimuths of the T (maximum extension) axes for dike systems 1, 2, and 3.

sive stress [*van Wyk de Vries and Matela*, 1998]. Second, the folds described here are associated with normal faults and axial plane parallel dikes, and not with thrusts and strike-slip faults, as is common in extruded substrata to volcanoes [*van Wyk de Vries et al.*, 2001]. Third, the basal complex is mostly composed of lava flows, basic dikes and plutons, ultramafic intrusives and stiff sedimentary

rocks. The volcano should have caused a very small deformation field on such a high-viscosity substratum [*van Wyk de Vries and Matela*, 1998], probably not enough to generate the observed structures. Last, the M-D$_1$ phase was contemporary with the early episodes of the Miocene volcanic complexes, dominated by fissural eruptions. Volcano was probably less than 1000 m high, which again implies small

Casillas *et al.*   *Crecimiento y evolución geológica de Fuerteventura*
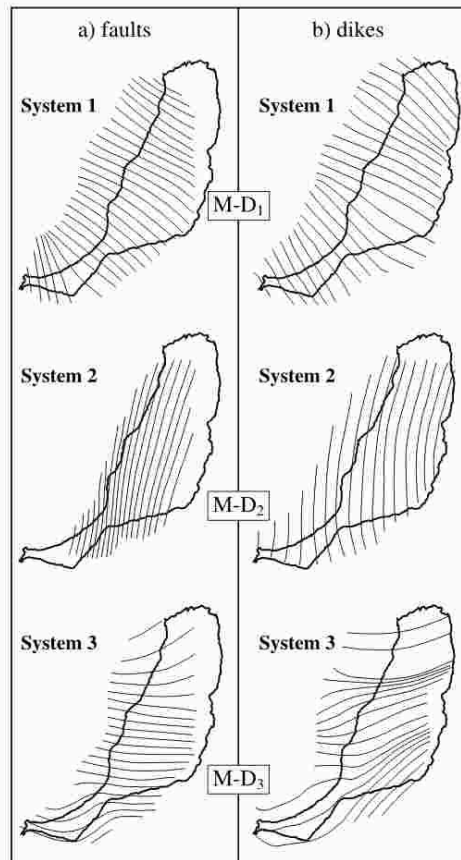
Figure 11. Maps of trajectories of the maximum horizontal extension axis. Results are shown for (a) faults and (b) dikes and are separated according to the distinguished systems (deformation phases M-D$_1$, M-D$_2$, and M-D$_3$). Trajectories obtained from the results of Tables 1 and 2 and using the interpolation program of *Lee and Angelier* [1994].

deformation of its substratum. The final hypothesis considered here for M-D$_1$ is that of a regional extensional tectonics, modulated by the intrusion of plutons and dikes and by the increasing load of the subaerial volcanic edifices. The structural data presented in this work highly support this hypothesis. However, the precise geometry of the extensional megastructure is debatable, although a possible interpretation is given below.

[37] The geometrical relationships between folds and faults in Las Hermosas area point to the activity during M-D$_1$ of a linked extensional fault system with a basal

detachment slightly dipping to the WNW or NW (cross section II-II', Figure 5). According to this interpretation, the faults show listric geometry in cross section and the arrangement of the fault system implies an asymmetric WNW to NW directed extension of the crust. Following the same logic, the geometrical analysis of cross section I-I' (Figure 4b) suggests that the large-scale folds could be associated with a hypothetical basal detachment, that must lie at greater depths in the center of the Fuerteventura Island than in Las Hermosas zone. Cross section I-I' has been continued until point I'' (Figure 13a; for location, see Figure 1) to obtain more information about the possible location of the hypothetical basal detachment in the center of the island. Cross section I-I'-I'' is based on the surface data and cross section of Figure 4b. The prediction of the geometry of the putative detachment at depth has been obtained by the use of conventional balanced cross section construction techniques and depth to detachment calculations [e.g., *Gibbs*, 1983; *Williams and Vann*, 1987]. Alternation of anticlines and synclines along the cross section has been interpreted as successive rollovers and ramp synclines formed above a complex ramp/flat listric detachment [*McClay and Scott*, 1991] (compare Figures 13a and 13b). The geometry of the subaerial volcanic group is very similar to the theoretical architecture of the synrift sediments in the analogue modeling, while most of the basal complex can be considered as prerift unit (Figure 13a). Also the lower part of the Miocene volcanic complexes can be considered as synrift materials. The converging pattern of system 1 dikes in Fuerteventura (Figure 3a) can be interpreted as a result of emplacement along the fracture system defining the central collapse graben that shows a fan-shaped geometry (Figure 13b). Alternatively, the dikes could have been tilted with respect to the graben axis to become almost parallel to the fan-shaped fault system, like that observed in the Solea graben of Troodos ophiolite [*Allerton and Vine*, 1987]. The association of large folds, dike swarm and normal faults is therefore an essential characteristic of this model. Interestingly, the Miocene plutonic rocks in the cross section I-I'-I'' are located above one of the hypothetical detachment ramps. Moreover, the center of the northern volcanic edifice lies above these plutonic roots (Figure 13a), suggesting a tectonic control on volcanic activity. The breakaway of the basal detachment should be located beneath the lava flows of the upper episodes of the Miocene volcanic complexes (near point I'' in Figure 13a), and it continues to the east of Las Hermosas area, as explained before. The probable trace of the hypothetical breakaway approximately follows the eastern boundary of the central depression of Fuerteventura, a conspicuous morphological feature of the island, although rocks of the episodes II and III of the Miocene volcanic edifices cover the breakaway trace.

[38] The present-day depth to the proposed basal detachment beneath the anticline is of around 5 km. This value, obtained from the techniques used to draw and evaluate cross section I-I'-I'', probably increases to $\geq$6 km below the Atlantic Ocean (left tip of that cross section). Around 2 to 3 km are deduced for the zone to the east of point I', therefore coinciding with the value in Las Hermosas area
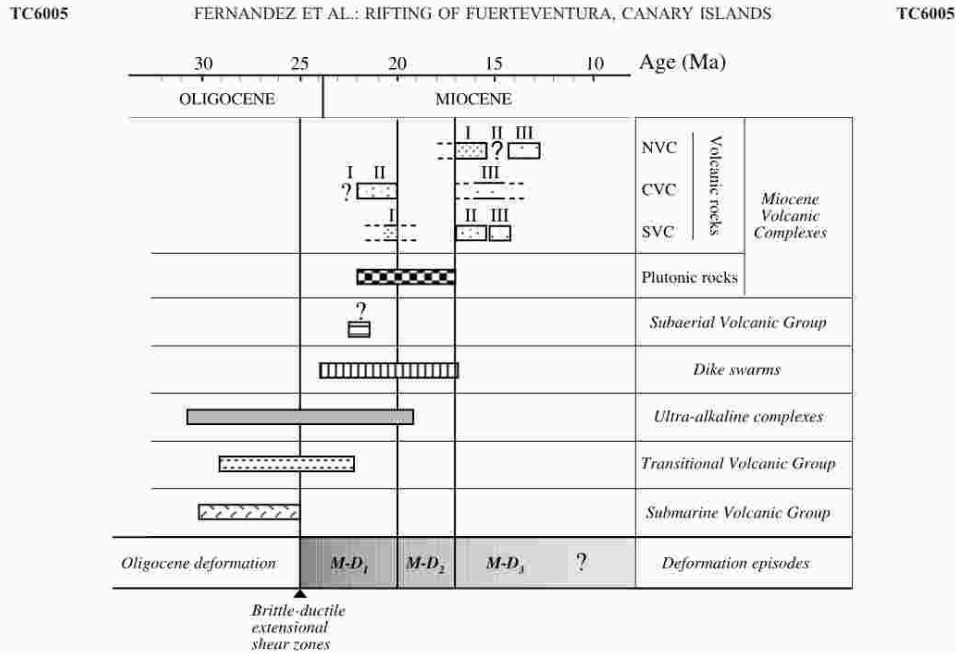
177

Figure 12. Chronological diagram representing the age of the main units of the basal complex, subaerial volcanic group, and Miocene volcanic complexes of the Fuerteventura Islands (references in the main text). The relative age of the deformation phases distinguished in this work (M-D$_1$, M-D$_2$, and M-D$_3$) is shown for comparison. Age determinations are from *Feraud* [1981], *Feraud et al.* [1985], *Le Bas et al.* [1986], *Ibarrola et al.* [1989], *Cantagrel et al.* [1993], *Ahijado* [1999], *Balogh et al.* [1999], *Gutiérrez* [2000], and *Muñoz et al.* [2005] for the basal complex, the dike swarm and the subaerial volcanic group and *Coello et al.* [1992], *Balcells et al.* [1994], and *Ancochea et al.* [1996] for the Miocene volcanic complexes.

(Figure 5). This is probably due to the vicinity of this zone to the breakaway fault. Figure 14a shows an idealized block diagram depicting the proposed tectonovolcanic activity during the M-D$_1$ phase. Cross sections I-I′-I″ and II-II′ are shown in the right frontal walls of the block diagram. The thickness of the oceanic crust agrees with the crustal models obtained from seismic profiles [*Banda et al.*, 1981; *Watts*, 1994; *Dañobeitia and Canales*, 2000]. The lower crust in the block diagrams also include a layer with high P wave velocities (7.4 km s^{-1}) found at 14–15 km beneath the surface in Fuerteventura and Lanzarote, and interpreted as due to underplated mafic rocks [*Dañobeitia and Canales*, 2000]. The subaerial volcanic group (and probably the lower units of episode I in the central and southern volcanic complexes) is considered as a synrift unit. The system I dike swarm acted as a feeder structure of these volcanic units, and therefore the emission model proposed for these successions consists in an elongate ridge with fissural volcanic activity (Figure 14a). In this sense, the results of this work coincide with the interpretation of *Fúster*

[1975] and *Stillman et al.* [1975], at least for the early stages of the subaerial volcanic history of Fuerteventura.

[39] The model of extension favored in this work is asymmetric (Figure 14). The exposed basal complex and subaerial volcanic rocks affected by M-D$_1$ show predominant east dipping bedding (Figure 4a), and the main mapped faults dip to the west (Figures 5 and 7a). This large-scale architecture recalls that of an asymmetric normal-faulting province (Figure 14). Other arguments are the presence of the central depression to the east of the basal complex exposure, and the distinct geological characteristics of the east and west coasts of Fuerteventura (Figure 1), including the contrasted bathymetry offshore both coasts of the island [e.g., *Acosta et al.*, 2003]. Finally, the giant landslides that partially destroyed the Miocene subaerial shield volcanoes show consistent dips to the west or WNW (Figure 13a), a fact already described by many authors [e.g., *Ancochea et al.*, 1996; *Stillman*, 1999; *Acosta et al.*, 2003]. Recent analogue models suggest that volcano spreading becomes concentrated on downslope sectors even with small (<1°) substrata tilt [*Wooller et al.*, 2004]. Therefore the polarity of
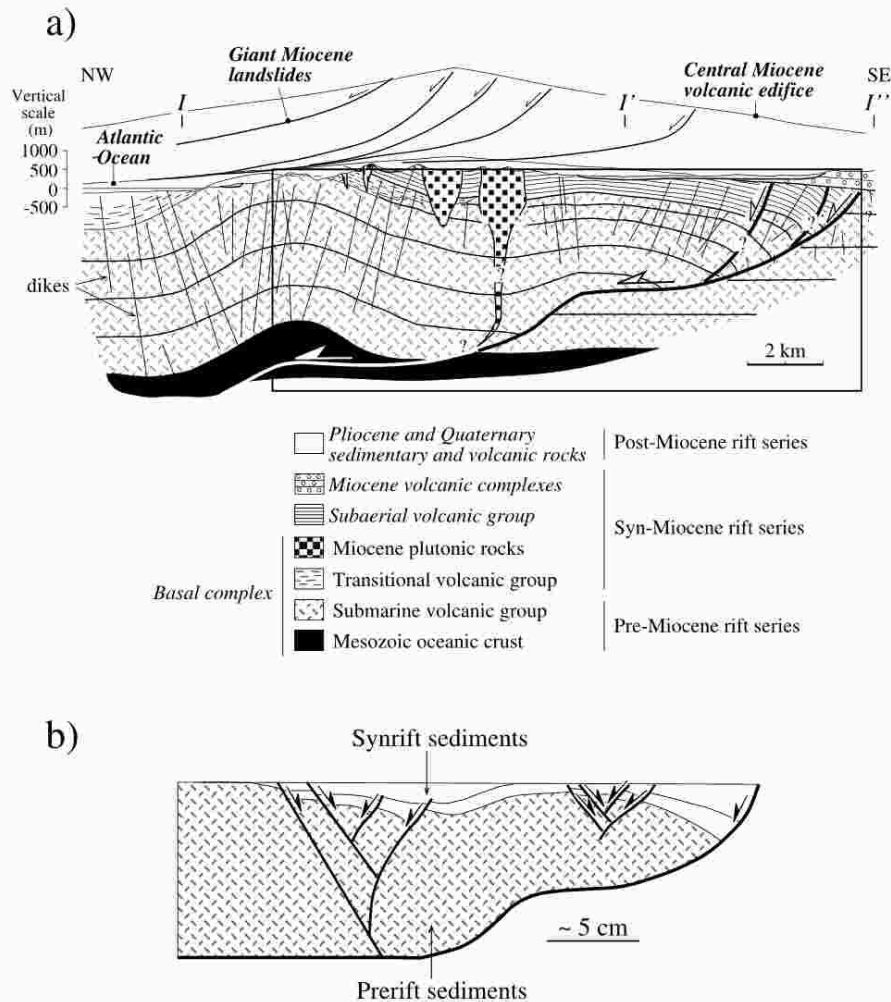
Figure 13. (a) I-I′-I″ cross section (see Figure 1 for location) with interpretation of the geometry and location of a stepped basal detachment. Shape of the large Miocene landslides affecting the volcanic edifice according to *Stillman* [1999]; the rectangle marks the area comparable with the analogue model (Figure 13b). (b) Analogue model of extension above a ramp/flat basal listric detachment (modified after *McClay and Scott* [1991]).

the giant landslides in Fuerteventura can be a consequence of a basement regionally tilted to the west or WNW, which is easy to explain with an asymmetric mode of extension. The absence of accurate geological and geophysical data offshore the west coast of Fuerteventura, does not allow a complete confirmation of the proposed model. Reactivation of the old structures imprinted in the oceanic crust since its birth in the Atlantic ridge, and the influence of younger structures such as the proposed Oligocene detachment [*Gutiérrez et al.*, 2006] have not been evaluated in this work, although these structural inheritances cannot be dis-

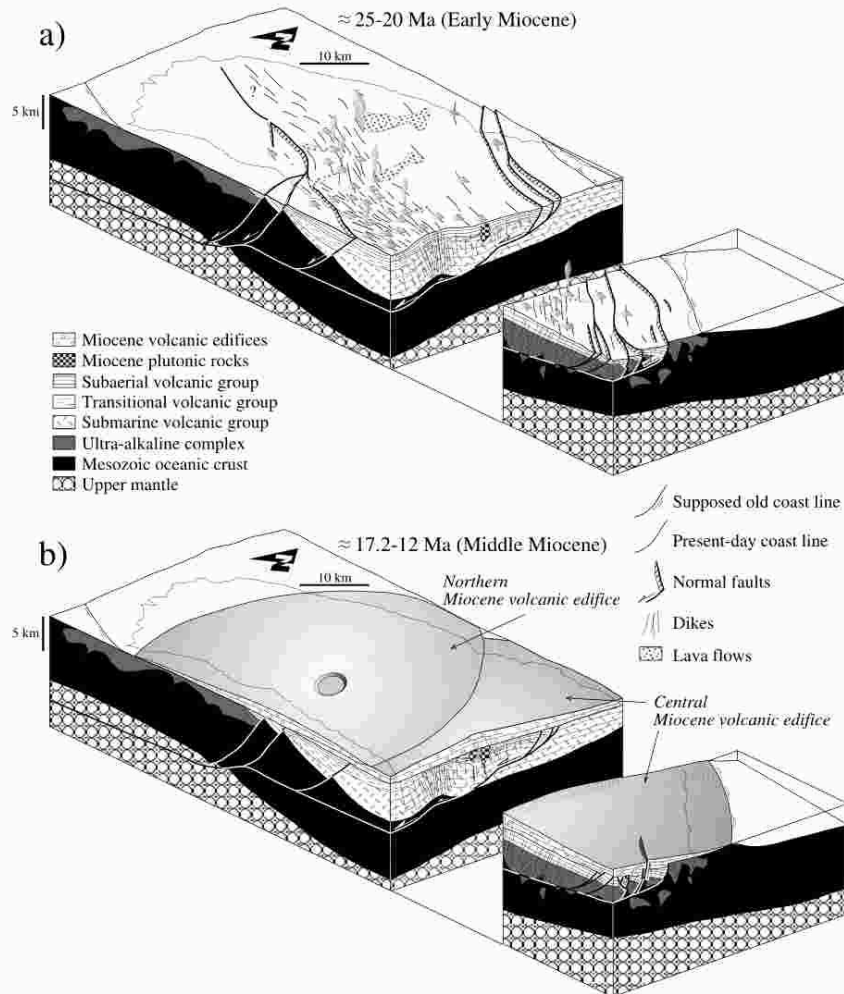Casillas *et al.*   *Crecimiento y evolución geológica de Fuerteventura*

Figure 14. Idealized block diagrams showing the geometry of the structures resulting from the Miocene deformation in the Fuerteventura Island. (a) Reconstruction during the M-D₁ phase depicting the displacement along a basal extensional detachment, the upward arching of the crust and the fissural volcanism generating the subaerial volcanic group. (b) Reconstruction during the M-D₃ phase representing the northern and central Miocene volcanic edifices (approximate size and geometry after *Ancochea et al.* [1993]). The three seismic layers identified in Fuerteventura by *Dañobeitia and Canales* [2000] correspond broadly to the Miocene volcanic edifices (upper crust), the submarine and transitional volcanic groups (middle crust), and the Mesozoic oceanic crust variably intruded by mantle magmas (lower crust). However, exact coincidence cannot be expected, due to the complex three-dimensional architecture of the crust in Fuerteventura. Thinning of the crust toward north is also observed in the seismic profile studied by *Dañobeitia and Canales* [2000]. The present-day coastline of Fuerteventura is shown for reference.
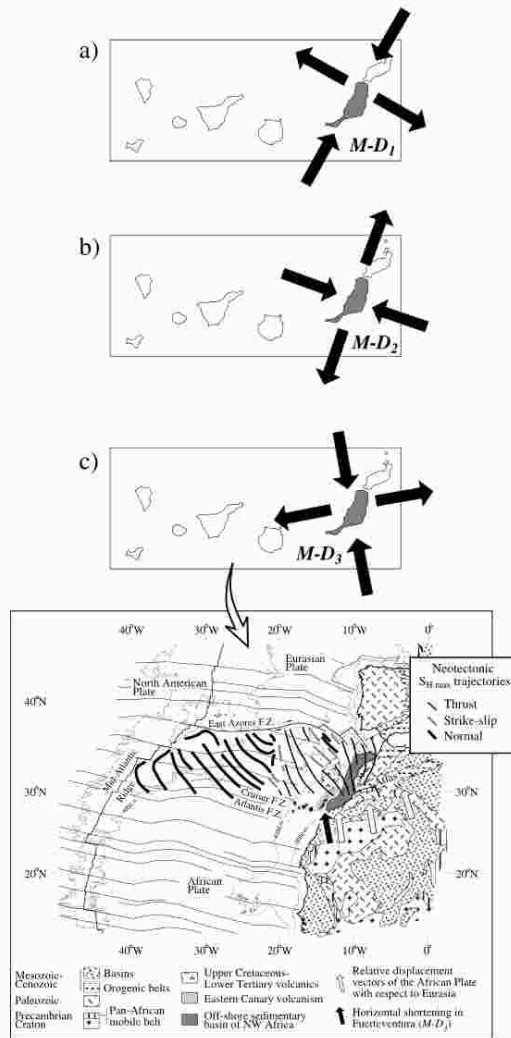
180

Figure 15. Time evolution of the average deformation fields in Fuerteventura. Black converging arrows: maximum horizontal shortening; black diverging arrows: maximum horizontal extension. (a) M-D$_1$ phase (25–20 Ma). (b) M-D$_2$ phase (20–17.2 Ma). (c) M-D$_3$ phase (17.2–12 Ma); sketch showing the large-scale tectonic framework of the Canary Islands. Patterns of important fracture zones (FZ), bathymetric contours, and plate boundaries are according to *Klitgord and Schouten* [1986] and *Steiner et al.* [1998]; geological features of continental northwestern Africa are after *Guiraud et al.* [1987]; tectonic map of the Atlas system and Iberian Peninsula are modified from *Seber et al.* [1996]; arrows indicating the relative displacement of Africa with respect to Eurasia follow the model of *Argus et al.* [1989]; curves marking the neotectonic stress trajectories and regimes in the NW corner of the African plate are after *Jiménez-Munt and Negredo* [2003].

carded in a model of Miocene asymmetric extension of Fuerteventura.

[40] In summary, it is here proposed that the M-D$_1$ phase gave place during the early Miocene to an asymmetric extension of the Fuerteventura oceanic lithosphere. The arcuate geometry in plan view of this asymmetric graben recalls the patterns described by *Rosendahl* [1987] in the East Africa Rift. Therefore it is possible to propose a process of Miocene rifting of Fuerteventura. The probable extrapolation of these structures to the north (Lanzarote and Conception Bank, Figure 1), and perhaps to the SW (from the Jandia Peninsula toward the Gran Canaria Island) suggests that this rifting process can be a fundamental characteristic of the eastern Canary ridge (Figure 15a). Magnetic anomalies follow the trend of the eastern Canary ridge, and show a curved, concave northward pattern at the south of Fuerteventura [*Catalán et al.*, 2003], therefore mimicking the arcuate geometry of rifting described in this work.

5.2. Phase M-D$_2$

[41] The transition to the M-D$_2$ phase took place at around 20 Ma, and it is marked by the intrusion of plutonic complexes with annular structure [*Ancochea et al.*, 1996]. The faults and dikes assigned to this phase affect the same materials than the M-D$_1$ phase and most of the Miocene plutonic rocks. It is responsible for the unconformities between episodes CVC-II and CVC-III and between SVC-I and SVC-II. *Feraud* [1981] and *Feraud et al.* [1985] have determined ages ranging from 20 Ma to 17.3 Ma for NW-SE trending dikes (system 2) from the southern part of Fuerteventura. The older SVC-II lava flows have been dated as 17.2 Ma [cf. *Ancochea et al.*, 1996, Table 1]. Accordingly, this phase lasted from 20 Ma to 17.2 Ma (Figure 12), and thus it approximately coincides with phase F$_2$ of *Ancochea et al.* [1996]. It represents the transition from a predominantly fissural to a central volcanic activity in the Miocene volcanic complexes. In fact, *Ancochea et al.* [1996] described complex dike systems that they have used, among other criteria, to determine the emission centers of the three large volcanic edifices. The radial patterns of dike systems described by *Ancochea et al.* [1996], mostly coincident in age with our systems 2 and 3, geometrically differ from our more constant dike trajectories (Figure 3). As explained before, this is a result of considering the dike trends in the younger episodes of the Miocene volcanic complexes [*Ancochea et al.*, 1996], while in this work we have measured dike data in the basal complex and in the older episodes of the Miocene edifices. More variable dike trends have been observed in the Jandia Peninsula (Figure 10), where radial dike patterns can reflect either volcano spreading or the effect of shallow intrusions exerting magma pressure on their walls and therefore increasing the volcano circumference [e.g., *Odè*, 1957; *Walker*, 1993; *van Wyk de Vries and Merle*, 1996]. However, in the stiff rocks of the basal complex, the subaerial volcanic group and the older units of the Miocene complexes, dike trends are more constant and define regional-scale deformation fields, with minor in-

fluence of the overlying edifices, which is indicative of the high viscosity of their substratum, as stated before.

[42] In any case, extension direction changed to NNE-SSW around 20 Myr ago, which is the average trend of the M-D$_2$ phase (Figures 12 and 15b). To explain this change in the extension direction two hypotheses can be advanced. First, it can be proposed a local switching of deformation axes during the same tectonic phase, a feature observed in the continental crust [e.g., *Simón Gomez*, 1989]. In fact, analysis of the brittle-ductile shear zones that acted during the first stages of the M-D$_1$ phase indicates a WNW-ESE predominant extension, with a minor extension along the NNE-SSW axis. However, the field structures in Fuerteventura show systematic crosscut relationships, and the trajectories of both deformation fields are not strictly normal (Figure 11). Therefore, in this work a second hypothesis of progressive permutation of deformation axes is favored. This permutation was responsible for a change from a mostly orthogonal rifting (MD-D$_1$) to an oblique rifting (MD-D$_2$). Similar tectonic evolutions have been found in many other rift systems, like for instance the Main Ethiopian Rift [*Boccaletti et al.*, 1999].

5.3. Phase M-D$_3$

[43] Phase MD-D$_3$ is contemporary with the main stages of growth of the huge volcanic edifices, particularly with respect to the northern volcanic complex (Figures 12 and 14b). It is responsible for the unconformities between episodes SVC-II and SVC-III in the southern volcanic complex and between episodes NVC-I and NVC-II-III in the northern volcanic complex. Dikes of system 3 have yielded ages ranging from 15.4 Ma to 12 Ma in the Jandía Peninsula [*Feraud*, 1981; *Feraud et al.*, 1985]. Therefore MD-D$_3$ approximately coincides with phase F$_3$ of *Ancochea et al.* [1996]. The average extension direction is E-W to ENE-WSW (Figure 11). No signs of this phase have been found in the Pliocene and Quaternary sediments and volcanic rocks of Fuerteventura. Therefore phase MD-D$_3$ can be dated between 17.2 and 12 Ma (Figure 12). Interestingly, the horizontal shortening direction deduced for phase MD-D$_3$ agrees with that of the present-day relative displacement vector of the African plate with respect to Eurasia in the studied area (Figure 15c) (displacement vectors traced according to the model of *Argus et al.* [1989]). At Lanzarote Island, *Marinoni and Pasquarè* [1994] have identified two strike-slip deformation phases with N-S to WNW-ESE horizontal shortening axes. The age of these events is less than 6 Ma. The orientation of the horizontal deformation axes for these phases in Lanzarote is roughly comparable with that of the MD-D$_3$ phase of Fuerteventura, and they can represent a time evolution of this phase (from extensional to strike-slip regimes) in the realm of the relative plate motions between Africa and Eurasia. In fact, as stated in the introduction, the theoretical model of *Jiménez-Munt and Negredo* [2003] suggests the present-day predominance of thrust to strike-slip regimes immediately to the north of the Canary Archipelago (Figure 15c), with N-S to NNW-SSE shortening directions. Also the available seismotectonic information for the zone between Gran Canaria and Tenerife, west of

Fuerteventura (Figure 1), supports a NNW-SSE trending maximum horizontal shortening favoring present-day displacement along strike-slip and reverse faults [*Mezcua et al.*, 1992].

5.4. Possible Causes of the Miocene Rifting of Fuerteventura

[44] The relative plate motion between Africa and Eurasia has remained stable since at least 30 Myr to the present [e.g., *Morgan*, 1983; *Roest and Srivastava*, 1991]. Therefore only the orientation of the maximum horizontal shortening associated with the MD-D_3 phase (N-S to NNW-SSE) can be partly explained with the relative plate motions between the African and Eurasian plates, and the origin of the MD-D_1 and MD-D_2 phases must be assigned to more local sources. Rifting and seafloor spreading is a tectonic characteristic of the western Mediterranean region since the Eocene and early Miocene, a paradoxical feature taking into account the colliding tectonic scenario between the African and Eurasian plates. *Hoernle et al.* [1995] suggested that this rifting, and its associated alkaline volcanism, is a consequence of lithosphere uplift above a large region of mantle upwelling. Indeed, *Hoernle et al.* [1995] have shown the presence of a low S wave velocity anomaly beneath the central east Atlantic and the western Mediterranean, depicting a huge sheet-like body. *Teixell et al.* [2005] have discussed the effect in the tectonic evolution of the Atlas Mountains of mantle upwelling in an otherwise contractive setting. The lithosphere thinning (from 180 to 80–60 km) beneath the Atlas could explain its high relief and occurrence of Miocene to recent alkaline magmatism. *Missenard et al.* [2006] proposed that this thermal anomaly can be followed from the Atlas Mountains to the south, across the Atlantic margin, and they relate this thermal anomaly to a shallow mantle plume. According to *Teixell et al.* [2005], mantle upwelling would be associated with upper mantle flow influenced by the thickening of the lithosphere at the Iberia-Africa plate boundary. With respect to the Canary Islands, *Canales and Dañobeitia* [1998] have described a swell rather obscured by the weight of the islands, and probably due to a thermal anomaly ($\sim$360°C) at the base of the lithosphere and upper asthenosphere. Geochemical data show a multicomponent mixture of lithospheric, asthenospheric and deep mantle sources [e.g., *Hoernle et al.*, 1991]. Therefore geophysical and geochemical data support the presence of a sublithospheric thermal anomaly, with mantle upwelling beneath the Canary Islands. The debate over whether this mantle upwelling represents a Miocene to recent plume, remnants of an old, Mesozoic plume, or it is rather a result of large-scale horizontal flow in the upper mantle, is beyond the scope of this work.

[45] Lithosphere uplift and later collapse through the activity of large-scale faults during the MD-D_1 and MD-D_2 phases should have overcome the effect of the deformation field related to the Africa-Eurasia relative convergent displacement. The end of phase MD-D_3 coincides with the waning of the volcanic activity in Fuerteventura. It is possible to relate this feature to the increasing relative importance of the deformation fields associated with the

African plate kinematics. The mantle anomaly was almost exhausted beneath Fuerteventura by the end of the middle Miocene, thus decreasing the importance of the local versus plate-scale strain fields. This transition corresponds to the switching between the extensional regime of phase MD-D_3 and the strike-slip regimes prevailing in more recent times, always with a N-S to NNW-SSE trending axis of maximum horizontal shortening. Interestingly, E-W trending extension still predominated until around 1.2 Ma in La Palma (location in Figure 1) [*Fernández et al.*, 2002]. This suggests that the transition from local to plate-scale strain fields probably suffered a westward migration with time, from the eastern Canary ridge (more than 6 Ma and less than 12 Ma in Fuerteventura and Lanzarote) toward the western Canary Islands (less than 1.2 Ma in La Palma). Similar age variations have been cited for the history of the subaerial volcanic activity in the Canaries [e.g., *Ancochea*, 2004].

[46] The evolution from phases MD-D_1 to MD-D_2, and then to MD-D_3, is characterized by the change from fissural volcanic activity toward predominantly central volcanic emissions. The model suggested by *Walter et al.* [2005] to explain the evolution of the Anaga volcano on the island of Tenerife (location in Figure 1) can also be applied to the Fuerteventura example. The model of *Walter et al.* [2005] considers the evolution of a linear rift that suffers local reorganization through flank instability and consequent generation of giant landslides. As a result of the variation in geometry and stress field triggered by the landslides, the linear rift evolves to triple-armed rifts that focus volcanic emissions on central edifices. *Walter et al.* [2005] have tested the model with a numerical elastic dislocation model. Giant landslides dominated the episodic growth of the volcanic edifices of Fuerteventura [*Ancochea et al.*, 1996; *Stillman*, 1999; *Acosta et al.*, 2003]. This instability can be partly explained by the syntectonic evolution of these volcanic edifices. Therefore it seems possible to apply the model of rift zone reorganization to the Miocene volcanic evolution of Fuerteventura. Apart from the possible mechanical effects of large landslides, tectonic switching from NW-SE to NNE-SSW and then to ENE-WSW extension directions should have collaborated in the construction of large central edifices. During the MD-D_2 and MD-D_3 phases the magmas could have profited the intersections between fractures resulting from the distinct tectonic events, such that ascent conduits could have taken a vertical elongate shape (Figure 14b). In this sense, the center of the northern edifice (Figure 1 for location) coincides with the inland prolongation of NW-SE faults observed in the west coast (Figure 7a) and that can be assigned to phase M-D_2. The age differences in the construction of the three large edifices in Fuerteventura are probably a consequence of local structural patterns and local evolution of volcanic emission and flank instabilities. The center of the older edifice (the CVC, Figure 12) coincides with the central segment of the sigmoid extensional structure (Figure 14b), probably the most mature part of the fault system that shows the larger extension factor.

[47] The complex image that emerges from this study can be used to constrain the models proposed for the origin

of the Canary Islands. The long and changing tectonic history of Fuerteventura, with a long-living rifting activity, is more akin to the unifying model of *Anguita and Hernán* [2000], which integrates the thermal and mechanical history and properties of the lithosphere and the sublithospheric mantle, than to any of the single hypotheses described in section 1.

6. Conclusions

[48] Three Miocene extensional deformation phases (M-D$_1$, M-D$_2$, and M-D$_3$) are recognized in the Fuerteventura Island. M-D$_1$ is characterized by a NW-SE directed extension. This phase, which lasted from 25 to 20 Ma, probably generated a large asymmetrical fault system, with predominantly top-to-NW sense of displacement. Syntectonic with this phase were the emplacement of a dense dike swarm, and the deposition of several volcanic units. Volcanic activity was essentially fissural during this stage. Folding of the pretectonic and syntectonic successions is interpreted as due to the accommodation of these series to complex ramp/flat geometry in the hypothetical basal detachment. The extensional structures are sigmoid in plan view, recalling the arcuate geometry of grabens in some continental rift systems. A switching to NNE-SSW extension directions took place during phase M-D$_2$ (20–17.2 Ma). This phase

is contemporary to the inception of the large central volcanic edifices in Fuerteventura. This change in the extension directions is believed to have conditioned the transition from fissural to central volcanic emission types. Finally, phase M-D$_3$ (17.2–12 Ma) was characterized by ENE-WSW extension or NNW-SSE shortening, which coincides with the displacement trajectories predicted by plate tectonic models in this part of the African plate. The Miocene rifting of Fuerteventura is considered as the tectonic result of the upwelling of a large body of anomalous sublithosphere mantle, which exceeded the deformation associated with plate motions, and generated a voluminous, tectonically controlled, basic volcanism. This evolution is akin to that of the Atlas province during the same time period, and it should be taken into account in any model for the origin of the Canary Islands.

References

Acosta, J., E. Uchupi, A. Muñoz, P. Herranz, C. Palomo, M. Ballesteros, and ZEE Working Group (2003), Geologic evolution of the Canarian Islands of Lanzarote, Fuerteventura, Gran Canaria and La Gomera and comparison of landslides at these islands with those at Tenerife, La Palma and El Hierro, *Mar. Geophys. Res.*, 24, 1–40.

Ahijado, A. (1999), Las intrusiones plutónicas e hipoabisales del sector meridional del Complejo Basal de Fuerteventura, Ph.D. thesis, 392 pp., Univ. Complutense de Madrid, Madrid, Spain.

Ahijado, A., and A. Hernández-Pacheco (1990), Las rocas ultramáficas alcalinas del Jable de Salinas, Fuerteventura, Islas Canarias, *Rev. Soc. Geol. Esp.*, 3, 275–287.

Ahijado, A., R. Casillas, and A. Hernández-Pacheco (2001), The dike swarms of the Amanay Massif, Fuerteventura, Canary Islands, *J. Asian Earth Sci.*, 19, 333–345.

Allerton, S., and F. J. Vine (1987), Spreading structure of the Troodos ophiolite, Cyprus: Some paleomagnetic constraints, *Geology*, 15, 593–597.

Ancochea, E. (2004), Canarias: Evolución de la actividad volcánica, in *Geología de España*, edited by J. A. Vera, pp. 639–641, Inst. Geol. y Minero de Esp.-Soc. Geol. de Esp., Madrid.

Ancochea, E., J. L. Brandle, C. R. Cubas, F. Hernán, and M. J. Huertas (1993), La Serie I de la Isla de Fuerteventura, *Mem. R. Acad. Cien. Ex. Fís. Nat.*, 27, 151 pp.

Ancochea, E., J. L. Brandle, C. R. Cubas, F. Hernán, and M. J. Huertas (1996), Volcanic complexes in the eastern ridge of the Canary Islands: The Miocene activity of the Island of Fuerteventura, *J. Volcanol. Geotherm. Res.*, 70, 183–204.

Anguita, F., and F. Hernán (1975), A propagating fracture model versus a hot-spot origin for the Canary Islands, *Earth Planet. Sci. Lett.*, 27, 11–19.

Anguita, F., and F. Hernán (2000), The Canary Islands origin: A unifying model, *J. Volcanol. Geotherm. Res.*, 103, 1–26.

Araña, V., and R. Ortiz (1991), The Canary Islands: Tectonics, magmatism and geodynamic framework, in *Magmatism in Extensional Structural Settings—The Phanerozoic Agrican Plate*, edited by A. B. Kampunzu and R. T. Lubala, pp. 209–249, Springer, New York.

Argus, D. F., R. G. Gordon, C. DeMets, and S. Stein (1989), Closure of the Africa-Eurasia-North America plate motion circuit and tectonics of the Gloria fault, *J. Geophys. Res.*, 94, 5585–5602.

Balcells, R., J. L. Barrera, J. A. Gómez, L. A. Cueto, E. Ancochea, M. J. Huertas, E. Ibarrola, and N. Snelling (1994), Edades radiométricas de los edificios miocenos de Fuerteventura (Islas Canarias), *Bol. Geol. Minero*, 105, 50–56.

Balogh, K., A. Ahijado, R. Casillas, and C. Fernández (1999), Contributions to the chronology of the Basal Complex of Fuerteventura, Canary Islands, *J. Volcanol. Geotherm. Res.*, 90, 81–102.

Banda, E., J. J. Dañobeitia, E. Suriñach, and J. Ansorge (1981), Features of crustal structure under the Canary Islands, *Earth Planet. Sci. Lett.*, 55, 11–24.

Boccaletti, M., R. Mazzuoli, M. Bononi, T. Trua, and B. Abebe (1999), Plio-Quaternary volcanotectonic activity in the northern sector of the Main Ethiopian Rift: Relationships with oblique rifting, *J. Afr. Earth Sci.*, 29, 679–698.

Bull, J. M., T. A. Minshull, N. C. Mitchell, K. Thors, J. K. Dix, and A. I. Best (2003), Fault and magmatic interaction within Iceland's western rift over the last 9 kyr, *Geophys. J. Int.*, 154, F1–F8.

Canales, J. P., and J. Dañobeitia (1998), The Canary Islands swell: A coherence analysis of bathymetry and gravity, *Geophys. J. Int.*, 132, 479–488.

Cantagrel, J. M., J. M. Fúster, C. Pin, U. Renaud, and E. Ibarrola (1993), Age Miocene inférieur des carbonatites de Fuerteventura, *C. R. Acad. Sci.*, 316, 1147–1153.

Carracedo, J. C., S. Day, H. Guillou, E. Rodríguez, J. A. Canas, and F. J. Pérez (1998), Hotspot

volcanism close to a passive continental margin, *Geol. Mag.*, 135, 591–604.

Casillas, R., A. Ahijado, and A. Hernández-Pacheco (1994), Zonas de cizalla dúctil en el complejo basal de Fuerteventura, *Geogaceta*, 15, 117–120.

Catalán, M., J. Martín Dávila, and ZEE Working Group (2003), A magnetic anomaly study offshore the Canary Archipelago, *Mar. Geophys. Res.*, 24, 129–148.

Cecchi, E., B. van Wyk de Vries, and J. M. Lavest (2005), Flank spreading and collapse of weak-cored volcanoes, *Bull. Volcanol.*, 67, 72–91.

Coello, J., J. M. Cantagrel, F. Hernán, J. M. Fúster, E. Ibarrola, E. Ancochea, C. Casquet, J. R. Jamond, and A. Cendrero (1992), Evolution of the eastern volcanic ridge of the Canary Islands based on new K-Ar data, *J. Volcanol. Geotherm. Res.*, 53, 251–274.

Dañobeitia, J. J. (1988), Reconocimiento geofísico de estructuras submarinas situadas al norte y sur del Archipiélago Canario, *Rev. Soc. Geol. Esp.*, 1, 143–155.

Dañobeitia, J. J., and J. O. Canales (2000), Magmatic underplating in the Canary Archipelago, *J. Volcanol. Geotherm. Res.*, 103, 27–41.

Feraud, G. (1981), Datation de resseaux de dykes et de roches volcaniques sous-marines par le methods K-Ar et ^{40}Ar-^{39}Ar: Utillisation des dykes comme marqueur de paleoconstraintes, Ph.D. thesis, 130 pp., Univ. de Nice, Nice, France.

Feraud, G., G. Giannérini, R. Campredon, and C. J. Stillman (1985), Geochronology of some Canarian dike swarms: Contribution to the volcano-tectonic evolution of the Archipelago, *J. Volcanol. Geotherm. Res.*, 25, 29–52.

Fernández, C., R. Casillas, A. Ahijado, V. Perelló, and A. Hernández-Pacheco (1997), Shear zones as result of intraplate tectonics in oceanic crust: An example of the Basal Complex of Fuerteventura (Canary Islands), *J. Struct. Geol.*, 19, 41–57.

Fernández, C., J. De la Nuez, R. Casillas, and E. García (2002), Stress fields associated with the growth of a large shield volcano (La Palma, Canary Islands), *Tectonics*, *21*(4), 1031, doi:10.1029/2000TC900038.

Foulger, G. R., J. H. Natland, D. C. Presnall, and D. L. Anderson (Eds.) (2005), *Plates, Plumes and Paradigms*, Spec. Pap. Geol. Soc. Am., *388*, 861 pp.

Fúster, J. M. (1975), Las Islas Canarias: Un ejemplo de evolución temporal y espacial del vulcanismo oceánico, *Estud. Geol.*, *31*, 439–463.

Fúster, J. M., A. Cendrero, P. Gastesi, E. Ibarrola, and J. Lopez Ruiz (1968), *Geología y volcanología de las Islas Canarias–Fuerteventura*, Instituto "Lucas Mallada", Consejo Superior de Invest. Cient., Madrid.

Fúster, J. M., M. Muñoz, J. Sagredo, A. Yébenes, T. Bravo, and A. Hernández-Pacheco (1980), Excursión n° 121 A + c del 26° I.G.C. a las Islas Canarias, *Bol. Inst. Geol. Min. Esp.*, *92*, 351–390.

Fúster, J. M., J. L. Barrera, M. Muñoz, J. Sagredo, and A. Yébenes (1984a), Mapa y Memoria explicativa de la Hoja de Pájara (1106 IV) del mapa geológico nacional a escala 1:25.000, Inst. Geol. y Minero de Esp., Madrid.

Fúster, J. M., A. Yébenes, J. L. Barrera, M. Muñoz, and J. Sagredo (1984b), Mapa y Memoria explicativa de la Hoja de Betancuria (1106 II) del mapa geológico nacional a escala 1:25.000, Inst. Geol. y Minero de Esp., Madrid.

Gastesi, P. (1969), Petrology of the ultramafic and basic rocks of Betancuria massif, Fuerteventura Island (Canarian Archipelago), *Bull. Volcanol.*, *33*, 1008–1038.

Gibbs, A. D. (1983), Balanced cross-section construction from seismic sections in areas of extensional tectonics, *J. Struct. Geol.*, *5*, 153–160.

Guiraud, R., Y. Bellion, J. Benkhelil, and C. Moreau (1987), Post-Hereynian tectonics in northern and western Africa, *Geol. J.*, *22*, 433–466.

Gutiérrez, M. (2000), Estudio petrológico, geoquímico y estructural de la serie volcánica submarina del Complejo Basal de Fuerteventura (Islas Canarias): Caracterización del crecimiento submarino y de la emersión de la Isla, Ph.D. thesis, 533 pp., Univ. de La Laguna, La Laguna, Spain.

Gutiérrez, M., R. Casillas, C. Fernández, K. Balogh, A. Ahijado, C. Castillo, J. R. Colmenero, and E. García-Navarro (2006), The submarine volcanic succession of the Basal Complex of Fuerteventura, Canary Islands: A model of submarine growth and emersion of some tectonic volcanic islands, *Geol. Soc. Am. Bull.*, *118*, 785–804.

Hobson, A., F. Bussy, and J. Hernández (1998), Shallow-level migmatization of gabbros in a metamorphic contact aureole, Fuerteventura Basal Complex, Canary Islands, *J. Petrol.*, *39*, 125–137.

Hoernle, K., and H. U. Schmincke (1993), The role of partial melting in the 15–Ma geochemical evolution of Gran Canaria: A blob model for the Canary hotspot, *J. Petrol.*, *34*, 599–626.

Hoernle, K., G. Tilton, and H. W. Schmincke (1991), Sr-Nd-Pb isotopic evolution of Gran Canaria: Evidence for shallow enriched mantle beneath the Canary Islands, *Earth Planet. Sci. Lett.*, *106*, 44–63.

Hoernle, K., Y. S. Zhang, and D. Graham (1995), Seismic and geochemical evidence of large-scale mantle upwelling beneath the eastern Atlantic and western and central Europe, *Nature*, *374*, 34–39.

Holik, J. S., P. D. Rabinowitz, and J. A. Austin (1991), Effects of the Canary hotspot volcanism on structure of oceanic crust off Morocco, *J. Geophys. Res.*, *96*, 12,039–12,067.

Homberg, C., J. Angelier, F. Bergerat, and O. Lacombe (2004), Using stress deflections to identify slip events in fault systems, *Earth Planet. Sci. Lett.*, *2217*, 409–424.

Ibarrola, E., J. M. Fúster, and J. M. Cantagrel (1989), Edades K-Ar de las rocas volcánicas submarinas del sector norte del Complejo Basal de Fuerteventura, paper presented at ESF Meeting on Canarian Volcanism, Eur. Sci. Found., Lanzarote, Spain.

Jackson, M. D., and D. D. Pollard (1990), Flexure and faulting of sedimentary host rocks during growth of igneous domes, Henry Mountains, Utah, *J. Struct. Geol.*, *12*, 185–206.

Javoy, M., C. J. Stillman, and C. Pineau (1986), Oxygen and hydrogen isotope studies on the basal complexes of the Canary Islands: Implications on the conditions of their genesis, *Contrib. Mineral. Petrol.*, *92*, 225–235.

Jiménez-Munt, I., and A. M. Negredo (2003), Neotectonic modelling of the western part of the Africa-Eurasia plate boundary: From the Mid-Atlantic Ridge to Algeria, *Earth Planet. Sci. Lett.*, *205*, 257–271.

Kamb, W. B. (1959), Ice petrofabric observations from Blue Glacier, Washington, in relation to theory and experiment, *J. Geophys. Res.*, *64*, 1891–1909.

Klitgord, K. D., and H. Schouten (1986), Plate kinematics of the central Atlantic, in *The Geology of North America*, vol. M, *The Western North Atlantic Region*, edited by P. R. Vogt and B. E. Tucholke, pp. 351–378, Geol. Soc. of Am., Boulder, Colo.

Lawn, B. R., and T. R. Wilshaw (1975), *Fracture of Brittle Solids*, Cambridge Univ. Press, New York.

Le Bas, M. J., D. C. Rex, and C. J. Stillman (1986), The early magmatic chronology of Fuerteventura, *Geol. Mag.*, *123*, 287–298.

Lee, C., and J. Angelier (1994), Paleostress trajectory maps based on the results of local determinations: The "LISSAGE" program, *Comput. Geosci.*, *20*, 161–191.

López Ruiz, L. (1970), Estudio petrográfico y geoquímico del Complejo filoniano de Fuerteventura (Islas Canarias), *Estud. Geol.*, *26*, 173–208.

Mardia, K. V. (1972), *Statistics of Directional Data*, Elsevier, New York.

Marinoni, L. B. (2001), Crustal extension from exposed sheet intrusions: Review and method proposal, *J. Volcanol. Geotherm. Res.*, *107*, 27–46.

Marinoni, L. B., and A. Gudmundsson (2000), Dykes, faults and palaeostresses in the Teno and Anaga massifs of Tenerife (Canary Islands), *J. Volcanol. Geotherm. Res.*, *103*, 83–103.

Marinoni, L. B., and G. Pasquaré (1994), Tectonic evolution of the emergent part of a volcanic ocean island: Lanzarote, Canary Islands, *Tectonophysics*, *239*, 111–135.

Marret, R., and R. W. Allmendinger (1990), Kinematic analysis of fault-slip data, *J. Struct. Geol.*, *12*, 973–986.

McClay, K. R., and A. D. Scott (1991), Experimental models of hangingwall deformation in ramp-flat listric extensional fault systems, *Tectonophysics*, *188*, 85–96.

McGuire, W. J., , A. P. Jones, and J. Neuberg (Eds.) (1996), *Volcano Instability on the Earth and Other Planets*, Geol. Soc. Spec. Publ., *110*, 388 pp.

McPhie, J., M. Doyle, and R. Allen (1993), *Volcanic Textures: A Guide to the Interpretation of Textures in Volcanic Rocks*, 1st ed., 198 pp., Center for Ore Deposit and Explor. Stud., Univ. of Tasmania, Tasmanian Govt. Print. Off., Hobart.

Meco, J., and R. S. Pomel (1985), Les formations marines et continentales intervolcaniques des Iles Canaries Orientales (Grande Canarie, Fuerteventura et Lanzarote), stratigraphie et signification paleoclimatique, *Estud. Geol.*, *41*, 223–227.

Meco, J., and C. E. Stearns (1981), Emergent littoral deposits in the Eastern Canary Islands, *Quat. Res.*, *15*, 199–208.

Merle, O., and A. Borgia (1996), Scaled experiments of volcanic spreading, *J. Geophys. Res.*, *101*, 13,805–13,817.

Mezcua, J., E. Buforn, A. Udias, and J. Rueda (1992), Seismotectonics of the Canary Islands, *Tectonophysics*, *208*, 447–452.

Missenard, Y., H. Zeyen, D. Frizon de Lamotte, P. Leturmy, C. Petit, M. Sébrier, and O. Saddiqi (2006), Crustal versus asthenospheric origin of relief of the Atlas Mountains of Morocco, *J. Geophys. Res.*, *111*, B03401, doi:10.1029/2005JB003708.

Morgan, W. J. (1971), Convection plumes in the lower mantle, *Nature*, *230*, 42–43.

Morgan, W. J. (1983), Hotspot tracks and the early rifting of the Atlantic, *Tectonophysics*, *94*, 123–139.

Muñoz, M. (1969), Estudio petrológico de las formaciones alcalinas de Fuerteventura (Islas Canarias), *Estud. Geol.*, *25*, 257–310.

Muñoz, M., and J. Sagredo (1994), Reajustes mineralógicos y geoquímicos producidos durante el metamorfismo de contacto de diques basálticos (Fuerteventura, Islas Canarias), *Bol. Soc. Esp. Min.*, *17*, 86–87.

Muñoz, M., J. Sagredo, P. J. Rincón-Calero, and R. Vegas (1997), Emplazamiento en una zona de cizalla dúctil-frágil transtensiva para el plutón de Pájara, Fuerteventura, Islas Canarias, *Geogaceta*, *21*, 171–174.

Muñoz, M., J. Sagredo, C. de Ignacio, J. Fernández-Suárez, and T. E. Jeffries (2005), New data (U-Pb, K-Ar) on the geochronology of the alkaline-carbonatitic association of Fuerteventura, Canary Islands, Spain, *Lithos*, *85*, 140–153.

Odé, H. (1957), Mechanical analysis of the dyke pattern of the Spanish Peaks area, Colorado, *Geol. Soc. Am. Bull.*, *68*, 567–576.

Oehler, J. F., B. van Wyk de Vries, and P. Labazuy (2005), Landslides and spreading of oceanic hotspot and arc shield volcanoes on low strength layers (LSLs): An analogue modeling approach, *J. Volcanol. Geotherm. Res.*, *144*, 169–189.

Pollard, D. D., and P. Segall (1987), Theoretical displacements and stresses near fractures in rock: With applications to fault, joints, veins, dikes, and solution surface, in *Fracture Mechanism of Rocks*, edited by B. K. Atkinson, pp. 227–349, Elsevier, New York.

Robertson, A. H. F., and D. Bernoulli (1982), Stratigraphy, facies and significance of Late Mesozoic and early Tertiary sedimentary rocks of Fuerteventura (Canary Islands) and Maio (Cape Verde Islands), in *Geology of the Northwest African Continental Margin*, edited by U. Von Rad et al., pp. 498–525, Springer, New York.

Robertson, A. H. F., and C. J. Stillman (1979a), Late Mesozoic sedimentary rocks of Fuerteventura, Canary Islands: Implications for West Africa continental margin evolution, *J. Geol. Soc. London*, *36*, 47–60.

Robertson, A. H. F., and C. J. Stillman (1979b), Submarine volcanic and associated sedimentary rocks of the Fuerteventura Basal Complex, Canary Islands, *Geol. Mag.*, *116*, 203–214.

Roest, W. R., and S. P. Srivastava (1991), Kinematics of the plate boundaries between Eurasia, Iberia, and Africa in the North Atlantic from the Late Cretaceous to the present, *Geology*, *19*, 613–616.

Rosendahl, B. R. (1987), Architecture of continental rifts with special reference to East Africa, *Annu. Rev. Earth Planet. Sci.*, *15*, 445–503.

Sagredo, J., E. Ancochea, J. L. Brándle, C. R. Cubas, J. M. Fúster, A. Hernández-Pacheco, and M. Muñoz (1989), Magmatismo hipoabisal-subvolcánico y vulcanismo en un ámbito geodinámico distensivo (Fuerteventura, Islas Canarias), paper presented at ESF Meeting on Canarian volcanism, Eur. Sci. Found., Lanzarote, Canary Islands, Spain.

Sagredo, J., M. Muñoz, and C. Galindo (1996), Características petrológicas y edad K-Ar de las sienitas nefelínicas del Morro del Recogedero (Fuerteventura, Islas Canarias), *Geogaceta*, *20*, 506–509.

Scheidegger, A. E. (1965), On the statistics of the orientation of bedding planes, grain axes and similar sedimentological data, *U.S. Geol. Surv. Prof. Pap.*, *525C*, 164–167.

Searle, R. (1980), Tectonic pattern of the Azores spreading centre and triple junction, *Earth Planet Sci. Lett.*, *51*, 415–434.

Seber, D., M. Barazangi, B. A. Tadili, M. Ramdani, A. Ibenbrahim, and D. Ben Sari (1996), Three-dimensional upper mantle structure beneath the intraplate Atlas and interplate Rif mountains of Morocco, *J. Geophys. Res.*, *101*, 3125–3138.

Simón Gomez, J. L. (1989), Late Cenozoic stress field and fracturing in the Iberian Chain and Ebro Basin (Spain), *J. Struct. Geol.*, *11*, 285–294.

Steiner, C., A. Hobson, P. Favre, and G. M. Stampli (1998), Early Jurassic sea-floor spreading in the central Atlantic -the Jurassic sequence of Fuerteventura (Canary Islands), *Geol. Soc. Am. Bull.*, *110*, 1304–1317.

Stillman, C. J. (1987), A Canary Islands dyke swarm: Implications for the formation of oceanic islands by extensional fissural volcanism, in *Mafic Dyke Swarms*, edited by H. C. Halls and W. F. Fahrig, *Spec. Pap. Geol. Assoc. Can.*, *34*, 243–255.

Stillman, C. J. (1999), Giant Miocene landslides and the evolution of Fuerteventura, Canary Islands, *J. Volcanol. Geotherm. Res.*, *94*, 89–104.

Stillman, C. J., and A. H. F. Robertson (1977), The dyke swarm of the Fuerteventura Basal Complex, Canary Islands, *Abstr. Geol. Soc. London Newslett.*, *6*, 8.

Stillman, C. J., J. M. Fuster, M. J. Bennell-Baker, M. Muñoz, J. D. Smewing, and J. Sagredo (1975), Basal Complex of Fuerteventura (Canary Islands) is an oceanic intrusive complex with rift-system affinities, *Nature*, *257*, 469–471.

Teixell, A., P. Ayarza, H. Zeyen, M. Fernández, and M. L. Arboleya (2005), Effects of mantle upwelling in a compressional setting: The Atlas Mountains of Morocco, *Terra Nova*, *17*, 456–461.

van Wyk de Vries, B., and R. Matela (1998), Styles of volcano-induced deformation: Numerical models of substratum flexure, spreading and extrusion, *J. Volcanol. Geotherm. Res.*, *81*, 1–18.

van Wyk de Vries, B., and O. Merle (1996), The effect of volcanic constructs on rift fault patterns, *Geology*, *24*, 643–646.

van Wyk de Vries, B., S. Self, P. W. Francis, and L. Keszthelyi (2001), A gravitational spreading origin for the Socompa debris avalanche, *J. Volcanol. Geotherm. Res.*, *105*, 225–247.

Walker, G. P. L. (1987), The dike complex of Koolau volcano, Oahu: Internal structure of a Hawaiian rift zone, *U.S. Geol. Surv. Prof. Pap.*, *1350*, 961–993.

Walker, G. P. L. (1993), Basaltic-volcano systems, in *Magmatic Processes and Plate Tectonics*, edited by H. M. Prichard et al., *Geol. Soc. Spec. Publ.*, *76*, 3–38.

Walter, T. R., V. R. Troll, B. Cailleau, A. Belousov, H. U. Schmincke, F. Amelung, and P. v. d. Bogaard (2005), Rift zone reorganization through flank instability in ocean island volcanoes: An example from Tenerife, Canary Islands, *Bull. Volcanol.*, *67*, 281–291.

Watts, A. B. (1994), Crustal structure, gravity anomalies and flexure of the lithosphere in the vicinity of the Canary Islands, *Geophys. J.*, *119*, 648–666.

Weigel, W., P. Goldflam, and K. Hinz (1978), The crustal structure of the Conception Bank, *Mar. Geophys. Res.*, *3*, 381–392.

Williams, G., and I. Vann (1987), The geometry of listric normal faults and deformation in their hangingwalls, *J. Struct. Geol.*, *9*, 789–795.

Wooller, L., B. van Wyk de Vries, J. B. Murray, H. Rymer, and S. Meyer (2004), Volcano spreading controlled by dipping substrata, *Geology*, *32*, 573–576.

Zazo, C., J. L. Goy, C. Hillaire-Marcell, P. Y. Gillot, V. Soler, J. A. González, C. J. Dabrio, and B. Ghaleb (2002), Raised marine sequences of Lanzarote and Fuerteventura revisited: A reappraisal of relative sea-level changes and vertical movements in the eastern Canary Islands during the Quaternary, *Quat. Sci. Rev.*, *21*, 2019–2046.

———————————

A. Ahijado and R. Casillas, Departamento de Edafología y Geología, Universidad de La Laguna, 38206-La Laguna, Tenerife, Canary Islands, Spain.

M. A. Camacho, C. Fernández, and E. García Navarro, Departamento de Geodinámica y Paleontología, Universidad de Huelva, E-21071 Huelva, Spain. (fcarlos@uhu.es)

M. Gutiérrez, Estudios del Terreno S.L., C/España 21, locales 13 y 14, 38390-Santa Ursula, Santa Cruz de Tenerife, Canary Islands, Spain.

Facies asociadas a deslizamientos gigantes en Fuerteventura (Islas Canarias)

Facies associated with giant landslides in Fuerteventura (Canary Islands)

R. Casillas[1], J.R. Colmenero [2], S. Harani[3]

1. Departamento de Edafología y Geología. Fac. de Biología. C/Astrofísico Sánchez s/n. Universidad de La Laguna. 38206. La Laguna. Santa Cruz de Tenerife. rcasilla@ull.es
2. Departamento de Geología, Facultad de Ciencias, Univ. de Salamanca, Plaza de la Merced s/n 37008 Salamanca. colme@usal.es
3. Departement of Petrology and Geochemistry, Institute of Geography and Earth Sciences, Eötvös Loránd University, Pázmány sêtány 1/C, H-1117, Budapest (Hungría), szabolcs.harangi@geology.elte.hu

Resumen: Hace unos 16 millones de años, el edificio Dorsal Inicial de la Isla de Fuerteventura sufrió un deslizamiento gravitacional de toda la parte septentrional de su flanco occidental. Los restos de la avalancha rocosa producida tapizan el fondo del océano al oeste de la Isla y también están presentes en el sector septentrional y central de la misma. El estudio detallado de los depósitos relacionados con este gigantesco deslizamiento permite diferenciar un conjunto de facies, cuya interpretación revela los procesos involucrados en el deslizamiento y en el relleno del anfiteatro resultante del mismo. La decapitación de la cámara magmática profunda del edificio volcánico por el deslizamiento produjo una explosión lateral dirigida ("*blast*") que generó un flujo piroclástico denso estratificado (PDF) que cubrió los depósitos de avalancha rocosa previamente depositados. El deslizamiento produjo una enorme depresión abierta al oeste, que continuó rellenándose con materiales epiclásticos procedentes de deslizamientos secundarios que afectaron a las paredes de la depresión, y con los resultantes del retrabajamiento erosivo de los propios depósitos del "*blast*" y de la avalancha. El proceso de relleno estuvo acompañado por la reanudación de la actividad volcánica en forma de erupciones subaéreas, algunas de ellas hidrovolcánicas.

Palabras clave: Fuerteventura, deslizamiento gravitacional, litofacies, "*blast*".

Abstract: Sixteen million years ago, the northern part of the Initial Ridge volcano of the island of Fuerteventura underwent a gravitational slide throughout its western flank. At present, the remains of the debris avalanche produced by the sliding blanket the ocean floor to the west of the island and are also present in the northern and central parts of Fuerteventura. A field study of these deposits has permitted to establish a series of lithofacies, whose sedimentological and lithological characteristics allow the reconstruction of the processes involved. The decapitation of the interior of the volcano (the magma chamber) during the slide produced a laterally directed blast that generated a stratified pyroclastic dense flow (PDF) that covered the previous debris avalanche deposits. The slide created a huge depression open to the West, which continued to be filled by epiclastic materials from secondary slides that affected the walls of the large depression, and also by the materials resulting from the reworking of both the debris avalanche and the blast deposits. This filling process was accompanied by renewed volcanic activity in the form of subaerial eruptions, some of them of hydrovolcanic character.

Key words: Fuerteventura, gravitational landslide, lithofacies, blast.

INTRODUCCIÓN

En las Islas Canarias se han contabilizado hasta 30 grandes deslizamientos gravitacionales ocurridos a lo largo de su historia. Estos colapsos laterales de los edificios volcánicos produjeron avalanchas rocosas (*debris avalanches*) integradas por grandes volúmenes de materiales (varios Km^3) que se desplazaron pendiente abajo a altas velocidades (100 ms^{-1}), y cuyos depósitos ocupan grandes áreas con espesores que alcanzan cientos de metros. Algunos de estos deslizamientos fueron acompañados de erupciones laterales explosivas ("*blast*"), cuyos depósitos

piroclásticos aparecen interestratificados con los de las avalanchas. La disponibilidad de agua hace que parte de los materiales de la avalancha puedan ser retrabajados por corrientes acuosas u otras más densas de tipo lahar (debris flows y flujos hiperconcentrados). Estos procesos pueden ir seguidos por actividad volcánica, que da lugar a lavas, piroclastos de caída o niveles hidrovolcánicos. En las Canarias, como en otras muchas islas volcánicas oceánicas, la mayor parte de los materiales de los deslizamientos se encuentran en los fondos oceánicos adyacentes y sólo una parte reducida de los mismos aflora en las islas. Fuerteventura ha sufrido varios de estos deslizamientos a lo largo de su historia (Ancochea et al., 1993;

Stillman et al., 1999; Acosta et al., 2003). En este trabajo se describen e interpretan las litofacies del deslizamiento más septentrional, el de Puerto del Rosario, acaecido hace unos 16 millones de años, relacionado con el desplome del flanco occidental de la Dorsal Inicial (que constituye el Edificio Inferior Norte o de Tetir de Ancochea et al., 1993) y que dio lugar a una avalancha rocosa cuyos depósitos tapizan el fondo oceánico al oeste de la isla. El estudio se ha realizado a lo largo de los numerosos barrancos de la región donde se han levantado 130 columnas estratigráficas, algunas con más de 300 metros de espesor. El trabajo constituye un avance de otro más completo en curso de realización.

BREVE RESEÑA GEOLÓGICA DE FUERTEVENTURA

La isla de Fuerteventura está formada por cuatro conjuntos volcánicos relacionados con su crecimiento submarino, emersión y posterior evolución subaérea (Ancochea et al., 1993): a) el Complejo Basal; b) los restos de los grandes edificios volcánicos de tipo escudo; c) los restos de los edificios volcánicos del Plioceno y el Cuaternario y d) los sedimentos del Plioceno y el Cuaternario. El Complejo Basal (CB, Fúster et al., 1968) aflora fundamentalmente en el sector occidental (Macizo de Betancuria) y representa, esencialmente, el crecimiento submarino y la emersión de la isla, constando esencialmente de materiales volcánicos submarinos (Grupo Volcánico Submarino, GVSM), de transición (Grupo Volcánico de Transición, GVT) y subaéreos (Grupo Volcánico Subaéreo, GVSA), apoyados sobre un fragmento de corteza oceánica. Todos ellos se encuentran intruidos por una secuencia de cuerpos plutónicos y un importante enjambre de diques. El GVSA integra los restos de una gran dorsal volcánica (Dorsal Inicial) que se formó en los primeros momentos de emersión de la isla, previamente a los edificios volcánicos de tipo escudo (Casillas et al., 2008). Los restos de los grandes edificios volcánicos de tipo escudo representan un vulcanismo subaéreo ocurrido entre 23 y 13 Ma (Ancochea et al., 1993), que dio lugar a tres edificios volcánicos (Meridional o de Jandía, Gran Tarajal o Central y de Tetir o Septentrional). Estos volcanes se desarrollaron por acumulación de lavas muy fluidas y material piroclástico dispuestos sobre o interestratificados con aglomerados y brechas correspondientes a avalanchas rocosas y depósitos sedimentarios relacionados con deslizamientos de flanco de los edificios más tempranos. Los restos de los edificios volcánicos del Plioceno y el Cuaternario (<5 Ma) representan la reactivación volcánica ocurrida a finales del Plioceno tras un intenso período erosivo. Junto a estas formaciones volcánicas aparecen niveles de playas levantadas, paleodunas con aluviones y paleosuelos.
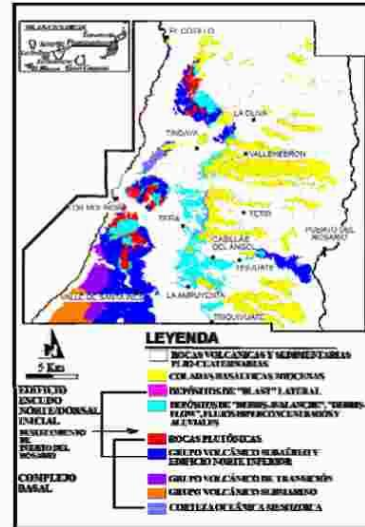

FIGURA 1. *Mapa geológico de la parte norte de la Isla de Fuerteventura.*

Los materiales objeto del presente estudio (Fig. 1) aparecen sobre las rocas volcánicas y plutónicas del CB, en formaciones de transición del CB (Brecha de Salinas, Cueto et al., 2004) y también intercalados en los niveles medios del edificio mioceno Escudo Septentrional (Formación Ampuyenta de Fúster et al., 1968; Edificio Septentrional Medio, de Ancochea et al., 1993; o brechas de tipo Ampuyenta y sedimentos y depósitos epiclásticos de Cueto et al., 2004).

DESCRIPCIÓN E INTERPRETACIÓN DE LAS LITOFACIES ENCONTRADAS

Las tablas I y II resumen, respectivamente, los caracteres y la interpretación de las facies epiclásticas y de las facies piroclásticas e hidroclásticas subaéreas, diferenciadas. Las facies A y B1 corresponden a depósitos de avalancha rocosa formados por los deslizamientos gravitacionales principal y secundarios. Las facies B2, B3, B4, C1, C2 y C3 representan depósitos formados por el retrabajamiento erosivo posterior de los niveles de avalancha rocosa mediante flujos hiperconcentrados cargados de clastos gruesos-muy gruesos, angulosos o redondeados. En el caso de las facies C4 y C5 el mecanismo de transporte parece haber sido corrientes acuosas de alta energía. Las facies D y E se interpretan como pequeñas llanuras de inundación. La tabla II incluye un conjunto de litofacies en depósitos producidos por flujos relacionados con la explosión lateral dirigida ("*blast*") simultánea al deslizamiento gravitacional (H-Q) y por erupciones subaéreas posteriores con importante interacción agua-magma (F).

FACIES	LITOLOGÍA Y ESTRATIFICACIÓN	TEXTURAS Y ESTRUCTURAS SEDIMENTARIAS	INTERPRETACIÓN
A: MEGABLOQUES	Megabloques decamétricos y hectométricos muy pobremente clasificados de basaltos plagioclásicos, diques y gabros. Matriz abundante de granulometría variable entre arcilla y canto. Espesor: 20->200 m	Fábrica desordenada y caótica. Abundantes diques clásticos arenosos y megabloques con *jigsaw cracks*	Facies de Megabloques de *debris avalanches* formada por un deslizamiento gravitacional "seco"
B1: BRECHAS MATRIZ-SOPORTADAS	Muy heterométricas. Bloques de hasta 1,5 m de diámetro, muy pobremente clasificados, de basaltos, traquitas, diques y gabros. Matriz muy abundante de grava fina-arena gruesa muy mal clasificada. Espesor: 2->100 m	Fábrica desordenada. Las capas tienen bases graduales e inversamente gradadas y los techos son netos o con gradación normal. Escasos clastos con *jigsaw-cracks*. Diques clásticos arcillosos	Facies de Matriz de *debris avalanches*
B2: BRECHAS CLASTO-SOPORTADAS	Muy heterométricas. Clastos de tamaño bloque y canto, menores que los de la facies B1. Matriz de arena gruesa-grava fina, escasa y bien a moderadamente clasificada. Espesor: 1,5-20 m	Fábrica desordenada o con gradación inversa a normal	*Flujos hiperconcentrados* generados por removilización del material del *debris avalanche*. La fábrica desordenada y escasa abrasión de los clastos indican un transporte muy reducido
B3: BRECHAS CLASTO-SOPORTADAS CON GRADACIÓN INVERSA	Clastos de 4,5 cm de tamaño medio y 70 cm de máximo, mal clasificados. Matriz escasa de arena gruesa-grava fina bien a moderadamente clasificada. Espesor: 0,7-2 m	Gradación inversa y base gradual o ligeramente erosiva: clastos groseramente ordenados paralelamente a la estratificación o imbricados con el eje a.	*Flujos hiperconcentrados* con transporte mayor que el de la facies B2. Soporte de los clastos principalmente por presión dispersiva
B4: BRECHAS CON INTERCALACIONES DE GRAVAS Y ARENAS	Las brechas son clasto y matriz-soportadas, muy heterométricas y con clastos <2 m; la matriz es abundante y de grava fina-arena gruesa, mal clasificada. Las gravas son finas y las arenas gruesas-muy gruesas, ambas con cantos y bloques dispersos. Los limos son escasos, con clastos de tamaño grava-canto. Capas irregulares <2 m, lateralmente discontinuas	Las brechas están desordenadas o con los clastos groseramente orientados o imbricados con el eje a; gradación inversa y normal. Las arenas y gravas muestran una grosera laminación paralela y cruzada de bajo ángulo. Los limos están laminados y tienen colores rojizos. Forman secuencias granodecrecientes groseras	*Flujos hiperconcentrados* probablemente canalizados con transición vertical a flujos acuosos arenosos
C1: CONGLOMERADOS MATRIZ-SOPORTADOS	Clastos de 20 cm tamaño medio y 1,20 de máximo, polimodales y bimodales, redondeados a subredondeados. Matriz abundante de arena gruesa-grava fina bien seleccionada	Fábrica desordenada	*Flujos hiperconcentrados* locales con clastos erosionados y retrabajados de zonas adyacentes. Escaso transporte y capacidad de selección. Idéntico a B2
C2: CONGLOMERADOS CLASTO-SOPORTADOS	Clastos de hasta 1,20 m de diámetro de basaltos y diques principalmente. Matriz: arena gruesa-grava fina, bien clasificada. Espesor: 0,7-20 m	Masivos o groseramente estratificados; los clastos se hallan dispuestos con el eje a paralelo a la estratificación o imbricado. Pueden mostrar gradación inversa en la base y normal en el techo	*Flujos hiperconcentrados con gravas*, con fuerte interacción entre los clastos y rápida sedimentación. Soporte de los clastos principalmente por presión dispersiva, similar a B3
C3: CONGLOMERADOS, GRAVAS Y ARENAS INTERESTRATIFICADOS	Los conglomerados tienen diámetro medio de 10 cm y máximo de 30 cm, con bloques dispersos de hasta 2 m. Las gravas y arenas (gruesas a muy gruesas y mal clasificadas) forman capas irregulares y tienen cantos dispersos o en pequeñas lentes. Espesor: 10-30 m	Estratos irregulares y lenticulares con base erosiva y clastos orientados paralelamente a la estratificación. En ocasiones las litologías forman secuencias inversas y normales. Laminación paralela y cruzada planar y en surco en las arenas	*Flujos hiperconcentrados* probablemente canalizados con transición vertical a flujos acuosos arenosos, similar a B4
C4: CONGLOMERADOS Y ARENAS EN SECUENCIAS CANALIFORMES	Conglomerados de cantos (15 cm de diámetro máximo) y gravas, en capas de 1-5 m. Arenas limosas en capas de 30-50 cm. Espesor: <35 m	Se ordenan formando secuencias granodecrecientes con base erosiva. Es frecuente la estratificación cruzada en surco de mediana-gran escala, la laminación paralela y la bioturbación figurativa	Flujos acuosos tractivos canalizados de energía decreciente de tipo *stream floods*
C5: GRAVAS FINAS Y ARENAS INTERESTRATIFICADAS	Arenas de grano muy grueso con cantos y bloques de hasta 1 m, dispersos u ordenados en láminas y lentes. Espesor: 0,5-3 m	Forman secuencias granodecrecientes con bases netas o ligeramente erosivas; las arenas muestran laminación paralela y cruzada de mediana-gran escala; imbricación del eje a en los clastos	Corrientes acuosas de tipo *stream* y *flash floods*. Posibles equivalentes distales de los flujos hiperconcentrados, que podrían llegar a estar representados en las lentes de cantos y bloques
D: ALTERNANCIA DE ARENAS Y LIMOS	Grano fino con clastos de 2-3 cm dispersos o formando lentes delgadas. Espesor: <2 m	Masivas o laminadas y con bioturbación vegetal	Débiles corrientes tractivas y desarrollo de paleosuelos inmaduros en llanuras de inundación efímeras
E: LIMOLITAS	Grano fino	Laminación paralela; color ocre	Llanuras de inundación efímeras

TABLA I. *Descripción e interpretación de las principales litofacies epiclásticas relacionadas con el deslizamiento gravitacional estudiado.*

189

FACIES	LITOLOGÍA Y ESTRATIFICACIÓN	TEXTURAS Y ESTRUCTURAS SEDIMENTARIAS	INTERPRETACIÓN
F: NIVELES HIDROVOLCÁNICOS	Brechas matriz-soportadas, gravas de grano fino, arenas de grano grueso y arenas limosas, con cantos dispersos de hasta 20 cm. Fragmentos juveniles (60%) y accidentales (40%)	Laminación paralela y cruzada de bajo ángulo. Colores amarillentos y verdosos	Erupciones hidrovolcánicas subaéreas por interacción explosiva agua-magma
H: BRECHAS CLASTOSOPORTADAS	Brechas clasto-soportadas bien clasificada con clastos de hasta 80 cm de tamaño, de gabros, sienitas, traquitas, diques y basaltos olivínicos vacuolares, plagioclásicos y olivínico-piroxénicos. Matriz (< 20%) de arena gruesa-grava fina	Gradación normal, inversa a normal o, más raramente, sólo inversa. En ocasiones los clastos muestran el eje mayor paralelo a la estratificación.	Nivel A1 de un depósito de flujo piroclástico denso estratificado de alta energía (PDC) producido por un "blast" lateral dirigido
I: BRECHAS MATRIZ-SOPORTADAS	Brechas matriz-soportadas, muy heterométricas, con matriz (50%) de arena gruesa-grava fina con clastos de 2-3 cm de tamaño, de basaltos plagioclásicos, traquitas, gabros y basaltos vacuolares (bombas?).	Gradación normal y más raramente inversa a normal o masiva. Grosera laminación paralela. A veces, contacto erosivo sobre facies H	Nivel A2 de un depósito de flujo piroclástico denso estratificado de alta energía (PDC) producido por un "blast" lateral dirigido
J: BRECHAS MATRIZ SOPORTADAS	Brecha matriz-soportada, heterogranular, con 40-70% de matriz de arcilla-arena gruesa-grava fina. Clastos de hasta 1 m dispersos de basaltos plagioclásicos, traquitas, basaltos vacuolares, gabros y diques. Localmente puede pasar a ser clastos-soportada y presentar niveles de concentración de cantos de hasta 30 cm de tamaño	Masiva o con gradación normal. Grosera laminación paralela. Clastos con el eje mayor paralelo a la estratificación o vertical. Puede tener base erosiva sobre facies H y mostrar en el techo chimeneas de desgasificación. Puede formar diques clásticos en las facies H y A.	Facies A2A de un depósito de flujo piroclástico denso estratificado de alta energía (PDC) producido por un "blast" lateral dirigido
K: ALTERNACIAS DE ARENAS Y GRAVAS LAMINADAS CON CANTOS DISPERSOS	Arenas y gravas alternando; clastos dispersos de tamaño variable entre 2-3 cms y 30 cms, angulosos a subredondeados, de gabros, rocas volcánicas, tobas traquíticas soldadas, diques y restos de bombas de basalto. En ocasiones hacia techo aparece lapilli acreccionado de tipo RIM y fragmentos de pómez	Laminación paralela y cruzada de bajo ángulo en forma de dunas. Gradación normal. Clastos orientados al azar, paralelamente a la estratificación u orientados con el eje mayor vertical. Estructuras de deformación por impacto y chimeneas de desgasificación	Nivel A2B de un depósito de flujo piroclástico denso estratificado de alta energía (PDC) producido por un "blast" lateral dirigido
L: CINERITA	Cinerita con lapilli acreccionado de tipo RIM.	En ocasiones pequeñas chimeneas de desgasificación con granos orientados con el eje vertical.	Nivel A3 de un depósito de flujo piroclástico denso estratificado de alta energía (PDC) producido por un "blast" lateral dirigido.
M: BRECHA CLASTOSOPORTADA	Brecha clasto-soportada con clastos de tamaño medio de 10 cm y máximo de 3 m. Misma composición que las facies H, I, J, y K.	Desordenada o con gradación inversa en la base. Ocupa depresiones entre los megabloques de la facies A	Depósito proximal de "blast" lateral acumulado en valles
O: BRECHA MATRIZ Y CLASTO-SOPORTADA	Brecha clasto y matriz-soportada con cantos de gabros, basaltos, etc. Clastos de tamaño medio 7 cm. Bloques aislados de 1 m.	Desordenada. A su techo aparece siempre la facies L	Flujos piroclásticos secundarios depositados en depresiones entre los megabloques de la facies A, procedentes de los depósitos de "blast" lateral acumulados en pendientes
P: BRECHA CLASTOSOPORTADA	Brecha clasto-soportada rellenando los espacios entre los megabloques de la Facies A. Clastos y matriz de la misma composición que las facies H, I, J, y K. En ocasiones pasa a las facies H	Desordenada	Depósito de "blast" lateral incorporado en la avalancha rocosa por la simultaneidad entre ambos flujos
Q: DIQUES CLÁSTICOS	Diques clásticos inyectados en las facies A y B1, de espesor entre 5 cm y 4 m, color blanco y matriz arenosa-grava fina con clastos aislados de hasta 1 m. Composición similar a la de las facies H, I, J y K	Subverticales. Granulometría menor en los márgenes que en el centro donde forma una brecha caótica, matriz- o clasto-soportada muy rica en fragmentos de gabro	Inyección ascendente en la facies A del material fluidificado de la facies P acumulado en la misma, inmediatamente después de producido el deslizamiento

TABLA II. *Descripción e interpretación de las principales litofacies piroclásticas e hidroclásticas relacionadas con el deslizamiento gravitacional.*

REFERENCIAS

Acosta, J., Uchupi, E., Muñoz, A., Herranz, P., Palomo, C., Ballesteros, M., y ZEE Working Group, (2003): Geologic evolution of the Canarian Islands of Lanzarote, Fuerteventura, Gran Canaria and La Gomera and comparison of landslides at these islands with those at Tenerife, La Palma and El Hierro. *Mar. Geophysical Researches*, 24: 1-40.

Ancochea, E., Brandle, J.L., Cubas, C. R., Hernán, F. y Huertas, M. J. (1993): La Serie I de la Isla de Fuerteventura. *Memoria de la Real Acad. de Cien. Ex. Fis. y Nat. Serie de Ciencias Nat.*, 27. 151 pp.

Casillas, R., Fernández, C., Ahijado, A., Gutiérrez, M., García-Navarro, E. y Camacho, M. (2008): Excursión postcongreso nº 2: Crecimiento temprano y evolución tectónica de la Isla de Fuerteventura. En: Pérez-Torrado, F. y Cabrera, M.C. (Ed).

Itinerarios Geológicos por las Islas Canarias: Fuerteventura, Lanzarote, La Gomera y El Hierro. Sociedad Geológica de España. *Geoguías*, 6: 59-86.

Cueto, L.A., Gómez, J.A., Barrera, J.L., García, E., Nieto, M., Vidal, J.R. y Ruiz, M.T. (2004): *Mapa Geológico de España 1:25.000, hoja nº 92-77 (Los Molinos)*. IGME, Madrid. .

Fúster, J.M., Cendrero, A., Gastesi, P., Ibarrola, E. y Lopez Ruiz, J. (1968): *Geología y volcanología de las Islas Canarias- Fuerteventura*. Instituto "Lucas Mallada". Consejo Superior de Investigaciones Científicas, Madrid. 239 pp.

Stillman, C. J., (1999): Giant Miocene Landslides and the evolution of Fuerteventura, Canary Islands. J. *Volcanology and Geothermal Research*, 94: 89-104.